# NON-PLANAR ADAPTIVE ANTENNAS FOR GPS RECEIVERS

A Thesis

Presented in Partial Fulfillment of the Requirements for

the Degree Master of Science in the

Graduate School of The Ohio State University

By

Chad Slick, B.S.E.E., B.S.C.E.

* * * * *

The Ohio State University

2007

Master's Examination Committee:

Prof. Prabhakar H. Pathak, Advisor

Dr. Inder J. Gupta, Co-Advisor

Approved by

Prabhakar Pathak

Advisor

Inder J. Gupta

Co-Advisor

Graduate Program in Electrical and Computer Engineering

# ABSTRACT

The current state-of-the-art adaptive antennas for Global Positioning System (GPS) receivers are planar antenna arrays. Due to the planar nature of these antenna arrays, the resolution with respect to the elevation plane is limited if the antenna is mounted in a horizontal plane. The nulls formed by the adaptive antenna in response to low elevation radio frequency interference (RFI) signals extend significantly into the elevation plane resulting in performance degradation. One solution to combat this problem is to use non-planar adaptive antennas with GPS receivers. The non-planar adaptive antenna can exploit its geometry to provide RFI suppression against low elevation interfering signals while maintaining reception of low angle signals of interest (SOI) to yield highly accurate Position, Velocity, and Time (PVT) solutions. It will be shown that convex non-planar antenna arrays perform significantly better than planar antenna arrays as well as concave non-planar antenna arrays in the presence of low elevation RFI signals. Also, an increase in the curvature of the antenna array will result in AJ performance improvement. All antenna arrays studied in this thesis have similar projected area (looking from the top) relative to the current state-of-the-art planar adaptive antenna (GAS-1 CRPA). Moreover, the convex non-planar antenna arrays contains more surface area allowing the addition of more antenna elements resulting in further performance improvement. The antenna element used in this study is a dual stacked microstrip patch antenna designed to operate at the L1(1575.42 MHz) and L2(1227.6 MHz) GPS frequencies. Rigorous electromagnetic (EM) modeling, which takes into account mutual coupling of antenna elements and array structure, of the various antenna arrays is performed to obtain the *in situ* volumetric patterns of the individual antenna elements.

This thesis also focuses on determining the optimum number of elements as well as their distributions based upon antenna array performance for a fixed aperture size of a

six inch high and two inch high convex non-planar adaptive antenna. The antenna arrays investigated have a single constraint to have the reference element distributed at the top of the convex surface to provide upper hemispherical coverage. The adaptive antenna performance is evaluated with respect to the adaptive algorithms of simple power minimization and beam forming / null steering. The performance metrics are the output Signal-to-Interference plus Noise Ratio (SINR) and the average available region over the upper hemisphere for which the output SINR exceeds a selected value in the presence of multiple interfering signals, where the average value is obtained by performing Monte Carlo simulations.

It will be shown that for the six inch high surface, it is better to distribute the antenna elements along two rings, with the inner ring at an angle of 45° from the centroid (a height of 4.24"), and the other ring along the bottom outer edge of the hemisphere. However, if less surface area is available, as is the case with the two inch high surface, it is best to distribute the remaining elements on the periphery of the antenna array. Furthermore, it will be shown that when adaptive antenna is operating in the beam forming / null steering mode the addition of more elements always leads to improved performance; however, this does not hold true when the adaptive antenna is operating in the simple power minimization mode.

Dedicated to my Family and Friends for their continued encouragement and support.

# ACKNOWLEDGMENTS

I would like to thank my adviser, Dr. Inder J. Gupta for his thorough support and help during my time at The Ohio State University in pursuit of achieving a Master of Science in Electrical Engineering. Also, I would like to thank Professor Prabhakar H. Pathak for his additional guidance and support throughout my graduate study. Furthermore, I would also like to thank Applied EM, Inc., for their joint collaboration on this project and for providing the numerical EM simulations of the investigated adaptive antennas evaluated at the GPS frequencies.

# VITA

| | |
|---|---|
| December, 4, 1981 | Born - Youngstown, OH |
| April, 2002 - September, 2005 | Co-op student Sandia National Laboratories |
| June 18, 2005 | B.S. Electrical Engineering, B.S. Computer Engineering, Kettering University, Flint, Michigan, USA |
| October, 2005 - September, 2006 | Northrop Grumman Industrial Fellowship, ElectroScience Lab, The Ohio State University |
| October, 2006 - present | Graduate Research Associate, ElectroScience Lab, The Ohio State University |

# PUBLICATIONS

C.D. Slick, "'Real-Time Sinc Interpolator"', Thesis, Sandia National Laboratories, June 2006.

I.J. Gupta and C.D. Slick, "Non-Planar Adaptive Antenna Arrays for GPS receivers", Technical Report 60005799-4, The Ohio State University ElectroScience Laboratory, June 2006.

I.J. Gupta and C.D. Slick, "Non-Planar Adaptive Antenna Arrays for GPS receivers", Technical Report 60005799-5, The Ohio State University ElectroScience Laboratory, August 2006.

I.J. Gupta and C.D. Slick, "Non-Planar Adaptive Antenna Arrays for GPS receivers", Technical Report 60010108-1, The Ohio State University ElectroScience Laboratory, November 2006.

I. Gupta, C. Church, A. O'brien, C. Slick, "Prediction of Antenna and Antenna Electronics Induced Biases in GNSS Receivers", Proceedings of ION GNSS 2007, San Diego, CA, January 2007.

C.D. Slick and I.J. Gupta, "Non-Planar Adaptive Antenna Arrays for GPS receivers", Technical Report 60010108-2, The Ohio State University ElectroScience Laboratory, February 2007.

C.D. Slick and I.J. Gupta, "Non-Planar Adaptive Antenna Arrays for GPS receivers", Technical Report 60010108-3, The Ohio State University ElectroScience Laboratory, May 2007.

## FIELDS OF STUDY

Major Field: Electrical and Computer Engineering

Studies in:

Adaptive Antennas
Space-Time Adaptive Processing
Electromagnetics

# TABLE OF CONTENTS

# LIST OF FIGURES

# LIST OF TABLES

# CHAPTER 1

# INTRODUCTION

Adaptive antenna arrays possess the ability to dynamically modify their patterns in response to the incident signal environment. As a result, they are extremely useful in suppressing radio frequency interference (RFI), which can be either intentional or unintentional, while maintaining reception of the signal of interest (SOI). This performance is achieved by adjusting dynamic weights to steer nulls in the direction of incident RFI and maintaining gain in the direction of the desired signal or signals. Various factors affect the performance of adaptive antenna arrays. These factors consist of antenna array design issues as well as signal processing issues. The antenna array design issues involve the design of the individual antenna element, the number of antenna elements, the element spacing, and the platform [13, 4, 6, 5, 7]. The signal processing issues include the adaptive algorithms, the number of taps, the tap delay, the selection of the reference tap, and the the sampling rate [8, 9, 11, 12]. The focus of this thesis is with respect to the antenna array design issues with fixed signal processing parameters. Adaptive antennas are commonly used in radar, communication, and navigation systems. The focus of this study is Global Positioning System (GPS) receivers.

Providing accurate GPS information is extremely critical for a wide variety of applications, and especially military applications. With the emergence of ultra-wideband (UWB) data systems and the growth of wireless communication systems, there are a number of potential sources to cause unintentional interference for GPS users. Moreover, intentional jamming from hostile sources is always an area of concern dealing with the availability of GPS. As a result, Anti-Jam (AJ) adaptive antennas must be designed to remain functional and maintain reception of GPS satellites throughout a wide range of harsh interference threat environments. The antenna is the connection between the receiver and the real world, and if the antenna is not properly designed to sufficiently suppress any type of incident interference, there is no possible means to recover the signal. Furthermore, the adaptive antenna should be designed to suppress RFI while maintaining maximum availability of GPS satellites.

The current state-of-the-art adaptive antennas used in conjunction with GPS receivers are planar antenna arrays. Due to the planar nature of these antenna arrays, the resolution with respect to the elevation plane is limited if the antenna is mounted in a horizontal plane. The nulls formed by the adaptive antenna in response to interference signals extend significantly into the elevation plane resulting in performance degradation. This is especially true for low elevation interfering signals. As a result, it can lead to reception loss of low elevation GPS satellites resulting in a less accurate Position, Velocity, Time (PVT) solution. One way to resolve this problem is to use non-planar adaptive antennas with GPS receivers. Non-planar antenna arrays have been proposed in [1, 10]; however, neither discussed the performance of non-planar antenna arrays in the presence of interfering signals. The non-planar adaptive antenna can exploit its geometry to provide RFI suppression against low elevation interfering signals while maintaining reception of low angle GPS satellites to yield highly accurate navigation solutions.

In this thesis, the performance of planar and non-planar GPS adaptive antenna arrays operating in harsh interference environments consisting of multiple low elevation interfering signals is investigated. All antenna array apertures studied in this work have similar projected area (looking from the top) of twelve inches. Also, the antenna arrays are constrained to having a single element distributed at the center of their respective surface. Rigorous electromagnetic modeling is carried out to include mutual coupling between the individual antenna elements as well as structure effects to obtain the *in situ* element volumetric patterns. This study is limited only to CW incident signals (desired as well as interference) and antenna electronics based on space-only processing. However, it has been shown in [14] that the performance of multi-tap Space-Time Adaptive Processing (STAP) based Antenna Electronics (AE) in the presence of wideband signals is almost identical to the performance of space-only processing in the presence of CW signals. Therefore, the conclusions of this thesis are also applicable to STAP based AE. This result yields a two-fold advantage in the reduction of computation time to evaluate the antenna array performance. First, the response of the individual antenna elements only needs to be analyzed at the L1 and L2 carrier frequencies instead of over the entire GPS frequency bands. Also, the reduction from multiple taps to a single tap yields a significant reduction in the computation time involved in the signal processing of the data to evaluate performance. The performance is examined using two adaptive algorithms, notably simple power minimization [8] and beam forming / null steering, which are both constrained to minimize the total output power. The performance metrics are output SINR and available angular region, which is defined as the region over the entire upper hemisphere for which the output SINR exceeds a selected level. This is calculated as the mean value over twenty-five independent trials for a given number of interfering signals, where their angle of arrival is varied randomly from one trial to the next.

The results of this thesis will show that convex non-planar antenna arrays perform significantly better than planar as well as concave non-planar antenna arrays. In fact, concave non-planar antenna arrays do not even perform as well as planar antenna arrays. It is shown that performance improvement can be achieved by increasing the amount of curvature of the convex non-planar surface geometry. As a result, it is shown that the six inch high geometry exhibits the best performance. Further investigation of the six inch high geometry reveals that one should distribute the elements in two rings, where the constraint of the reference element at the top of the hemisphere is met, and the remaining elements distributed on an inner ring of height 4.24 inches and an outer ring along the bottom of the hemisphere. All platforms may not be able to tolerate an antenna height of six inches, and one still wants to take advantage of the non-planar geometry; therefore, a two-inch high geometry is also investigated. It is shown that as the aperture becomes filled, there is an advantage to placing the elements along one ring instead of two rings; however, there is not a significant advantage between distributing antenna elements uniformly or non-uniformly. Furthermore, it will be shown that an increase in antenna elements will always lead to performance improvement if the AE is operating in the beam forming / null steering mode; whereas, this is not the case for the AE operating in simple power minimization mode. With respect to the AE operating in simple power minimization mode, it is shown that increasing elements will improve AJ performance up to a certain number, and increasing elements past this number will either cause the performance to increase only marginally, or in some cases, cause the performance to degrade.

The rest of this thesis is organized as follows: Chapter 2 introduces the basic concepts relating to the adaptive antenna. Furthermore, it will discuss the development of the adaptive processing (i.e., algorithms and processing techniques) as well as the simulation and signal scenarios used in conjunction with the array processing. Chapter 2 will also discuss the performance metrics utilized in this thesis to gauge the performance of the antenna array. Moreover, it will also describe the selected individual antenna element. Chapter 3 describes the non-planar surface selection for the geometry of the antenna array that yields the best performance, and that the addition of antenna elements also leads to improved performance. Chapter 4 shows that increasing the curvature of the non-planar surface results in improved performance and also yields more surface area, which allows one to increase the number of antenna elements in the array. Chapter 5 compares the performance of six inch high non-planar convex antenna array geometries. Three separate types of antenna distributions for the selected geometry are investigated. Moreover, the best antenna array for the six inch high surface will be presented. Chapter 6 compares the performance of two inch high non-planar convex antenna array geometries and yields a selected geometry based upon the adaptive performance. Chapter 7 compares the performance of three twelve element antenna arrays, a planar geometry, a two inch high geometry and a six inch high geometry and demonstrates performance improvement that can be achieved. Finally, Chapter 8 presents the conclusions and some ideas for future research.

# CHAPTER 2

# BACKGROUND AND UNDERSTANDING

This chapter lays the foundation for the work presented in this thesis. The antenna electronics (AE) used in this thesis is based on space-only adaptive processing, which is a special case of space-time adaptive processing. Therefore, we first derive the analytical model for space-time adaptive processing for completeness, and then relate it specifically to space-only adaptive processing. Moreover, it derives the STAP algorithms used in conjunction with this thesis. This chapter then describes the signal scenario, as well as, the individual antenna element that is employed in this study.

## 2.1 Analytical model of Space-Time Adaptive Processing

Figure 2.1 shows a block diagram of STAP, consisting of L antenna elements and N taps behind each element. The signal component denoted by $x_{ln}$ is the received voltage at the output of a antenna element for the $l$th element and the $n$th tap. At this point, the signal component is a combination of the desired signal, the interference signal and thermal noise, which is combined after passing through the RF front end, which is assumed to be ideal, of the antenna. It is important to note, the signals (desired and interference) incident upon the antenna as well as the thermal noise are assumed to be mutually uncorrelated, Wide Sense Stationary (WSS) zero-mean random processes. Each tap delays the signal component through the antenna by $T_0$, where $T_0$ is the inverse of the sampling rate, and the signal, $x_{ln}(t)$, is given in discrete time by:

$$x_{ln}(t) = x_l(t - (n-1)T_0) \tag{2.1}$$

The complex weights are assumed steady state and are denoted $w_{ln}$ for the weight at the $l$th element and the $n$th tap. Next, the voltage signals are multiplied by their respective corresponding weights and summed together to form the the array output $y(t)$ given by:

$$y(t) = \sum_{l=1}^{L} \sum_{n=1}^{N} w_{ln} x_{ln}(t) \tag{2.2}$$

By expressing the tap voltage signals and their corresponding weight vectors in vector form as follows

$$\mathbf{x} = [x_{11} ... x_{1N} x_{21} ... x_{2N} x_{L1} ... x_{LN}]^T \tag{2.3}$$

$$\mathbf{w} = [w_{11} ... w_{1N} x_{21} ... w_{2N} x_{L1} ... w_{LN}]^T \tag{2.4}$$

(where superscript T denotes the transpose operator and lowercase boldface characters represent vectors), one can express the array output as

$$y(t) = \mathbf{x}^T \mathbf{w} = \mathbf{w}^T \mathbf{x} \tag{2.5}$$

In general, the signal vector $\mathbf{x}$ and the array output are dependent upon current time, t; however, this will be dropped in the following equations for convenience. The mean square output of the array is given as

$$\begin{aligned} P &= \frac{1}{2} E\{y^* y\} \\ &= \frac{1}{2} E\left\{(\mathbf{w}^T \mathbf{x})^* (\mathbf{x}^T \mathbf{w})\right\} \\ &= \frac{1}{2} E\left\{\mathbf{w}^H \mathbf{x}^* \mathbf{x}^T \mathbf{w}\right\} \\ &= \frac{1}{2} \mathbf{w}^H E\left\{\mathbf{x}^* \mathbf{x}^T\right\} \mathbf{w} \\ &= \frac{1}{2} (\mathbf{w}^H \Phi \mathbf{w}) \end{aligned} \tag{2.6}$$

where $\Phi$ is the $LN$ x $LN$ covariance matrix defined as

$$\Phi = E\left\{\mathbf{x}^* \mathbf{x}^T\right\} \tag{2.7}$$

In the above equations, $E\{\bullet\}$ denotes the expectation operator, superscript * denotes the complex conjugate and superscript H denotes Hermitian or complex conjugate transpose operator. The weights $\mathbf{w}$ can be pulled outside of the expectation because they are not a random process and are independent of time, t. The total received signal vector $\mathbf{x}$ can be decomposed into its various signal components,

$$\mathbf{x} = \mathbf{x}_d + \mathbf{x}_i + \mathbf{x}_n \tag{2.8}$$

where $\mathbf{x}_d$ represents the received voltages due to the desired signal, $\mathbf{x}_i$ represents the voltages due to the interference signals, and $\mathbf{x}_n$ represents the voltages due to thermal noise of the system. By expressing the signal vector in terms of its three components one can now expand the total covariance matrix as

$$\begin{aligned} \Phi &= E\left\{(\mathbf{x}_d + \mathbf{x}_i + \mathbf{x}_n)^*(\mathbf{x}_d + \mathbf{x}_i + \mathbf{x}_n)^T\right\} & (2.9) \\ &= E\left\{\mathbf{x}_d^*\mathbf{x}_d^T\right\} + E\left\{\mathbf{x}_d^*\mathbf{x}_i^T\right\} + E\left\{\mathbf{x}_d^*\mathbf{x}_n^T\right\} + E\left\{\mathbf{x}_i^*\mathbf{x}_d^T\right\} + E\left\{\mathbf{x}_i^*\mathbf{x}_i^T\right\} + \\ &\quad E\left\{\mathbf{x}_i^*\mathbf{x}_n^T\right\} + E\left\{\mathbf{x}_n^*\mathbf{x}_d^T\right\} + E\left\{\mathbf{x}_n^*\mathbf{x}_i^T\right\} + E\left\{\mathbf{x}_n^*\mathbf{x}_n^T\right\} & (2.10) \end{aligned}$$

Under the assumption that the desired signal, interference signal and noise signal are all mutually uncorrelated and zero mean, the cross terms in (2.10) are equal to zero, and $\Phi$ can be expressed as

$$\begin{aligned} \Phi &= E\left\{\mathbf{x}_d^*\mathbf{x}_d^T\right\} + E\left\{\mathbf{x}_i^*\mathbf{x}_i^T\right\} + E\left\{\mathbf{x}_n^*\mathbf{x}_n^T\right\} \\ &= \Phi_d + \Phi_i + \Phi_n & (2.11) \end{aligned}$$

where $\Phi_d$ represents the desired signal covariance matrix, $\Phi_i$ represents the interference signal covariance matrix, and $\Phi_n$ represents the noise signal covariance matrix. Therefore, the individual covariance matrices can be solved for independently and the total covariance matrix can be found by 2.11. Each individual covariance matrix is $LN$ x $LN$ and represents the correlation between all taps and elements. The covariance matrix for arbitrary signal k, corresponding to either the desired or interference signal, can be subdivided into element-to-element submatrices and written as

$$\Phi_k = \begin{bmatrix} [\Phi_{k_{11}}]_{N\mathrm{x}N} & [\Phi_{k_{12}}]_{N\mathrm{x}N} & \cdots & [\Phi_{k_{1L}}]_{N\mathrm{x}N} \\ [\Phi_{k_{21}}]_{N\mathrm{x}N} & [\Phi_{k_{22}}]_{N\mathrm{x}N} & & \vdots \\ \vdots & & \ddots & \\ [\Phi_{k_{L1}}]_{N\mathrm{x}N} & \cdots & & [\Phi_{k_{LL}}]_{N\mathrm{x}N} \end{bmatrix} \tag{2.12}$$

where $[\Phi_{k_{pq}}]_{N\mathrm{x}N}$ denotes the the $N$ x $N$ covariance matrix between elements $p$ and $q$. The covariances matrices with respect to two elements are defined by

$$[\Phi_{k_{pq}}]_{mn} = E\left\{\mathbf{x}_{k_{pm}}^*\mathbf{x}_{k_{qn}}^T\right\} \tag{2.13}$$

we can further expand the received signal voltage $\mathbf{x}$ as the convolution of the time domain incident signal $k(t)$ and the time domain antenna response of element $p$, denoted $h_p(t)$. It is also important to note that the antenna response is dependent upon look direction $(\theta_k, \phi_k)$ which is taken into account; thus,

$$\begin{aligned}
[\Phi_{k_{pq}}]_{mn} &= E\big\{[h_p(\theta_k,\phi_k,t)\otimes k(t-(m-1)T_0)]^* \quad \ldots \\
&\qquad [h_q(\theta_k,\phi_k,t)\otimes k(t-(n-1)T_0)]\big\} \qquad (2.14)\\
&= E\Big\{\Big[\int_{-\infty}^{\infty} k(t-(m-1)T_0-\alpha)h_p(\theta_k,\phi_k,\alpha)\partial\alpha\Big]^* \quad \ldots \\
&\qquad \Big[\int_{-\infty}^{\infty} k(t-(n-1)T_0-\beta)h_q(\theta_k,\phi_k,\beta)\partial\beta\Big]\Big\} \\
&= \int_{-\infty}^{\infty}\int_{-\infty}^{\infty} E\left\{k^*(t-(m-1)T_0-\alpha)k(t-(n-1)T_0-\beta)\right\} \quad \ldots \\
&\qquad h_p^*(\theta_k,\phi_k,\alpha)h_q(\theta_k,\phi_k,\beta)\partial\alpha\partial\beta \\
&= \int_{-\infty}^{\infty}\int_{-\infty}^{\infty} E\left\{k^*(t-(m-1)T_0+(n-1)T_0-\alpha+\beta)k(t)\right\} \quad \ldots \\
&\qquad h_p^*(\theta_k,\phi_k,\alpha)h_q(\theta_k,\phi_k,\beta)\partial\alpha\partial\beta \\
&= \int_{-\infty}^{\infty}\int_{-\infty}^{\infty} E\left\{k^*(t-((m-n)T_0+\alpha-\beta)k(t)\right\} \\
&\qquad h_p^*(\theta_k,\phi_k,\alpha)h_q(\theta_k,\phi_k,\beta)\partial\alpha\partial\beta \\
&= \int_{-\infty}^{\infty}\int_{-\infty}^{\infty} R_k((m-n)T_0+\alpha-\beta)\ h_p^*(\theta_k,\phi_k,\alpha) \quad \ldots \\
&\qquad h_q(\theta_k,\phi_k,\beta)\partial\alpha\partial\beta \qquad (2.15)
\end{aligned}$$

where $\otimes$ is the convolution operator and $R_k(\tau)$ is the autocorrelation of signal k and is defined as

$$R_k(\tau) = E\left\{k^*(t)k(t+\tau)\right\} = E\left\{k^*(t-\tau)k(t)\right\} \qquad (2.16)$$

As a result, the entries of the covariance matrix are given by

$$\begin{aligned}
[\Phi_{k_{pq}}]_{mn} &= \left[R_k(\tau+(m-n)T_0)\otimes h_p^*(\theta_k,\phi_k,-\tau)\otimes h_q(\theta_k,\phi_k,\tau)\right]|_{\tau=0} \\
&= \mathcal{F}^{-1}\left\{S_k(\omega)H_p^*(\theta_k,\phi_k,f)H_q(\theta_k,\phi_k,f)\right\}|_{\tau=(m-n)T_0} \qquad (2.17)
\end{aligned}$$

where $S_k(\omega)$ is the power spectral density of the signal k and is defined as

$$S_k(\omega) = \mathcal{F}\left\{R_k(\tau)\right\} \qquad (2.18)$$

$\mathcal{F}$ and $\mathcal{F}^{-1}$ are the Fourier Transform and Inverse Fourier Transform operators, respectively. Furthermore, $H_p(\theta_k, \phi_k, f)$ and $H_q(\theta_k, \phi_k, f)$ denote the frequency response of antenna elements $p$ and $q$, respectively, for a given incident direction $(\theta_k, \phi_k)$. It is imperative the elements share a common phase center. Moreover, if one knows the power spectral density of the Signal Of Interest (SOI) and the antenna response over the bandwidth of the signal, one can analytically generate the individual covariance matrices $\Phi_d$ and $\Phi_i$. These covariance matrices are constructed for only a single signal; however, when multiple interference signals are incident upon the antenna array, the interference covariance matrix is the sum of the individual interference covariance matrices, again under the assumption they are mutually uncorrelated. The interference covariance matrix in the presence of K interfering signals is written as

$$\Phi_i = \sum_{k=1}^{K} \Phi_{i,k} \tag{2.19}$$

The thermal noise is assumed to have a flat power spectral density over the system bandwidth, which is determined by the bandwidth of the RF front end electronics. The thermal noise is assumed to be uncorrelated between channels and has a power spectral density of $N_0$, and the noise covariance matrix is given as

$$\Phi_n = \begin{bmatrix} [\Phi_{n_{11}}]_{N\text{x}N} & 0 & \cdots & 0 \\ 0 & [\Phi_{n_{22}}]_{N\text{x}N} & \ddots & \vdots \\ \vdots & \ddots & \ddots & 0 \\ 0 & \cdots & 0 & [\Phi_{k_{LL}}]_{N\text{x}N} \end{bmatrix} \tag{2.20}$$

where the submatrices, $[\Phi_{k_{pq}}]_{N\text{x}N}$ denotes the the $N$ x $N$ noise covariance matrix between elements $p$ and $q$ and is equal to zero for $p \neq q$. This yields a block diagonal matrix. Furthermore the noise covariance matrix is equal to a unitary matrix, when the tap spacing is equal to the inverse of the system bandwidth, and the noise becomes temporally uncorrelated; whereas, it is already spatially uncorrelated[12]. Again, the total covariance matrix is the sum of the individual noise and signal covariance matrices.

## 2.2 Space-Only Adaptive Processing

Space-only adaptive processing can be thought of as a special case of space-time adaptive processing where the number of taps is reduced from N to 1. By reducing the taps to 1, one sacrifices the ability to perform any nulling in the temporal domain and is only able to null signals relative to the spatial domain. It has been shown in [14] that space-only processing in the presence of CW signals is almost identical to space-time adaptive processing in the presence of wideband signals. This is related by the fact that STAP does not add anymore spatial degrees of freedom, but it does help in the nulling of wideband signals in the temporal domain. Space only processing in the presence of CW signals requires less a priori knowledge of various system parameters. The power spectral density, or signal structure, of various incident signals is no longer required over the signal bandwidth, and one only needs to know the power at the carrier frequency, since one is only concerned with CW signals. Also, one only needs to know the antenna response at the carrier frequencies of the SOI, and no longer over the entire bandwidth of the system. This result leads to a significant computation reduction in solving for the submatrices of the individual covariance matrices between two elements seen in equation 2.17. They are reduced from size $N$ x $N$ to a single scalar, and the size of the covariance matrix is reduced from $LN$ x $LN$ to $L$ x $L$, which is very useful.

## 2.3 STAP weights

The purpose of this section is to provide more insight into the development of the steady-state weights, $\mathbf{w}$, as well as, the two STAP algorithms used in conjunction with this study. The algorithms utilized in this study adapt the weights in order to minimize the output power under a single constraint. The output power is given in (2.6) where $\Phi$ is the total covariance matrix stated in (2.11). The output power is minimized under a single constraint [8],

$$\mathbf{u}^H \mathbf{w} = 1 \tag{2.21}$$

where $\mathbf{u}$ represents the constraint vector, and the the generalized weight solution can be calculated through a method of Lagrange Multipliers to minimize the total output power under the above constraint, and the weights can be written as

$$\mathbf{w} = \frac{\Phi^{-1}\mathbf{u}}{\mathbf{u}^H\Phi^{-1}\mathbf{u}} \tag{2.22}$$

The first algorithm studied is referred to as Simple Power Minimization, (also known as Null-Steering and Power Inversion), and it minimizes the output power through the constraint that the reference tap of the reference element is fixed to unity. It has been shown in [11] that an odd number of taps should be implemented, and for good performance the reference tap should be the center tap or $\lceil \frac{N}{2} \rceil$. This algorithm is often implemented due to its convenience. It does not require any *a priori* knowledge of antenna or the SOI. Simple power minimization should only be selected when the SOI is sufficiently weak (as is the case with GPS signals), because it suppresses all incident high powered signals indiscriminately . The weights are given by (2.22) where the constraint vector is given by

$$\mathbf{u} = [\mathbf{u}_1 \cdots \mathbf{u}_l]^T \tag{2.23}$$

The $l$th subvector is given by

$$\mathbf{u}_l = \begin{cases} [0, 0, \cdots, 1, \cdots, 0, 0], & \text{if} l = l_r \\ \mathbf{0}, & \text{if} l \neq l_r \end{cases} \tag{2.24}$$

where $l_r$ is the index of the reference element. A more detailed derivation for simple power minimization is given in [8].

The other algorithm used in this study is referred to as Beam Forming / Null Steering (also known as Simple Beam Steering). It constrains the array to steer a beam (enhance the gain) in the direction of SOI while the remaining degrees of freedom are used to minimize the total output power. This method requires *a priori* knowledge of the look direction of the SOI as well as the antenna response in that direction. The weights are given in (2.22) and the constraint vector is of the same form as (2.23). The $l$th subvector is given by

$$\mathbf{u}_l = [0, 0, \cdots, u_l^*, \cdots, 0, 0] \tag{2.25}$$

where $u_l^*$ is located at the reference tap and corresponds to the complex conjugate of the voltage induced by the SOI at the $l$th element.

## 2.4 Performance Metrics

In this study, two performance metrics are used to evaluate the performance of the space-time adaptive array. The metrics are based upon the received signal powers and are used to determine whether the SOI will be detectable in the receiver. The first metric used is output Signal-to-Interference plus Noise ratio (SINR), and this output power ratio can be solved for analytically using the steady state adapted weights and the individual covariance matrices. Recall that the total output power given in (2.6), where the total covariance matrix (Equation 2.11) can be separated into a sum of individual covariance matrices assuming the signals are mutually uncorrelated, and one can write the individual output powers as

$$P_d = \frac{1}{2}\mathbf{w}^H \Phi_d \mathbf{w} \tag{2.26}$$

$$P_i = \frac{1}{2}\mathbf{w}^H \Phi_i \mathbf{w} \tag{2.27}$$

$$P_n = \frac{1}{2}\mathbf{w}^H \Phi_n \mathbf{w} \tag{2.28}$$

where $P_d$, $P_i$, and $P_n$ are the output powers of the desired, interference, and noise signals, respectively. The SINR is then defined as

$$SINR = \frac{P_d}{P_i + P_n} \tag{2.29}$$

Furthermore, it is more common to measure SINR in terms of decibels (dB) and is given as

$$SINR_{dB} = 10 \log_{10} \frac{P_d}{P_i + P_n} \tag{2.30}$$

For the remainder of this thesis, output SINR is referred to in its dB form.

The the other metric is Available Angular Region. It is defined as the available region over the entire upper hemisphere for which the output SINR exceeds a selected threshold. These two metrics will be used to evaluate the performance of the various antenna arrays examined in this study.

## 2.5 Simulation and Signal Scenario

The incident signal scenario consists of a single desired signal and multiple interfering signals. The noise signal is Additive White Gaussian Noise (AWGN) assumed uncorrelated between channels and equal to 0 dB. The desired signal has a Signal-to-Noise Ratio (SNR) of -30 dB at an isotropic element and its Angle of Arrival (AoA) is varied to sweep the entire upper hemisphere. Each interfering signal has an Interference-to-Noise Ratio (INR) equal to 50 dB at an isotropic element and its AoA is limited to the angular region of $-10^\circ$ to $20^\circ$ elevation and at least $15^\circ$ separation in azimuth. Moreover, twenty-five independent trials are carried out for a given number of interfering signals, where their directions are varied randomly from one trial to the next. All signal incident upon the antenna array are assumed to be uncorrelated with each other as well as the thermal noise. The incident signals are assumed to be in the L1 (1575.42 MHz) and L2 (1227.6 MHz) GPS bands.

In this study, the Antenna Electronics (AE) is based on Space-Only Processing and all incident signals are assumed to be narrow band (CW) signals. As stated above and in [14], the performance of space-only processing in the presence of CW signals is similar to the performance of multi-tap space-time adaptive processing in the presence of wide band signals. Therefore, the results and conclusions of this study are applicable to STAP based AE. This result yields a two-fold advantage in the reduction of computation time to evaluate the antenna array performance. First, the response of the individual antenna elements only needs to be analyzed at the L1 and L2 carrier frequencies instead of the entire the GPS frequency bands. Also, the reduction from N taps to a single tap yields a significant reduction in the computation time involved in the signal processing of the data to evaluate performance. As a result, this reduction enables the study of more antenna configurations. Rigorous electromagnetic modeling is carried out to include the mutual coupling and structure effects of the antenna arrays. A numerical electromagnetic (EM) code, FEKO [15], is used to calculate the *in situ* volumetric patterns of each individual antenna element at the L1 and L2 band carrier frequencies.

## 2.6 Individual Antenna Element

This study utilizes actual antenna elements to evaluate the performance of the antenna arrays. The selected element is a dual-band stacked microstrip patch antenna designed with input impedance and radiation characteristics at L1 and L2 frequency bands. Proper design of stacked patch antennas can be achieved by feeding the lower patch with the upper patch being parasitic, or by feeding the upper patch with the lower patch being parasitic, as is the case for the element in this study. Figure 2.2 shows the antenna configuration. The dielectric layers are of the same permittivity with a dielectric constant equal to 9.2. However, the thicknesses of the two layers are different. The upper layer's thickness is equal to 2.54 mm, and the lower layer's thickness is equal to 7.62 mm. It is noted that the substrate used with these thickness parameters is readily available from Rogers Corporation (Microwave Materials Division, Chandler, AZ), and will not have to be a specialized fabrication. The complete antenna dimensions are equal to 1.75" x 1.75" x 0.4 ". In order to realistically evaluate the non-planar antenna array performance the antenna element must be analyzed *in situ* using a finite dielectric substrate and a finite ground plane shown. The analysis and optimization for a single isolated element is carried out using the EM software FEKO. The geometry considered for this simulation is shown in Figure 2.3. The calculated return loss and right-hand circularly polarized radiation patterns are displayed in Figures 2.4 and 2.5, respectively. The peak gains are 7 dB and 5 dB and the gains at 80° are approximately -3 dB and -5 dB for at the L2 and L1 carrier frequencies respectively. Notice that a small asymmetry is observed in the radiation patterns; however, it can be eliminated by a symmetric feed.

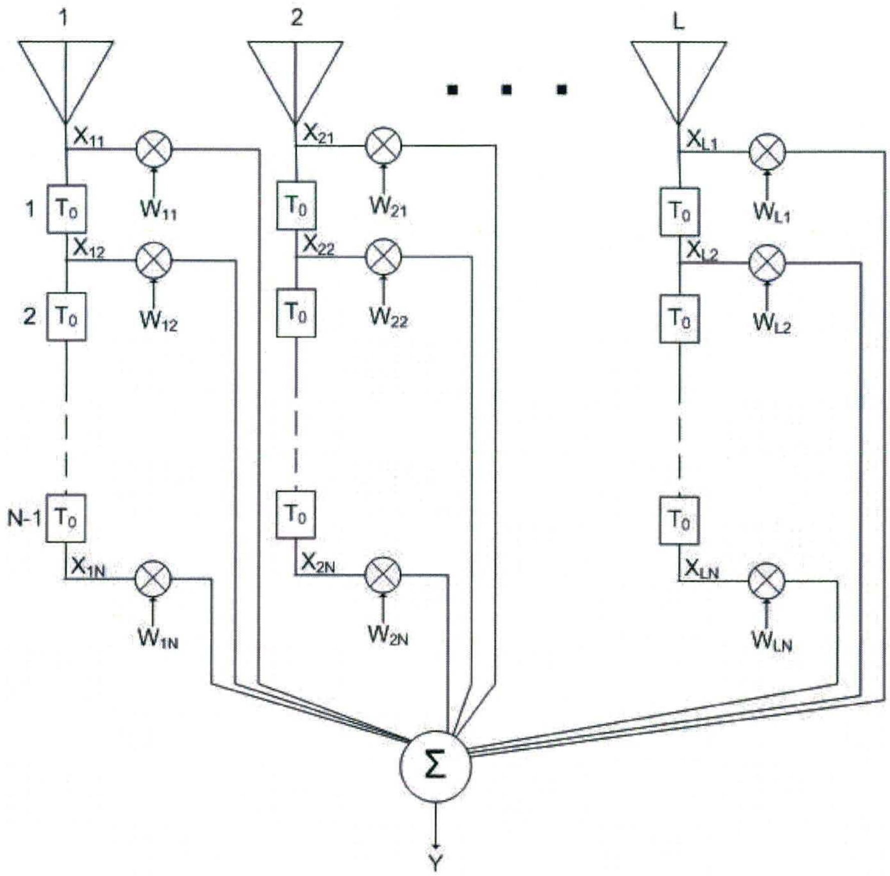


Figure 2.1: The space-time adaptive filter model.

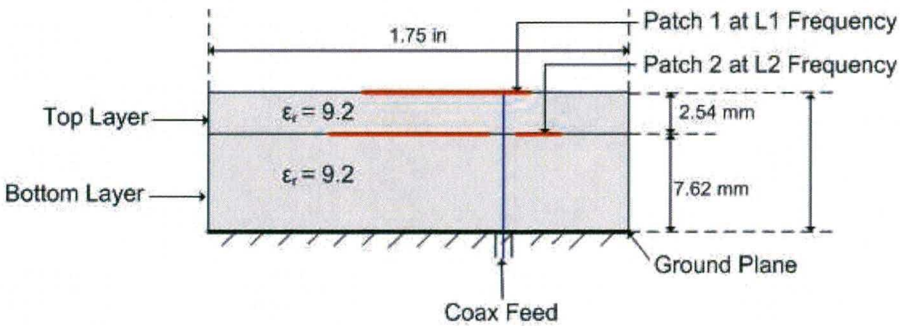


Figure 2.2: Stacked Microstrip Antenna.

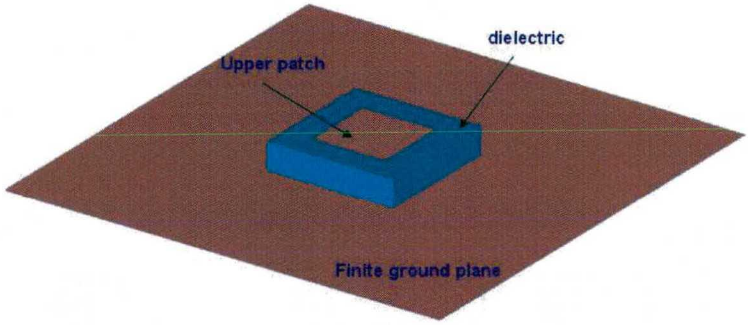


Figure 2.3: Stacked Microstrip antenna (lower patch hidden in dielectric) with finite dielectric and ground plane.

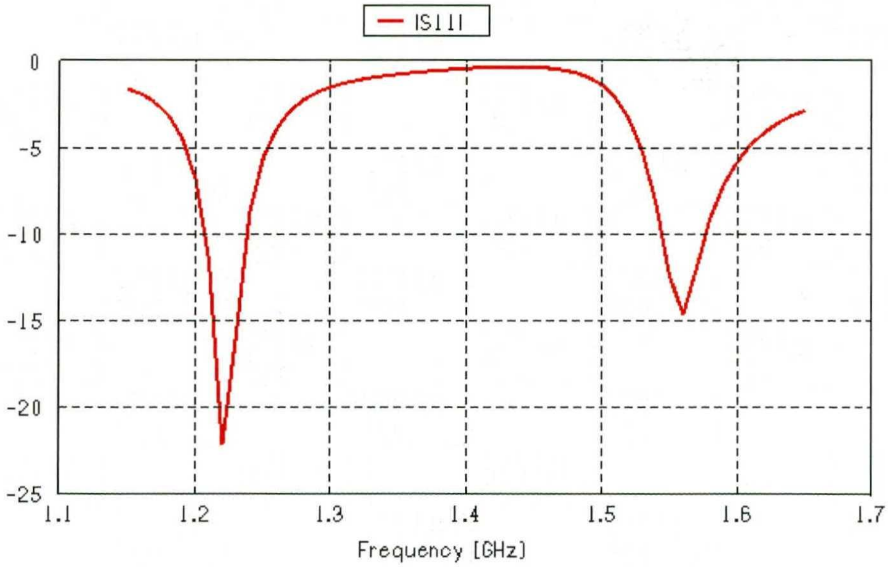


Figure 2.4: Return Loss of the antenna element on finite dielectric.

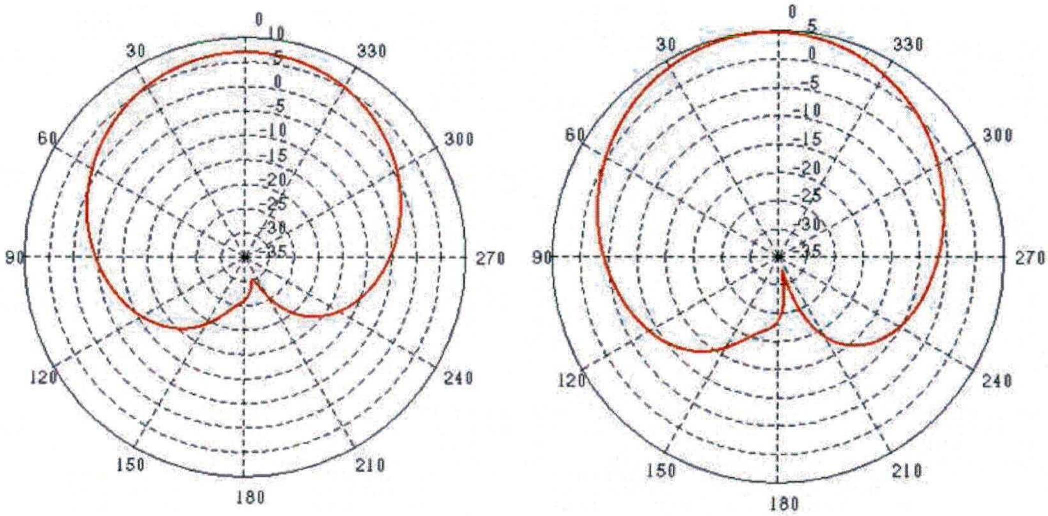


(a) 1.23 GHz

(b) 1.575 GHz

Figure 2.5: Circularly Polarized Radiation Patterns of the antenna element at 1.23 GHz (a) and 1.575 GHz (b).

# CHAPTER 3

# SURFACE SELECTION

The main purpose of this chapter is to establish the type of surface geometry the antenna array will be conformed to in order to yield improved performance. The conclusions and results presented in this chapter are similar to the one reported in a previous research effort [3], and are given here for completeness. Three different types of surface geometries are included in this study: planar, non-planar convex, and non-planar concave. All antenna arrays have similar projected area (looking from the top). The performance of the three surface geometries will be evaluated using an array of seven and ten elements in the presence of various low elevation interfering signals for both the L1 and L2 bands. All incident signals (desired as well as interference) are assumed to be CW signals and the AE is based on space-only processing. The two versions of AE being used are simple power minimization and beam forming / null steering, and the performance metrics used to evaluate performance are output SINR and available angular region. The results of this chapter will conclude that the non-planar convex surface yields significantly better performance than planar as well as non-planar concave antenna arrays. Moreover, the non-planar concave antenna arrays exhibit worse performance than planar arrays.

## 3.1 Antenna Arrays

The performance of six antenna arrays is studied in this chapter. The surface geometry of the non-planar antenna arrays is a three inch high surface for the convex surface and three inch deep surface for the concave surface both with curvature relative to a sphere of radius 7.5 inches. The measuring reference point of the non-planar arrays is the circular aperture of the planar array. The convex surface extends upwards and will be referred to as a X inch high geometry, and the concave surface extends downwards and will be referred to as a X inch deep geometry, where X is the number of inches the geometry is extended relative to the planar surface. The first set of three antenna arrays have seven elements; whereas, the second set contains ten elements. Antenna array A1 (Figure 3.1) is a planar array consisting of seven elements, with one element placed in the center and the remaining elements distributed uniformly on the periphery. Antenna array A2 (Figure 3.2) is a non-planar convex array with seven elements, with one element placed at the top of the surface, and the remaining elements distributed uniformly around the bottom of the hemisphere. Antenna array A3 (Figure 3.3) is a non-planar concave array with seven elements, with one element placed at the bottom of the surface, and the remaining elements distributed uniformly around the top of the surface. The remaining three antenna arrays utilize the same three surface geometries, but now have ten elements. All three antenna arrays exhibit similar element distribution as the reference element is distributed in the center of the array, three elements located along an inner ring, and the remaining six elements distributed along an the periphery of the surface. Antenna array A4 (Figure 3.4) is a planar array, A5 (Figure 3.5) is a non planar convex array, and A6 (Figure 3.6) is a non-planar concave array.

## 3.2 Performance Results

### 3.2.1 Output SINR

First, it is important to examine the performance of the various antenna arrays in an interference-free environment to set a general baseline as performance will degrade with the presence of interfering signals. Figures 3.7 and 3.8 show the output SINR (dB) in the absence of all interfering signals for the L1 and L2 bands, respectively. Note, in this case, SINR is equal to SNR as there are no interfering signals; however, we will still use the term SINR. The antenna electronics is operating in simple power minimization mode. In the figure, the output SINR over the entire upper hemisphere is plotted. In each plot, the center of the circle corresponds to zenith and the outer ring corresponds to horizon. The radial direction represents elevation and phi represents azimuth. Note that antenna arrays A2 and A5 have the largest area of coverage where the SINR is greater than -30 dB in the upper hemisphere for both the L1 and L2 bands. Also, the planar antenna arrays (A1 and A4) perform better than the non-planar concave antenna arrays (A3 and A6). It is important to note that the performance of the antenna arrays degrades with the addition of more elements. The reason for this behavior is strong mutual coupling between individual antenna elements and ,also, shadowing of individual antenna elements in the case of the concave non-planar antenna arrays. When the AE is operating in simple power minimization mode the overall antenna array response in the absence of interference is equal to the response of the reference element which is the only element that remains on. Therefore, if one causes significant degradation to the response of the reference element due to mutual coupling, one will cause significant degradation to the overall antenna array response.

Figures 3.9 and 3.10 show the output SINR for the L1 and L2 bands while the antenna electronics is operating in beam / forming null steering mode. All other parameters are the same as in Figures 3.7 and 3.8. One observes that the entire upper hemisphere has output SINR performance greater than -30 dB SINR with antenna arrays A2 and A5 exhibiting the best performance. Again, the concave non-planar antenna arrays do not perform as well as the planar antenna arrays. Also, it is important to note that increasing the number of elements leads to increased performance for all the antenna array surfaces when the AE is operating in beam forming / null steering mode. One notices that beam forming / null steering yields significantly better performance over simple power minimization when comparing Figures 3.7 and 3.8 with Figures 3.9 and 3.10.

Figures 3.11 and 3.12 shows the output SINR of the six antenna arrays in a signal scenario consisting of four incident interfering signals for the L1 and L2 bands, respectively. The AE is operating in simple power minimization mode. The angle of arrival of the four interfering signals is marked by a white 'o' with a red 'x' in the various plots. Notice that the output SINR in the angular region in proximity of an interfering signal is quite low, as expected. Furthermore, the output SINR improves as the desired signal moves away from the interfering signal. Again, note that the antenna arrays A2 and A5 have the best performance. Moreover, one observes the limited resolution of the elevation plane for the planar and concave non-planar antenna arrays. This is seen by the fact that the nulls along the interfering signal directions extend significantly in the elevation plane. Again, the concave non-planar antenna arrays yield the worst performance.

Figures 3.13 and 3.14 shows the output SINR while the AE is operating in beam forming / null steering mode for the L1 and L2 bands, respectively. All other parameters are the same as Figures 3.11 and 3.12. Again, the same characteristics are observed in that the output SINR within the vicinity of the interfering signals is dismal, and it increases as one moves away from interfering signal. Antenna arrays A2 and A5 yield the best performance, with A5 having significantly better performance than A2. Also, with respect to the planar and convex non-planar antenna arrays, one observes that the addition of antenna elements allows the array to place more concise nulls along the interfering signal direction leading to an increase in performance. However, in the case of the concave non-planar geometry there is not much performance difference and they are not performing as well as the other antenna arrays. Also, when comparing Figures 3.13 and 3.14 with Figures 3.11 and 3.12, one sees that beam forming / null steering has a significant performance advantage.

### 3.2.2 Available Angular Region

Due to the fact that one will not know the direction of the incident interference signals, it is better to evaluate the anti-jam (AJ) performance of the antenna arrays using Monte Carlo simulations and examining the mean value. As a result, the average available angular region will be the performance metric of choice. The available angular region is defined as the portion of the upper hemisphere over which the output SINR exceeds a selected value. The data is obtained by averaging over twenty-five independent trials, where the interference angle of arrival directions are varied randomly from one trial to the next.

### Seven Element Antenna Arrays

Figures 3.15 and 3.16 show the available angular region in the upper hemisphere for the three seven element antenna arrays in the presence of one to six interfering signals for the L1 and L2 bands, respectively. The antenna electronics is operating in the simple power minimization mode. It is important to note that one needs N+1 antenna elements to null N jammers, and that AJ performance degrades with an increase in the number of jammers. Again, the results conclude that antenna array A2 performs better than antenna arrays A1 and A3. For the L1 band, as the number of interfering signals increases to six, antenna arrays A1 and A3 are performing dramatically worse as compared to antenna array A2. In the case of the L2 band, antenna array A2 still performs significantly better; however, the performance improvement is not as much as in the L1 band. Antenna array A3 exhibits poor performance in both bands.

Figures 3.17 and 3.18 display the available angular region for the L1 and L2 bands, respectively, while the antenna electronics is operating in the beam forming / null steering mode. All other parameters are the same as in Figures 3.15 and 3.16. As expected, convex non-planar antenna array A2 has significantly better performance than A1 and A3. The beam forming / null steering algorithm yields better performance than simple power minimization algorithm, and array A3 does not perform as well.

### Ten Element Antenna Arrays

Figures 3.19 and 3.20 show the available angular region in the upper hemisphere for the three ten element antenna arrays for the L1 and L2 bands, respectively, in the presence of four to nine interfering signals. Everything else is the same as Figures 3.15 and 3.16. The same exact conclusions drawn above also hold true here and it comes as no surprise that antenna array A5 has far better performance than the other antenna arrays with the concave non-planar array yielding the worst performance in both the L1 and L2 bands.

Figures 3.21 and 3.22 show the available angular region for the ten element arrays for the L1 and L2 bands, respectively, in the presence of four to nine interfering signals. The antenna electronics is operating in beam forming / null steering mode.

As expected, the convex non-planar antenna geometry (antenna array A5) performs the best, followed by the planar geometry (antenna array A4), and then the concave non-planar geometry (antenna array A6). Moreover, it is shown that beam forming / null steering yields significant performance improvement as compared to simple power minimization mode. Furthermore, comparing these figures with the seven element arrays in Figures 3.17 and 3.18, and comparing performance in the presence of the same number of jammers, one observes that the addition of more antenna elements leads to an increase in AJ performance.

As a matter of fact, it is seen for both adaptive algorithms that increasing the number of elements from seven to ten elements for the convex non-planar geometry leads to an improvement in AJ performance. This holds true for both the L1 and L2 bands. The performance improvement is more significant for beam forming / null steering. This observation can be made in Tables 3.1 through 3.4 which shows the percentage available angular region when the output SINR is -35 dB or more in the presence of zero to nine interfering signals for all six antenna arrays. Tables 3.1 and 3.2 display results while the AE is operating in simple power minimization mode, and Tables 3.3 and 3.4 yield results for the beam forming / null steering algorithm. In Table 3.1, one observes that antenna array A2 is performing better than antenna arrays A1 and A3, and antenna array A5 is performing better than antenna arrays A4 and A6. Also, it is seen that performance degrades with the presence of more interfering signals and one requires N+1 antenna elements to null N interfering signals. The seven element antenna arrays have (near) zero coverage of the upper hemisphere in the presence of seven or more interfering signals. The addition of elements allows one the capability to null more interfering signals and leads to a performance improvement of all three antenna arrays leads in the L1 band. For the L2 frequency band (Table 3.2), it is seen that the non-planar convex antenna arrays (A2 and A5) have better performance than the planar antenna arrays (A1 and A4) and the concave non-planar antenna arrays (A3 and A6). The addition of antenna elements results in a performance increase for the convex non-planar antenna array; however, this is not true for the planar and concave non-planar antenna array geometries. An increase in the number of elements results in a larger amount of mutual coupling between the reference element and auxiliary elements causing poorer performance when the antenna electronics is operating in simple power minimization mode. Comparing performance of the L1 (Table 3.1) and L2 (Table 3.2) frequency bands, one notices that the convex non-planar antenna arrays have better performance in the L1 band than in the L2 band. The reason for the performance difference is due to the antenna aperture being electrically larger in the L1 band. In Tables 3.3 (L1 band) and 3.3 (L2 band), one observes similar performance characteristics. The performance degrades for a more harsh interfering signal environment, and one requires N+1 antenna elements to null N interfering signals. Antenna array A2 is performing better than antenna arrays A1 and A3, and antenna array A5 exhibits better performance than antenna arrays A4 and A6. Also, one observes that an increase in the number of elements leads to performance improvement for all three antenna arrays for both the L1 and L2 bands. Furthermore, comparing Tables 3.1 and 3.2 with Tables 3.3 and 3.4, one observes a significant performance increase when the AE is operating in the beam forming / null steering mode over the simple power minimization mode.

## 3.3 Chapter Summary

In this chapter, the AJ performance of some planar and non-planar antenna arrays at GPS frequencies was discussed. All antenna apertures contained similar projected area (looking from the top). It was shown that convex non-planar antenna arrays have significantly better performance than the planar antenna arrays. Also, concave non-planar antenna arrays do not perform as well. Furthermore, one can add more elements to convex non-planar antenna arrays to enhance performance and provide the capability to null more interfering signals. This is true for simple power minimization adaptive antennas as well as beam forming / null steering adaptive antennas in both the L1 and L2 bands. It is shown that there is a significant performance advantage for the AE to be operating in the beam forming / null steering mode. Therefore, the best performance is exhibited by a convex non-planar surface geometry with a larger amount of antenna elements and the AE is operating in beam forming / null steering mode. The amount of curvature of the convex non-planar surface is investigated next in Chapter 4 for a seven and ten element antenna array. It will be shown that there is a performance advantage for a convex non-planar surface with a larger amount of curvature.

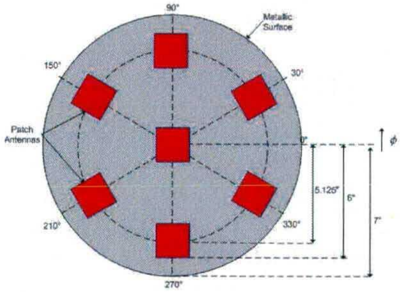


(a) Top Down View

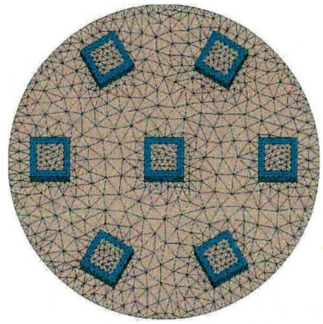

(b) Gridded Surface

Figure 3.1: Antenna Array A1.

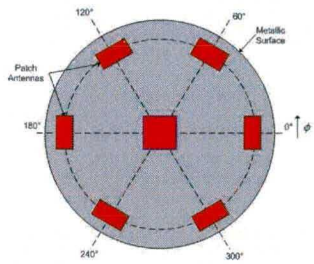


(a) Top Down View

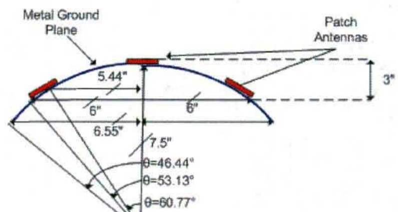


(b) Side View

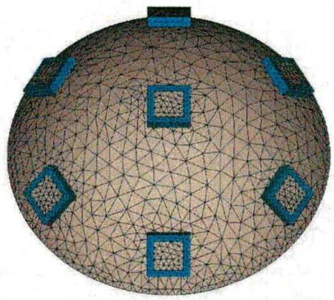

(c) Gridded Surface

Figure 3.2: Antenna Array A2.

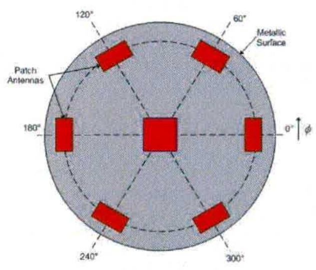


(a) Top Down View

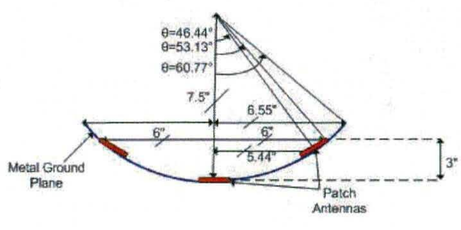


(b) Side View

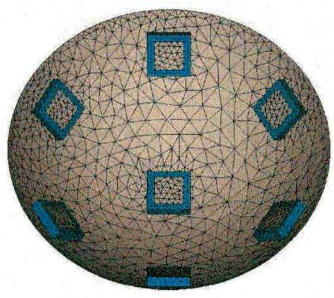

(c) Gridded Surface

Figure 3.3: Antenna Array A3.

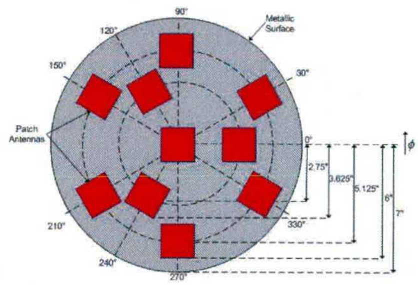


(a) Top Down View

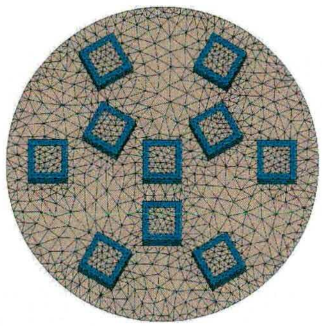

(b) Gridded Surface

Figure 3.4: Antenna Array A4.

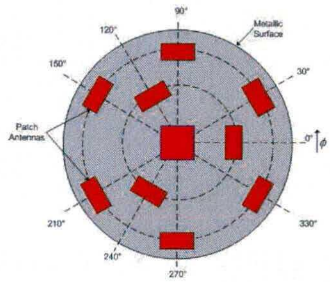


(a) Top Down View

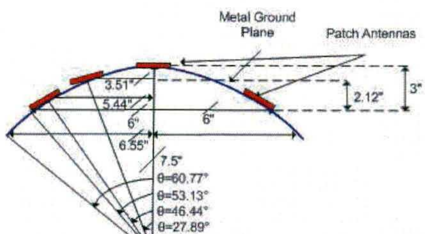


(b) Side View

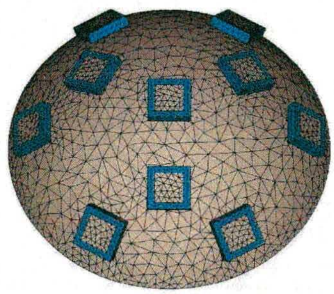

(c) Gridded Surface

Figure 3.5: Antenna Array A5.

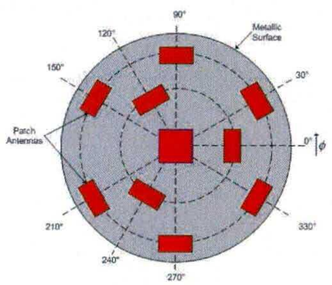


(a) Top Down View

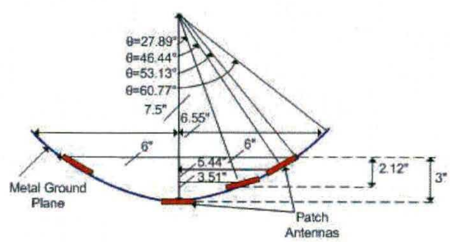


(b) Side View

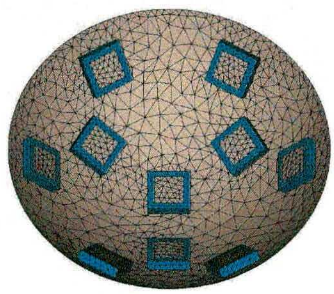

(c) Gridded Surface

Figure 3.6: Antenna Array A6.

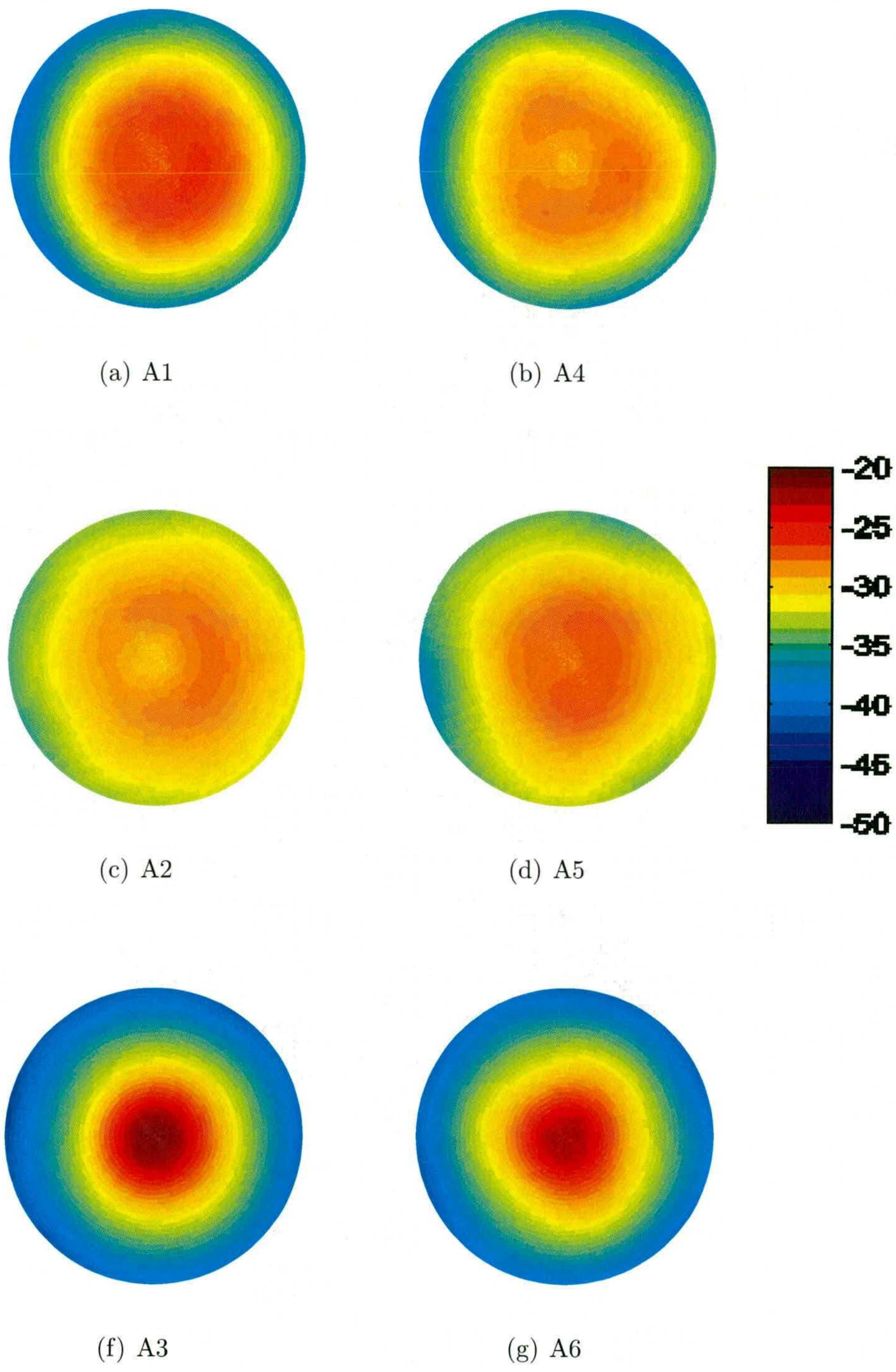


Figure 3.7: Output SINR (dB) of the six antenna arrays in the absence of interference. AE is operating in simple power minimization mode. L1 frequency band.

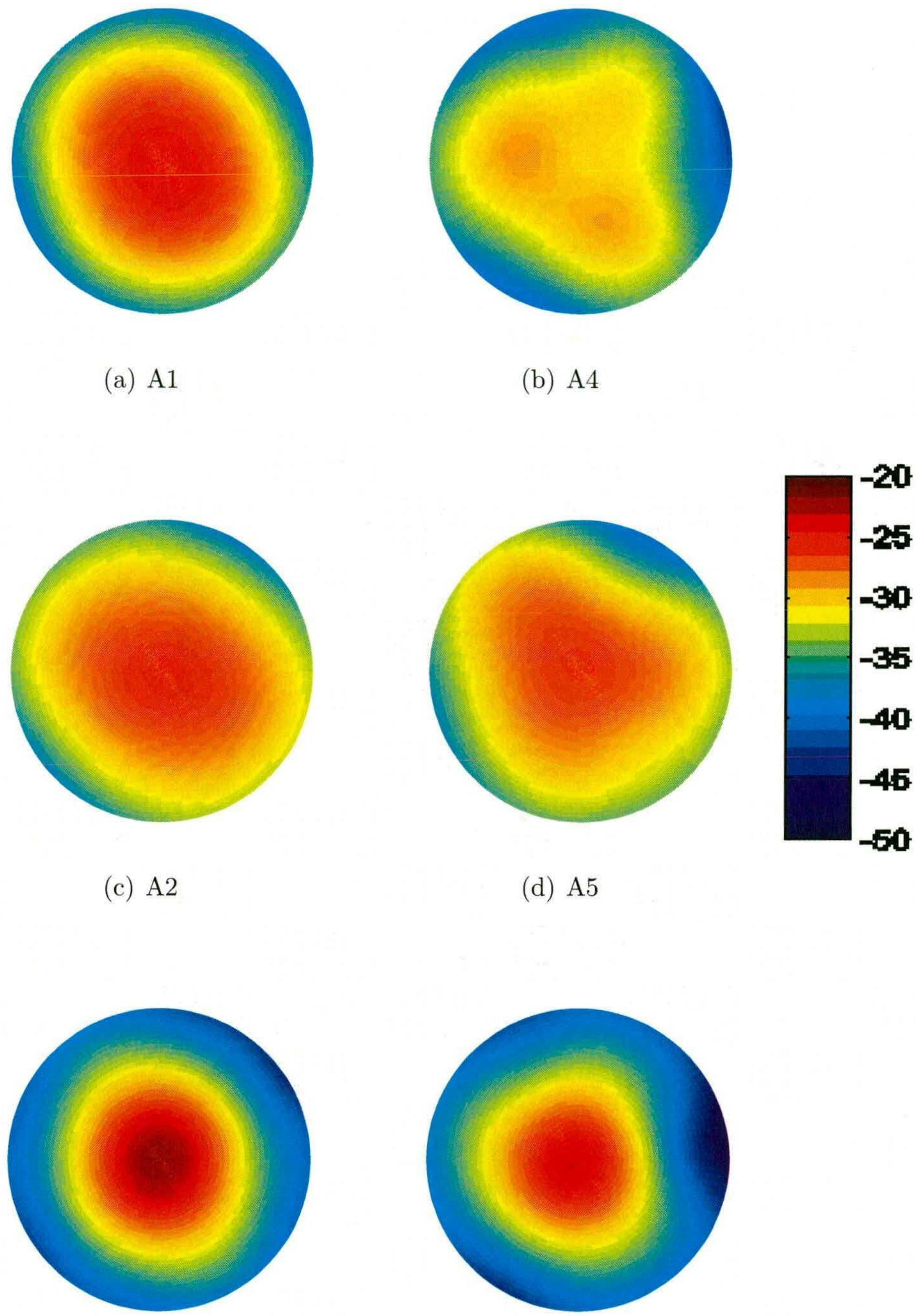


(a) A1 (b) A4

(c) A2 (d) A5

(f) A3 (g) A6

Figure 3.8: Output SINR (dB) of the six antenna arrays in the absence of interference. AE is operating in simple power minimization mode. L2 frequency band.

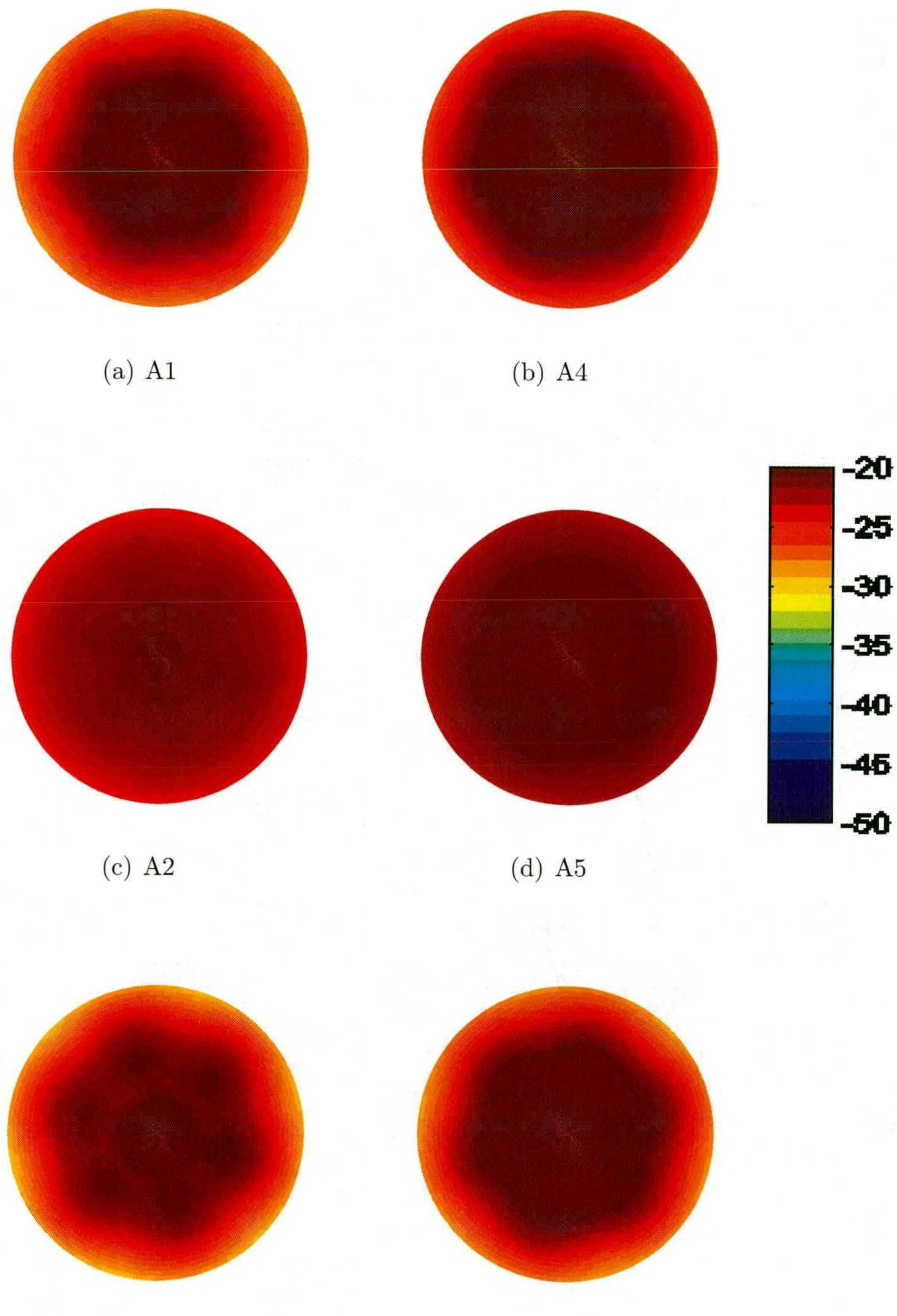


(a) A1 (b) A4

(c) A2 (d) A5

(f) A3 (g) A6

Figure 3.9: Output SINR (dB) of the six antenna arrays in the absence of interference. AE is operating in beam forming / null steering mode. L1 frequency band.

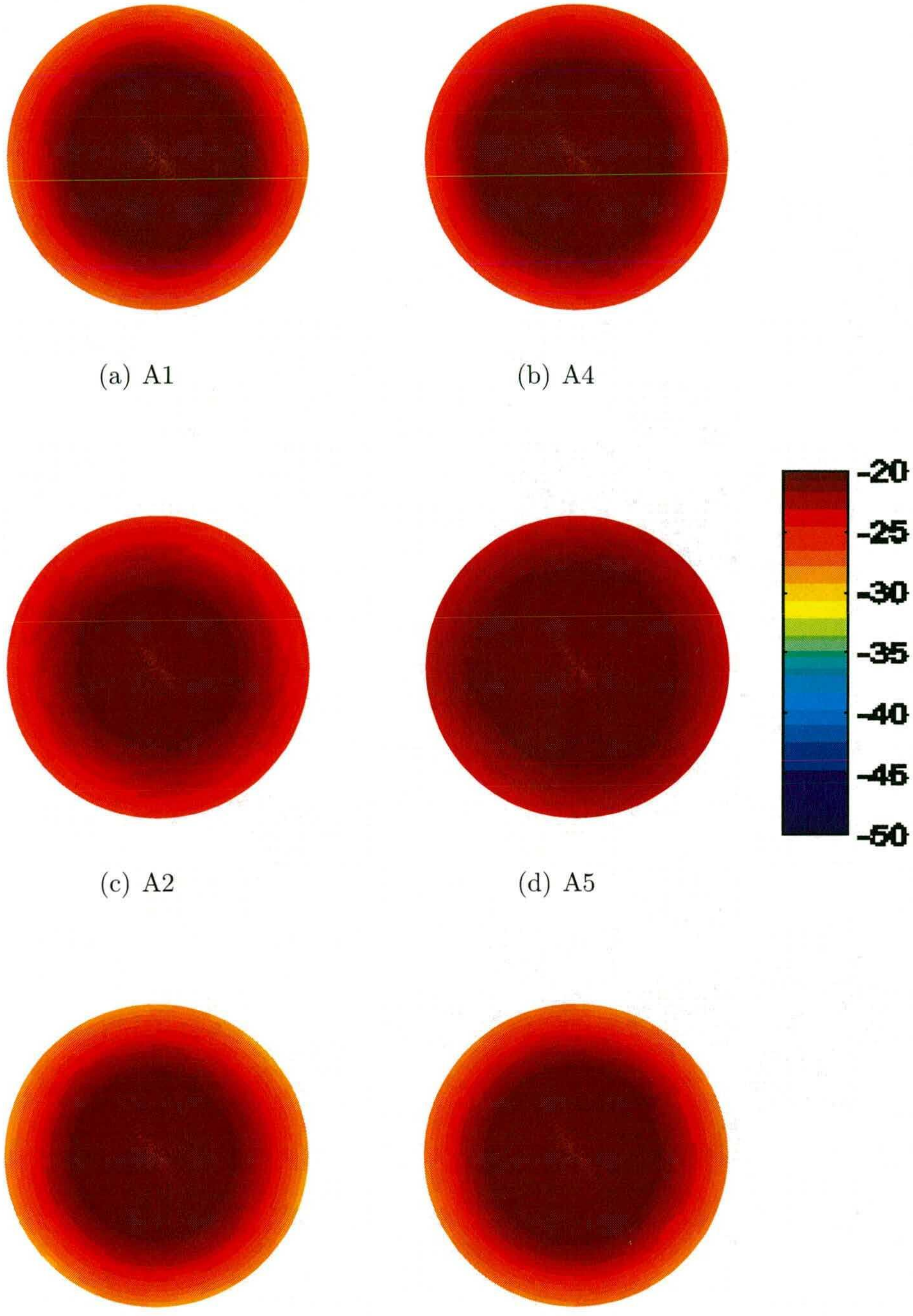


(a) A1 (b) A4

(c) A2 (d) A5

(f) A3 (g) A6

Figure 3.10: Output SINR (dB) of the six antenna arrays in the presence of four interfering signals. AE is operating in beam forming / null steering mode. L2 frequency band.

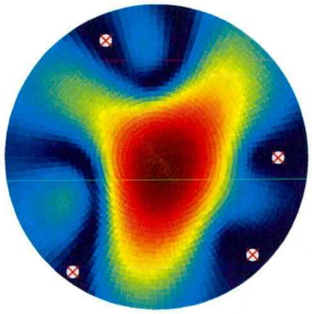

(a) A1

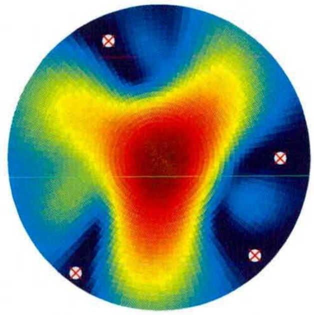

(b) A4

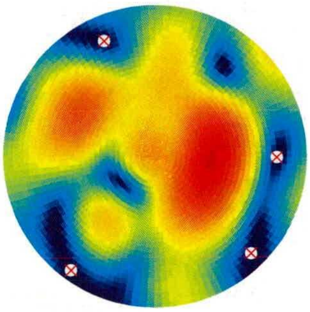

(c) A2

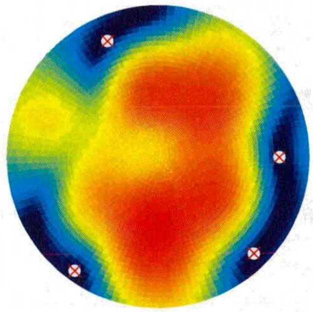

(d) A5

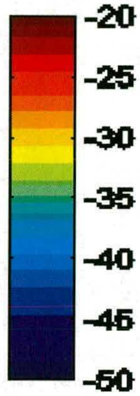


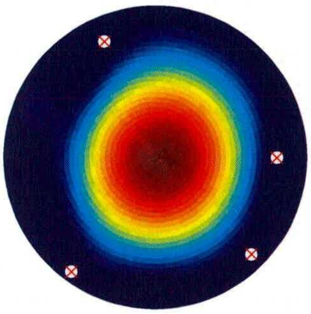

(f) A3

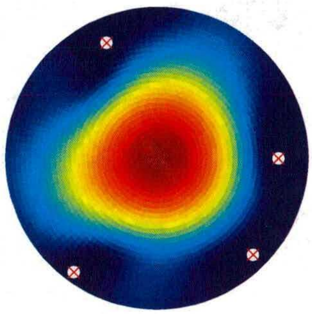

(g) A6

Figure 3.11: Output SINR (dB) of the six antenna arrays in the presence of four interfering signals. AE is operating in simple power minimization mode. L1 frequency band.

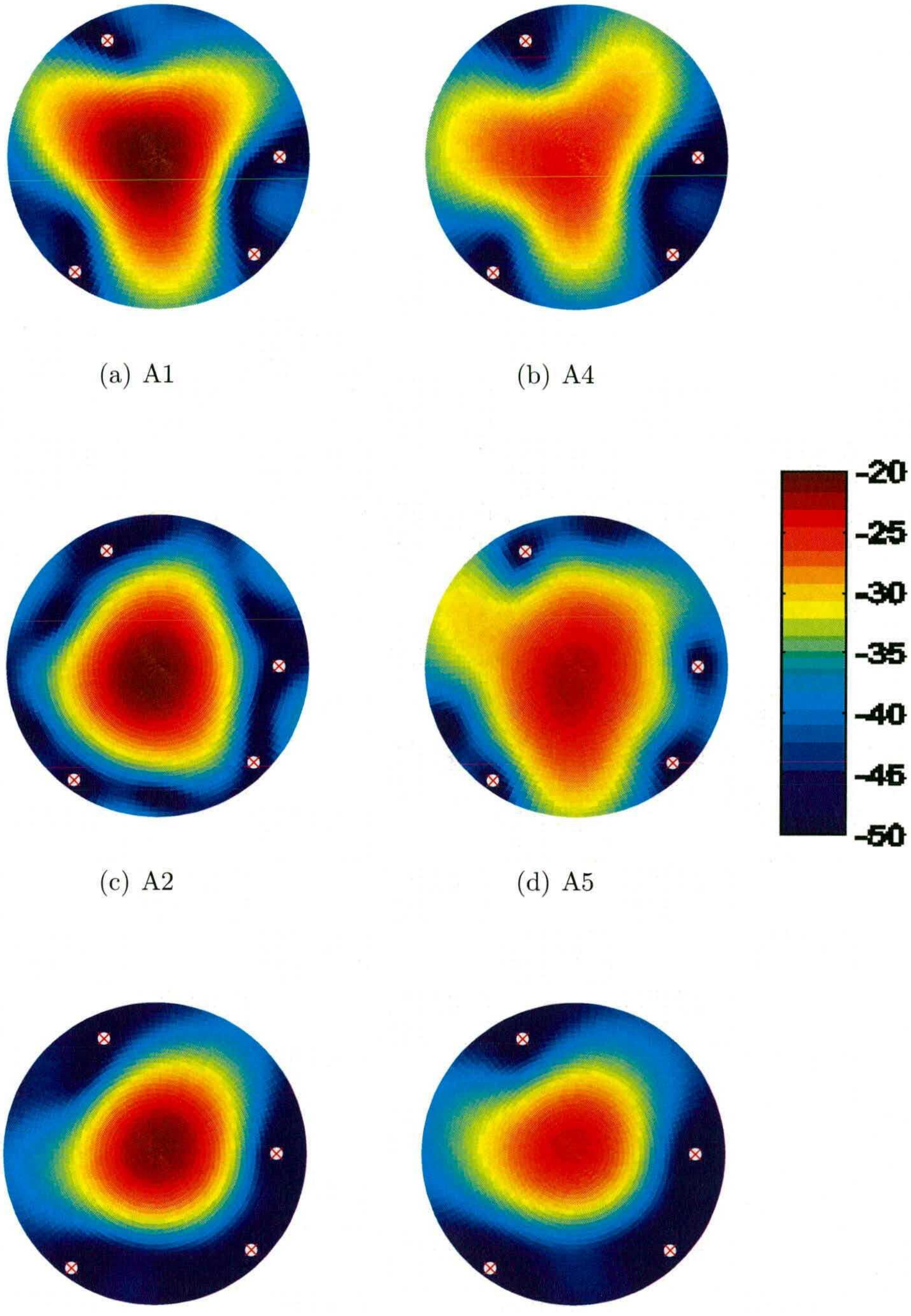


(a) A1 (b) A4

(c) A2 (d) A5

(f) A3 (g) A6

Figure 3.12: Output SINR (dB) of the six antenna arrays in the presence of four interfering signals. AE is operating in simple power minimization mode. L2 frequency band.

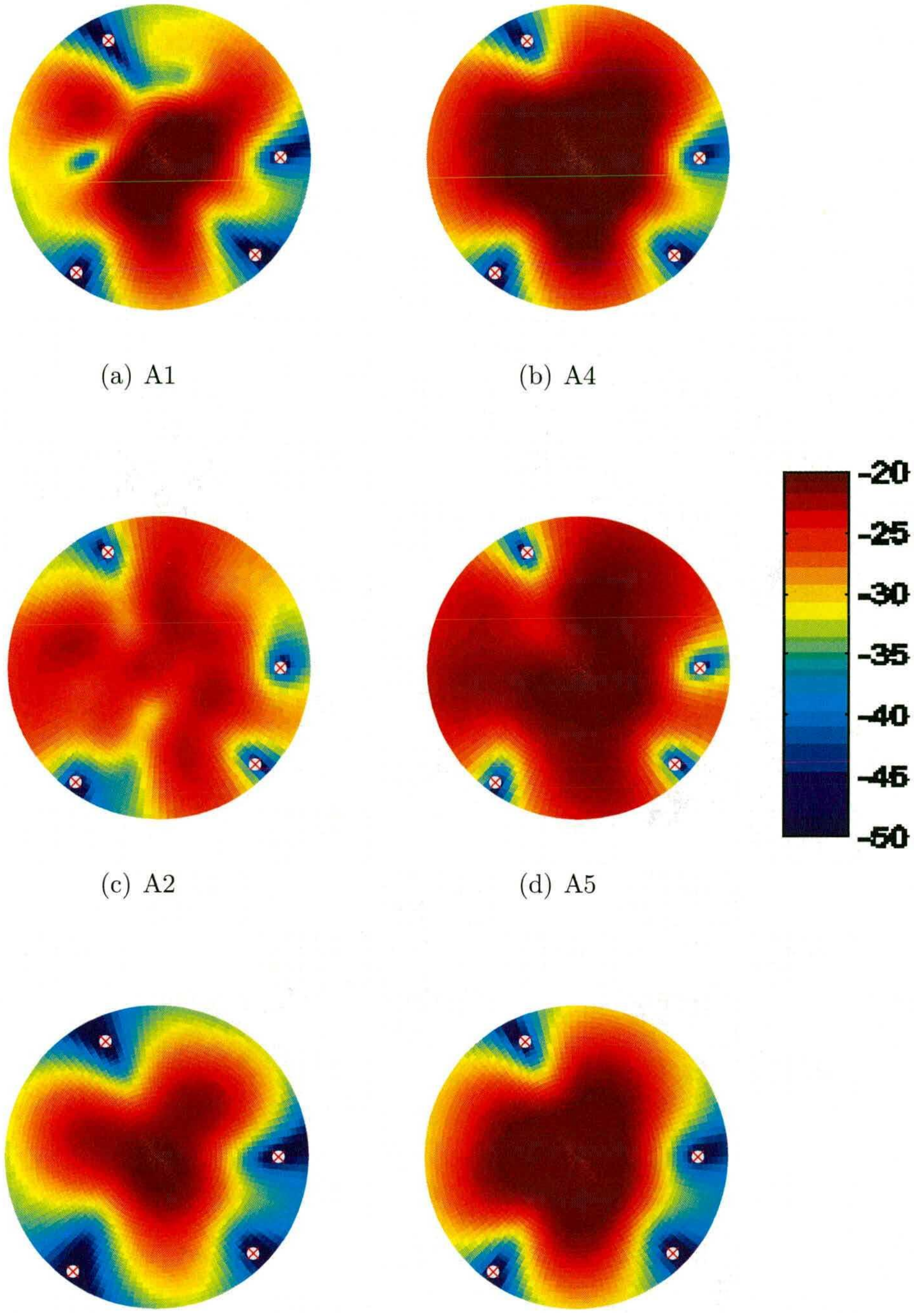


(a) A1 (b) A4

(c) A2 (d) A5

(f) A3 (g) A6

Figure 3.13: Output SINR (dB) of the six antenna arrays in the presence of four interfering signals. AE is operating in beam forming / null steering mode. L1 frequency band.

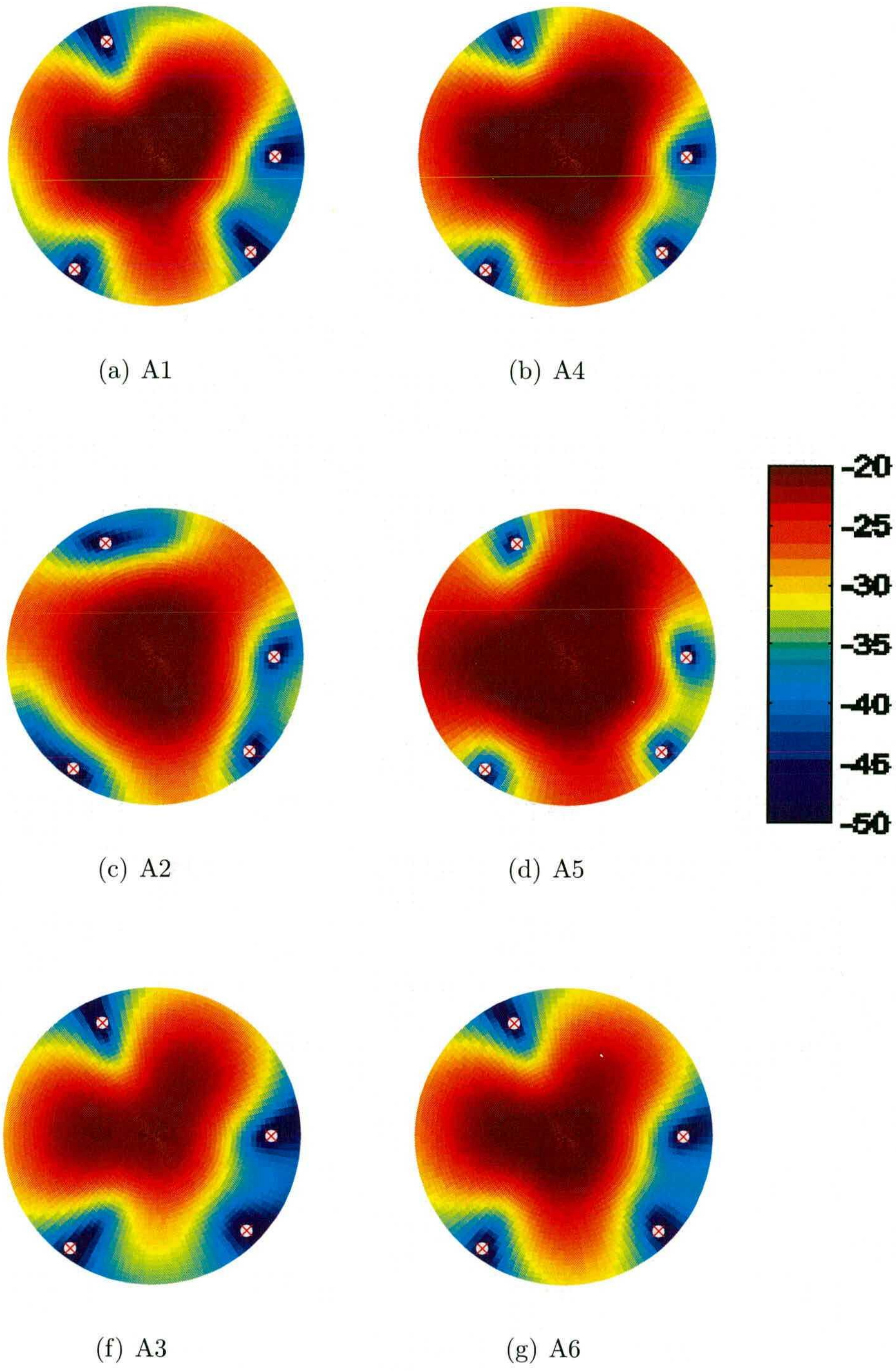


(a) A1

(b) A4

(c) A2

(d) A5

(f) A3

(g) A6

Figure 3.14: Output SINR (dB) of the six antenna arrays in the presence of four interfering signals. AE is operating in beam forming / null steering mode. L2 frequency band.

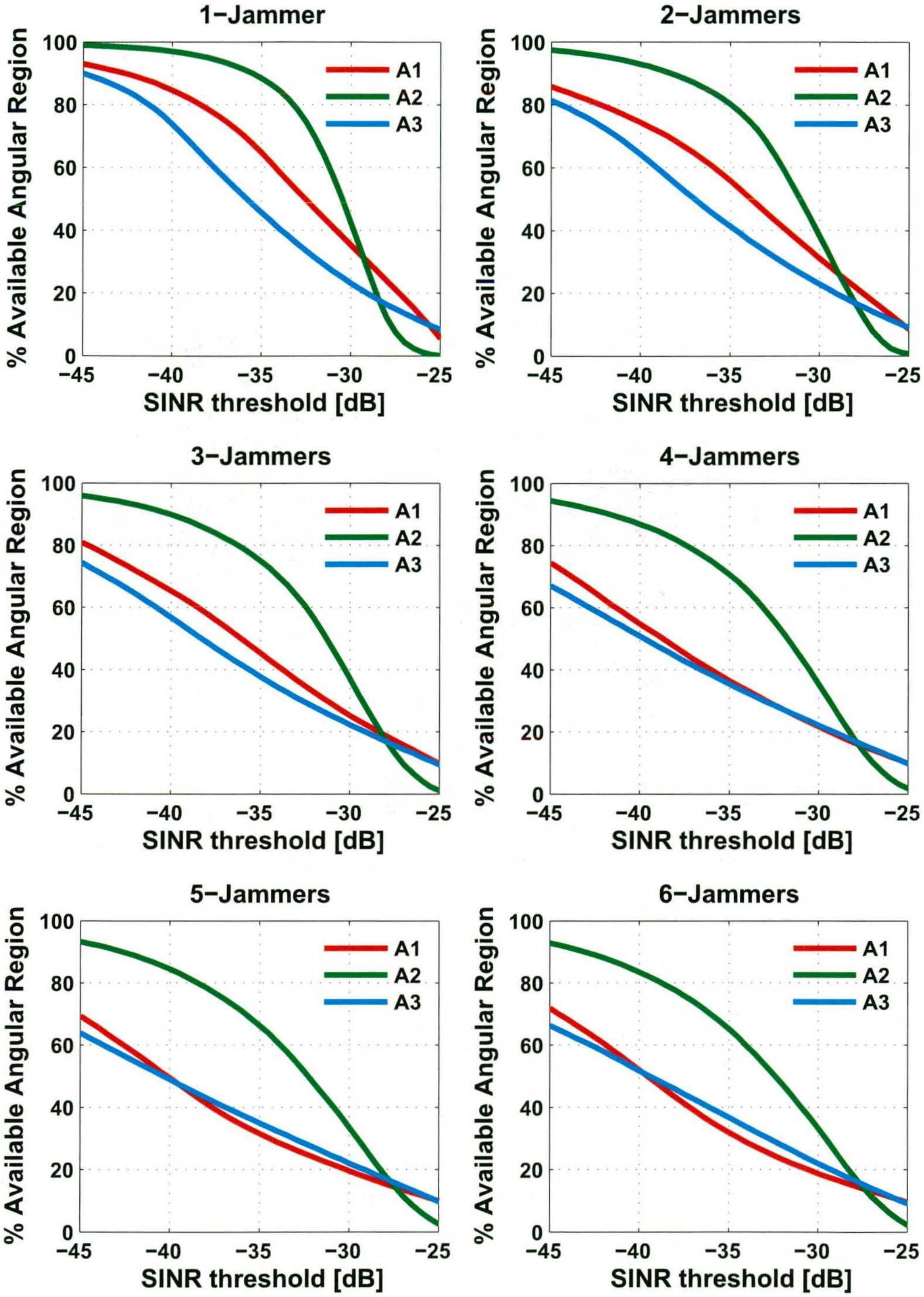


Figure 3.15: Performance of seven element antenna arrays in the presence of one to six interfering signals. AE is operating in simple power minimization mode. L1 frequency band.

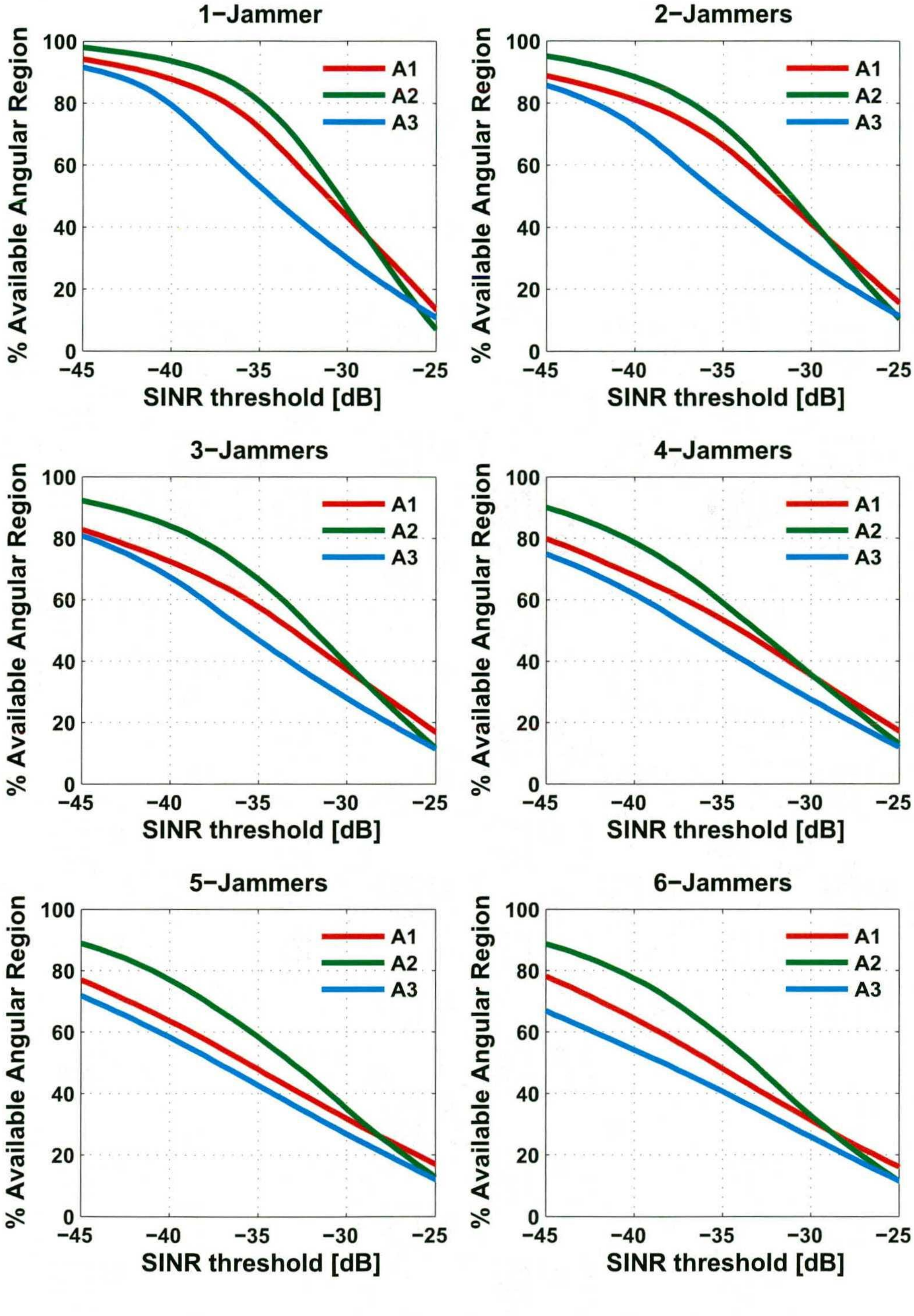


Figure 3.16: Performance of seven element antenna arrays in the presence of one to six interfering signals. AE is operating in simple power minimization mode. L2 frequency band.

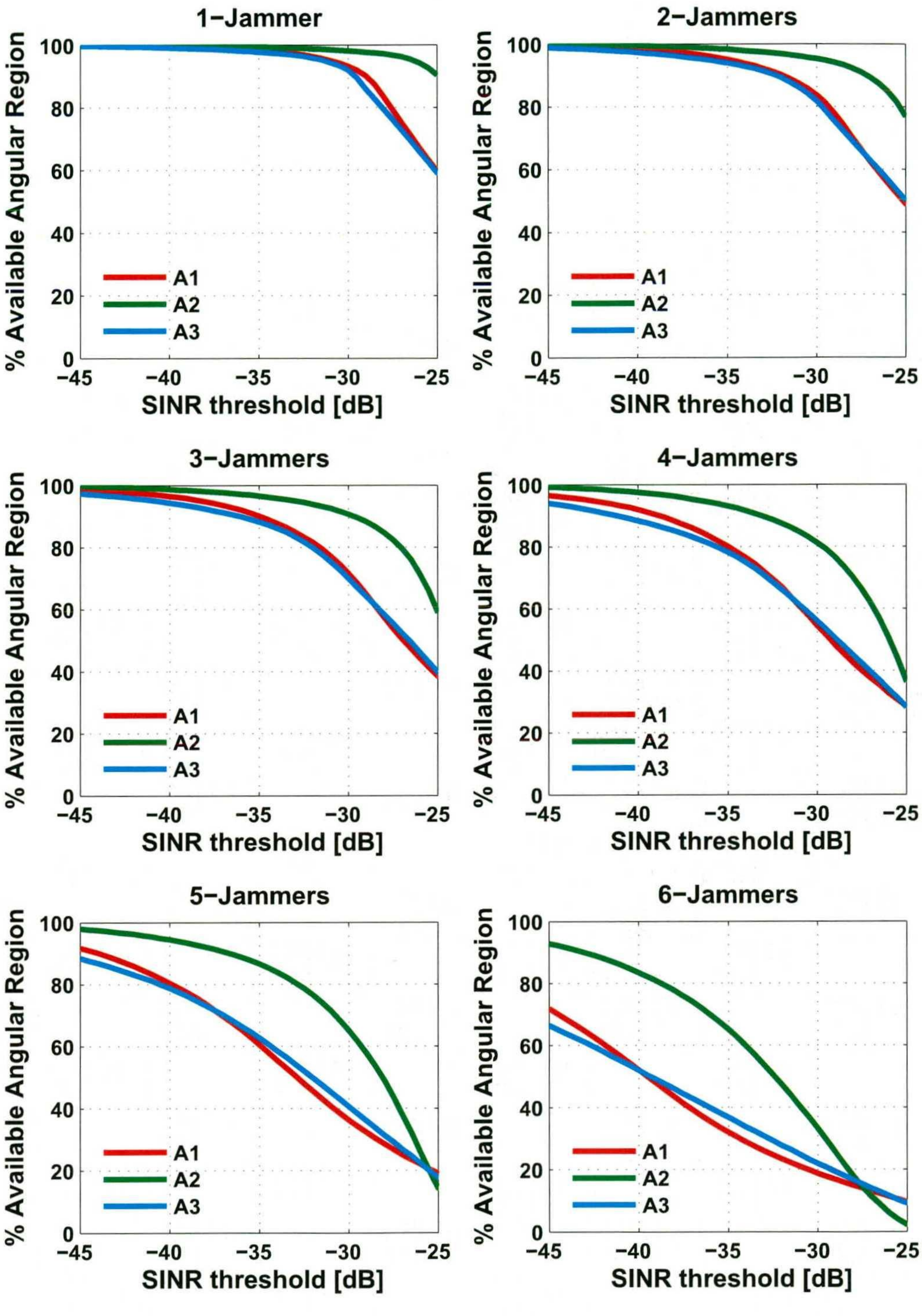


Figure 3.17: Performance of seven element antenna arrays in the presence of one to six interfering signals. AE is operating in beam forming / null steering mode. L1 frequency band.

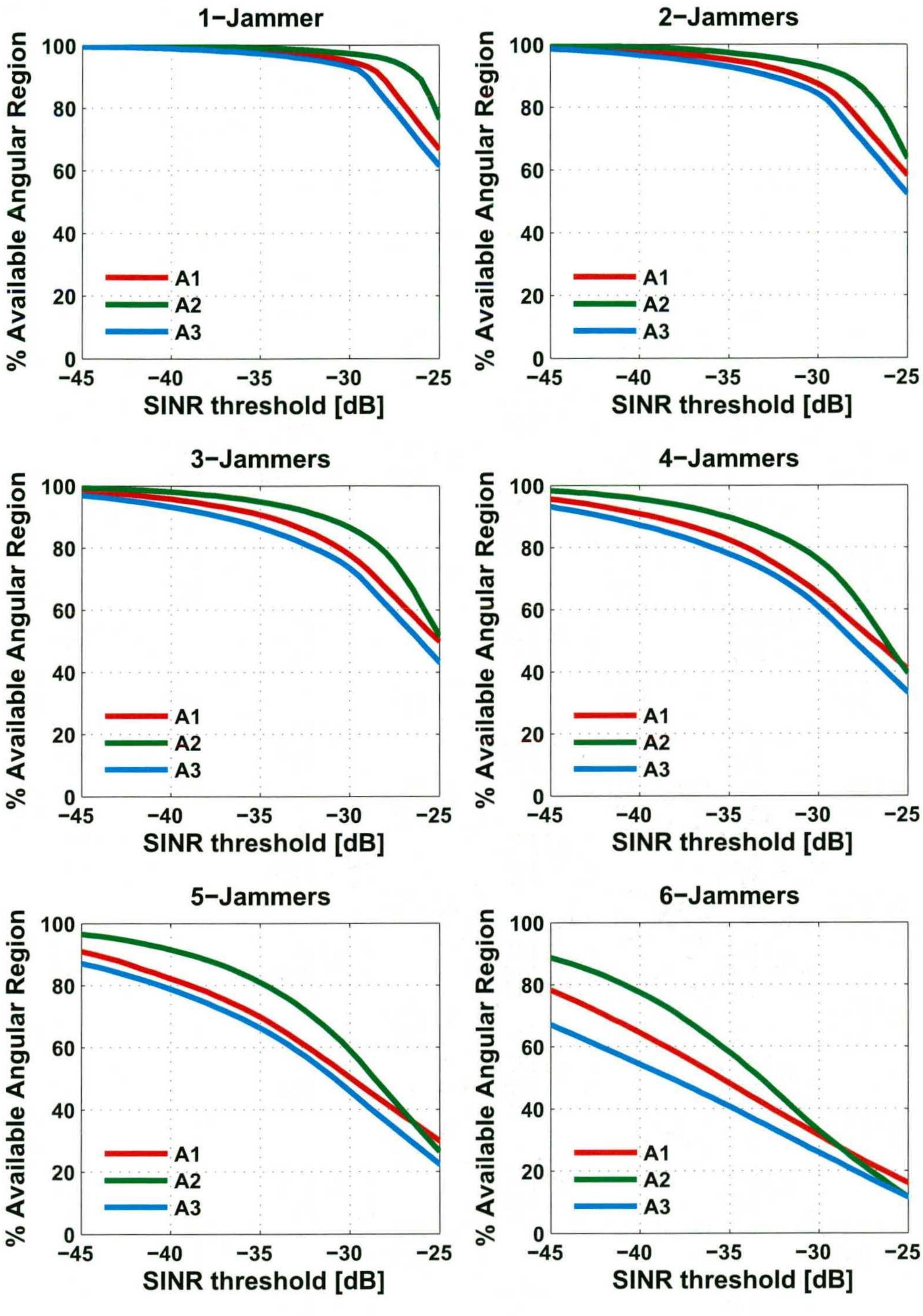


Figure 3.18: Performance of seven element antenna arrays in the presence of one to six interfering signals. AE is operating in beam forming / null steering mode. L2 frequency band.

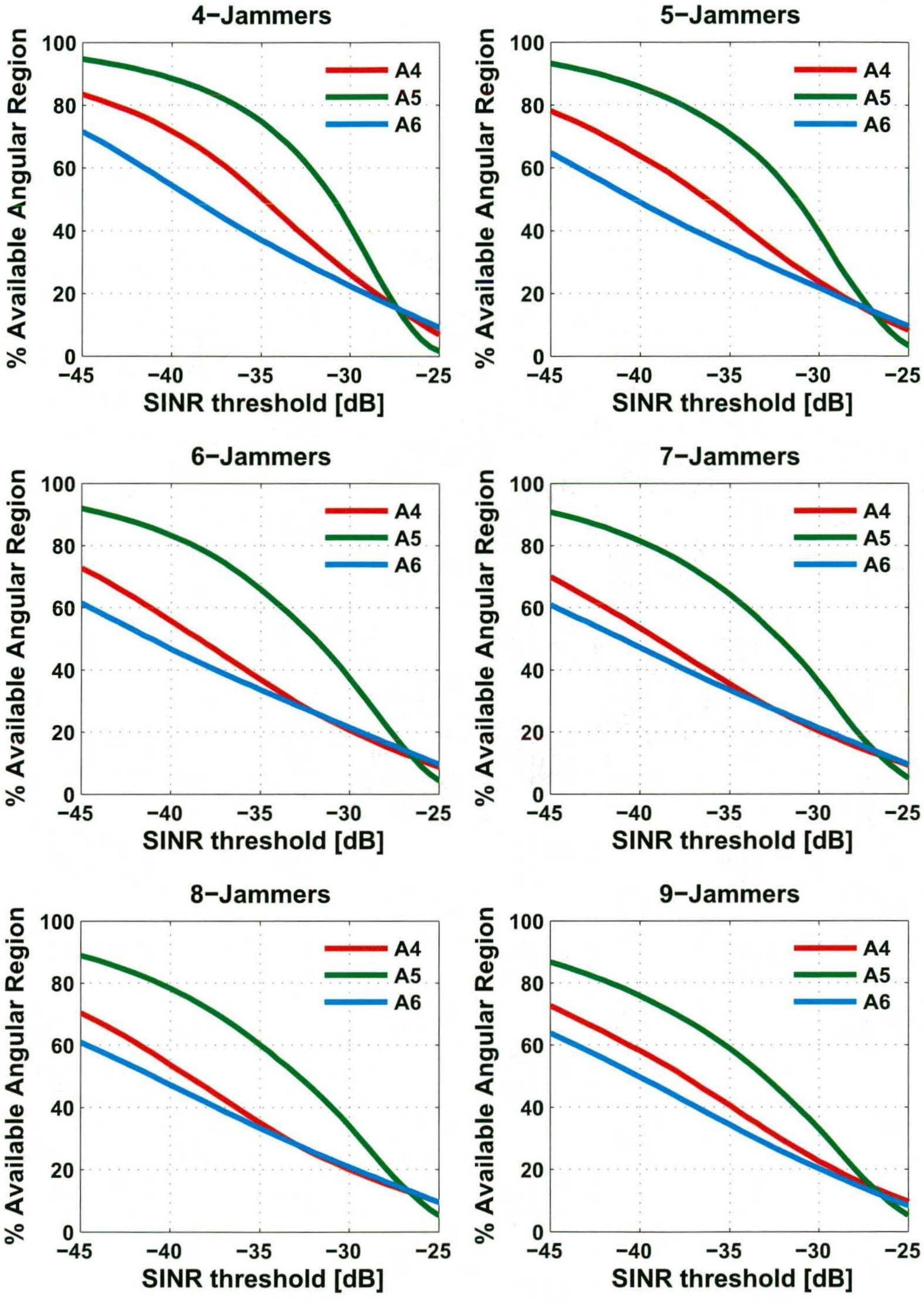


Figure 3.19: Performance of ten element antenna arrays in the presence of four to nine interfering signals. AE is operating in simple power minimization mode. L1 frequency band.

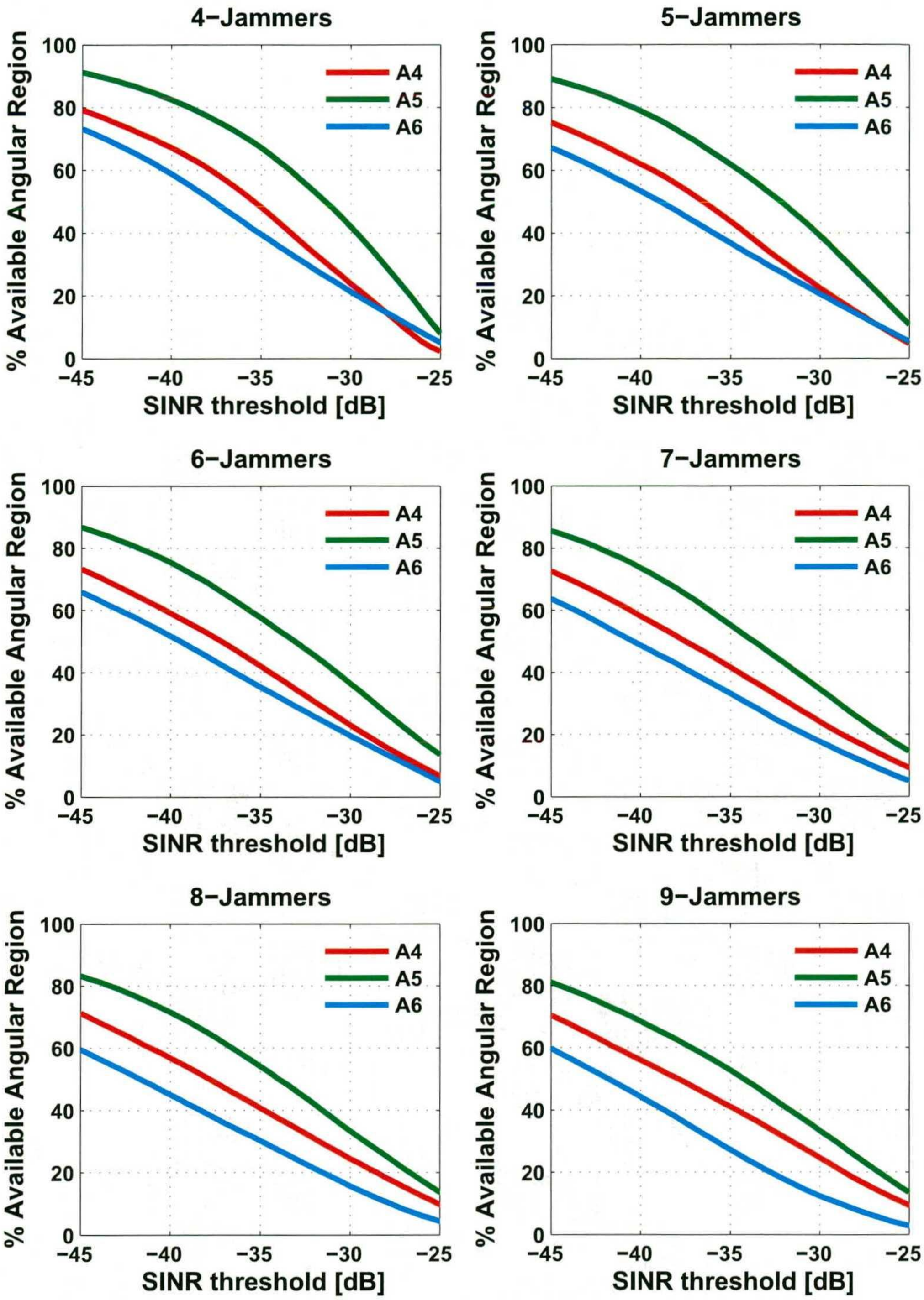


Figure 3.20: Performance of ten element antenna arrays in the presence of four to nine interfering signals. AE is operating in simple power minimization mode. L2 frequency band.

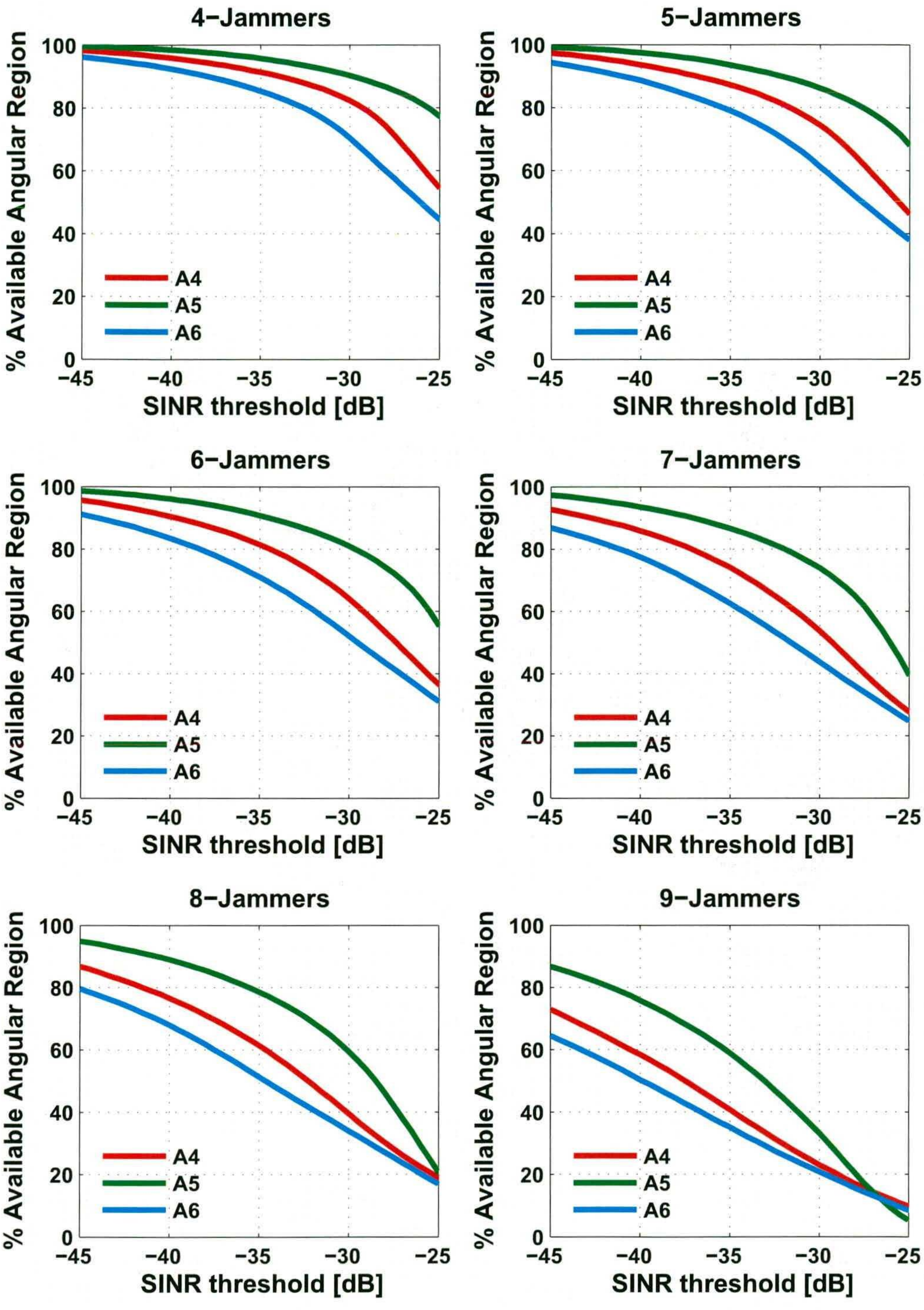


Figure 3.21: Performance of ten element antenna arrays in the presence of four to nine interfering signals. AE is operating in beam forming / null steering mode. L1 frequency band.

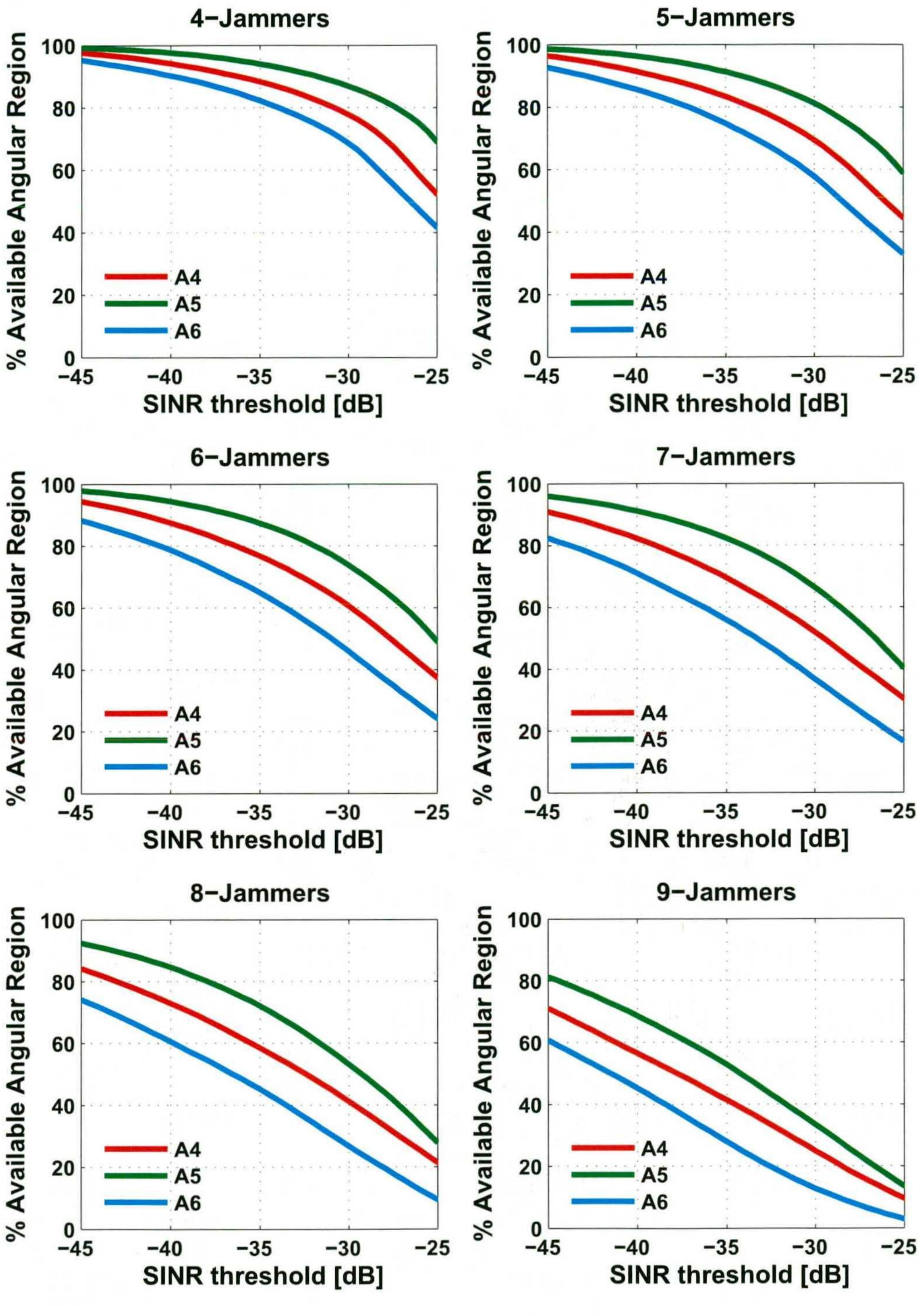


Figure 3.22: Performance of ten element antenna arrays in the presence of four to nine interfering signals. AE is operating in beam forming / null steering mode. L2 frequency band.

| No. of interfering signals | Antenna Array | | | | | |
|---|---|---|---|---|---|---|
| | A1 | A2 | A3 | A4 | A5 | A6 |
| **0** | 75.80 | 98.82 | 51.85 | 80.66 | 95.60 | 56.40 |
| **1** | 64.77 | 88.32 | 45.68 | 71.45 | 87.57 | 49.08 |
| **2** | 55.82 | 80.06 | 41.26 | 63.73 | 81.13 | 44.94 |
| **3** | 45.40 | 74.98 | 37.76 | 56.81 | 77.53 | 39.85 |
| **4** | 36.48 | 70.59 | 35.42 | 50.71 | 74.73 | 37.05 |
| **5** | 31.56 | 66.28 | 35.01 | 44.45 | 70.70 | 34.54 |
| **6** | 31.90 | 65.17 | 36.70 | 36.91 | 65.85 | 33.59 |
| **7** | 0.67 | 0.00 | 1.13 | 35.41 | 64.20 | 33.45 |
| **8** | 0.00 | 0.00 | 0.00 | 35.11 | 60.11 | 33.36 |
| **9** | 0.00 | 0.00 | 0.00 | 40.50 | 58.85 | 34.42 |

Table 3.1: Percentage of available angular region when SINR threshold is greater than -35 dB. AE is operating in simple power minimization mode. L1 frequency band.

| No. of interfering signals | Antenna Array | | | | | |
|---|---|---|---|---|---|---|
| | A1 | A2 | A3 | A4 | A5 | A6 |
| **0** | 81.10 | 92.39 | 56.05 | 72.24 | 91.06 | 50.43 |
| **1** | 71.88 | 80.41 | 53.12 | 62.15 | 83.26 | 46.69 |
| **2** | 66.25 | 72.75 | 49.61 | 57.11 | 75.38 | 43.81 |
| **3** | 57.56 | 66.54 | 46.78 | 50.66 | 71.55 | 40.81 |
| **4** | 53.48 | 58.96 | 44.38 | 48.15 | 67.13 | 39.53 |
| **5** | 47.84 | 58.40 | 42.70 | 43.62 | 61.71 | 36.69 |
| **6** | 47.98 | 58.10 | 40.62 | 42.10 | 57.64 | 35.36 |
| **7** | 0.19 | 0.00 | 4.05 | 41.58 | 55.20 | 33.18 |
| **8** | 0.00 | 0.00 | 0.00 | 40.76 | 54.18 | 30.24 |
| **9** | 0.00 | 0.00 | 0.00 | 41.03 | 52.75 | 27.21 |

Table 3.2: Percentage of available angular region when SINR threshold is greater than -35 dB. AE is operating in simple power minimization mode. L2 frequency band.

| No. of interfering signals | Antenna Array | | | | | |
|---|---|---|---|---|---|---|
| | A1 | A2 | A3 | A4 | A5 | A6 |
| **0** | 100.00 | 100.00 | 100.00 | 100.00 | 100.00 | 100.00 |
| **1** | 98.33 | 99.28 | 97.65 | 98.75 | 99.46 | 97.97 |
| **2** | 95.04 | 98.20 | 93.86 | 96.99 | 98.62 | 94.96 |
| **3** | 90.05 | 96.49 | 88.21 | 94.82 | 97.59 | 91.35 |
| **4** | 80.02 | 93.04 | 78.19 | 91.24 | 95.60 | 85.24 |
| **5** | 60.48 | 86.60 | 62.71 | 87.15 | 93.42 | 78.94 |
| **6** | 31.97 | 65.19 | 36.81 | 81.37 | 90.70 | 70.96 |
| **7** | 0.68 | 0.00 | 1.14 | 74.06 | 86.62 | 62.52 |
| **8** | 0.00 | 0.00 | 0.00 | 61.42 | 78.63 | 51.37 |
| **9** | 0.00 | 0.00 | 0.00 | 40.75 | 58.91 | 35.10 |

Table 3.3: Percentage of available angular region when SINR threshold is greater than -35 dB. AE is operating in beam forming / null steering mode. L1 frequency band.

| No. of interfering signals | Antenna Array | | | | | |
|---|---|---|---|---|---|---|
| | A1 | A2 | A3 | A4 | A5 | A6 |
| **0** | 100.00 | 100.00 | 100.00 | 100.00 | 100.00 | 100.00 |
| **1** | 98.15 | 98.96 | 97.11 | 98.44 | 99.21 | 97.44 |
| **2** | 95.01 | 97.24 | 92.71 | 96.00 | 97.99 | 93.79 |
| **3** | 90.62 | 94.81 | 86.58 | 93.08 | 96.48 | 89.10 |
| **4** | 82.45 | 89.66 | 77.90 | 88.29 | 93.88 | 82.19 |
| **5** | 69.76 | 80.95 | 66.30 | 83.32 | 91.12 | 74.63 |
| **6** | 48.07 | 58.19 | 40.72 | 76.71 | 87.26 | 64.90 |
| **7** | 0.19 | 0.00 | 4.06 | 69.58 | 82.30 | 55.96 |
| **8** | 0.00 | 0.00 | 0.00 | 58.39 | 72.05 | 45.16 |
| **9** | 0.00 | 0.00 | 0.00 | 41.37 | 52.83 | 27.96 |

Table 3.4: Percentage of available angular region when SINR threshold is greater than -35 dB. AE is operating in beam forming / null steering mode. L2 frequency band.

# CHAPTER 4

# ANTENNA CURVATURE EFFECTS

This chapter investigates the effects of surface curvature of the non-planar convex antenna arrays on their AJ performance. The study will consist of seven and ten element antenna arrays going from a planar geometry of zero curvature up through a six-inch high surface with curvature relative to a sphere of radius six inches. All antenna apertures studied will have similar projected area looking from the top. Due to the fact that all apertures have similar projected area, increasing the amount of curvature will yield more surface area, allowing one to physically distribute more antenna elements to the antenna array. The results of this chapter will conclude that there is an improvement in AJ performance as the amount of curvature is increased for the convex non-planar surface.

The chapter first presents the effect it has on seven element antenna arrays, where all of the antennas have a single reference element located at the center or top of the surface, and the remaining six elements are uniformly distributed along the periphery of the surface. Next, it examines the curvature effect on ten element antenna arrays. The ten element antenna arrays have a two ring distribution, where it has the reference element located at the center of the surface, three elements located on an inner ring, and the six other elements located along an outer ring on the bottom of the surface.

## 4.1 Seven Element Antenna Arrays

The antenna arrays range from zero curvature up to a curvature relative to a sphere of radius six inches. All antenna arrays have seven elements and identical distributions with the reference element located at the center of the surface and the remaining six elements uniformly distributed along the periphery. Antenna array A1 (Figure 4.1), introduced in Chapter 3, is a planar geometry which has zero curvature. Antenna Array B1 (Figure 4.2) is a one inch high geometry with curvature relative to a sphere of 18.5 inches. Antenna array B2 (Figure 4.3) is a two inch high geometry possessing curvature relative to a sphere of ten inches. Antenna array A2 (Figure 4.4), also introduced in Chapter 3, is a three inch high geometry with curvature relative to a sphere of 7.5 inches. Furthermore, antenna array B3 (Figure 4.5) has curvature relative to a sphere of 6.5 inches and is four inches high. Finally, antenna array B4 (Figure 4.6) is a spherical surface of radius six inches and is deemed the six inch high geometry.

Figures 4.13 and 4.14 show the AJ performance of the antenna arrays for the L1 and L2 bands, while the antenna electronics is operating in the simple-power minimization mode. One to six interfering signals are incident upon the antenna arrays. For the L1 Band, increasing the curvature yields a performance improvement, initially, for a given number of interfering signals; however, the performance improvement saturates around the three inch geometry resulting in antenna arrays A2, B3, and B4 having similar performance. One reason for the performance to saturate at the L1 band, which has a wavelength of approximately 7.49 inches (19.03 cm), is that as the curvature is increasing the inter-element spacing is becoming larger resulting in sympathetic nulls. In the L2 band, the AJ performance is constantly increasing as the curvature of the antenna array is increasing, resulting in the six inch high geometry (antenna array B4) having the best overall performance. Since the L2 band has a larger wavelength (9.61 inches or 24.42 cm), it is not affected by sympathetic nulls from the further inter-element spacing.

Furthermore, one can refer to Tables 4.1 and 4.2 corresponding to the L1 and L2 band, respectively, to get a more exact view of the percentage available angular region for which the output SINR is greater than -35 dB while the AE is operating in the simple power minimization mode. In Table 4.1, one observes that the performance increases as the amount of curvature increases up to four interfering signals. For the incident signal scenario of five and six jammers, the performance steadily increases and then saturates at the three inch high geometry (antenna array A2). Therefore, antenna arrays A2, B3, and B4 have similar performance. However, for the L2 band (Table 4.2), the AJ performance steadily increases as the amount of surface curvature increases for all given incident signal scenarios, thus, validating the advantage of a convex non-planar antenna array with large curvature.

The performance of the six antenna arrays while the AE is operating in the beam forming / null steering mode for the L1 and L2 bands can be viewed in Figures 4.15 and 4.16. All other parameters are the same as in Figures 4.13 and 4.14. In the L1 band, one observes similar results when the AE is operating in simple power minimization mode. Initially, increasing the surface curvature from planar results in improved AJ performance, however, the performance begins to saturate around the three inch high geometry and antenna arrays A2, B3, and B4 have similar performance. On the contrary, one observes that the performance within the L2 band is consistently improving as the amount of curvature increases as it did in the case of simple power minimization. Thus, it is shown that performance does improve as the curvature increases and that the six inch high geometry has the best overall performance.

Tables 4.3 and 4.4 are given below to examine the percentage where the output SINR exceeds -35 dB for the L1 and L2 bands, respectively. In the L1 band (Table 4.3), one notices that the performance is increasing for a larger amount of curvature for five or less interfering signals. When the antenna arrays are fully constrained (six interfering signals), performance initially increases and saturates at the three-inch high geometry and antenna arrays A2, B3, and B4 yield similar performance. Table 4.4 displays the results for the L2 band, and one sees the same result as the simple power minimization case. Increasing the amount of curvature of the convex non-planar surface yields better AJ performance for a given number of interfering signals. Comparing Tables 4.3 and 4.4 with Tables 4.1 and 4.2, as expected, one observes a significant performance advantage to the antenna electronics operating in the beam forming / null steering mode.

## 4.2 Ten Element Antenna Arrays

The curvature effect studied in this section has the same parameters as Section 4.1. However, all antenna arrays have ten elements and the two ring distribution as described above. They have the reference element located at the center of the surface, three elements located on an inner ring of a given height, and the six remaining elements located along an outer ring on the bottom of the surface. Antenna array A4 (Figure 4.7), introduced in Chapter 3 is a planar geometry. Antenna array B5 (Figure 4.8) is a one inch high geometry with an inner ring height of 0.75 inches. Note the inner ring height is the height to the center of the inner ring elements. Antenna array B6 (Figure 4.9) is a two inch high geometry with an inner ring height of 1.46 inches. Moreover, the three inch high geometry, antenna array A5 (Figure 4.10), introduced in Chapter 3 has an inner right that is 2.12 inches high. Antenna array B7 (Figure 4.11) has an inner ring height of 2.81 inches and is the four inch high geometry. Finally, antenna array B8 (Figure 4.12) is the six inch high geometry with an inner ring height of 4.24 inches.

Figures 4.17 and 4.18 show the AJ performance of the six ten element antenna arrays for the L1 and L2 bands, respectively, in the presence of four to nine interfering signals. The AE is operating in the simple power minimization mode. One observes similar results relative to the seven element antenna arrays. For the L1 band, performance begins to increase as the amount of curvature increases initially; however, it begins to saturate at the three-inch high geometry (antenna array A5). As a result, the three-inch high (antenna array A5), four-inch high (antenna array B7) and six-inch high geometries (antenna array B8) exhibit similar performance. In the L2 band, increasing the amount of curvature always results in improved AJ performance. Therefore, if one wishes to obtain the best overall AJ performance, one should select a convex non-planar surface with large curvature.

The percentage available angular region of the ten element antenna arrays for which the output SINR is more than -35 dB in the presence of zero to nine interfering signals is given below in Tables 4.5 and 4.6. The antenna electronics is operating in simple power minimization mode. For the L1 band, the conclusions drawn above are further supported in Table 4.5 in that for a given number of jammers, increasing the amount of surface curvature from planar yields improved performance initially and then trails off around the three inch high geometry (antenna array A5). In Table 4.6 one observes increasing the amount of surface curvature consistently results in improved AJ performance with the six inch high geometry (antenna array B8) having superior performance compared to the other antenna arrays.

Figures 4.19 and 4.20 display the AJ performance while the antenna electronics is operating in the beam forming / null steering mode for the L1 and L2 bands, respectively. All other parameters are the same as Figures 4.17 and 4.18. For the L1 band, one notices that performance is improved as the curvature is increased up to L-2 interfering signals, where L is the number of antenna elements. However, for nine interfering signals the performance initially increases as curvature increases and saturates around the three inch high geometry (antenna array A5). In Figure 4.20, one see that the AJ performance increases as the amount of surface curvature increases for all given incident signal scenarios. Therefore, we have came to the exact same conclusion as the case of simple power minimization, that increasing the amount of curvature will result in improved AJ performance. Thus, in our case the six-inch high geometry yields the best overall AJ performance.

Tables 4.7 and 4.8 further support this conclusion, where the AE is operating in the beam forming / null steering mode. All other parameters are the same as in Tables 4.5 and 4.6. In Table 4.7, one observes that performance increases as curvature increases up to eight interfering signals. For nine interfering signals, performance increases up to the four inch high geometry (antenna array B7); however, antenna arrays A5, B7, and B8 result in similar performance. For the L2 band (Table 4.8), one again see that performance increases as the amount of surface curvature increases for a given number of interfering signals. Also, by comparing Tables 4.7 and 4.8 against Tables 4.5 and 4.6 one easily observes the significant performance improvement one can obtain by the AE operating in the beam forming / null steering mode, as expected. Therefore, it is highly recommended to operate in the beam forming / null steering mode.

## 4.3 Chapter Summary

In this chapter, it has been shown that for a convex non-planar surface, increasing the amount of curvature of the surface will result in an improvement in the AJ performance for both seven and ten element antenna arrays. As a result, the six-inch high geometry exhibited the best overall AJ performance. Therefore, in the next chapter we will further investigate the six-inch high geometry. We will determine how many elements one can add to the antenna array as well as the best distribution for those elements. Also, it is important to note that beam forming / null steering significantly outperforms simple power minimization, and it is highly recommended to operate in beam forming / null steering mode.

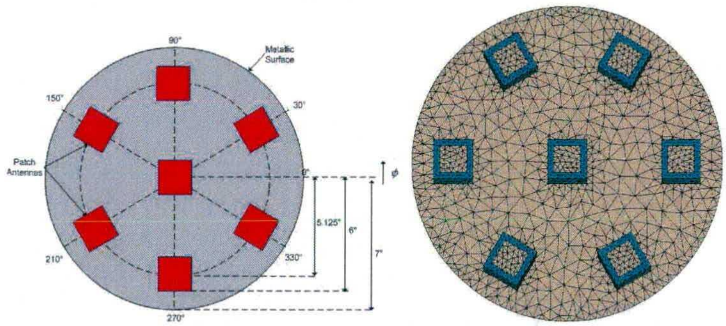


(a) Top Down View (b) Gridded Surface

Figure 4.1: Antenna Array A1.

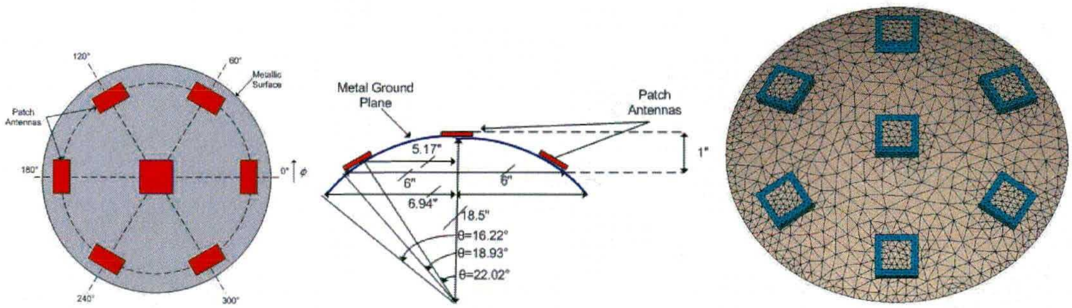


(a) Top Down View (b) Side View (c) Gridded Surface

Figure 4.2: Antenna Array B1.

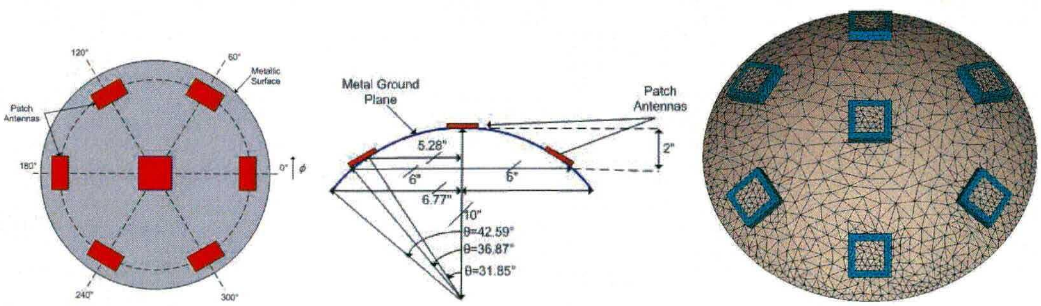


(a) Top Down View (b) Side View (c) Gridded Surface

Figure 4.3: Antenna Array B2.

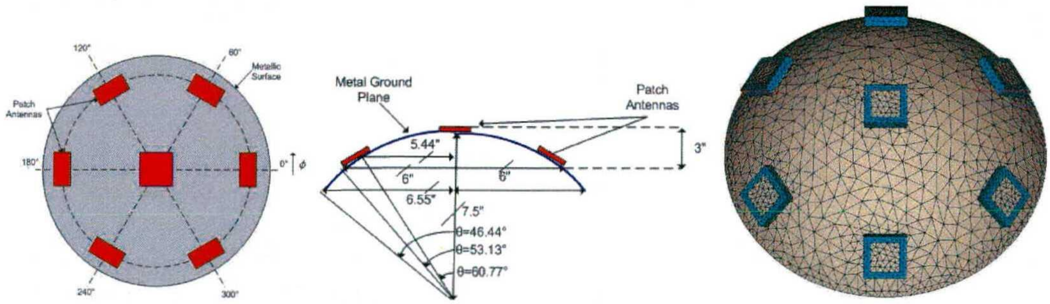


(a) Top Down View (b) Side View (c) Gridded Surface

Figure 4.4: Antenna Array A2.

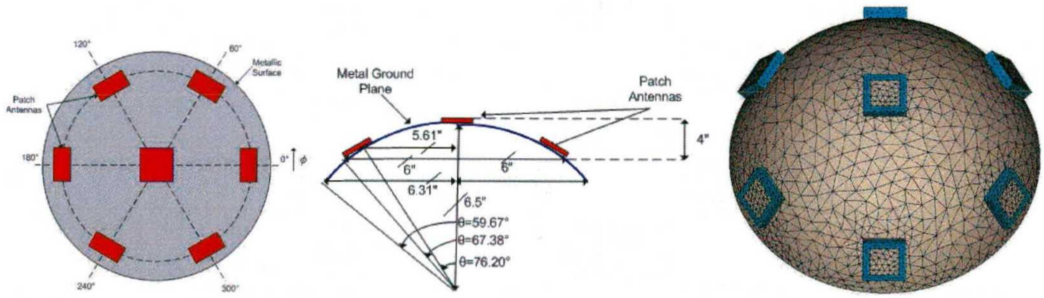


(a) Top Down View (b) Side View (c) Gridded Surface

Figure 4.5: Antenna Array B3.

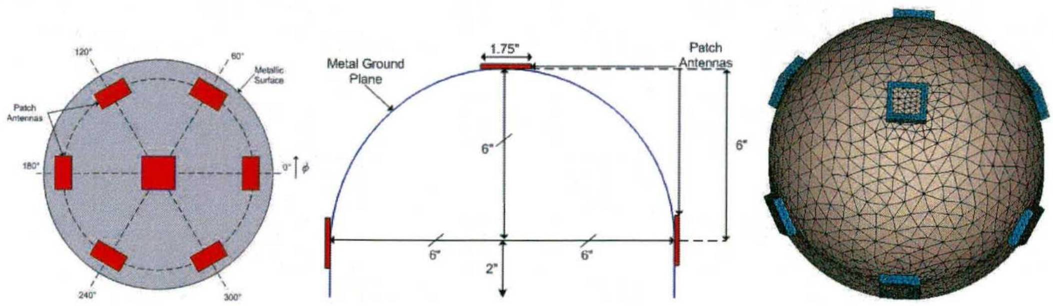


(a) Top Down View (b) Side View (c) Gridded Surface

Figure 4.6: Antenna Array B4.

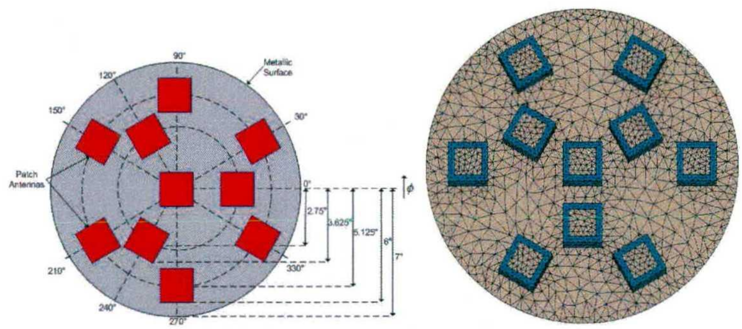


(a) Top Down View (b) Gridded Surface

Figure 4.7: Antenna Array A4.

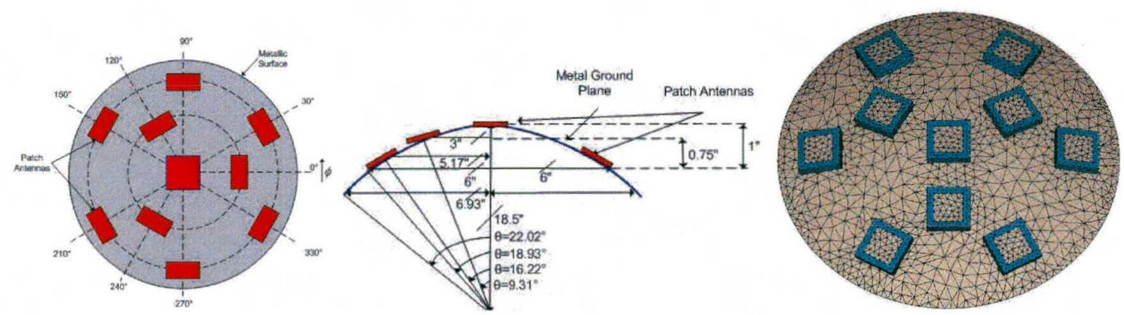


(a) Top Down View (b) Side View (c) Gridded Surface

Figure 4.8: Antenna Array B5.

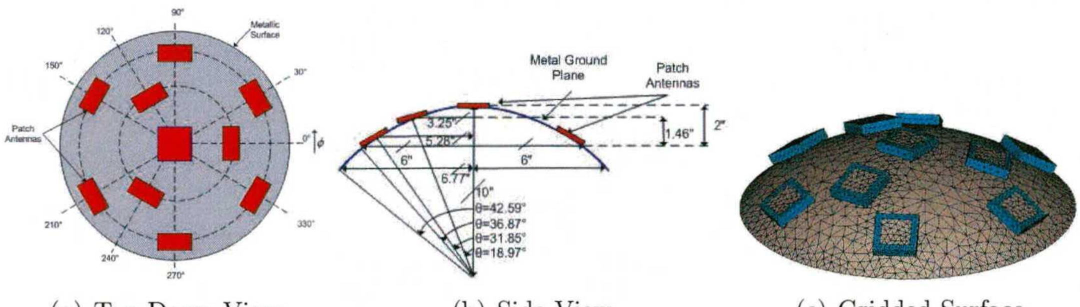


(a) Top Down View (b) Side View (c) Gridded Surface

Figure 4.9: Antenna Array B6.

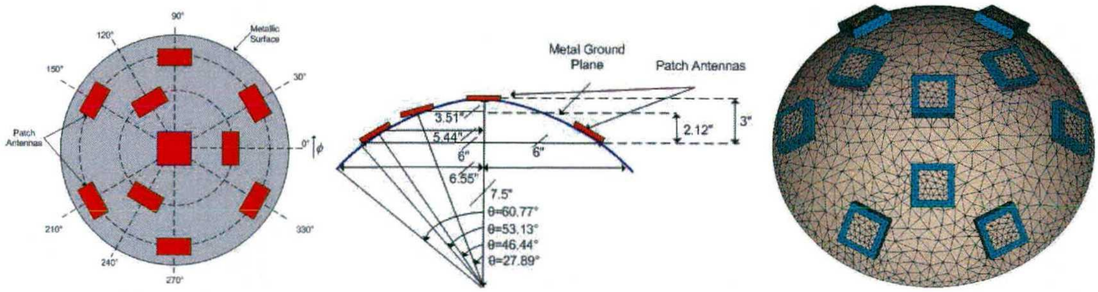


(a) Top Down View (b) Side View (c) Gridded Surface

Figure 4.10: Antenna Array A5.

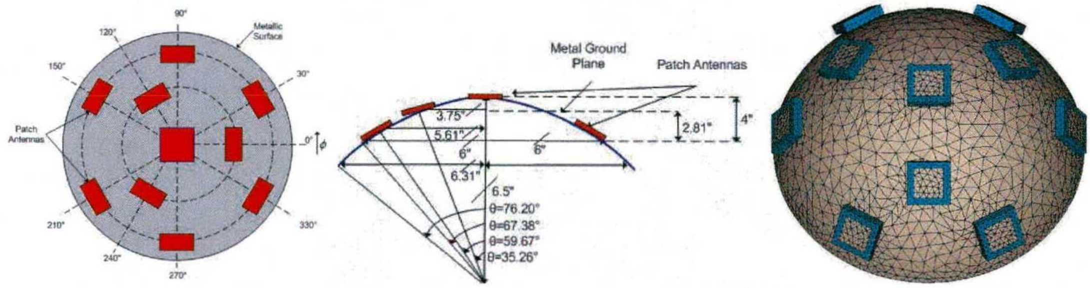


(a) Top Down View (b) Side View (c) Gridded Surface

Figure 4.11: Antenna Array B7.

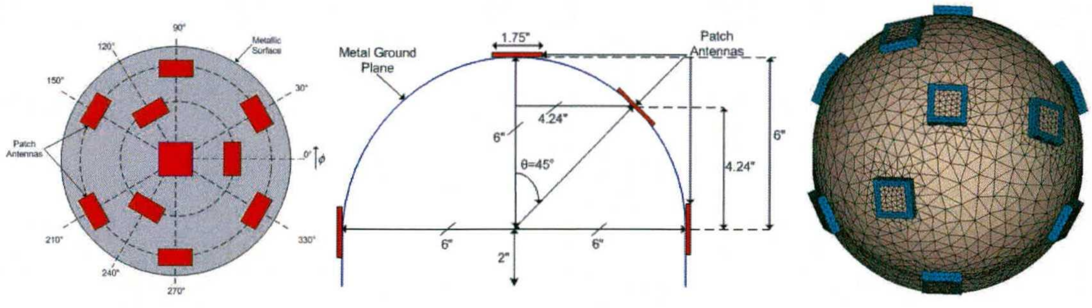


(a) Top Down View (b) Side View (c) Gridded Surface

Figure 4.12: Antenna Array B8.

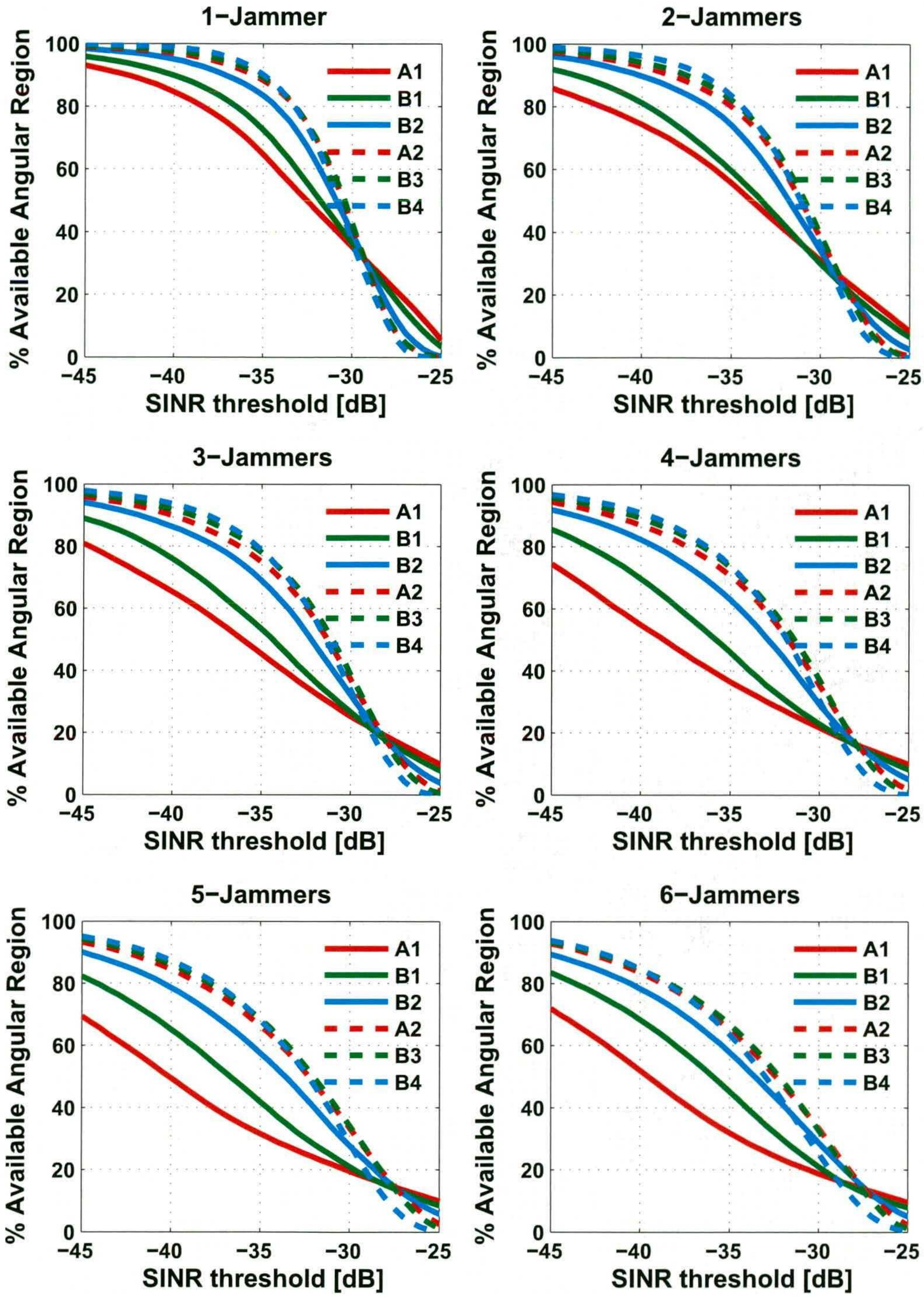


Figure 4.13: Performance of seven element antenna arrays in the presence of one to six interfering signals. AE is operating in simple power minimization mode. L1 frequency band.

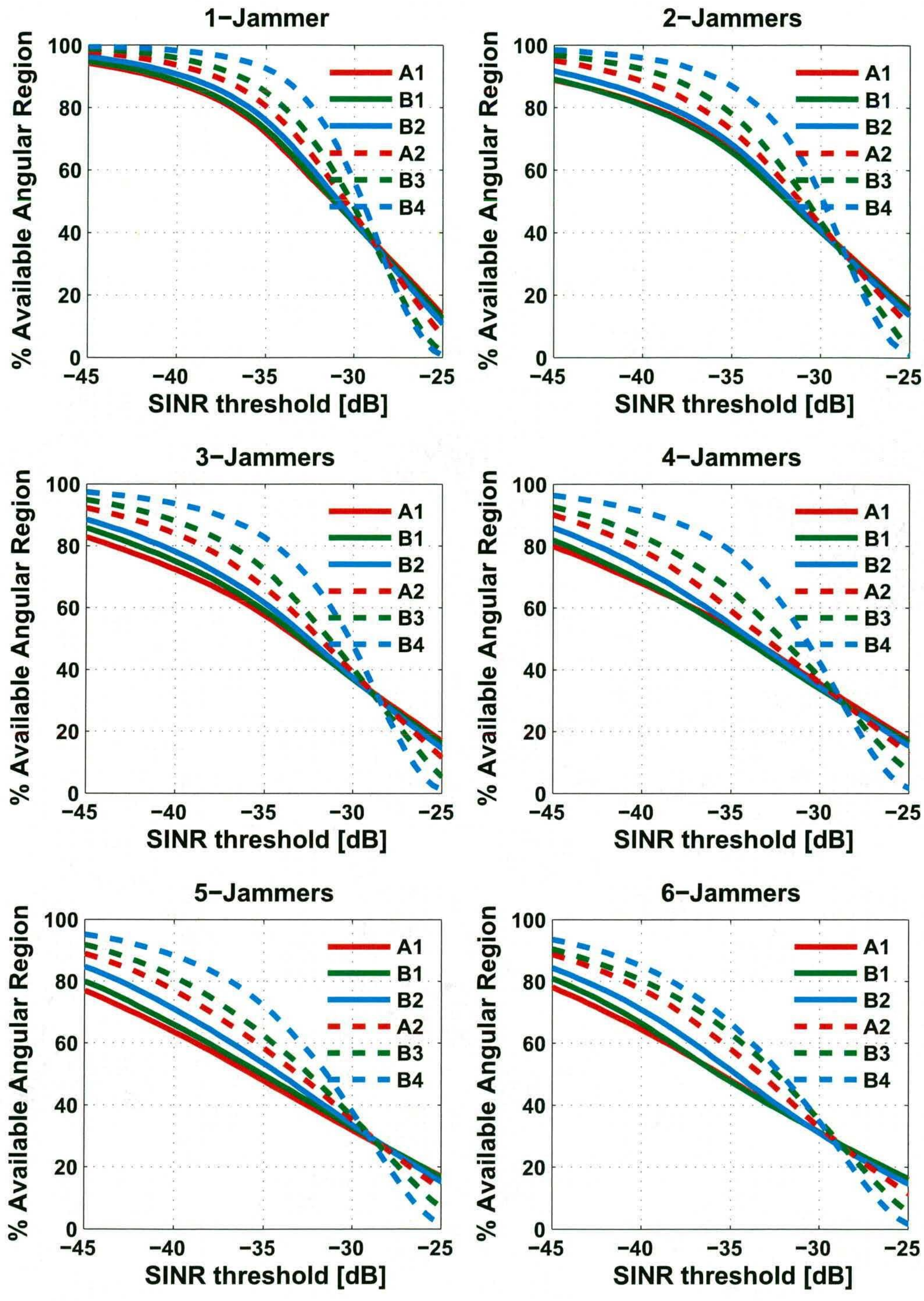


Figure 4.14: Performance of seven element antenna arrays in the presence of one to six interfering signals. AE is operating in simple power minimization mode. L2 frequency band.

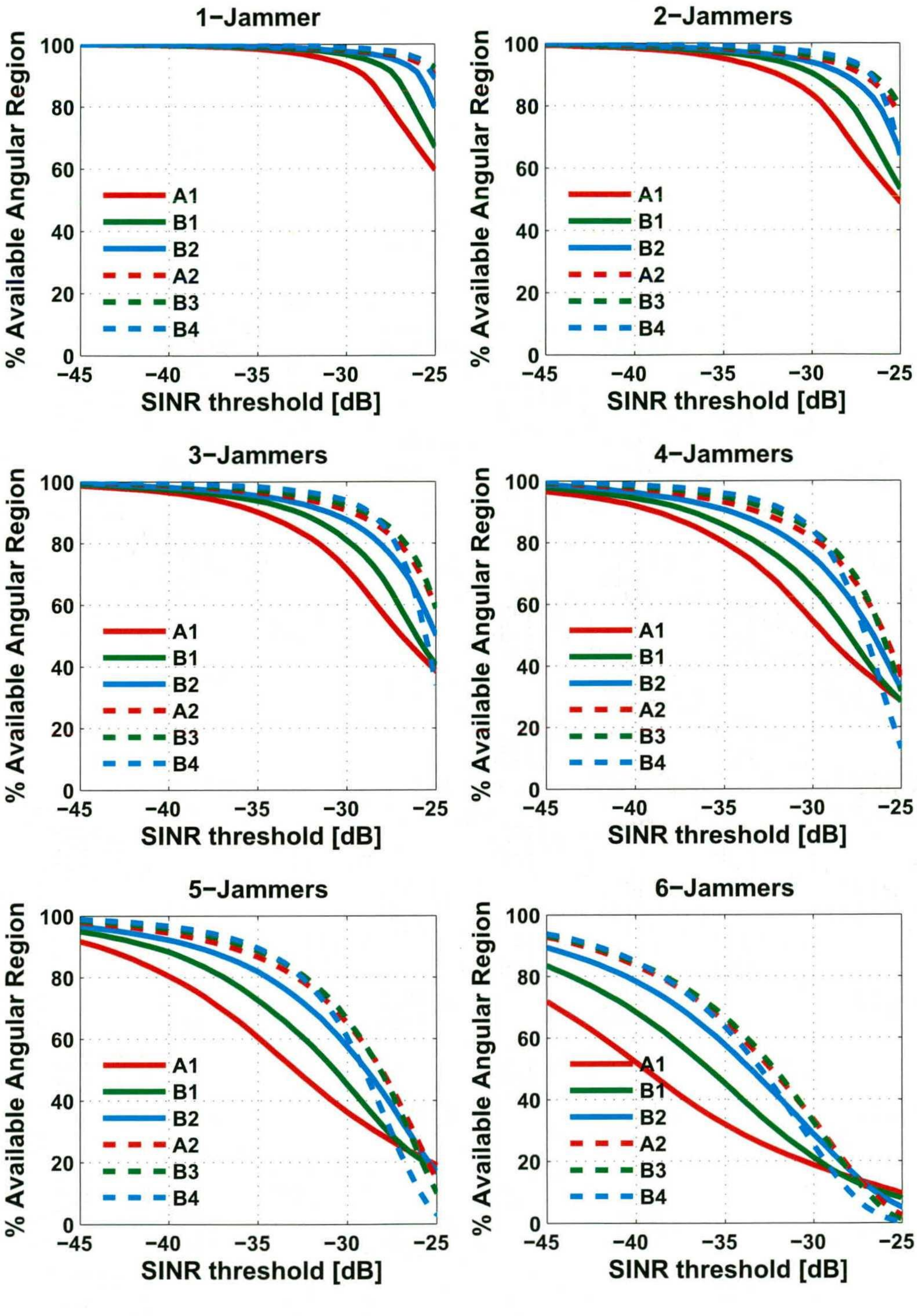


Figure 4.15: Performance of seven element antenna arrays in the presence of one to six interfering signals. AE is operating in beam forming / null steering mode. L1 frequency band.

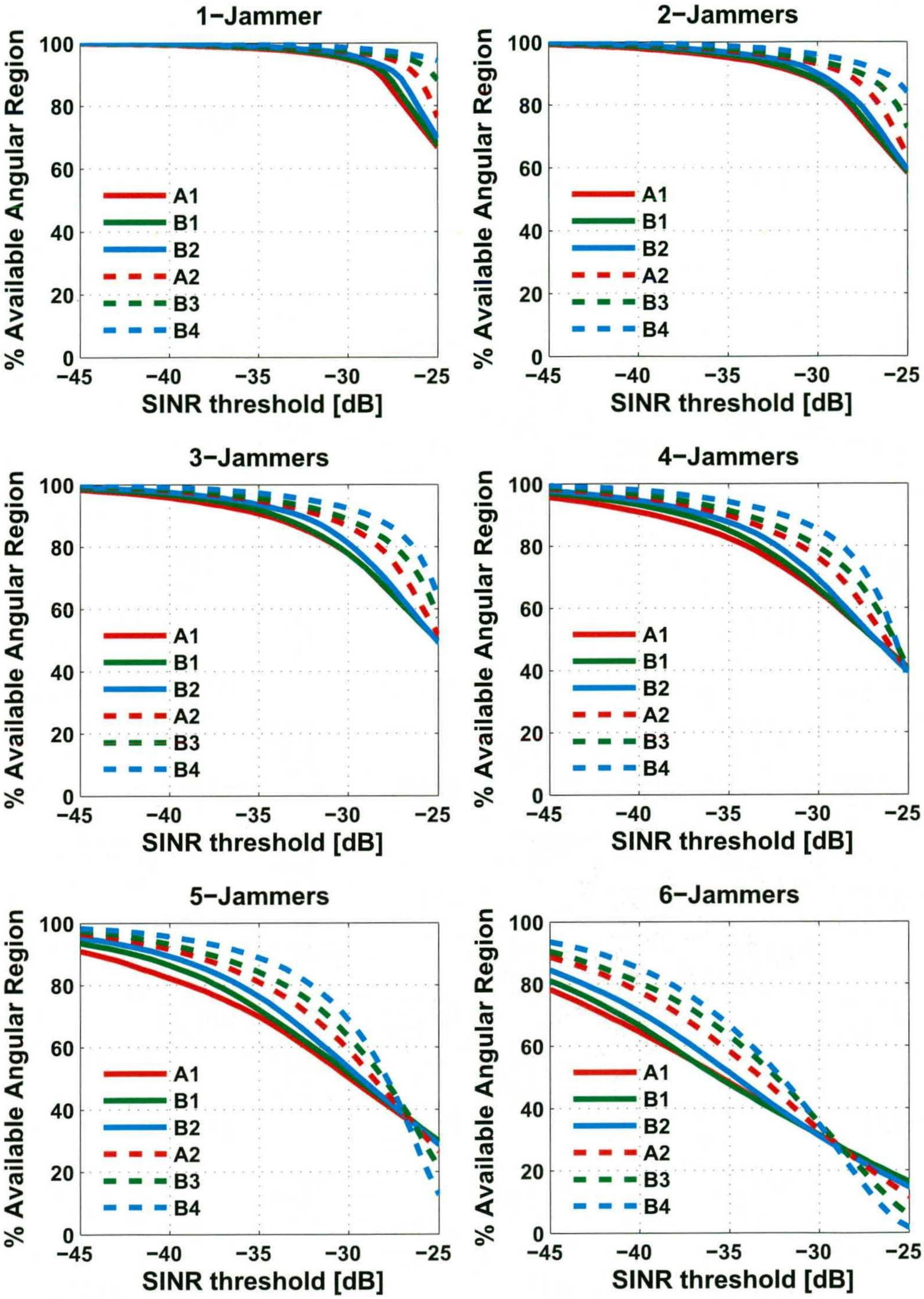


Figure 4.16: Performance of seven element antenna arrays in the presence of one to six interfering signals. AE is operating in beam forming / null steering mode. L2 frequency band.

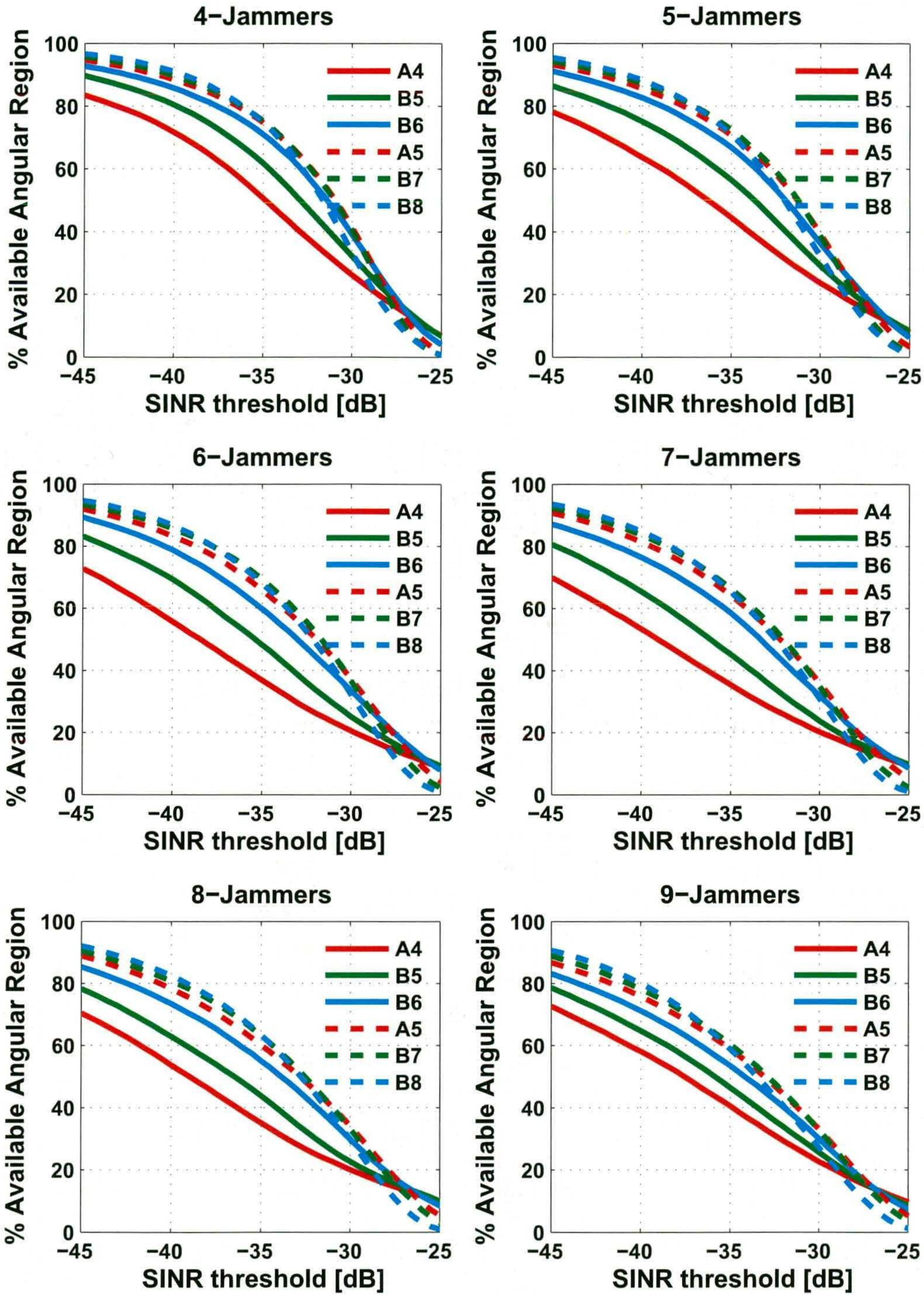


Figure 4.17: Performance of ten element antenna arrays in the presence of four to nine interfering signals. AE is operating in simple power minimization mode. L1 frequency band.

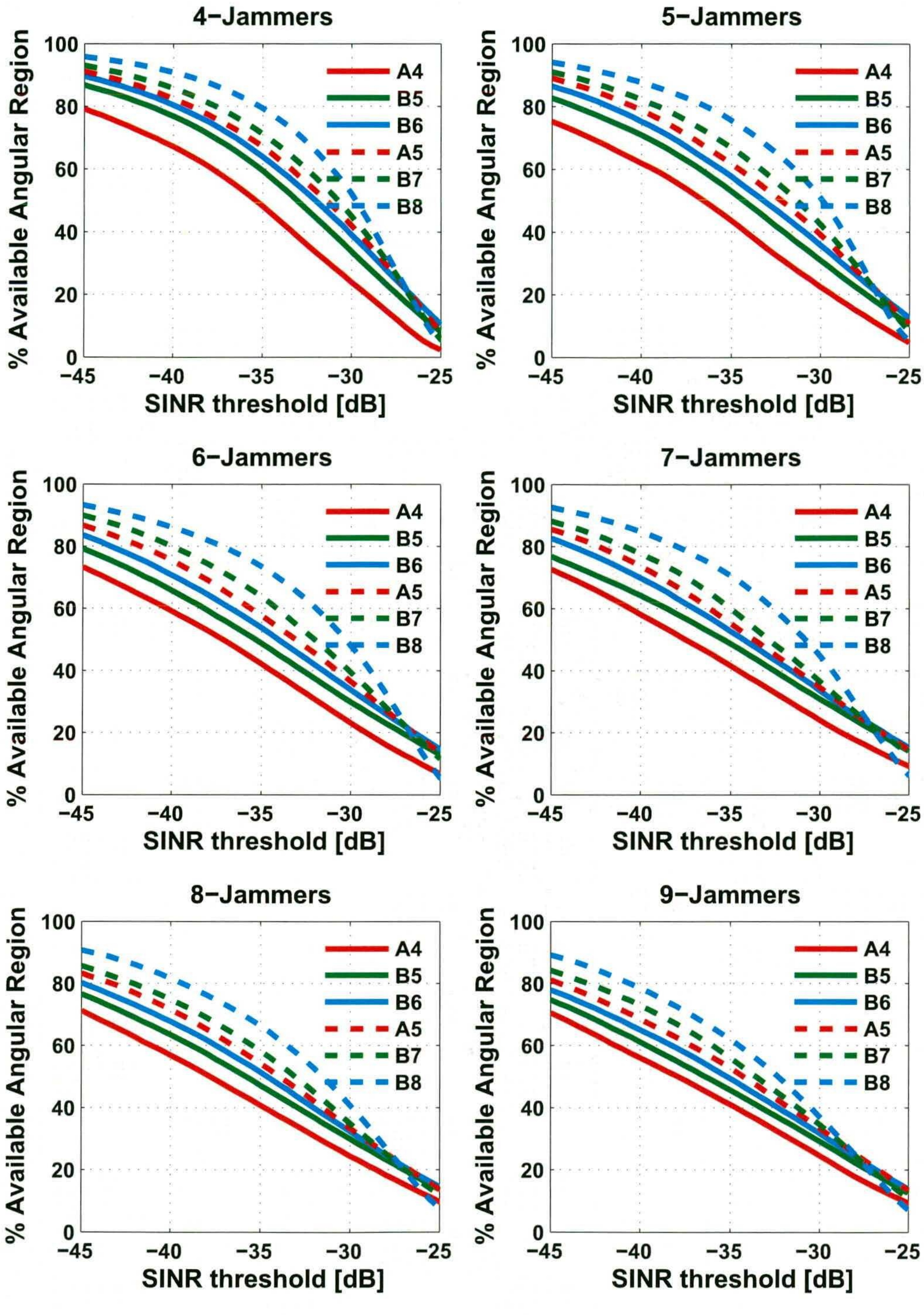


Figure 4.18: Performance of ten element antenna arrays in the presence of four to nine interfering signals. AE is operating in simple power minimization mode. L2 frequency band.

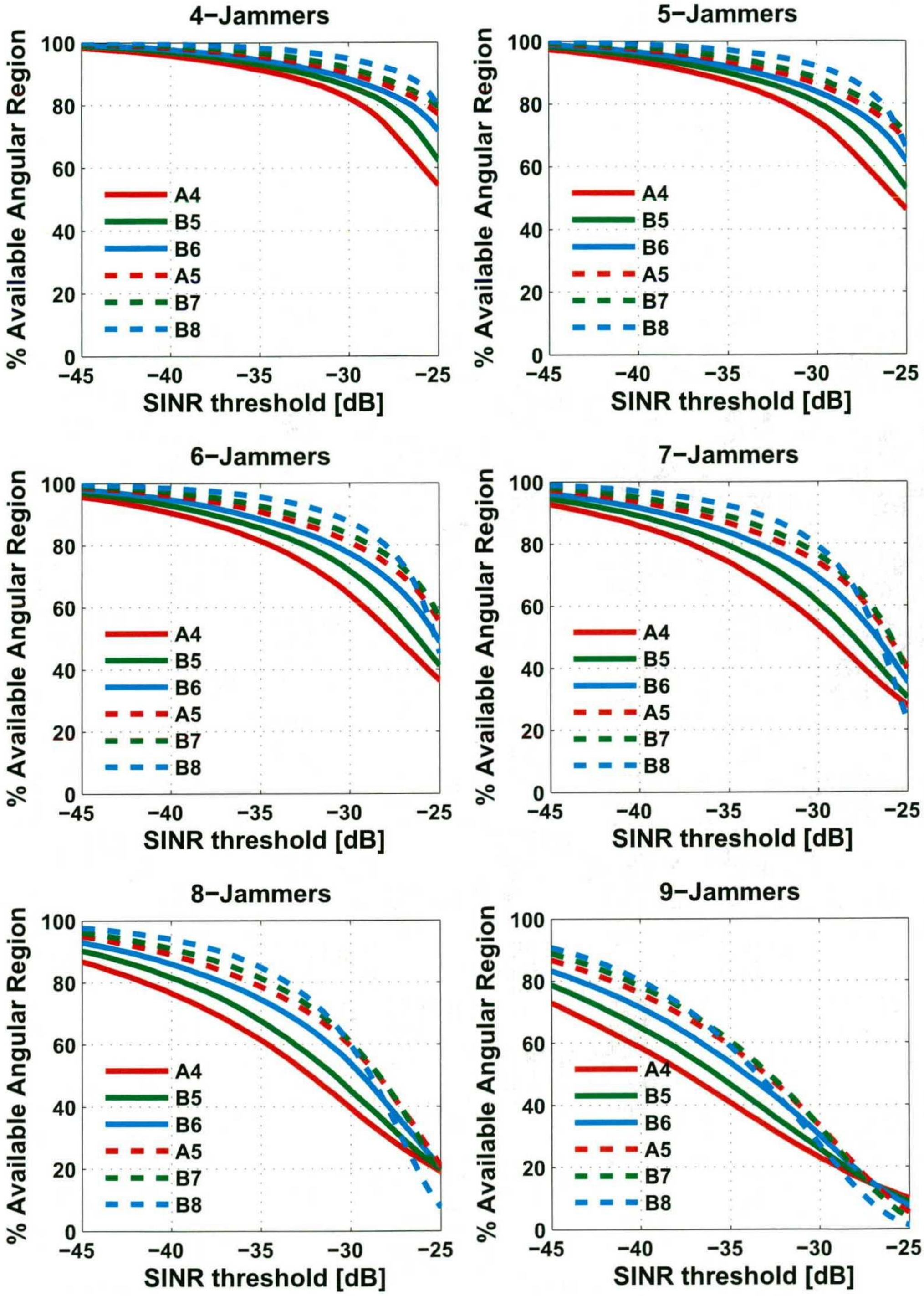


Figure 4.19: Performance of ten element antenna arrays in the presence of four to nine interfering signals. AE is operating in beam forming / null steering mode. L1 frequency band.

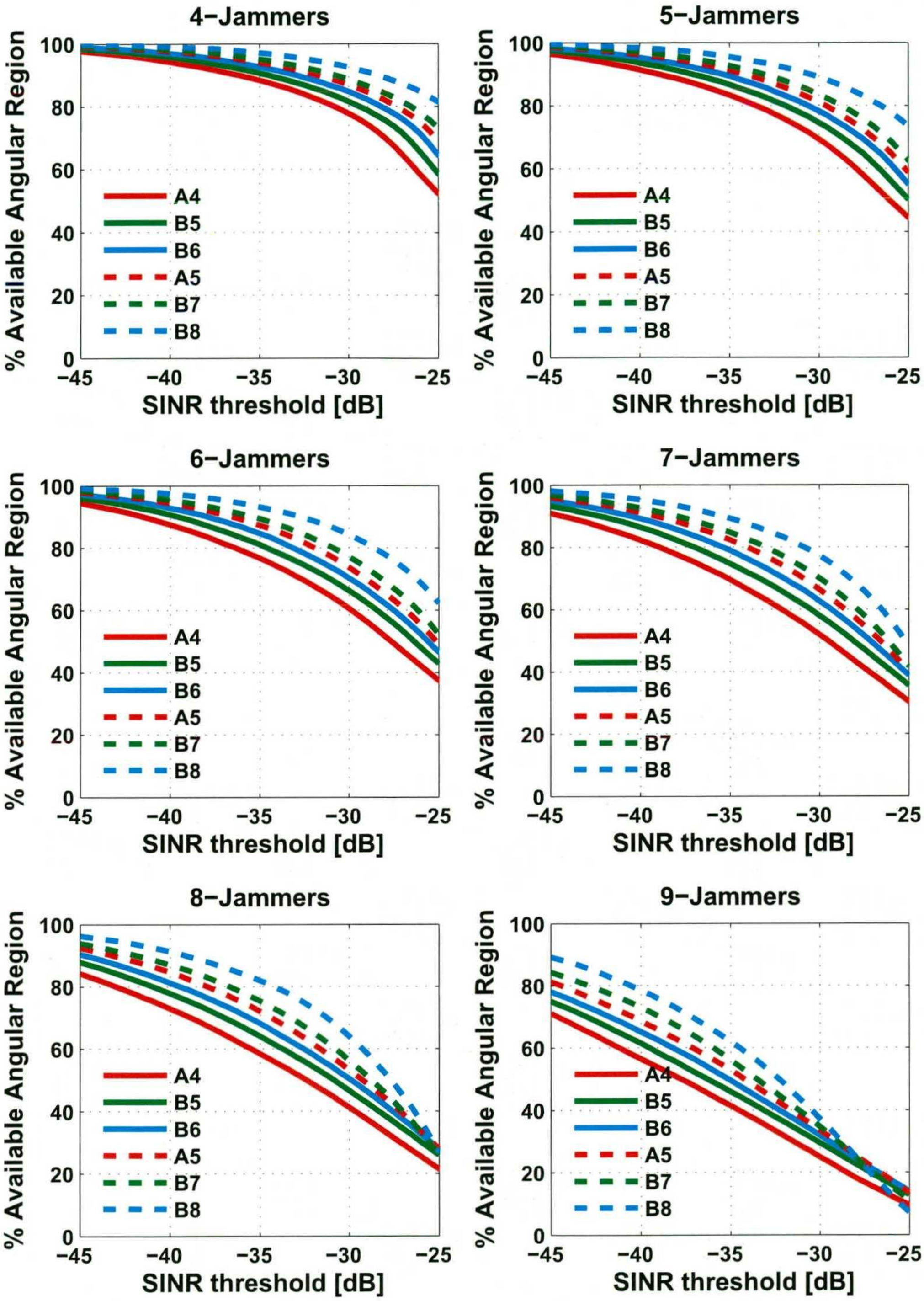


Figure 4.20: Performance of ten element antenna arrays in the presence of four to nine interfering signals. AE is operating in beam forming / null steering mode. L2 frequency band.

| No. of interfering signals | Antenna Array | | | | | |
|---|---|---|---|---|---|---|
| | A1 | B1 | B2 | A2 | B3 | B4 |
| **0** | 75.80 | 89.16 | 97.22 | 98.82 | 97.77 | 96.38 |
| **1** | 64.77 | 72.50 | 83.46 | 88.32 | 89.10 | 90.04 |
| **2** | 55.82 | 59.52 | 74.09 | 80.06 | 82.08 | 83.40 |
| **3** | 45.40 | 53.38 | 68.96 | 74.98 | 78.01 | 78.69 |
| **4** | 36.48 | 45.95 | 62.94 | 70.59 | 73.29 | 73.74 |
| **5** | 31.56 | 41.89 | 57.53 | 66.28 | 68.54 | 68.08 |
| **6** | 31.90 | 45.23 | 57.82 | 65.17 | 66.83 | 63.60 |

Table 4.1: Seven element antenna arrays. Percentage of available angular region when SINR threshold is greater than -35 dB. AE is operating in simple power minimization mode. L1 frequency band.

| No. of interfering signals | Antenna Array | | | | | |
|---|---|---|---|---|---|---|
| | A1 | B1 | B2 | A2 | B3 | B4 |
| **0** | 81.10 | 84.00 | 88.09 | 92.39 | 94.74 | 98.57 |
| **1** | 71.88 | 72.91 | 75.74 | 80.41 | 84.85 | 92.41 |
| **2** | 66.25 | 65.66 | 68.16 | 72.75 | 77.86 | 86.80 |
| **3** | 57.56 | 58.95 | 61.54 | 66.54 | 72.28 | 82.69 |
| **4** | 53.48 | 52.26 | 54.55 | 58.96 | 65.49 | 78.29 |
| **5** | 47.84 | 49.76 | 53.50 | 58.40 | 62.55 | 72.16 |
| **6** | 47.98 | 47.63 | 51.32 | 58.10 | 63.14 | 66.52 |

Table 4.2: Seven element antenna arrays. Percentage of available angular region when SINR threshold is greater than -35 dB. AE is operating in simple power minimization mode. L2 frequency band.

| No. of interfering signals | Antenna Array | | | | | |
|---|---|---|---|---|---|---|
| | A1 | B1 | B2 | A2 | B3 | B4 |
| **0** | 100.00 | 100.00 | 100.00 | 100.00 | 100.00 | 100.00 |
| **1** | 98.33 | 98.82 | 99.04 | 99.28 | 99.45 | 99.64 |
| **2** | 95.04 | 96.90 | 97.60 | 98.20 | 98.61 | 99.08 |
| **3** | 90.05 | 93.67 | 95.37 | 96.49 | 97.18 | 98.18 |
| **4** | 80.02 | 85.57 | 90.58 | 93.04 | 94.64 | 95.89 |
| **5** | 60.48 | 72.50 | 81.84 | 86.60 | 88.58 | 89.49 |
| **6** | 31.97 | 45.31 | 57.85 | 65.19 | 66.84 | 63.64 |

Table 4.3: Seven element antenna arrays. Percentage of available angular region when SINR threshold is greater than -35 dB. AE is operating in beam forming / null steering mode. L1 frequency band.

| No. of interfering signals | Antenna Array | | | | | |
|---|---|---|---|---|---|---|
| | A1 | B1 | B2 | A2 | B3 | B4 |
| **0** | 100.00 | 100.00 | 100.00 | 100.00 | 100.00 | 100.00 |
| **1** | 98.15 | 98.51 | 98.73 | 98.96 | 99.10 | 99.48 |
| **2** | 95.01 | 95.76 | 96.53 | 97.24 | 97.68 | 98.51 |
| **3** | 90.62 | 91.74 | 93.56 | 94.81 | 95.60 | 97.19 |
| **4** | 82.45 | 84.93 | 87.54 | 89.66 | 91.28 | 94.10 |
| **5** | 69.76 | 72.01 | 76.22 | 80.95 | 84.14 | 88.72 |
| **6** | 48.07 | 47.66 | 51.36 | 58.19 | 63.18 | 66.54 |

Table 4.4: Seven element antenna arrays. Percentage of available angular region when SINR threshold is greater than -35 dB. AE is operating in beam forming / null steering mode. L2 frequency band.

| No. of interfering signals | Antenna Array | | | | | |
|---|---|---|---|---|---|---|
| | A4 | B5 | B6 | A5 | B7 | B8 |
| **0** | 80.66 | 89.03 | 93.68 | 95.60 | 94.93 | 94.66 |
| **1** | 71.45 | 79.45 | 84.96 | 87.57 | 87.23 | 88.80 |
| **2** | 63.73 | 71.39 | 78.07 | 81.13 | 81.16 | 82.81 |
| **3** | 56.81 | 66.71 | 74.21 | 77.53 | 77.98 | 78.52 |
| **4** | 50.71 | 61.81 | 70.92 | 74.73 | 75.28 | 74.77 |
| **5** | 44.45 | 56.34 | 66.71 | 70.70 | 72.40 | 70.87 |
| **6** | 36.91 | 48.31 | 59.87 | 65.85 | 69.36 | 68.03 |
| **7** | 35.41 | 45.18 | 58.54 | 64.20 | 66.37 | 65.28 |
| **8** | 35.11 | 43.88 | 55.12 | 60.11 | 63.27 | 63.37 |
| **9** | 40.50 | 46.40 | 53.49 | 58.85 | 60.40 | 58.80 |

Table 4.5: Ten element antenna arrays. Percentage of available angular region when SINR threshold is greater than -35 dB. AE is operating in simple power minimization mode. L1 frequency band.

| No. of interfering signals | Antenna Array | | | | | |
|---|---|---|---|---|---|---|
| | A4 | B5 | B6 | A5 | B7 | B8 |
| **0** | 72.24 | 87.50 | 91.28 | 91.06 | 92.80 | 96.29 |
| **1** | 62.15 | 77.10 | 81.71 | 83.26 | 86.17 | 90.70 |
| **2** | 57.11 | 69.94 | 73.54 | 75.38 | 78.90 | 85.28 |
| **3** | 50.66 | 64.11 | 68.80 | 71.55 | 75.19 | 81.55 |
| **4** | 48.15 | 59.43 | 63.89 | 67.13 | 71.13 | 79.31 |
| **5** | 43.62 | 52.99 | 57.65 | 61.71 | 66.80 | 75.56 |
| **6** | 42.10 | 48.75 | 53.76 | 57.64 | 63.79 | 73.48 |
| **7** | 41.58 | 48.65 | 52.69 | 55.20 | 59.96 | 70.56 |
| **8** | 40.76 | 47.20 | 51.46 | 54.18 | 58.29 | 66.36 |
| **9** | 41.03 | 45.63 | 49.42 | 52.75 | 56.04 | 62.02 |

Table 4.6: Ten element antenna arrays. Percentage of available angular region when SINR threshold is greater than -35 dB. AE is operating in simple power minimization mode. L2 frequency band.

| No. of interfering signals | Antenna Array | | | | | |
|---|---|---|---|---|---|---|
| | A4 | B5 | B6 | A5 | B7 | B8 |
| **0** | 100.00 | 100.00 | 100.00 | 100.00 | 100.00 | 100.00 |
| **1** | 98.75 | 99.02 | 99.25 | 99.46 | 99.58 | 99.76 |
| **2** | 96.99 | 97.64 | 98.16 | 98.62 | 98.93 | 99.42 |
| **3** | 94.82 | 95.88 | 96.78 | 97.59 | 98.09 | 98.92 |
| **4** | 91.24 | 92.98 | 94.36 | 95.60 | 96.59 | 98.11 |
| **5** | 87.15 | 89.79 | 91.73 | 93.42 | 94.79 | 96.99 |
| **6** | 81.37 | 85.55 | 88.32 | 90.70 | 92.57 | 95.50 |
| **7** | 74.06 | 79.28 | 83.63 | 86.62 | 88.74 | 92.25 |
| **8** | 61.42 | 67.57 | 74.49 | 78.63 | 81.38 | 84.80 |
| **9** | 40.75 | 46.54 | 53.59 | 58.91 | 60.47 | 58.83 |

Table 4.7: Ten element antenna arrays. Percentage of available angular region when SINR threshold is greater than -35 dB. AE is operating in beam forming / null steering mode. L1 frequency band.

| No. of interfering signals | Antenna Array | | | | | |
|---|---|---|---|---|---|---|
| | A4 | B5 | B6 | A5 | B7 | B8 |
| **0** | 100.00 | 100.00 | 100.00 | 100.00 | 100.00 | 100.00 |
| **1** | 98.44 | 98.74 | 99.01 | 99.21 | 99.38 | 99.69 |
| **2** | 96.00 | 96.82 | 97.50 | 97.99 | 98.35 | 99.14 |
| **3** | 93.08 | 94.47 | 95.70 | 96.48 | 97.06 | 98.37 |
| **4** | 88.29 | 90.51 | 92.53 | 93.88 | 94.92 | 96.94 |
| **5** | 83.32 | 86.57 | 89.29 | 91.12 | 92.57 | 95.34 |
| **6** | 76.71 | 81.08 | 84.63 | 87.26 | 89.37 | 93.15 |
| **7** | 69.58 | 74.70 | 78.93 | 82.30 | 84.71 | 89.19 |
| **8** | 58.39 | 64.09 | 68.21 | 72.05 | 75.42 | 81.99 |
| **9** | 41.37 | 45.88 | 49.47 | 52.83 | 56.08 | 62.05 |

Table 4.8: Ten element antenna arrays. Percentage of available angular region when SINR threshold is greater than -35 dB. AE is operating in beam forming / null steering mode. L2 frequency band.

# CHAPTER 5

# SIX INCH HIGH GEOMETRIES

The purpose of this chapter is to determine how to distribute the antenna elements given a non-planar convex hemispherical surface of radius six inches. Three types of surface distributions are investigated. A one ring uniform distribution with a reference elements placed at the top of the hemisphere and the remaining elements distributed uniformly along the bottom of the hemisphere. A two ring distribution with a reference element placed at the top of the hemisphere with the remaining elements located along both the bottom or outer ring of the hemisphere and on an inner ring of height 4.24 inches. Moreover, a second two ring distribution will also be studied where there is an inner ring height of 3 inches and and the reference element and remaining elements are distributed similarly as above. It will be shown that it is best to distribute the antenna elements along two rings with an inner ring height of 4.24 inches. Also, if the AE is operating in simple power minimization mode, there is a point of diminishing returns in AJ performance that is reached at twelve elements. However, if the antenna electronics is operating in beam forming / null steering mode, the addition of more elements always leads to an improvement in AJ performance. Therefore, one should fill the antenna array aperture as full as possible to attain the best performance.

## 5.1 Seven Element Antenna Arrays

First, to set a baseline for the six inch high surface, five seven element antenna arrays are investigated first. Figures 5.1 through 5.5 show the various element distributions. Antenna array B4 shown in Figure 5.1 below has seven antenna elements with the reference element placed at the top of the hemisphere and the remaining elements distributed uniformly along the bottom of the hemisphere. Antenna array C1 (Figure 5.2) is a seven element antenna array with the reference element placed at the top of the hemisphere and the remaining six elements distributed non-uniformly on the bottom of the hemisphere. Moreover, antenna arrays C2 (Figure 5.3), C3 (Figure 5.4), and C4 (Figure 5.5) are two ring distributions where the reference element is distributed at the top of the hemisphere three elements distributed similarly along the bottom of the hemisphere and three elements with different distributions along an inner ring of height 4.24 inches.

We found that all five antenna arrays have similar performance. Thus for this seven element non-planar antenna, element distribution does not have any significant effect on its AJ performance. As an illustration, Figures 5.22 and 5.23 show the performance of the five antenna arrays at L1 and L2 frequencies, respectively, in the presence of one to six interfering signals when the AE is operating in the simple power minimization mode. It is important to note that as there is an increase in the number of jammers the overall performance of the antenna arrays begins to degrade. One can see that all five of the antenna arrays have similar performance.

Tables 5.1 and 5.2 show the percentage available angular region for the L1 and L2 bands, respectively, when the output SINR threshold is greater than -35 dB for a given number of jammers ranging from an interference free environment up to six interfering signals. The antenna electronics is operating in simple power minimization mode. It is seen in both Tables 5.1 and 5.2 that the two one ring distributions (antenna arrays B4 and C1) yield better performance over the three two ring distributions (antenna arrays C2, C3, and C4) for five or less interfering signals. For six interfering signals, all antenna arrays have similar performance with antenna array C4 exhibiting a marginal advantage. Also, it is noted that antenna array C2 exhibits the worst overall performance.

Figures 5.24 and 5.25 show the performance of the five antenna arrays when the AE is operating in a beam forming/null steering mode. Again, one can draw the same conclusions that all five antennas have similar AJ performance. If one compares the results in these figures with those in Figures 5.22 and 5.23, he or she can notice that beam forming/null steering AE performs much better than the AE operating in simple power minimization mode, as expected. This is especially true for five or less incident jammers. For six incident interfering signals, AE operating in the two modes have similar performance because the system is fully constrained in that the antenna has only seven elements.

Tables 5.3 and 5.4 show the percentage available angular region when the AE is operating in beam forming / null steering mode at the L1 and L2 carrier frequencies, respectively. All other parameters are the same as in Tables 5.1 and 5.2. It is shown that for both the L1 and L2 bands that all five antenna arrays have very similar performance for a given number of interfering signals. However, when the array is operating in a harsh signal environment and is fully constrained, antenna array C4 yields slightly better performance.

## 5.2 One Ring Uniform Distributions

As a result of observing that the element distribution of the seven element array did not have a significant effect on its AJ performance, we further investigate the effect of increasing elements for the one ring uniform distribution. Figures 5.6 though 5.9 show the studied antenna arrays, which have the reference element located at the top of the hemisphere and the remaining elements distributed uniformly along the bottom of the hemisphere. Antenna arrays C5, C6, C7, and C8 have 8, 9, 10 and 11 elements, respectively, and are shown below in Figures 5.6, 5.7, 5.8, and 5.9, respectively. The results for antenna array B4 are also included.

It was found that increasing the number of elements in the antenna array significantly improves the AJ performance of the antenna array. This is especially true when the antenna array is operating in beam forming / null steering mode. As an illustration, figures 5.26 and 5.27 show the performance of the five antenna arrays at L1 and L2 frequencies, respectively, in the presence of five to ten interfering signals when the AE is operating in the simple power minimization mode. The performance of the antenna arrays degrades with an increase in the number of interfering signals. Note that in the presence of N jammers, one needs at least N+1 antenna elements for good AJ performance. Also, increasing the number of antenna elements to greater than N+1 elements results in improved AJ performance.

Tables 5.5 through 5.6 show the percentage available angular region at the L1 and L2 carrier frequencies, respectively, for the when the output SINR exceeds a threshold of -35 dB in the presence of zero to ten interfering signals. The same conclusions can be drawn from both tables in that the the percentage available angular region degrades as one increases the number of interfering signals for a given antenna array. Also, one observes that performance increases when the number of antenna elements increases for a given number of jammers.

Figures 5.28 and 5.29 show the performance of the five antenna arrays at L1 and L2 frequencies, respectively, in the presence of five to ten interfering signals when the AE is operating in beam forming / null steering mode. The same conclusions are drawn in this case as with simple power minimization; however, the improvement of the beam forming / null steering antenna arrays is much more significant, as expected. One still needs N+1 antenna elements to null N jammers and performance degrades as the number of interfering signals increases. However, the performance degrades much slower than in simple power minimization. Also, as pointed out above, one can increase the number of antenna elements to make up for the loss in performance. Therefore, one should increase the amount of antenna elements in the array resulting in improved AJ performance.

Tables 5.7 and 5.8 show the percentages when the AE is operating in beam forming / null steering mode in the L1 and L2 bands, respectively. The same conclusions can be drawn here as for simple power minimization that an increase in the number of jammers leads to a decrease in the the percentage available angular region. Moreover, one observes that performance improved when the number of antenna elements increases for a given number of jammers. Comparing Tables 5.7 and 5.8 with Tables 5.5 and 5.6 one again observes that a significant performance improvement can be achieved when AE is operating in the beam forming / null steering mode.

## 5.3 Comparison of One Ring and Two Ring Distributions

One has observed that increasing the number of antenna elements yields improved AJ performance; however, now the question becomes how to distribute these elements. Due to the amount of surface area resulting from the six inch high surface, one may physically place more antenna elements on the surface and in different distributions. As a result, we distributed a number of antenna elements along an inner ring height of 4.24 inches. The antenna arrays introduced in this section have nine, ten, and eleven elements respectively with a two ring distribution and compared to the nine (antenna array C6), ten (antenna array C7) , and eleven (antenna array C8) element one ring distributions. Antenna array C9 (Figure 5.10) has nine elements with the reference element distributed at the top of the hemisphere, two elements distributed along the inner ring and the remaining six elements placed along the outer ring along the bottom of the hemisphere. Antenna array B8 (Figure 5.11), introduced in Chapter 4 has ten elements with one element at the top, three elements along the inner ring and six elements along the outer ring. Likewise, antenna array C10 (Figure 5.12) has eleven elements with one at the top, three along the inner ring and seven along the outer ring.

From the results it shows that as the array begins to become fully constrained (as N jammers approaches N+1 antenna elements), the two ring distribution is superior compared to the one ring distribution. Therefore, one should distribute the antenna elements for the six inch high surface on two rings. This result is observed in the following figures. Figures 5.30 and 5.31 show the performance of the six antenna arrays at L1 and L2 frequencies, respectively, in the presence of five to ten interfering signals when the AE is operating in the simple power minimization mode. One observes that two ring distribution is outperforming the one ring distribution as the array becomes fully constrained. For the case of eight jammers at L1 and L2 antenna array C9 is performing better than antenna array C6. Likewise, for eight and nine jammers, antenna array B8 outperforms C7 and the same for antenna array C10 outperforming C8 up to ten interfering signals.

The percentage of available angular region for which the output SINR exceeds a threshold of -35 dB in the presence of zero to ten interfering signals are tabulated below. Tables 5.9 and 5.10 show the percentages when the AE is operating in simple power minimization mode at the L1 and L2 carrier frequencies, respectively. In Table 5.9, one notices that the one ring distributions are performing better than their two ring complements up to L-3 interfering signals, where L is the number of antenna elements. Antenna array C6 is performing better than antenna array C9 for six or less interfering signals, antenna array C7 outperforms antenna array B8 for eight or less jammers, and antenna array C8 yields better performance compared to antenna array C10 for nine or less interfering signals. However, for the more harsh signal environments (L-2 interfering signals and above) the two ring distributions yield better performance. Similar results are observed for the L2 band (Table 5.10), in that the two ring distributions have better performance as the number of interfering signals increases and begins to completely constrain the antenna array.

Figures 5.32 and 5.33 show the performance of the six antenna arrays at L1 and L2 frequencies, respectively, in the presence of five to ten interfering signals when the AE is operating in the beam forming / null steering mode. One observes the same results as for the simple power minimization case. The two ring distribution of a given number of antenna elements is performing better than its one ring counterpart in both the L1 and L2 bands.

Tables 5.11 and 5.12 show the percentages when the AE is operating in beam forming / null steering mode at the L1 and L2 carrier frequencies, respectively. All other parameters are the same as in Tables 5.9 and 5.10. In both tables, one observes that the two ring distribution of a select number of antenna elements yields improved performance over the one ring distribution for a given number of jammers. Antenna array C9 outperforms antenna array C6, antenna array B8 performs better than antenna array C7, and antenna array C10 exhibits better performance than antenna array C8. Therefore, if the AE is operating in the beam forming / null steering mode it is better to distribute the elements in a two ring distribution to yield performance improvement for antennas operating in any interference signal environment. As expected, beam forming / null steering significantly outperforms simple power minimization and can be seen by comparing Tables 5.11 and 5.12 with Tables 5.9 and 5.10.

## 5.4 Two Ring Distributions

It has been established that distributing the antenna elements on two rings yields better performance. Now we are going to study the effect increasing the number of antenna elements and see if there is a point of diminishing returns. Also, we are going to investigate this effect as well as studying the effect of moving the inner ring further away from the reference element to an inner ring height of three inches. The effect of moving the inner ring elements further away from the reference element results in less mutual coupling between the reference element and inner ring elements. When the antenna array AE is operating in simple power minimization mode, in the absence of interference, the antenna response of the antenna array is the response of the reference element due to fact it is the only element remaining on with available degrees of freedom to null incoming interference signals incident upon the array. Therefore, for the simple power minimization case the antenna array should perform better in the presence of a low number of interfering signals. However, as the antenna array approaches a complete constraint due to the number of interfering signals, this may or may not result in improved performance. First, we are going to study the two ring distributions with an inner ring height of 4.24 inches.

### 5.4.1 Inner Ring Height of 4.24 Inches

The antenna arrays introduced in this section are shown below in Figures 5.13 through 5.16. Antenna arrays C9, B8, and C10 from the previous section will also be included in drawing the conclusion. Again all antenna arrays in this section have a reference element placed at the top of the hemisphere and the remaining elements placed both along an inner ring with height of 4.24 inches and on the outer ring along the bottom of the hemisphere. Antenna array C11 (Figure 5.13) has twelve elements with one element at the top, three elements along the inner ring and eight elements along the outer ring. Antenna array C12 (Figure 5.14) has thirteen elements, one at the top, four along the inner ring and eight elements on the outer ring. Antenna array

C13 (Figure 5.15) has fourteen elements with one at the top, five along the inner ring and eight distributed along the outer ring. Finally, antenna array C14 (Figure 5.16) has fifteen elements with one at the top, six along the inner ring and eight elements along the outer ring.

For the results, the same rules apply as before that one needs N+1 antenna elements to null N jammers, and that performance degrades with an increase in the number interfering signals. However, there is not always an improvement in AJ performance with an increase in the number of antenna elements with respect to the AE operating in simple power minimization mode. There is still always an improvement in AJ performance with an increase in the number of antenna elements with respect to AE operating in the beam forming / null steering mode. When the AE is operating in simple power minimization mode for N+1 or more antenna elements in the array, the AJ performance is more or less independent of the number of antenna elements. Figures 5.34 and 5.35 illustrate this below, and show the performance of the seven antenna arrays at L1 and L2 frequencies, respectively, in the presence of seven to fourteen interfering signals when the AE is operating in the simple power minimization mode. As one can see, the AJ performance is similar for both the L1 and L2 frequency bands as long as one has N+1 antenna elements. Actually one also observes in the figures that before the array is becoming fully constrained, antenna array C11 is outperforming antenna arrays with a larger number of elements.

This result can further be seen in Tables 5.13 and 5.14, which show the percentage available angular region for the L1 and L2 bands, respectively, when the AE is operating in simple power minimization mode. As one increases the number of elements, the AJ performance improves for nine or less interfering signals up to the twelve elements (antenna array C11) and then it saturates and actually becomes worse for a greater number of elements. For ten and eleven interference signals, the antenna arrays that are able to operate in the signal environment have similar performance. The point of diminishing returns with the AE operating in simple power minimization mode is achieved for twelve elements. In Table 5.14, one observes similar results in that the antenna array C11 exhibits the best performance up to eleven interfering signals, except for ten interfering signals. One observes that the performance degrades for a greater number of antenna elements, and this result is due to a larger number of antenna elements being distributed on the inner ring causing a larger amount of mutual coupling with the reference element.

Figures 5.36 and 5.37 show the performance of the seven antenna arrays at L1 and L2 frequencies, respectively, in the presence of seven to fourteen interfering signals when the AE is operating in the beam forming / null steering mode. From the figure results, one observes that increasing the number of antenna elements yields a significant AJ performance improvement. As expected, the antenna arrays with the AE operating in the beam forming / null steering mode perform much better as compared to the AE operating in the simple power minimization mode. The available angular region increases by at least 15% over simple power minimization. This leads one to the conclusion that as long as the AE is operating in the beam forming / null steering mode one can keep increasing the number of elements resulting in improved AJ performance. Note the addition of more antenna elements will result in an increase of mutual coupling effects; however, the antenna array is still constrained to point a beam in the direction of the desired signal and one should still see an improvement in the AJ performance.

Again, for completeness, the tables indicating the percentage of available angular region for which the output SINR exceeds a threshold of -35 dB are included. Tables 5.15 and 5.16 show the percentages when the AE is operating in beam forming / null steering mode at the L1 and L2 carrier frequencies, respectively. In both tables, one observes similar results characteristic of the AE operating in the beam forming / null steering mode, in that the addition of antenna elements always leads to improved AJ performance. Therefore, one can pack the antenna aperture as much as possible with antenna elements to achieve a greater attainable performance. As a result, the limiting factors of attainable AJ performance are the physical size of the individual antenna elements and hardware cost (antenna and antenna electronics). It is important to note that the physical size of the individual antenna elements can be reduced by selecting a higher dielectric constant substrate [2]. However, reducing the size of individual elements results in poorer performance with respect to bandwidth as well as antenna gain.

### 5.4.2 Inner Ring Height of 3 Inches

All of the antenna array included in this section have a single reference element located at the top of the hemisphere, with remaining elements distributed along a three inch high inner ring or along the outer ring along the bottom of the hemisphere. The antenna arrays are shown in Figures 5.17 through 5.21. Antenna arrays C15(Figure 5.17), C16(Figure 5.18),C17(Figure 5.19), C18(Figure 5.20), and C19(Figure 5.21) have nine, ten, eleven, twelve, and thirteen elements, respectively, and have their elements distributed exactly the same as their two ring counterparts with an inner ring height of 4.24 inches.

The performance results are very similar compared to the previous two ring distributions above. When the AE is operating in simple power minimization mode, shown in Figures 5.38 and 5.39 for the L1 and L2 bands, respectively, in the presence of five to twelve interfering signals, that as long as the antenna array contains more than N+1 antenna elements the AJ performance is more or less independent of the number of elements. All antenna arrays have similar performance.

Tables 5.17 and 5.18 show the percentage of available angular region for which the output SINR exceeds -35 dB for the L1 and L2 bands, respectively, when the AE is operating in simple power minimization mode. For the L1 band (Table 5.17), the AJ performance minimally increases from nine up to twelve elements for a given number of interfering signals. It is also shown that antenna array C18 has better or similar performance compared to antenna array C19 up to ten interfering signals. For eleven interfering signals, antenna array C19 performs better than antenna array C18, which is fully constrained. This same results holds true in Table 5.18 (L2 band). Performance slightly improves for a given number of interfering signals when the number of antenna elements is increased from nine to twelve elements. The thirteen element antenna array C19 has similar performance to the antenna array C18. Therefore, one would select the antenna array with less number of elements that does not make a difference in performance. Furthermore, it was mentioned previously that moving the elements along the inner ring further away from the would provide less mutual coupling for a low number of interfering signals and this result can be observed in comparing Tables 5.17 and 5.20 with its two ring complement viewed in Tables 5.13 and 5.16. This does show that there is improved performance in the simple power minimization case for a low number of interfering signals; however, we are more concerned of how the antenna arrays perform in harsh signal environments.

The instance when the AE is operating in beam forming / null steering mode, shown in Figures 5.40 and 5.41 for the L1 and L2 bands, respectively, in the presence of five to twelve interfering signals. There is a significant advantage as one increases the number of elements. In fact, it is a two fold advantage, where one possesses the ability to null more jammers while yielding improved AJ performance.

Tables 5.19 and 5.20 show the percentage available angular region results when the antenna electronics is operating in beam forming / null steering mode. All other parameters are the same as in Tables 5.17 and 5.18. As expected, it is shown that increasing the number of elements leads to a greater performance improvement. Also, as expected, the beam forming / null steering mode outperforms simple power minimization and can be seen by comparing Tables 5.19 and 5.20 with Tables 5.17 and 5.18.

## 5.5 Comparison of 12 Element Antenna Arrays

In order to get a better idea of how the two antenna arrays match up with respect to AJ performance, we will compare the performance of the different twelve element antenna array two ring distributions. This will be antenna arrays C11 (Figure 5.13) with an inner ring height of 4.24 inches and C18(Figure 5.20) with an inner ring height of three inches.

Figures 5.42 and 5.43 compare the performance of antenna arrays C11 and C18 at L1 and L2 carrier frequencies, respectively. The AE is operating in simple power minimization mode and in the presence of six to eleven interfering signals. Note that at L1 carrier frequency the two antenna arrays have similar performance; whereas, at L2 carrier frequency, antenna array C11 has slightly better performance. Therefore, the two ring distribution with an inner ring height of 4.24 inches exhibits better AJ performance, and one should select this distribution if one wants to achieve maximum AJ performance.

This result is further seen in Tables 5.21 and 5.22, which show the percentage available angular region for which the output SINR exceeds -35 dB when the antenna is operating in the presence of zero to eleven interfering signals. The AE is operating in simple power minimization mode. In Table 5.21, one sees that antenna array C18 has slightly better performance up to eight interfering signals and including ten interfering signals. However, as the antenna arrays are fully constrained antenna array C11 has better performance. For the L2 band (Table 5.22), antenna array C11 has better performance for any given number of interfering signals. Therefore, one should select antenna array C11 to provide maximum AJ performance operating in harsh signal environments.

Figures 5.44 and 5.45 show the performance of antenna arrays C11 and C18 when the AE is operating is the beam forming / null steering mode. All other parameters are the same as in Figures 5.42 and 5.43, respectively. Again from the results in the two figures, one can conclude that antenna array C11 is a better choice. This is especially true for operation in the L2 band. Therefore, it is shown that antenna array C11 and the two ring distribution with inner ring height of 4.24 inches is the recommended configuration.

This result is further supported by Tables 5.23 and 5.24, which show the performance percentages when the AE is operating in the beam forming / null steering mode at the L1 and L2 carrier frequencies, respectively. It is shown that antenna array C11 outperforms C18 in every incident interfering signal scenario. Thus, validating the advantage to distributing the elements in a two ring configuration with an inner ring height of 4.24 inches.

## 5.6 Comparison of 7 and 12 Element Antenna Arrays

We will now show the the performance advantage one can obtain from going from a seven element to twelve element antenna array. The seven element antenna array selected is antenna array C4 (Figure 5.5), which had the best AJ performance in the presence of six interfering signals, although it was very slight. Moreover, antenna array C11(Figure 5.13) is the selected twelve element antenna array.

The results are shown for the antenna arrays operating in simple power minimization mode in the presence of three to eight interfering signals in Figures 5.46 and 5.47 for the L1 and L2 bands, respectively. From the figures, as expected, one can see that antenna array C11 outperforms antenna array C4. This is especially true in the presence of seven and eight interfering signals. However, it should be noted that antenna array C4 only has seven elements yielding the capability to null six interfering signals; whereas, antenna array C11 has twelve elements. Taking this into account, the performance improvement when the antenna is operating in simple power minimization mode is not very significant unless one is operating in a severe interference environment.

Tables 5.25 and 5.26 have been provided showing the percentage available angular region for the L1 and L2 bands, respectively, for which the output SINR is greater than -35 dB in the presence of zero to eleven interfering signals. The AE is operating in the beam forming / null steering mode. One notices that in the presence of interfering signals there is only a slight advantage achieved with increasing the number of elements from seven to twelve with only approximately 7% performance advantage at the L1 band and approximately 4% performance advantage at the L2 band in the presence of six interfering signals. Therefore, the addition of elements allows one to null more interfering signals; however, there is not a significant performance advantage that is achieved.

However, as one uses the AE operating in the beam forming / null steering mode there is a significant advantage in moving from seven to twelve elements as the the seven element antenna array becomes constrained. This result can be viewed in Figures 5.48 and 5.49 where the antenna electronics is operating in the beam forming / null steering mode in the presence of three to eight interfering signals at the L1 and L2 bands, respectively. There is approximately a 30% increase in AJ performance for six interfering signals. Therefore, it is highly recommended to operate in the beam forming / null steering mode.

Tables 5.27 and 5.28 are for the AE operating in beam forming / null steering mode. All other parameters are the same as in Tables 5.25 and 5.26. One views the significant improvement in AJ performance that is achieved when the seven element antenna array becomes fully constrained and the twelve element array still has spare degrees of freedom. In the presence of six interfering signals, twelve element antenna array C11 has an approximate 31% performance advantage at the L1 band and 27% performance advantage at the L2 band over seven element antenna array C4. Therefore, there is a two fold advantage by operating in the beam forming / null steering mode. One contains the capability to null more interfering signals, and one provides a significant improvement in AJ performance.

## 5.7 Chapter Summary

In this chapter, it was shown that for a six inch high hemispherical surface it is best to distribute the antenna elements along two rings, with the inner ring being 4.24 inches high, and the outer ring encircling the bottom of the hemisphere. It was also shown that one can improve the performance of the antenna arrays by increasing the number of elements. However, when the antenna electronics is operating in simple power minimization mode, one observed that the point of diminishing returns was at about twelve elements and antenna array C11 is the best choice. On the other hand, if the antenna array can be used with AE operating in beam forming / null steering mode, there is significant performance improvement provided by increasing the number of antenna elements. It was concluded that one should pack the aperture as much as possible with antenna elements leading to further performance improvement. Moreover, the limiting factors of attainable AJ performance are the physical size of the individual antenna elements and hardware cost (antenna and antenna electronics). It is important to note that the physical size of the individual antenna elements can be reduced by selecting a higher dielectric constant substrate [2]. However, reducing the size of individual elements results in poorer performance with respect to bandwidth as well as antenna gain. We have studied the six inch high geometry, which is a possibility for ship-board application; however, it would not be desirable to the aerodynamic profile of an aircraft due to its physical size. Next, we will study the performance of a two inch high surface, which maintains a curvature relative to a spherical surface of radius ten inches. As we saw previously, this surface will not yield the performance of a six inch high geometry; however, it could still yield better performance than a planar geometry.

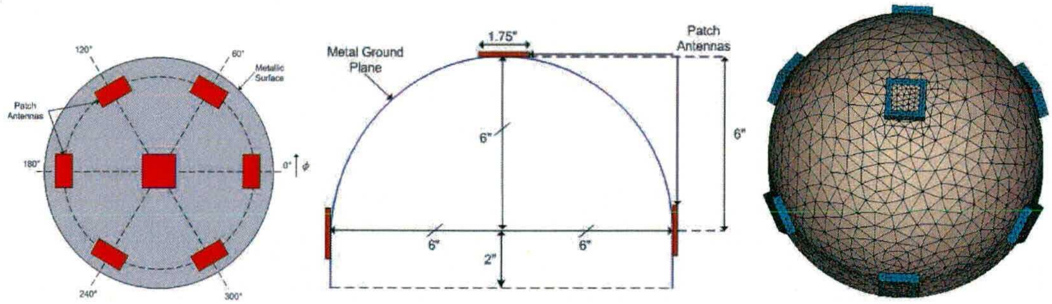


(a) Top Down View (b) Side View (c) Gridded Surface

Figure 5.1: Antenna Array B4.

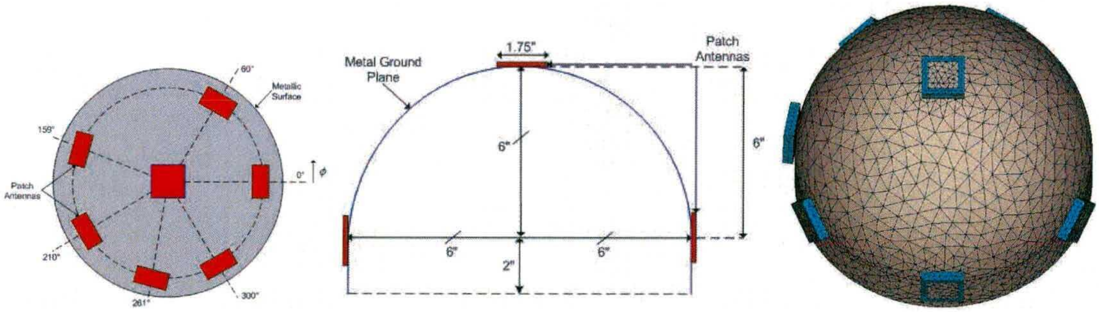


(a) Top Down View (b) Side View (c) Gridded Surface

Figure 5.2: Antenna Array C1.

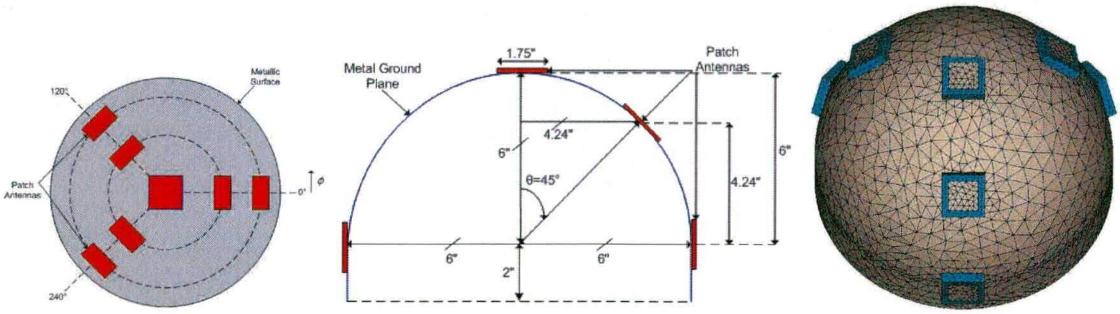


(a) Top Down View (b) Side View (c) Gridded Surface

Figure 5.3: Antenna Array C2.

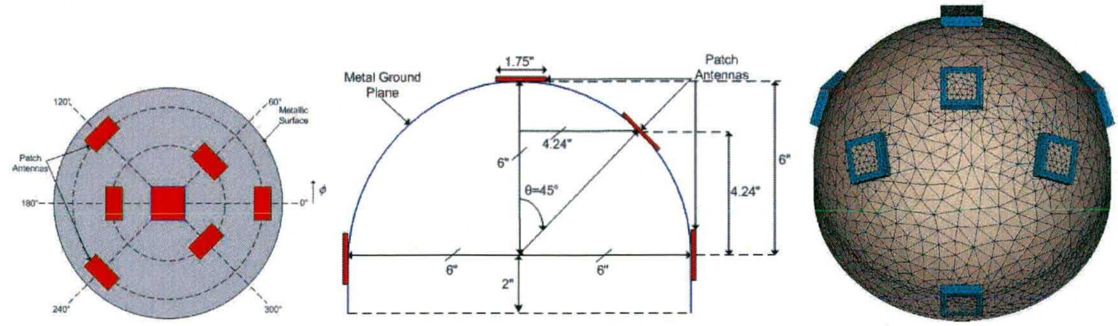

(a) Top Down View (b) Side View (c) Gridded Surface

Figure 5.4: Antenna Array C3.

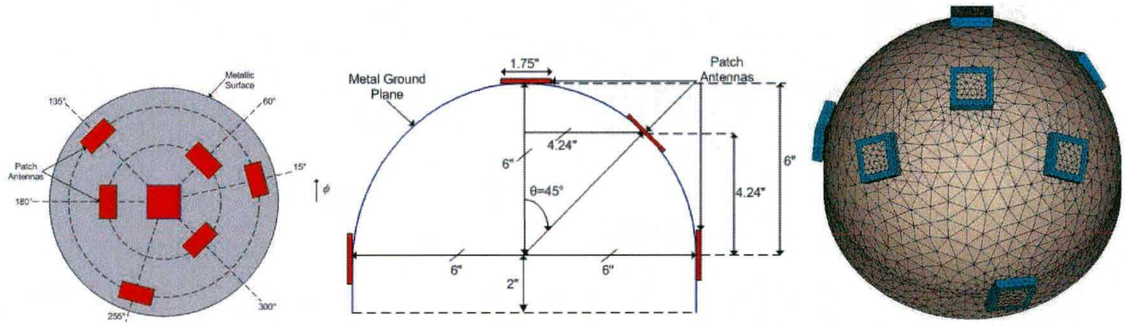

(a) Top Down View (b) Side View (c) Gridded Surface

Figure 5.5: Antenna Array C4.

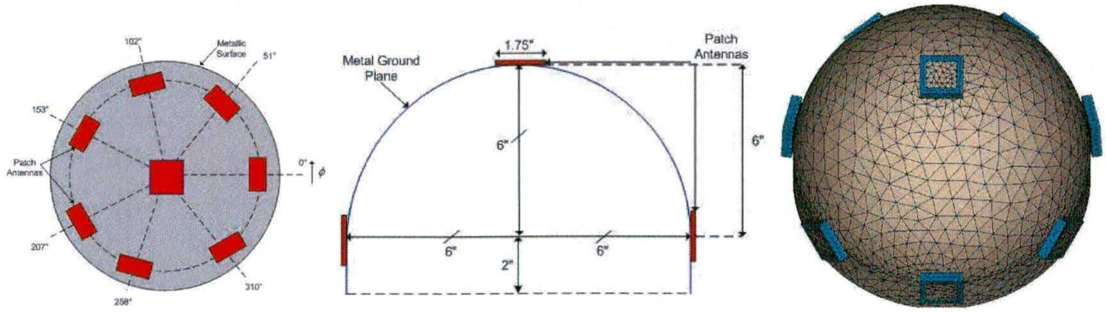

(a) Top Down View (b) Side View (c) Gridded Surface

Figure 5.6: Antenna Array C5.

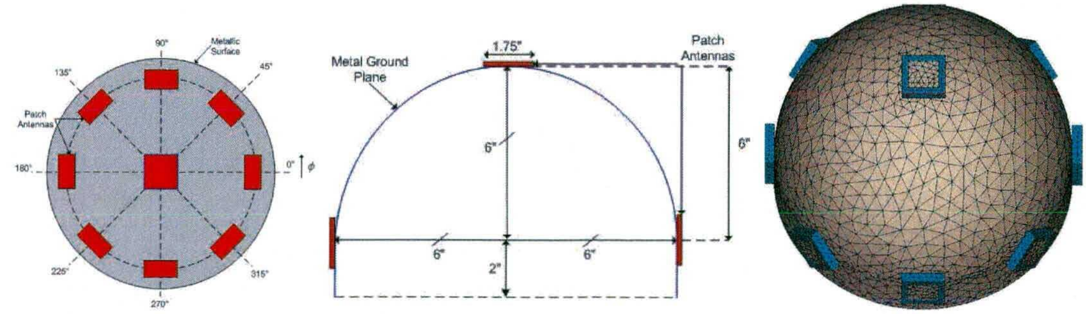


(a) Top Down View (b) Side View (c) Gridded Surface

Figure 5.7: Antenna Array C6.

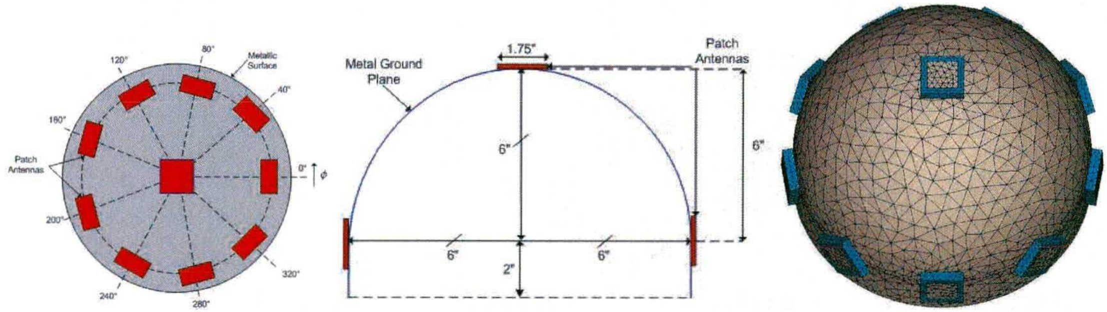


(a) Top Down View (b) Side View (c) Gridded Surface

Figure 5.8: Antenna Array C7.

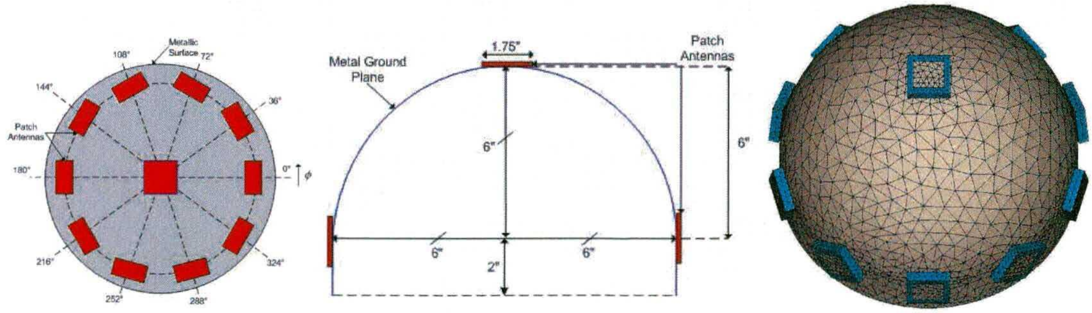


(a) Top Down View (b) Side View (c) Gridded Surface

Figure 5.9: Antenna Array C8.

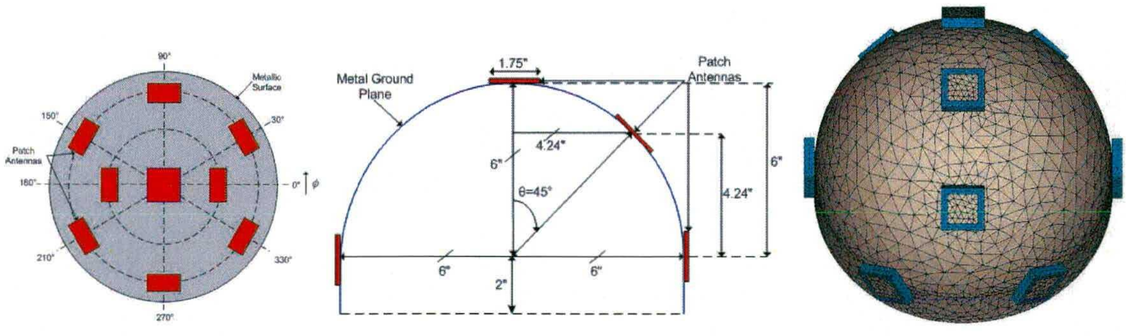


(a) Top Down View (b) Side View (c) Gridded Surface

Figure 5.10: Antenna Array C9.

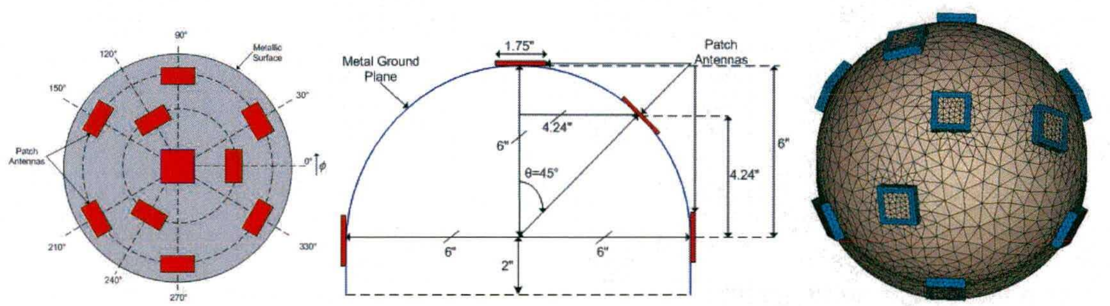


(a) Top Down View (b) Side View (c) Gridded Surface

Figure 5.11: Antenna Array B8.

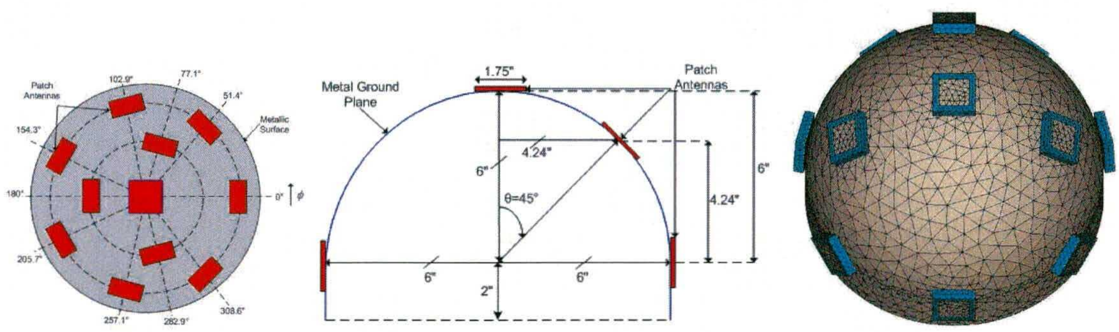


(a) Top Down View (b) Side View (c) Gridded Surface

Figure 5.12: Antenna Array C10.

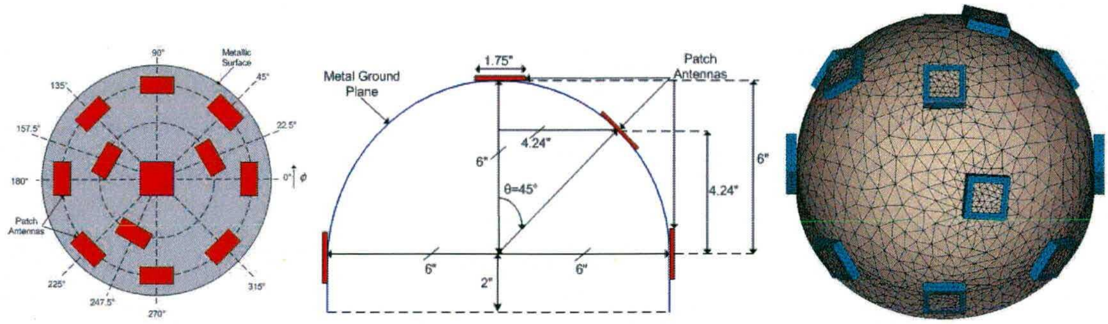


(a) Top Down View (b) Side View (c) Gridded Surface

Figure 5.13: Antenna Array C11.

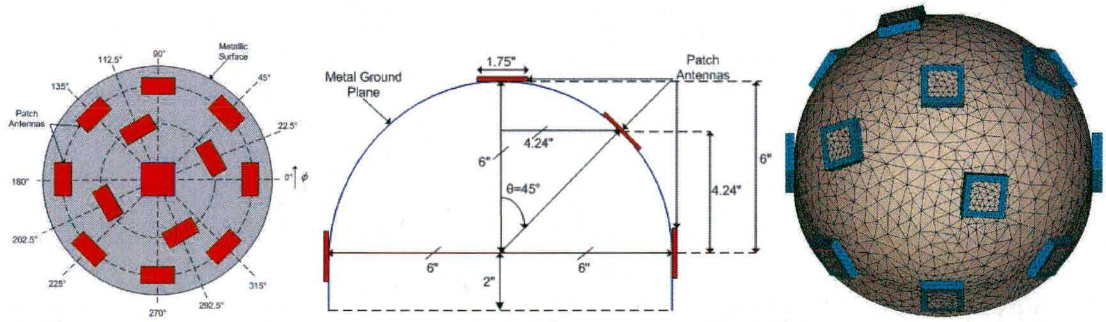


(a) Top Down View (b) Side View (c) Gridded Surface

Figure 5.14: Antenna Array C12.

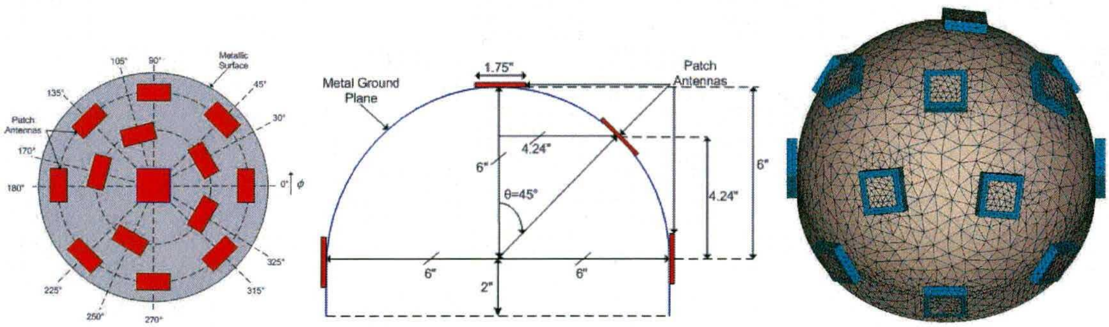


(a) Top Down View (b) Side View (c) Gridded Surface

Figure 5.15: Antenna Array C13.

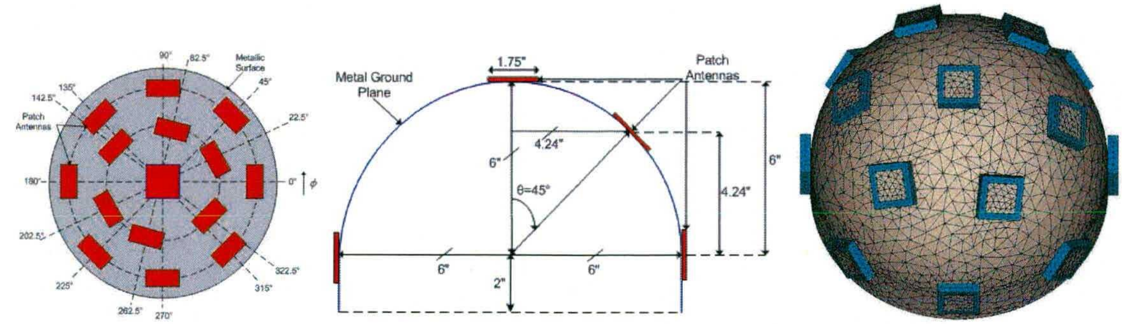


(a) Top Down View (b) Side View (c) Gridded Surface

Figure 5.16: Antenna Array C14.

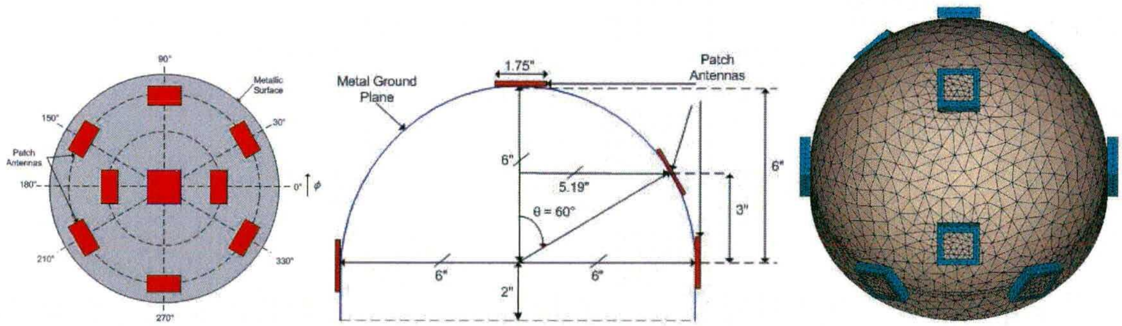


(a) Top Down View (b) Side View (c) Gridded Surface

Figure 5.17: Antenna Array C15.

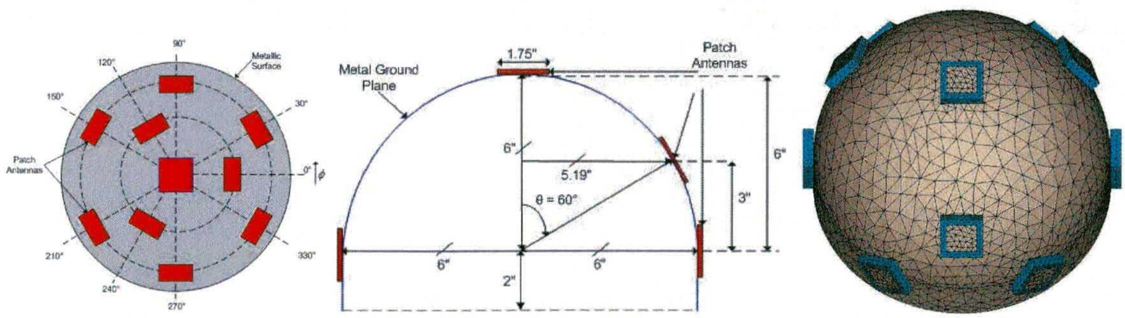


(a) Top Down View (b) Side View (c) Gridded Surface

Figure 5.18: Antenna Array C16.

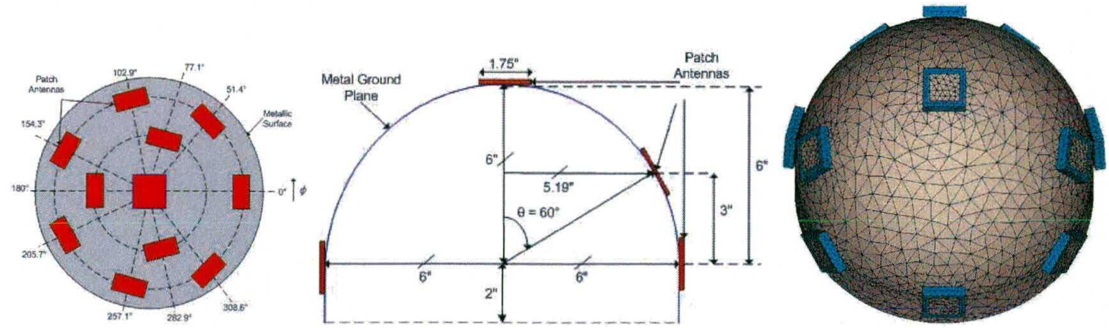


(a) Top Down View (b) Side View (c) Gridded Surface

Figure 5.19: Antenna Array C17.

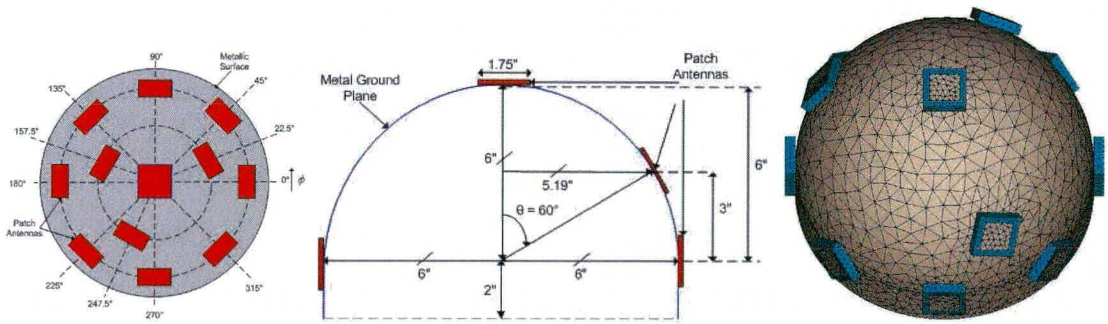


(a) Top Down View (b) Side View (c) Gridded Surface

Figure 5.20: Antenna Array C18.

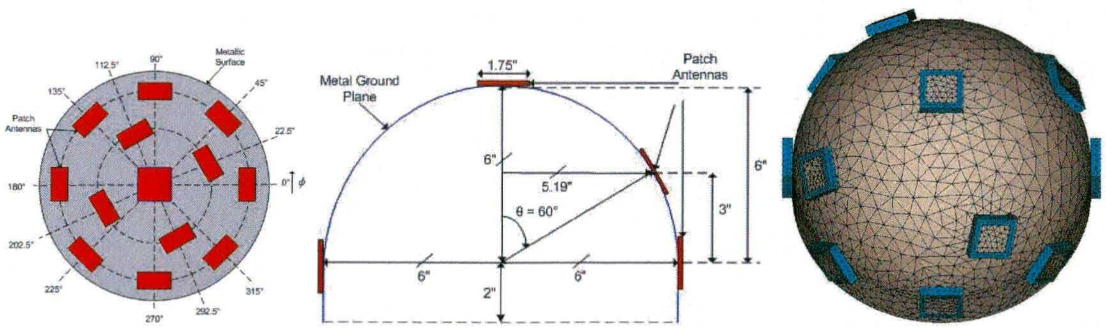


(a) Top Down View (b) Side View (c) Gridded Surface

Figure 5.21: Antenna Array C19.

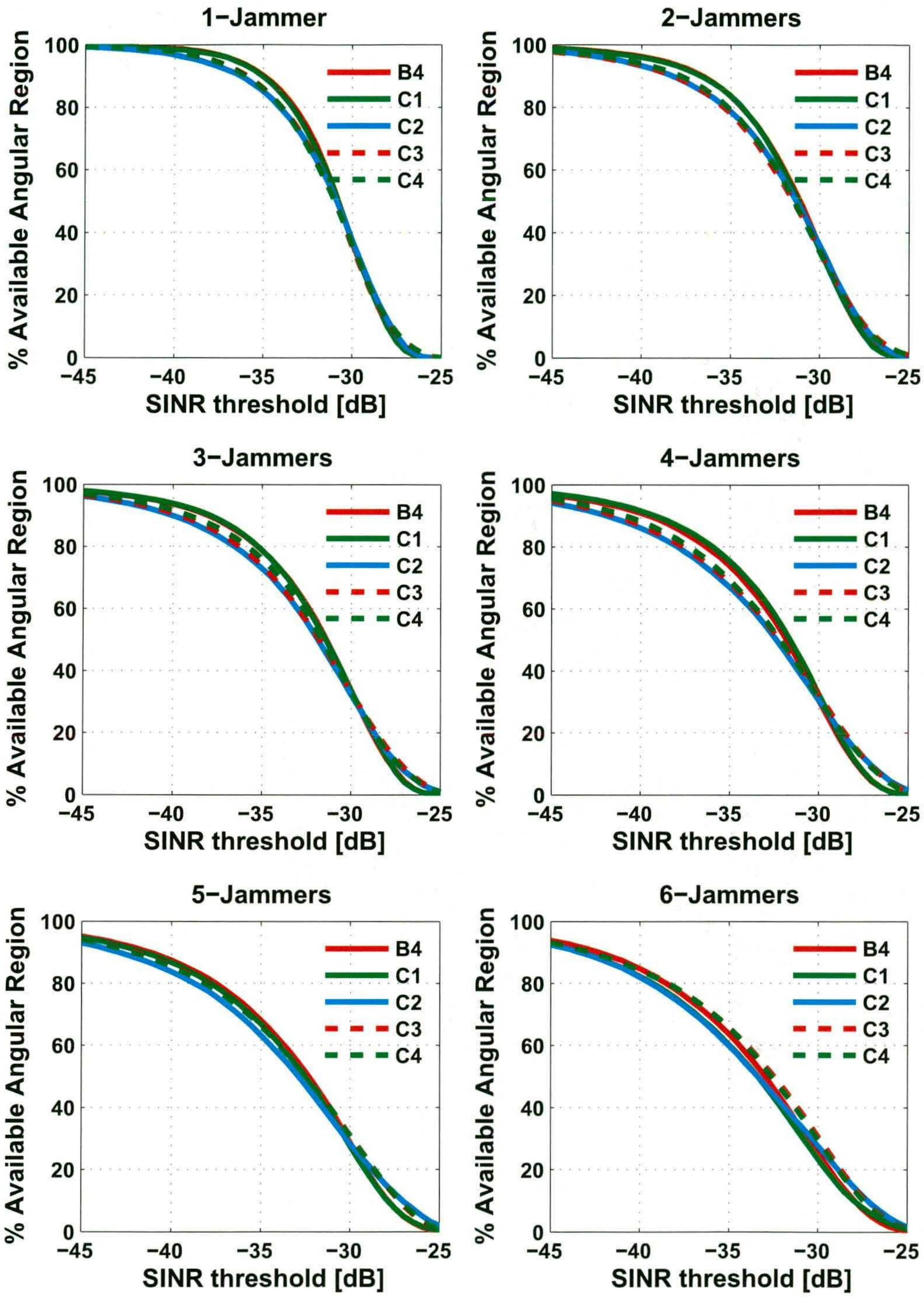


Figure 5.22: Performance of seven element antenna arrays in the presence of one to six interfering signals. AE is operating in simple power minimization mode. L1 frequency band.

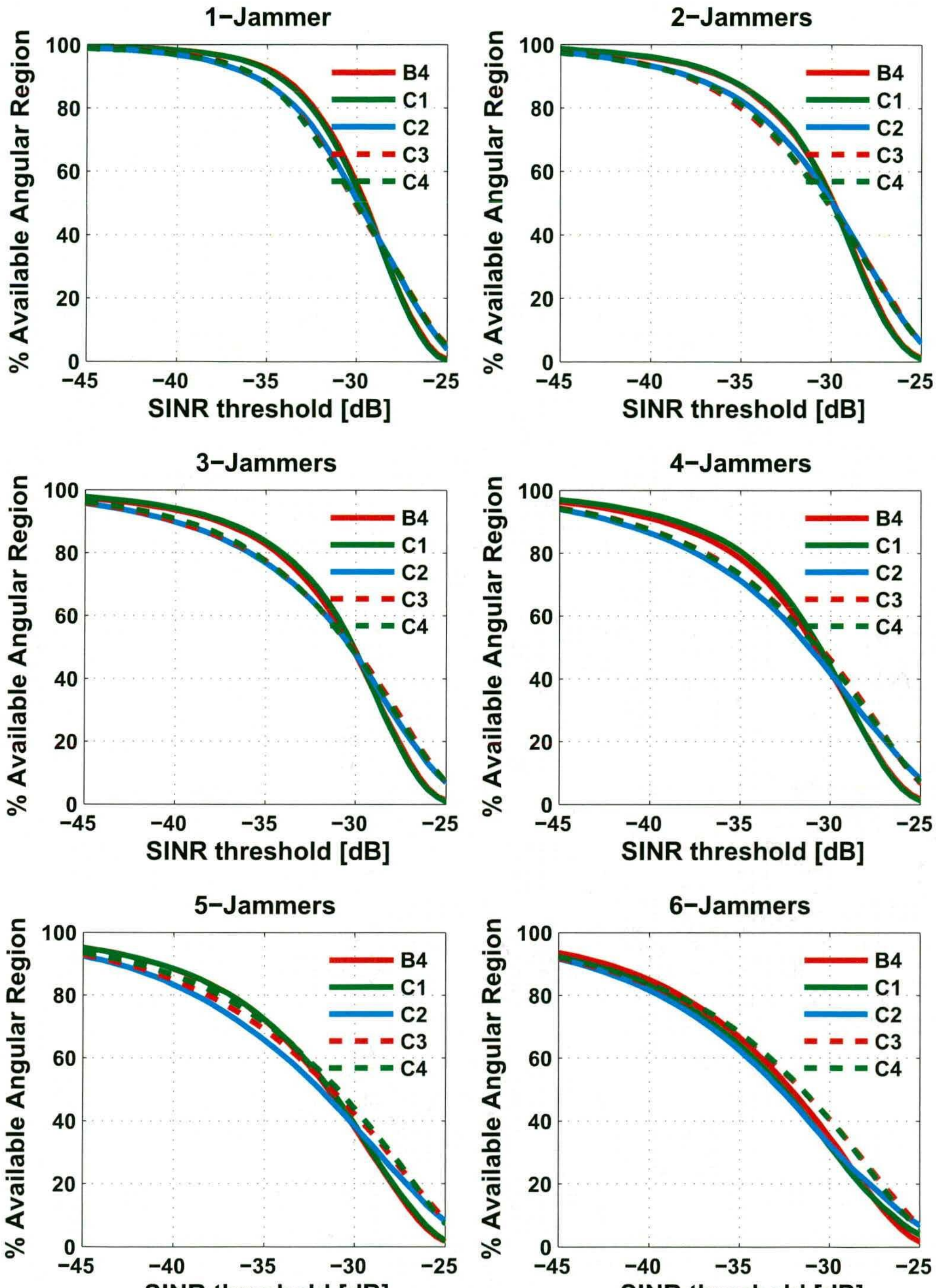


Figure 5.23: Performance of seven element antenna arrays in the presence of one to six interfering signals. AE is operating in simple power minimization mode. L2 frequency band.

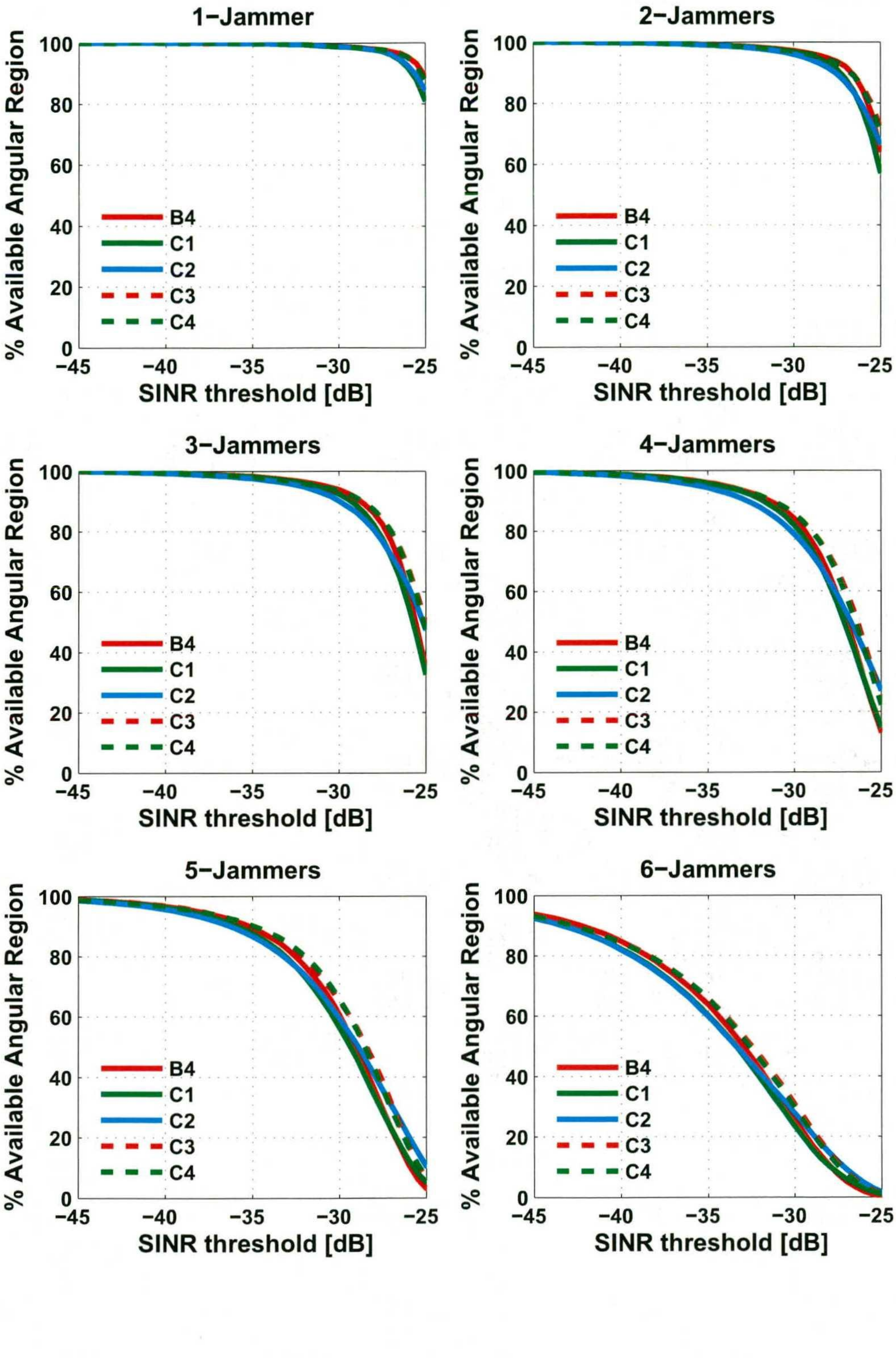


Figure 5.24: Performance of seven element antenna arrays in the presence of one to six interfering signals. AE is operating in beam forming / null steering mode. L1 frequency band.

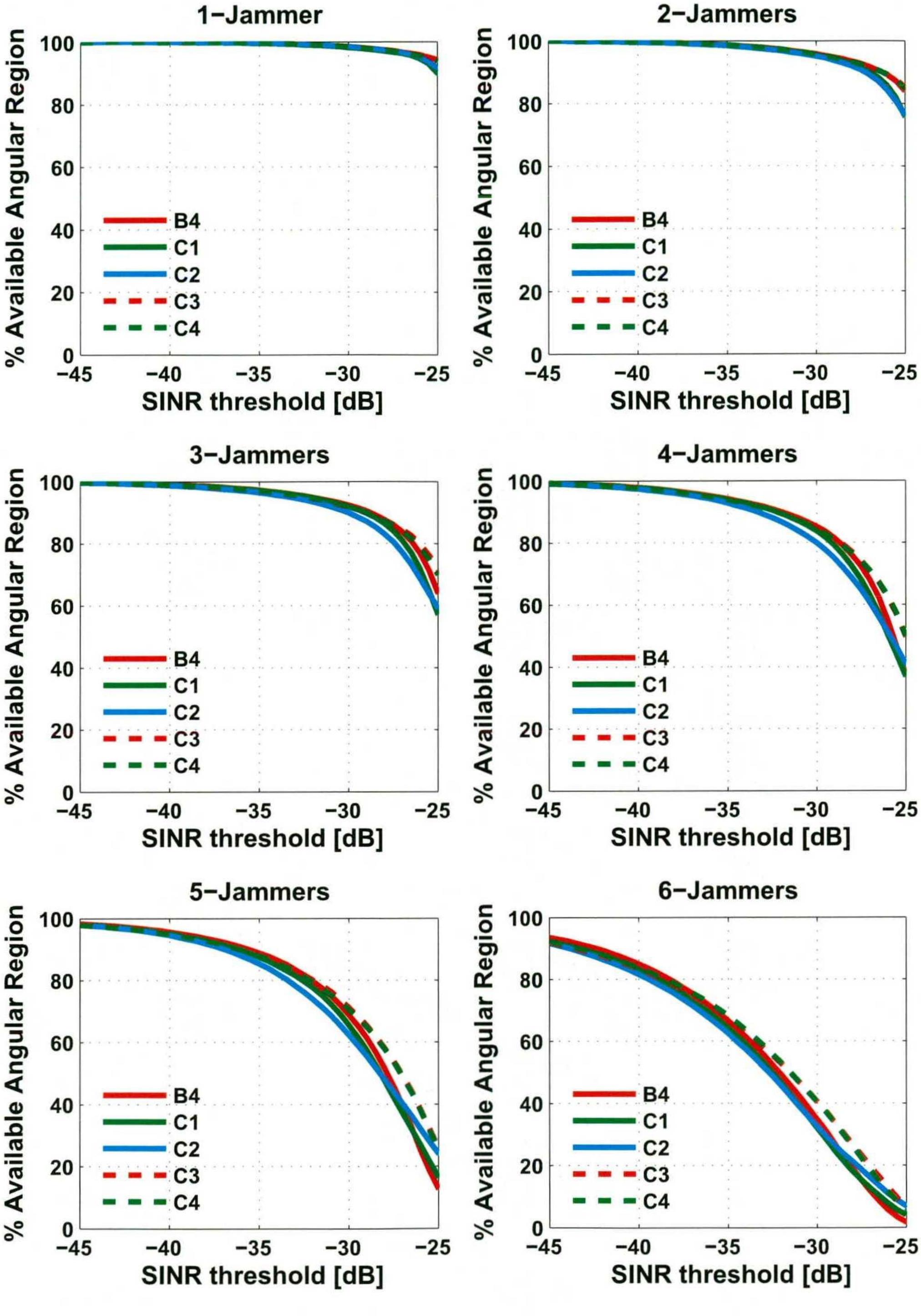


Figure 5.25: Performance of seven element antenna arrays in the presence of one to six interfering signals. AE is operating in beam forming / null steering mode. L2 frequency band.

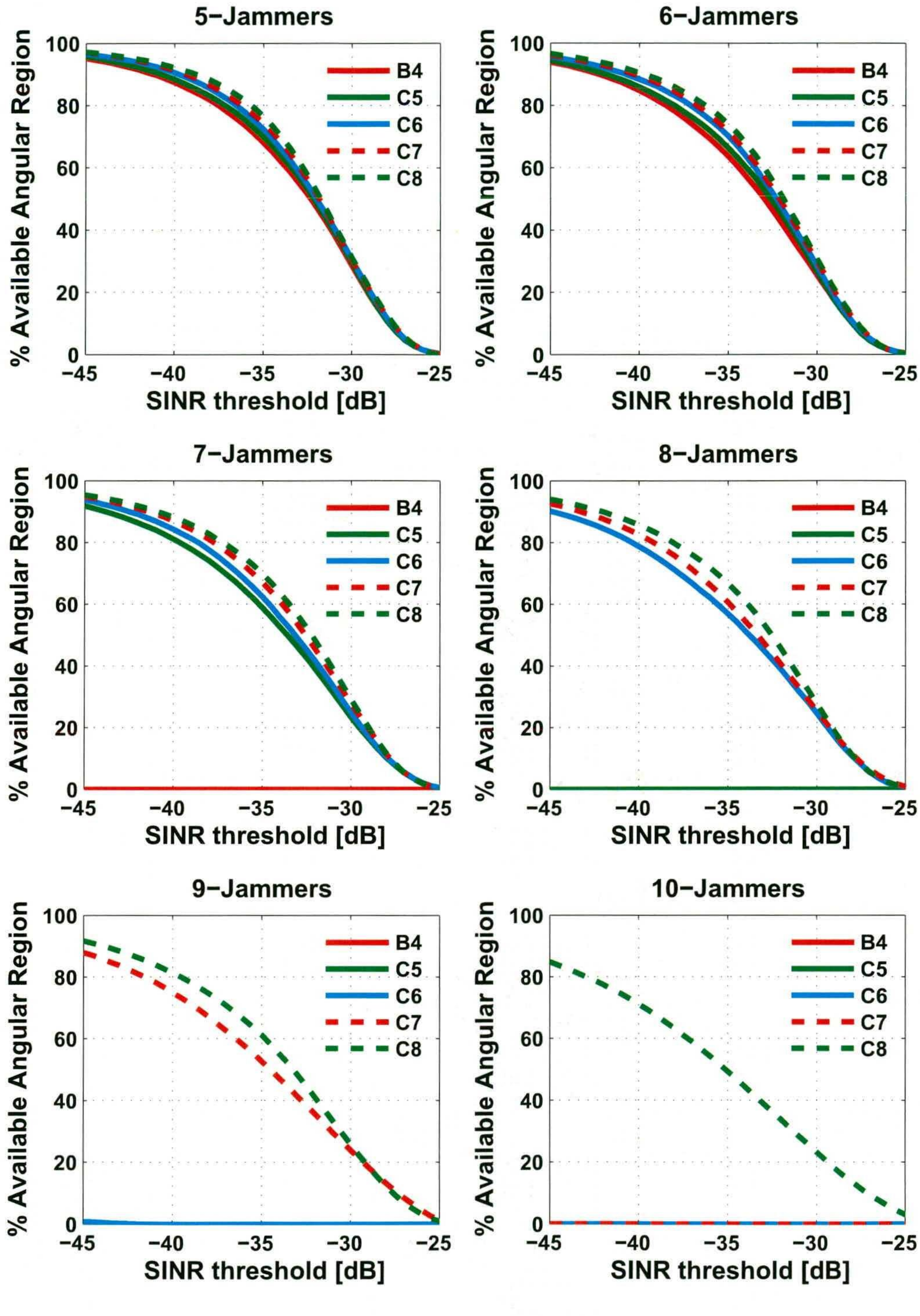


Figure 5.26: Performance of antenna arrays distributed uniformly along one ring in the presence of five to ten interfering signals. AE is operating in simple power minimization mode. L1 frequency band.

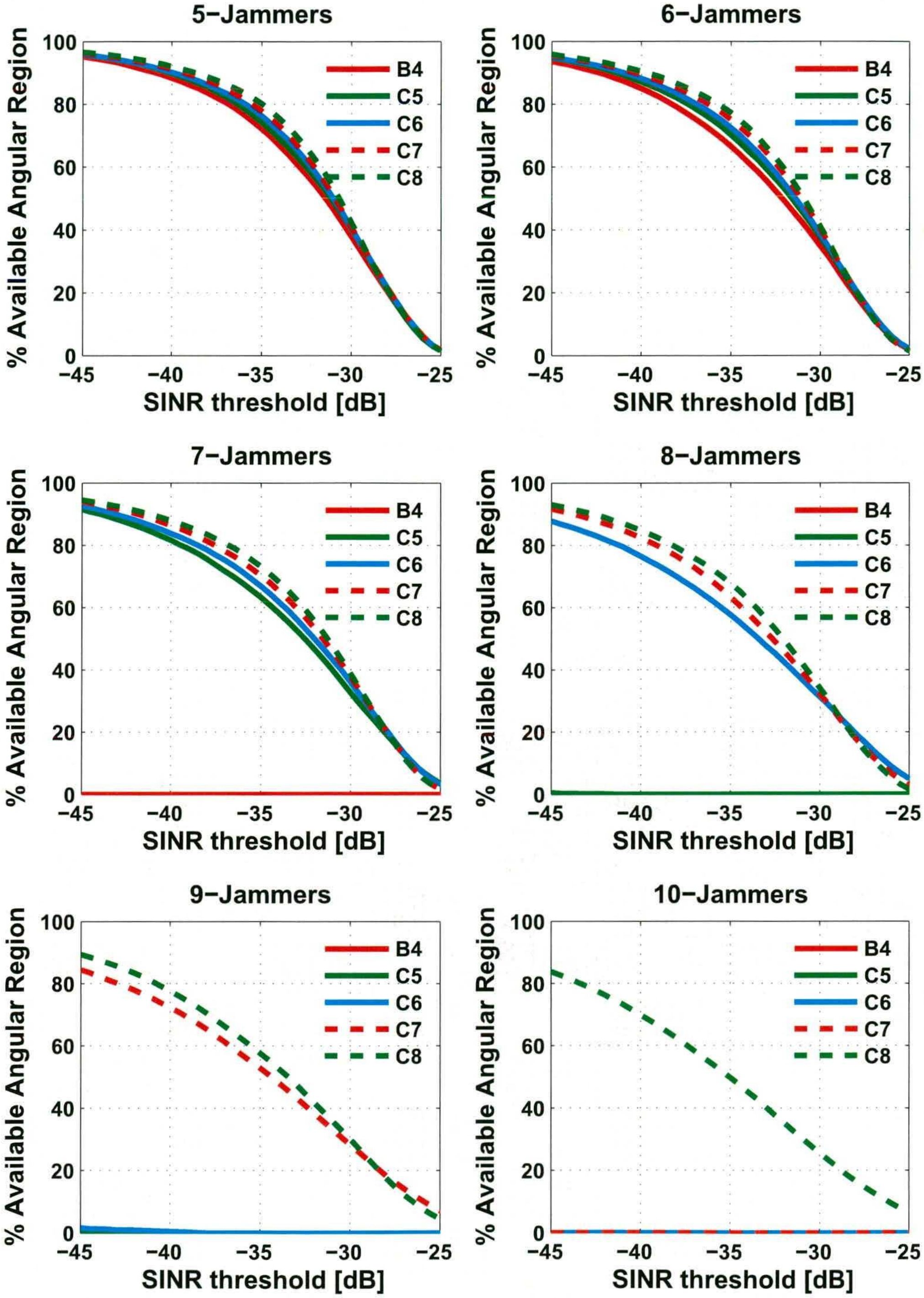


Figure 5.27: Performance of antenna arrays distributed uniformly along one ring in the presence of five to ten interfering signals. AE is operating in simple power minimization mode. L2 frequency band.

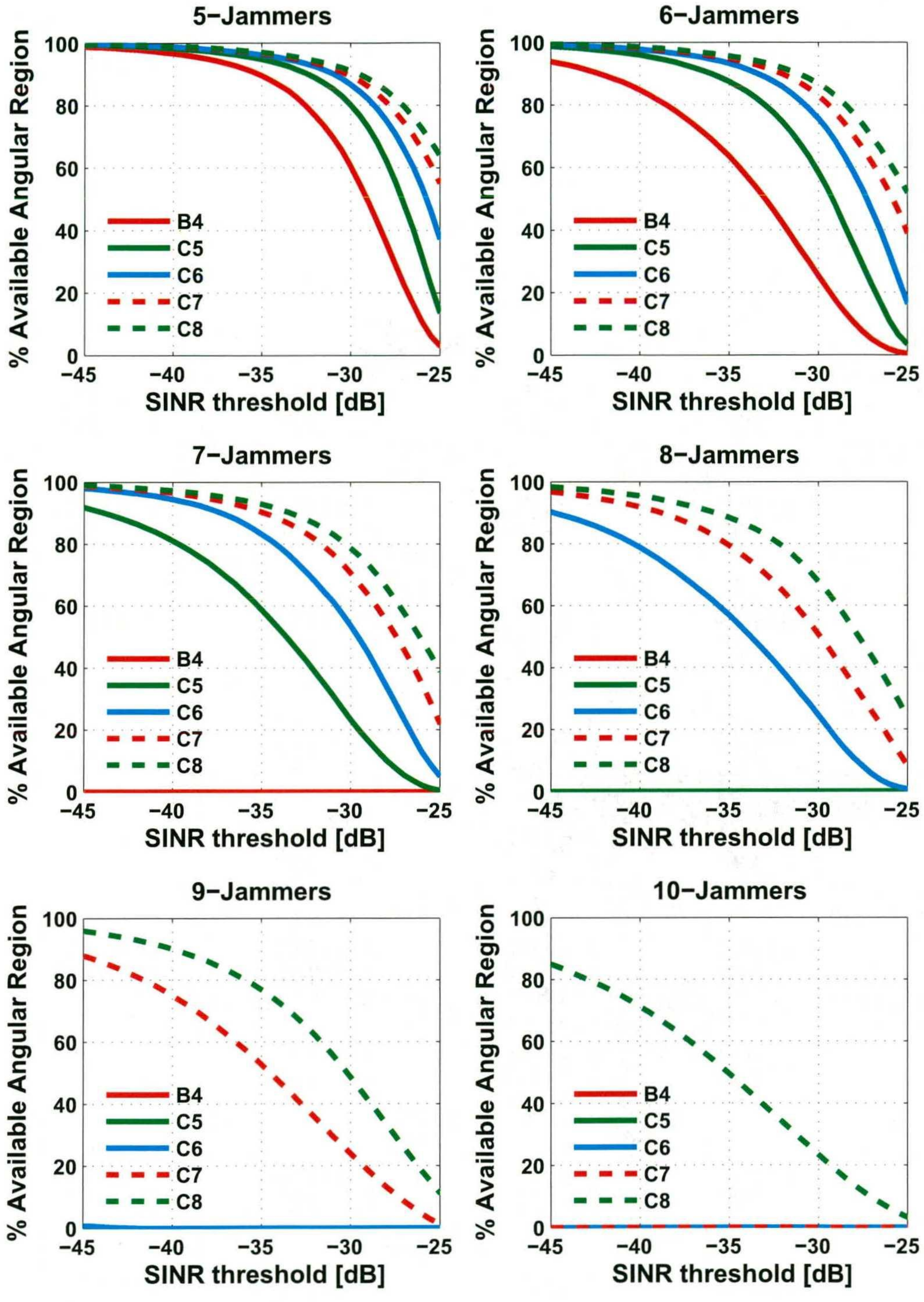


Figure 5.28: Performance of antenna arrays distributed uniformly along one ring in the presence of five to ten interfering signals. AE is operating in beam forming / null steering mode. L1 frequency band.

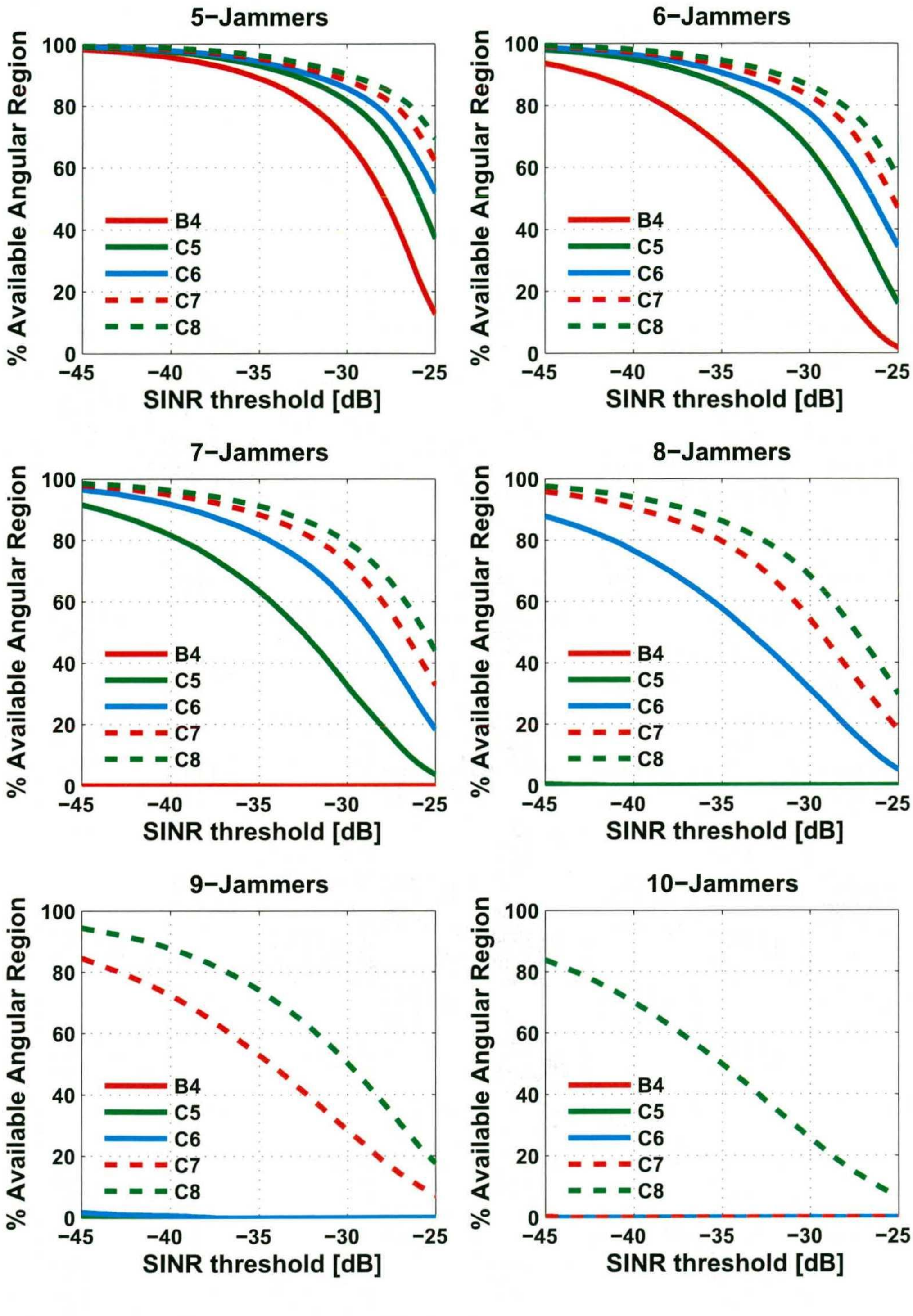


Figure 5.29: Performance of of antenna arrays distributed uniformly along one ring in the presence of five to ten interfering signals. AE is operating in beam forming / null steering mode. L2 frequency band.

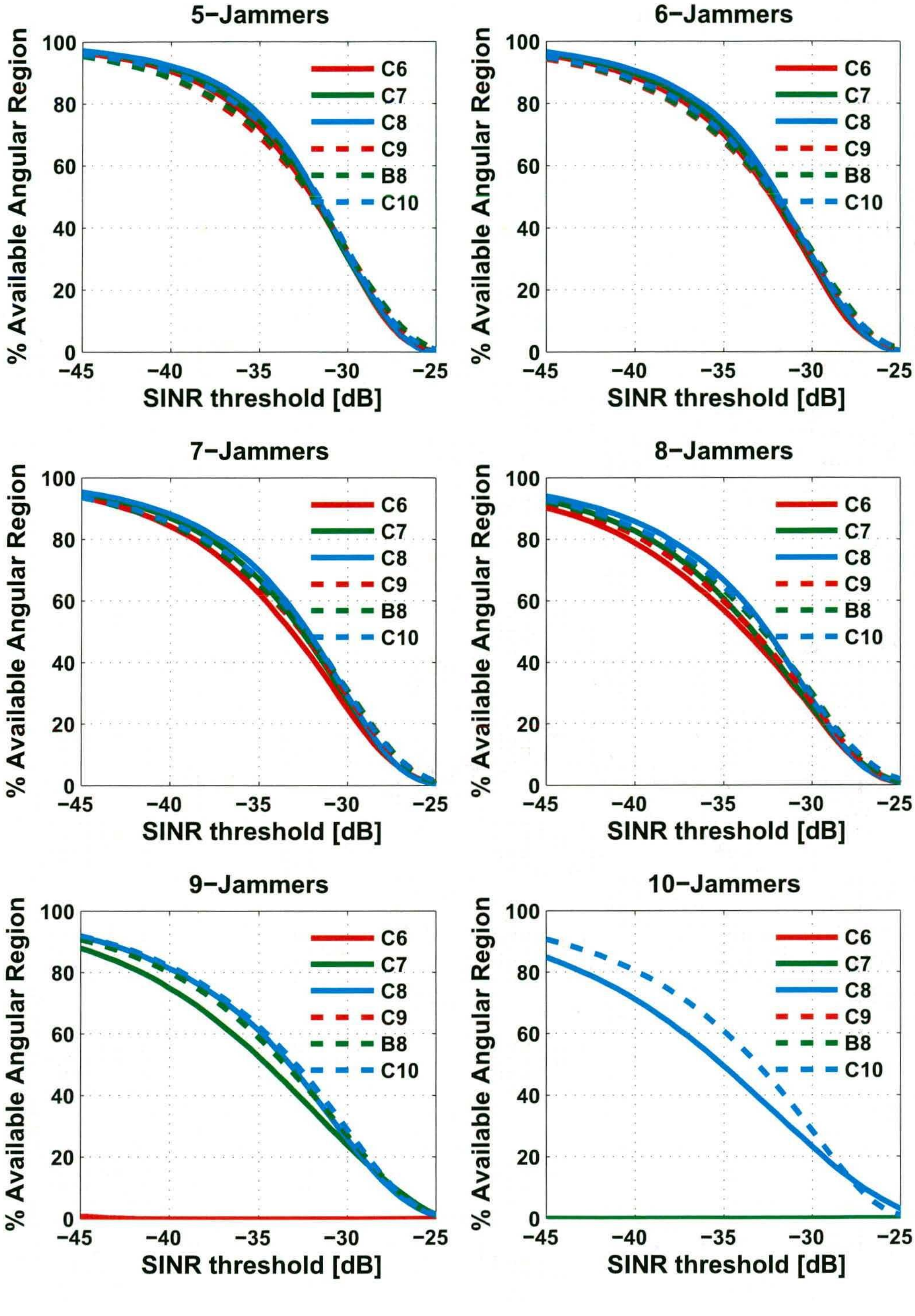


Figure 5.30: Performance of antenna arrays with one and two ring distributions in the presence of five to ten interfering signals. AE is operating in simple power minimization mode. L1 frequency band.

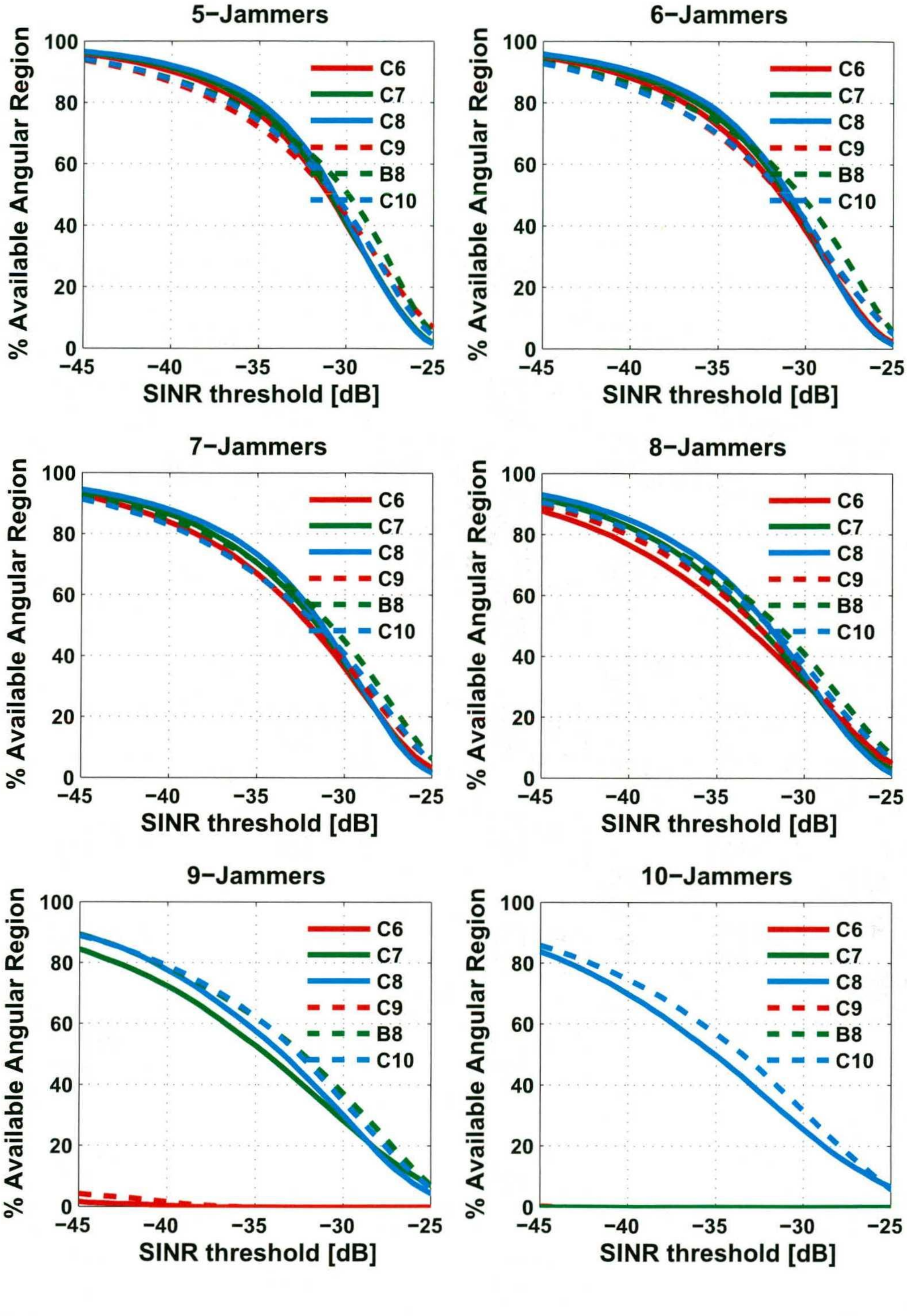


Figure 5.31: Performance of antenna arrays with one and two ring distributions in the presence of five to ten interfering signals. AE is operating in simple power minimization mode. L2 frequency band.

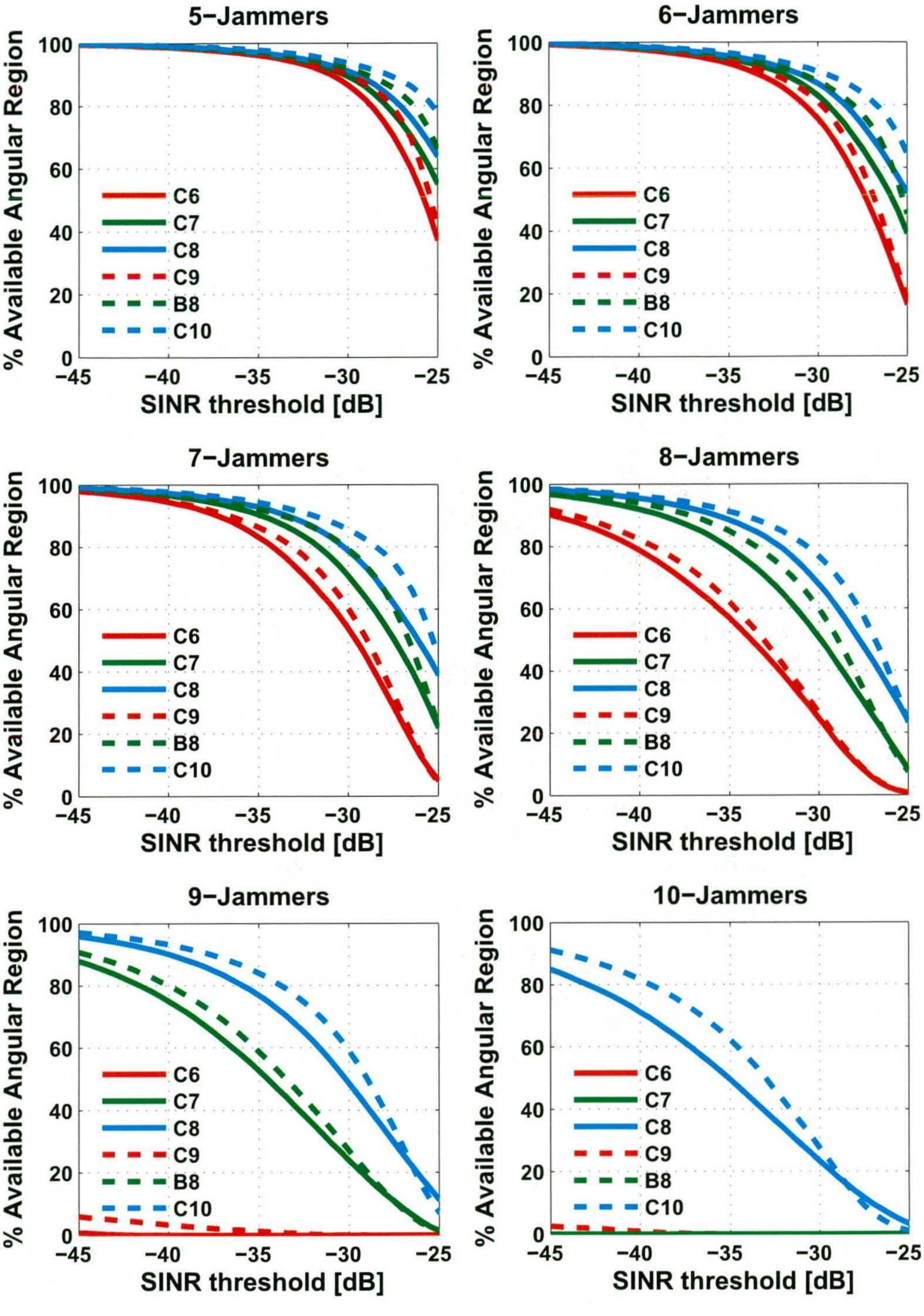


Figure 5.32: Performance of antenna arrays with one and two ring distributions in the presence of five to ten interfering signals. AE is operating in beam forming / null steering mode. L1 frequency band.

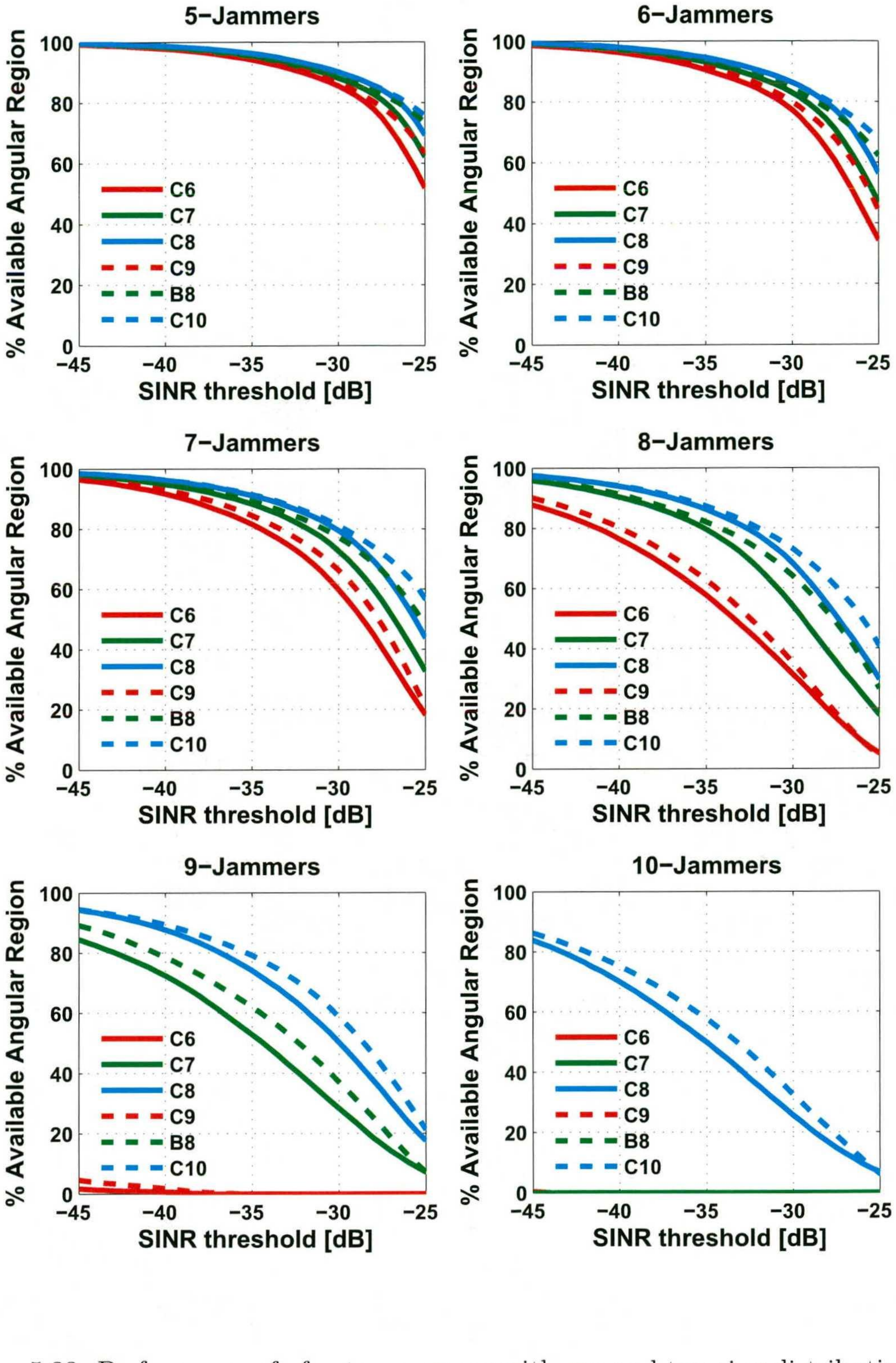


Figure 5.33: Performance of of antenna arrays with one and two ring distributions in the presence of five to ten interfering signals. AE is operating in beam forming / null steering mode. L2 frequency band.

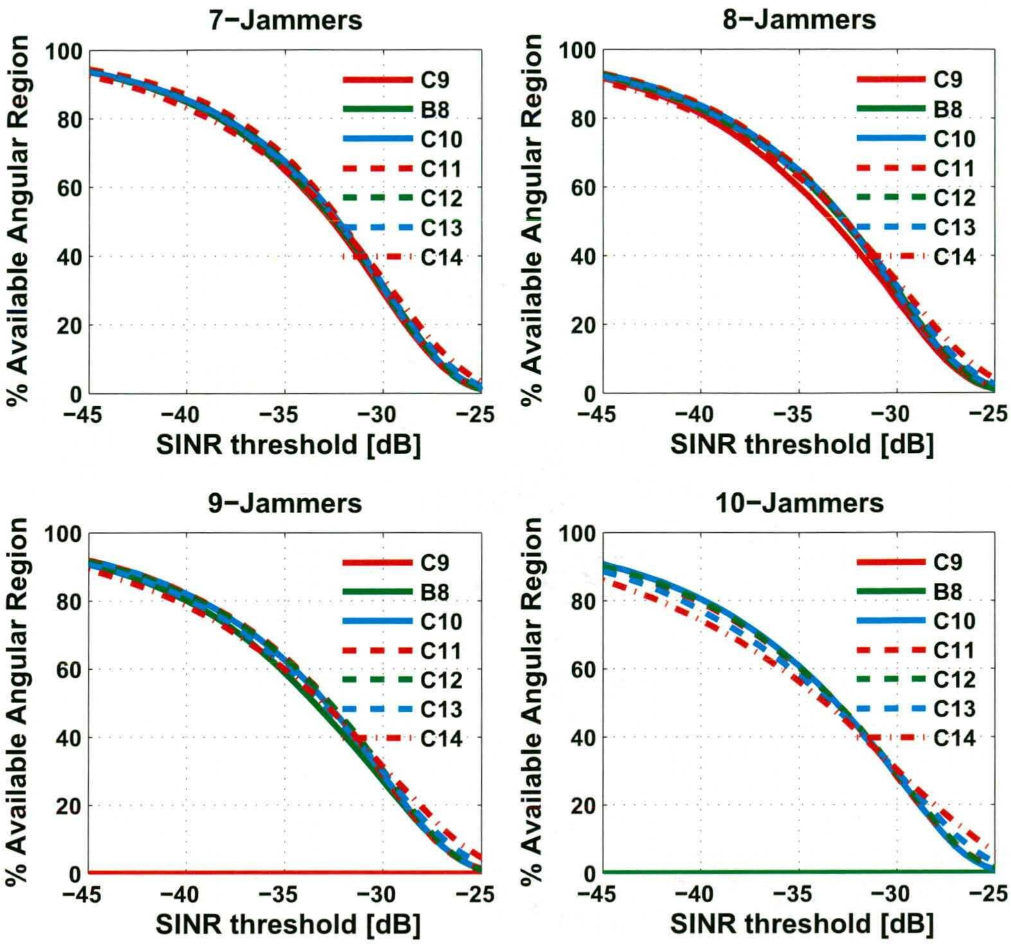


Figure 5.34: Performance of antenna arrays with elements distributed on two rings with an inner ring height of 4.24 inches in the presence of seven to fourteen interfering signals. AE is operating in simple power minimization mode. L1 frequency band. (Continued on the following page).

Figure 5.34 continued.

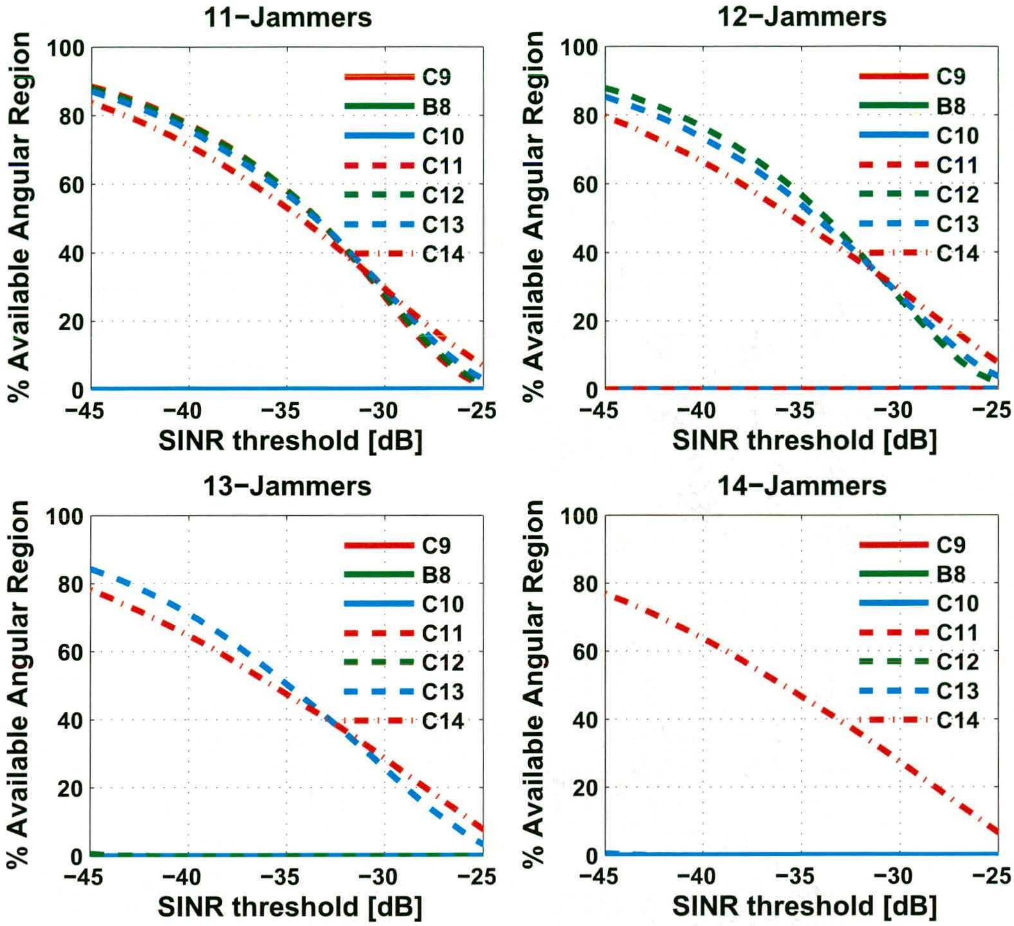

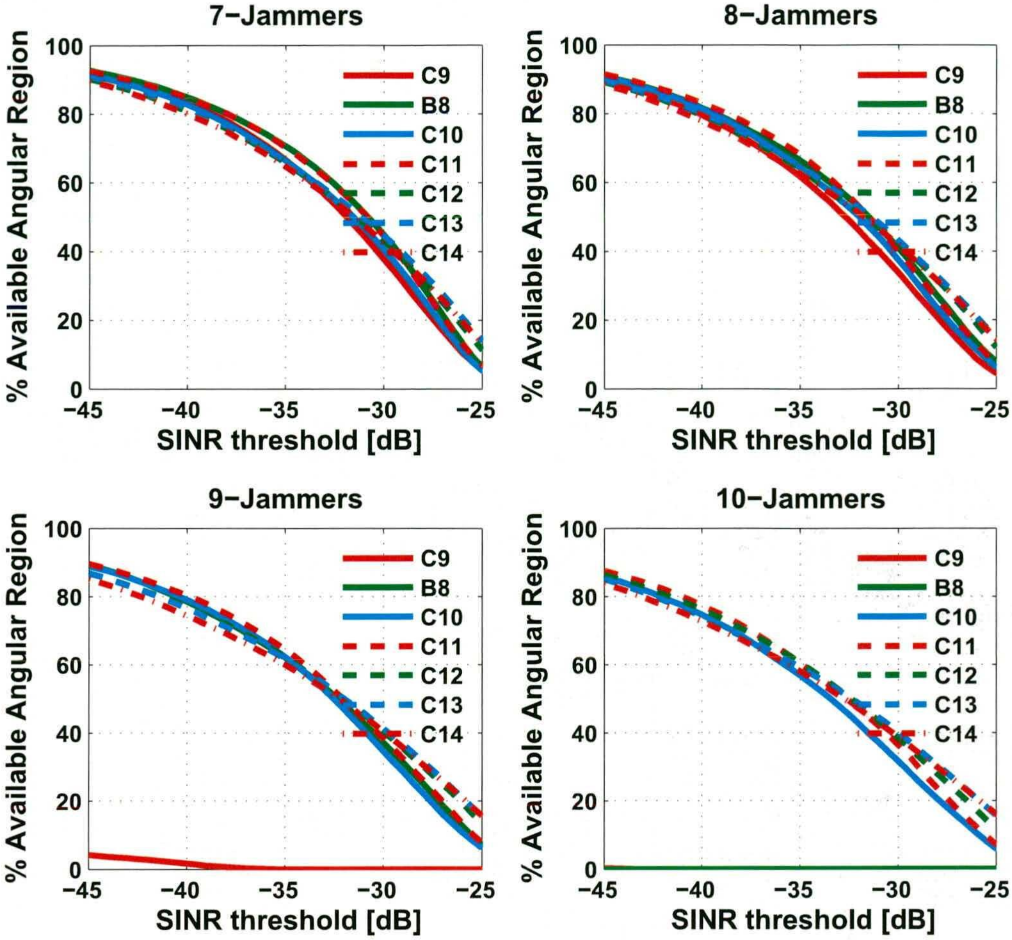


Figure 5.35: Performance of antenna arrays with elements distributed on two rings with an inner ring height of 4.24 inches in the presence of seven to fourteen interfering signals. AE is operating in simple power minimization mode. L2 frequency band. (Continued on the following page).

Figure 5.35 continued.

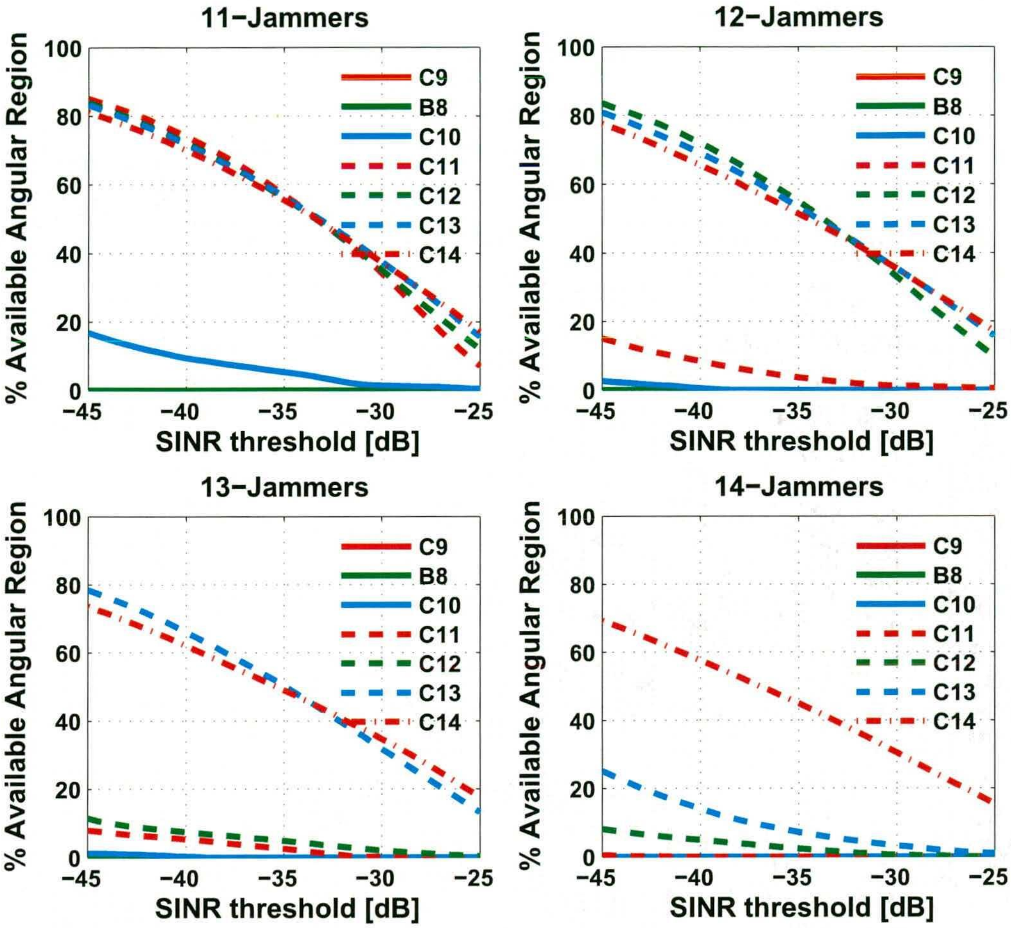

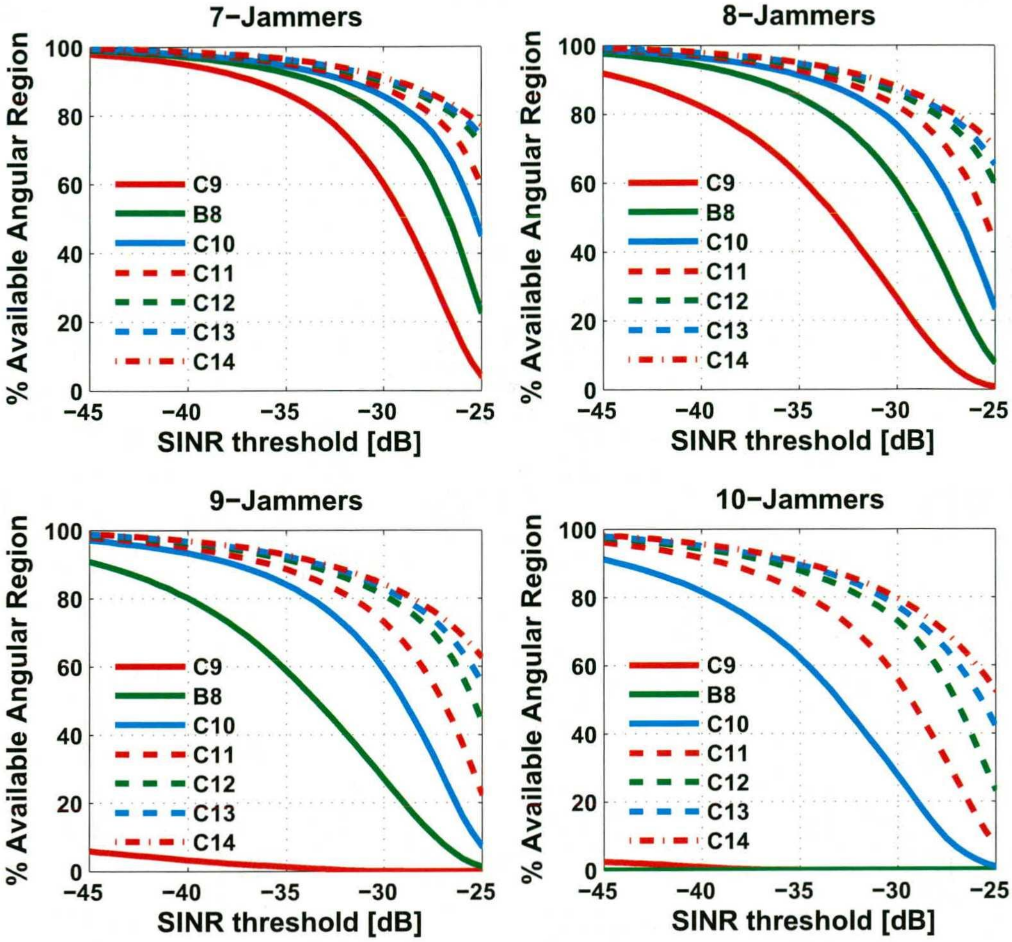


Figure 5.36: Performance of antenna arrays with elements distributed on two rings with an inner ring height of 4.24 inches in the presence of seven to fourteen interfering signals. AE is operating in beam forming / null steering mode. L1 frequency band. (Continued on the following page).

Figure 5.36 continued.

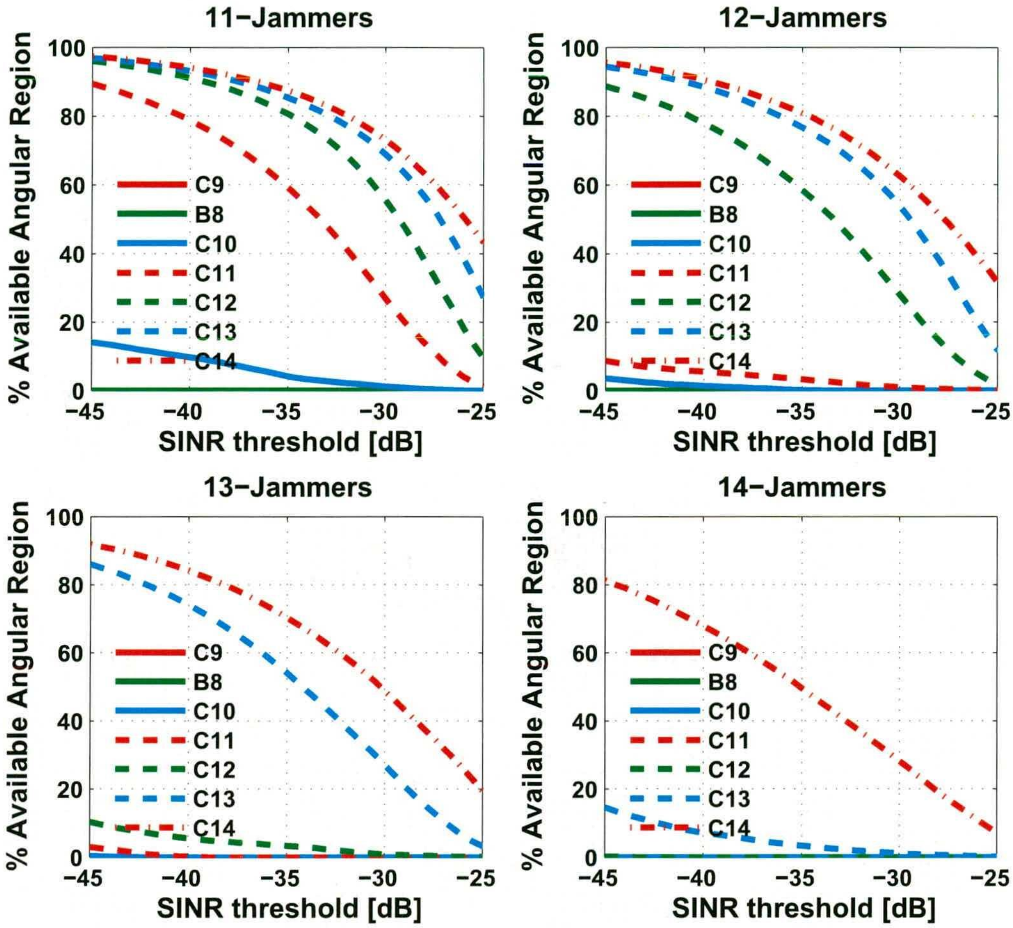

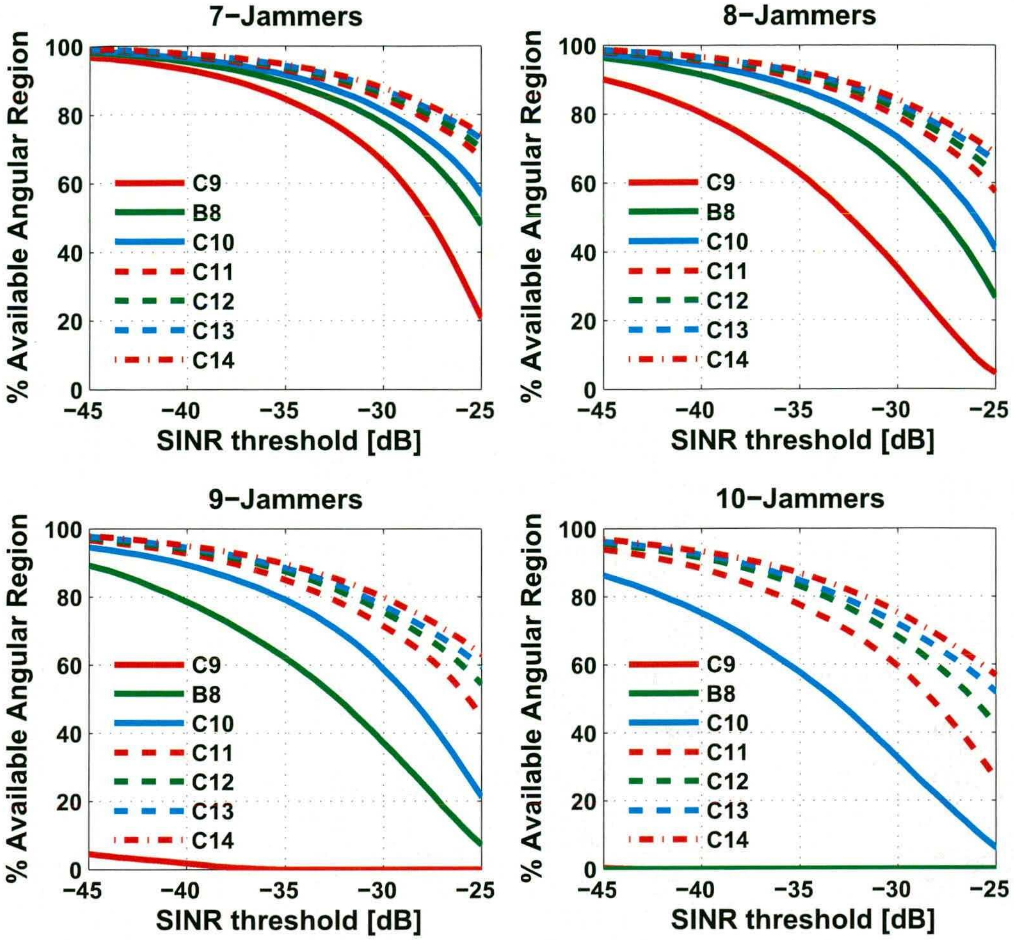


Figure 5.37: Performance of antenna arrays with elements distributed on two rings with an inner ring height of 4.24 inches in the presence of seven to fourteen interfering signals. AE is operating in beam forming / null steering mode. L2 frequency band. (Continued on the following page).

Figure 5.37 continued.

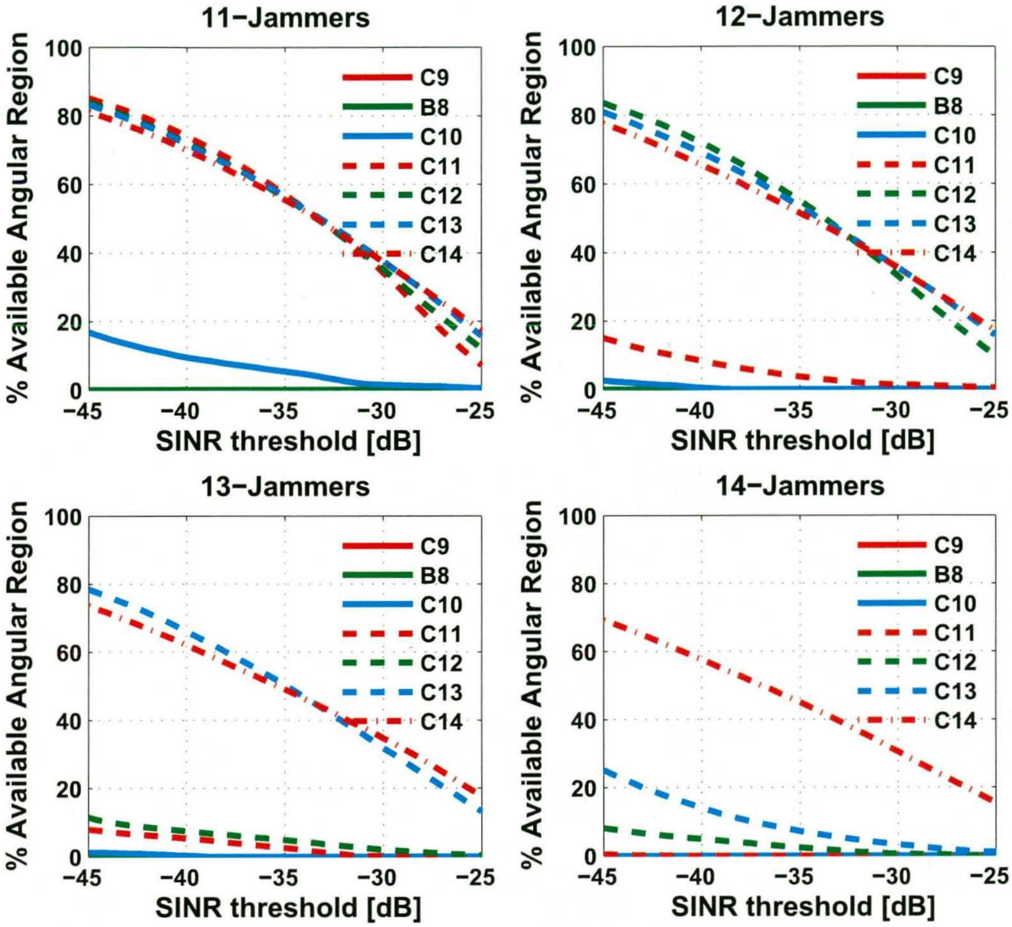

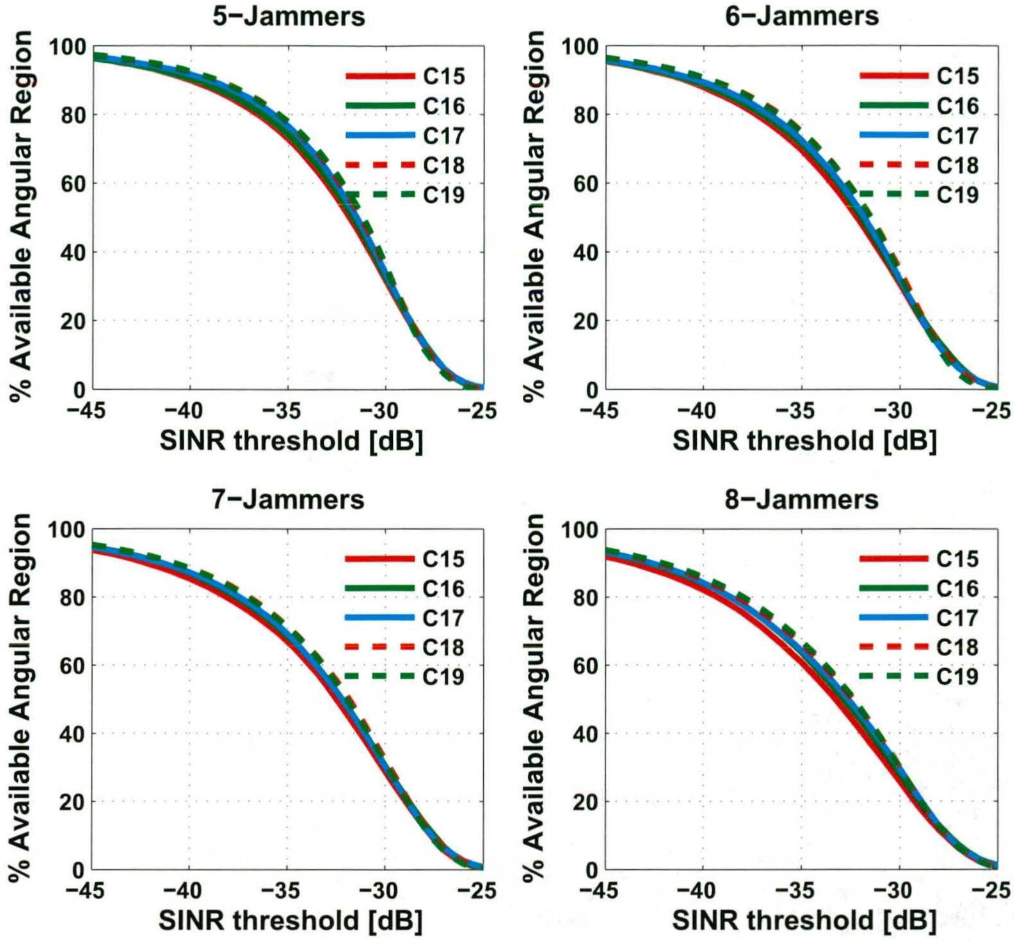


Figure 5.38: Performance of antenna arrays with elements distributed on two rings with an inner ring height of three inches in the presence of five to twelve interfering signals. AE is operating in simple power minimization mode. L1 frequency band. (Continued on the following page).

Figure 5.38 continued.

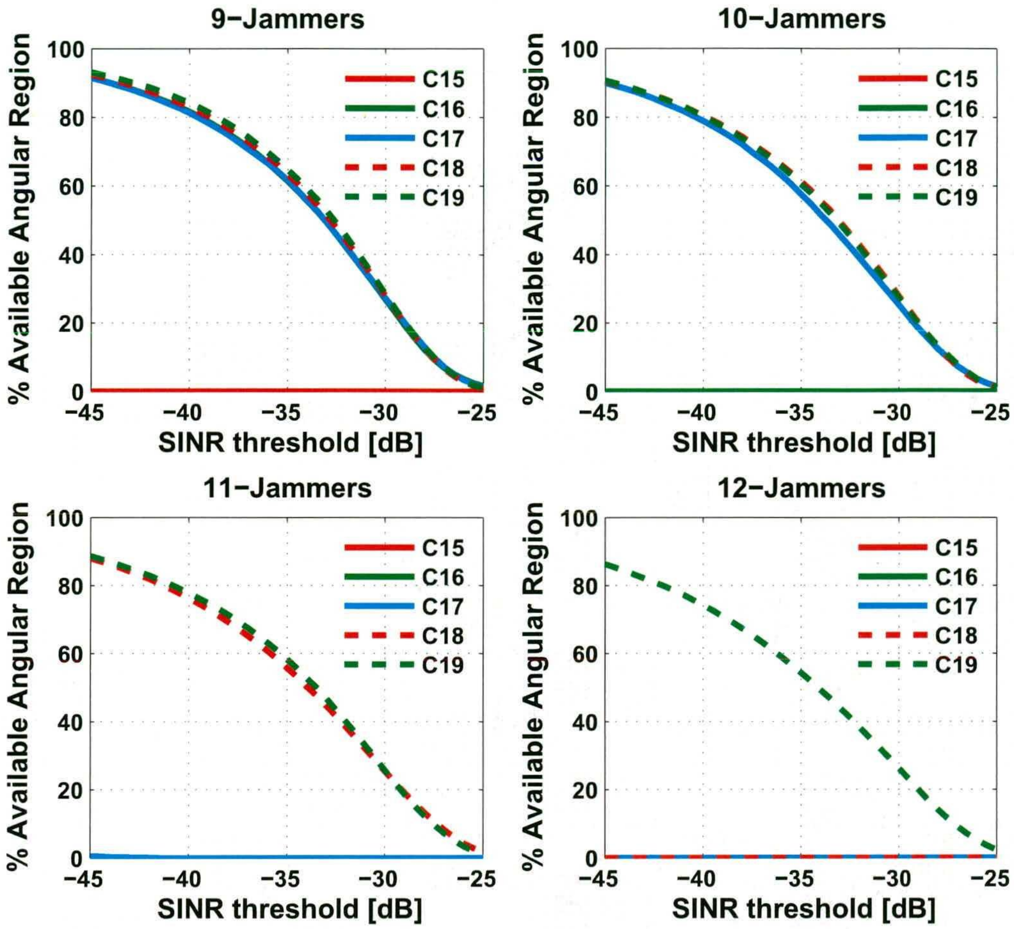

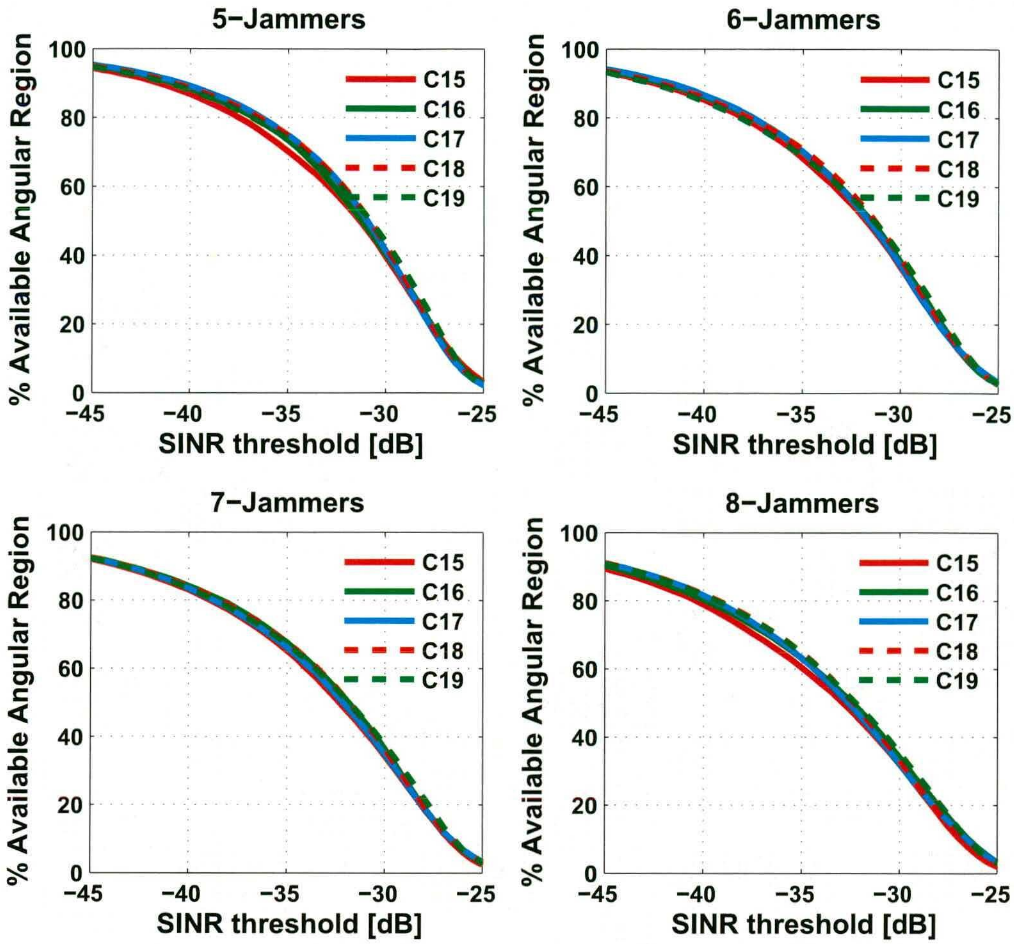


Figure 5.39: Performance of antenna arrays with elements distributed on two rings with an inner ring height of three inches in the presence of five to twelve interfering signals. AE is operating in simple power minimization mode. L2 frequency band. (Continued on the following page).

Figure 5.39 continued.

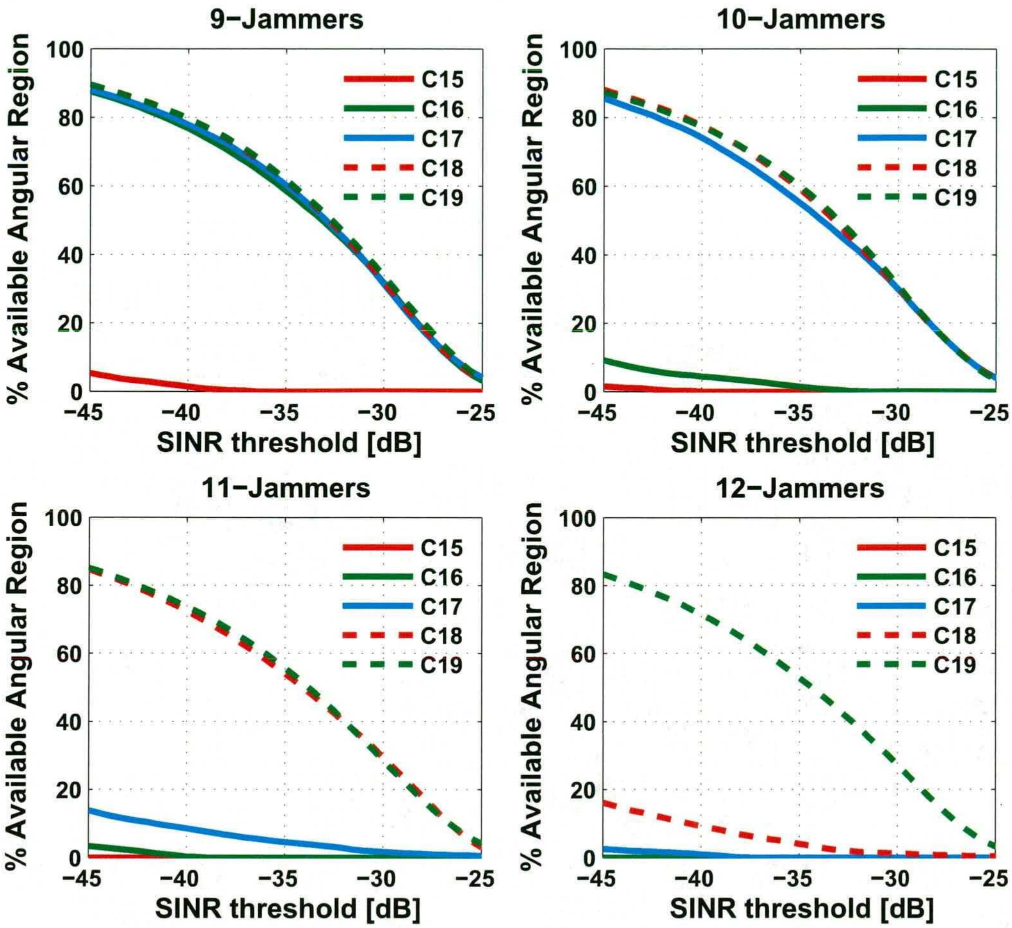

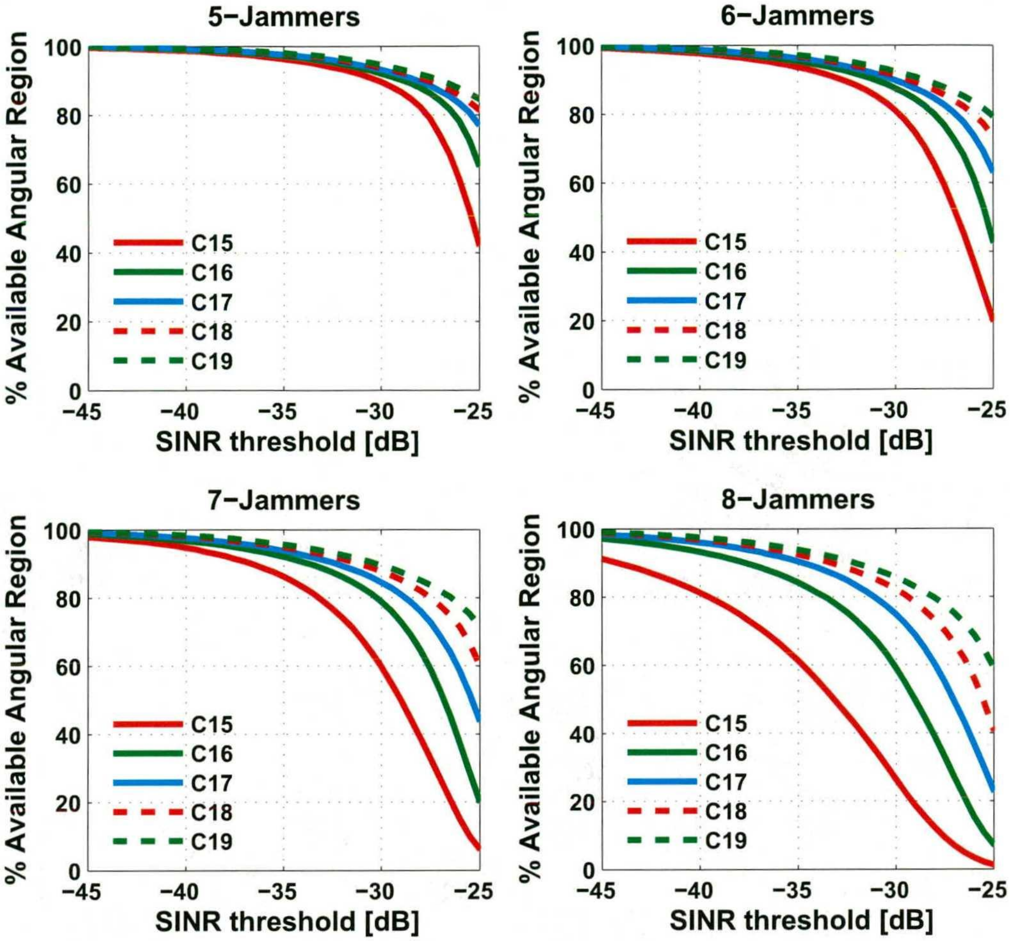


Figure 5.40: Performance of antenna arrays with elements distributed on two rings with an inner ring height of three inches in the presence of five to twelve interfering signals. AE is operating in beam forming / null steering mode. L1 frequency band. (Continued on the following page).

Figure 5.40 continued.

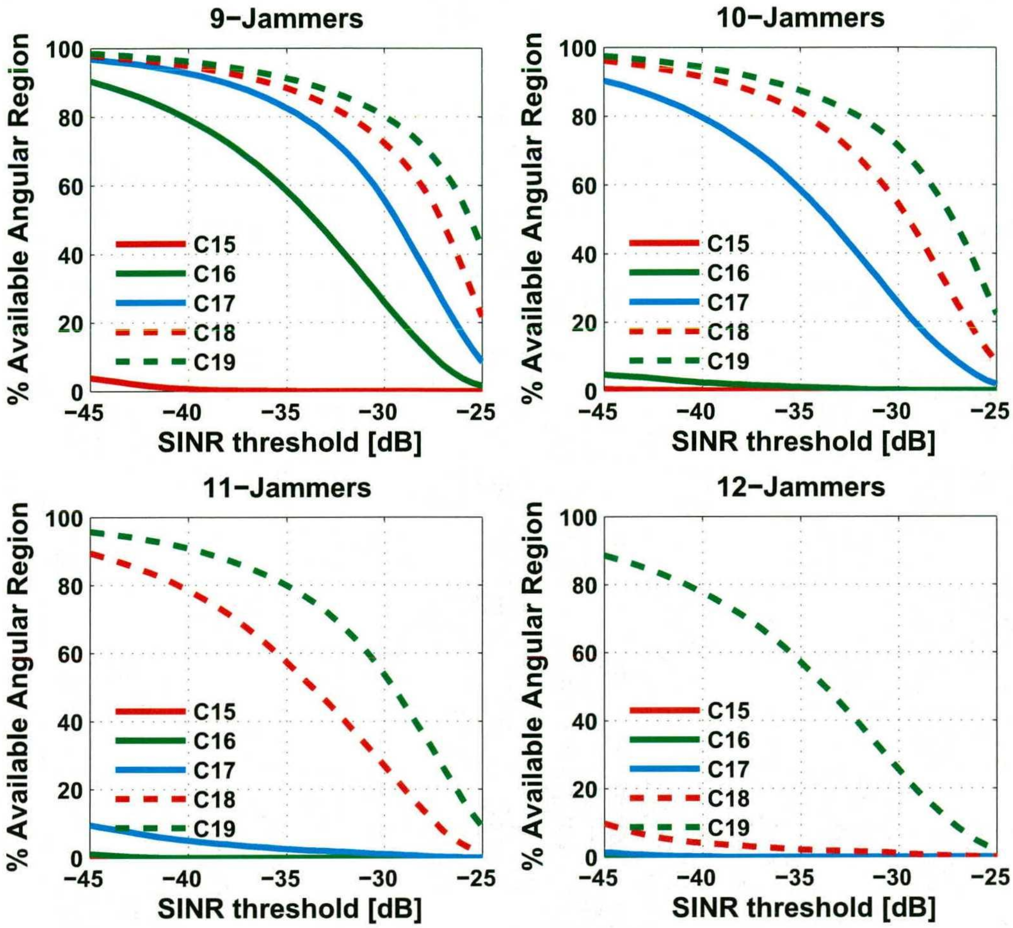

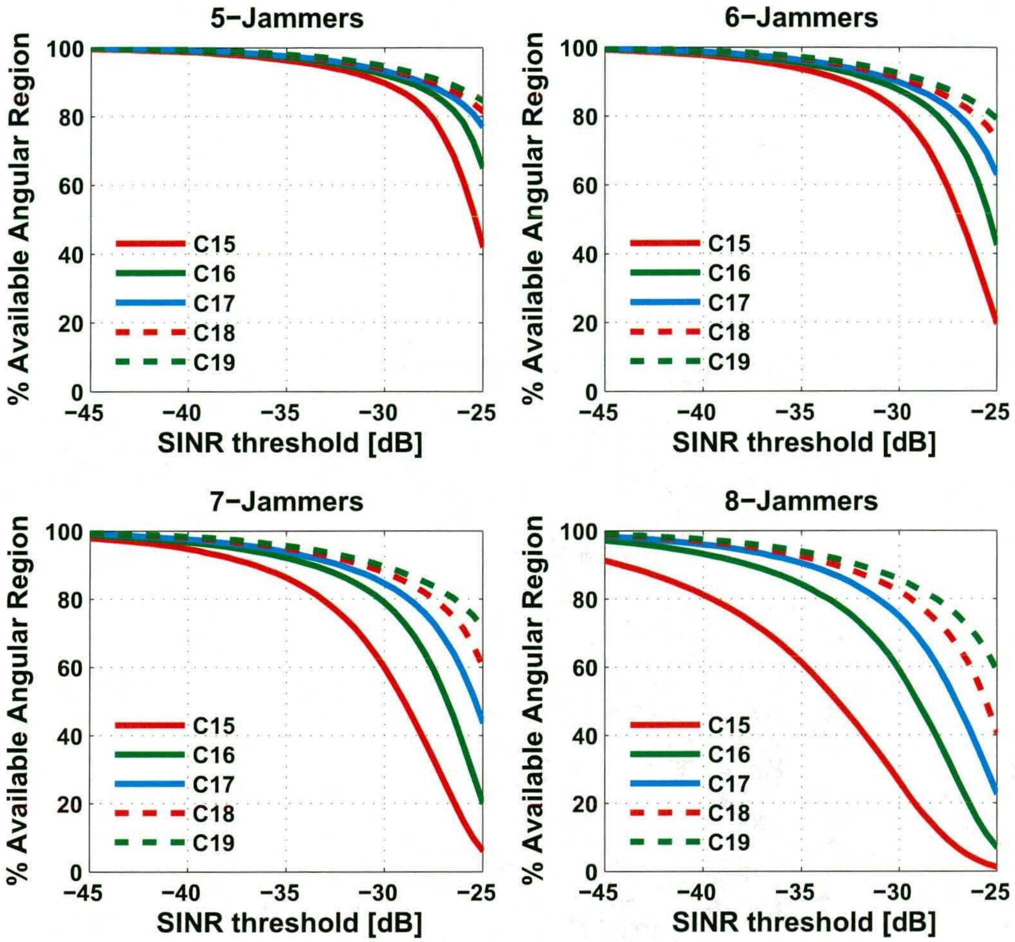


Figure 5.41: Performance of antenna arrays with elements distributed on two rings with an inner ring height of three inches in the presence of five to twelve interfering signals. AE is operating in beam forming / null steering mode. L2 frequency band. (Continued on the following page).

Figure 5.41 continued.

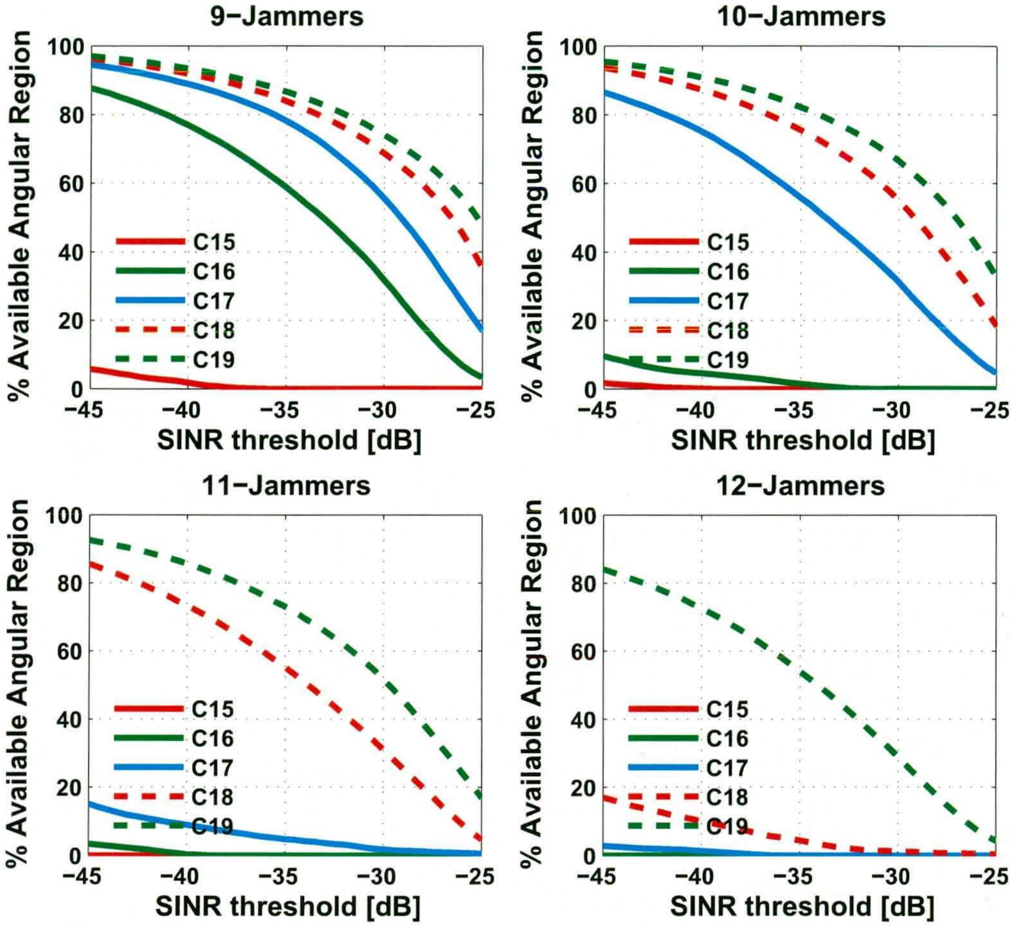

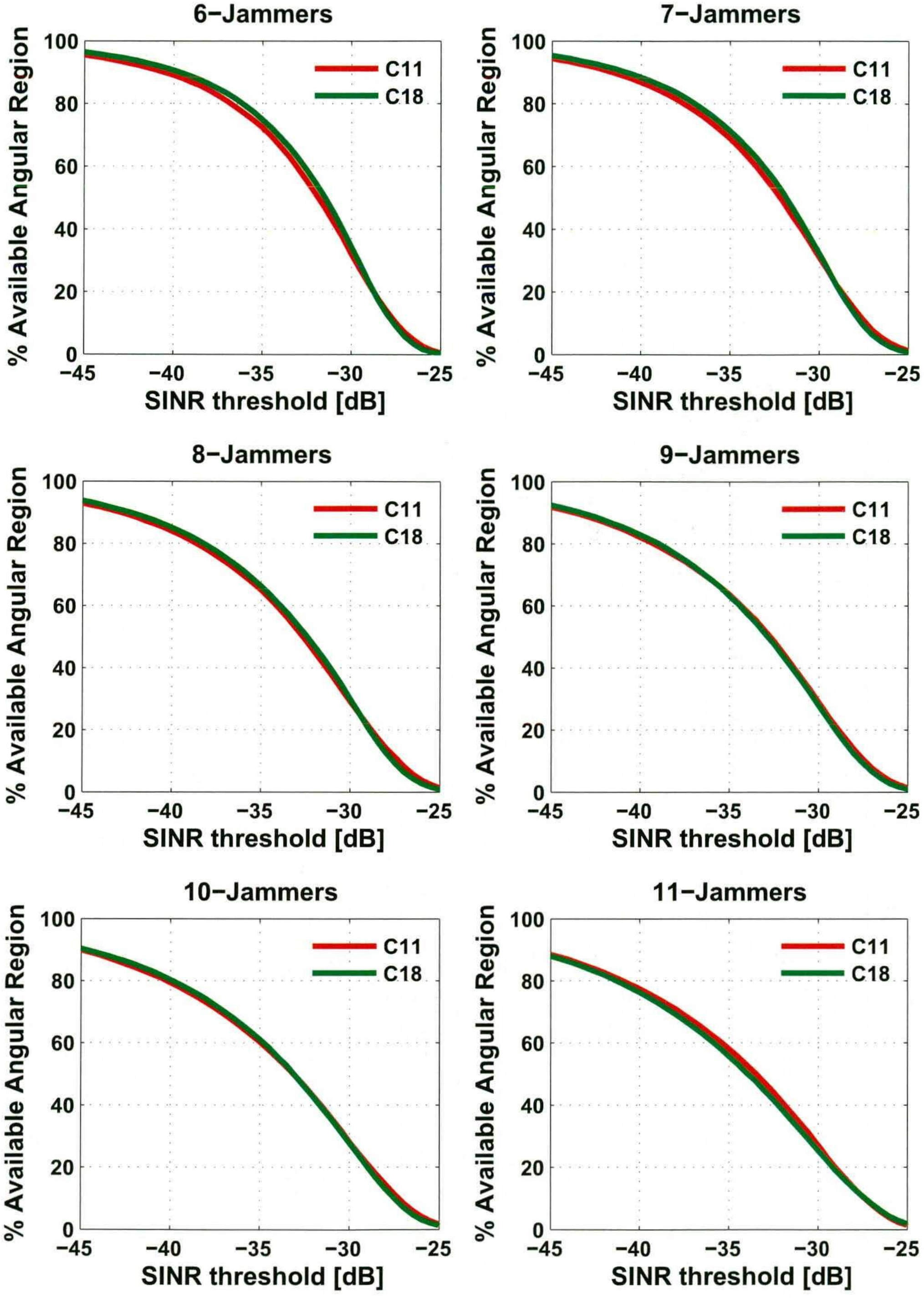


Figure 5.42: Performance of twelve element antenna arrays in the presence of six to eleven interfering signals. AE is operating in simple power minimization mode. L1 frequency band.

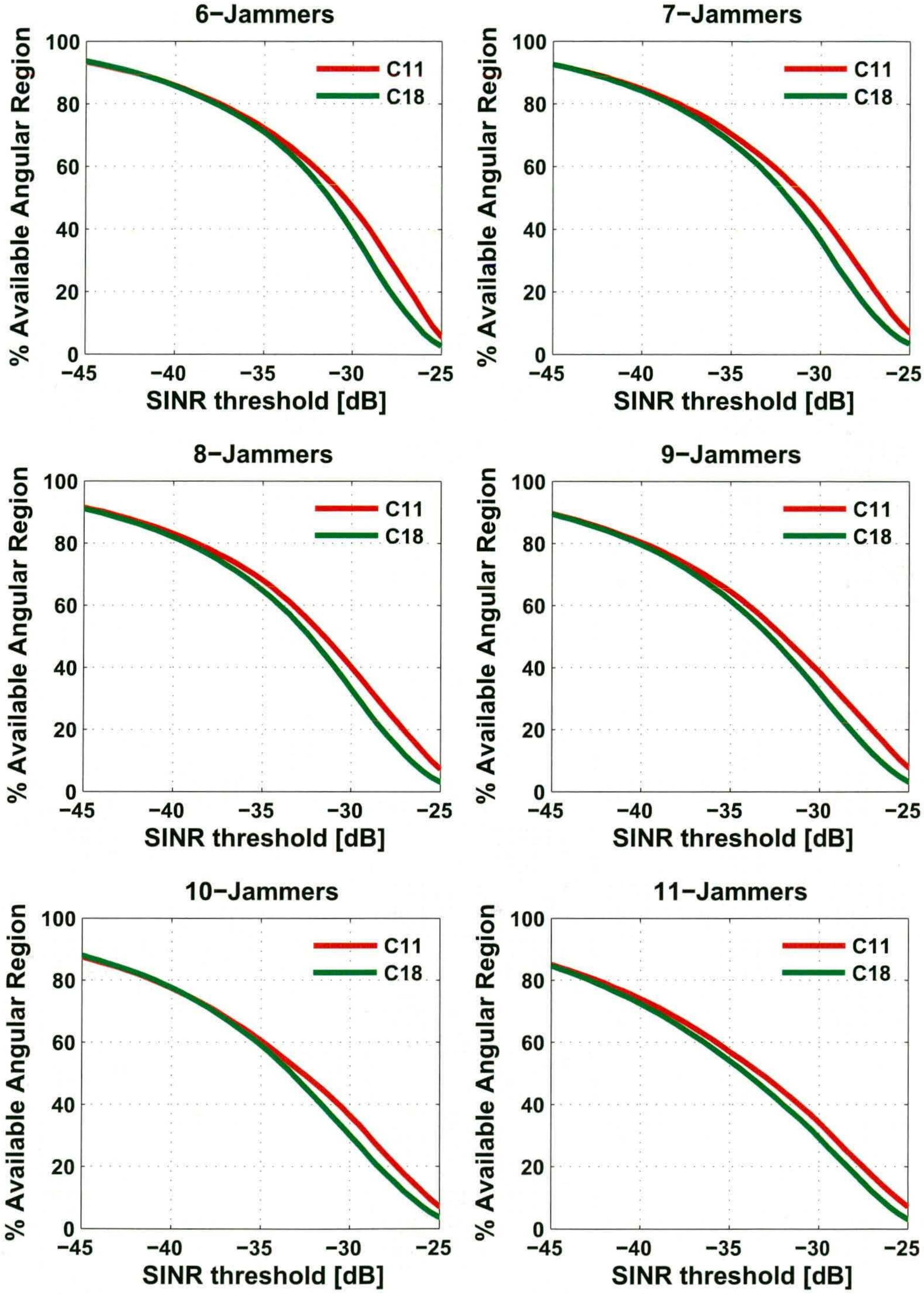


Figure 5.43: Performance of twelve element antenna arrays in the presence of six to eleven interfering signals. AE is operating in simple power minimization mode. L2 frequency band.

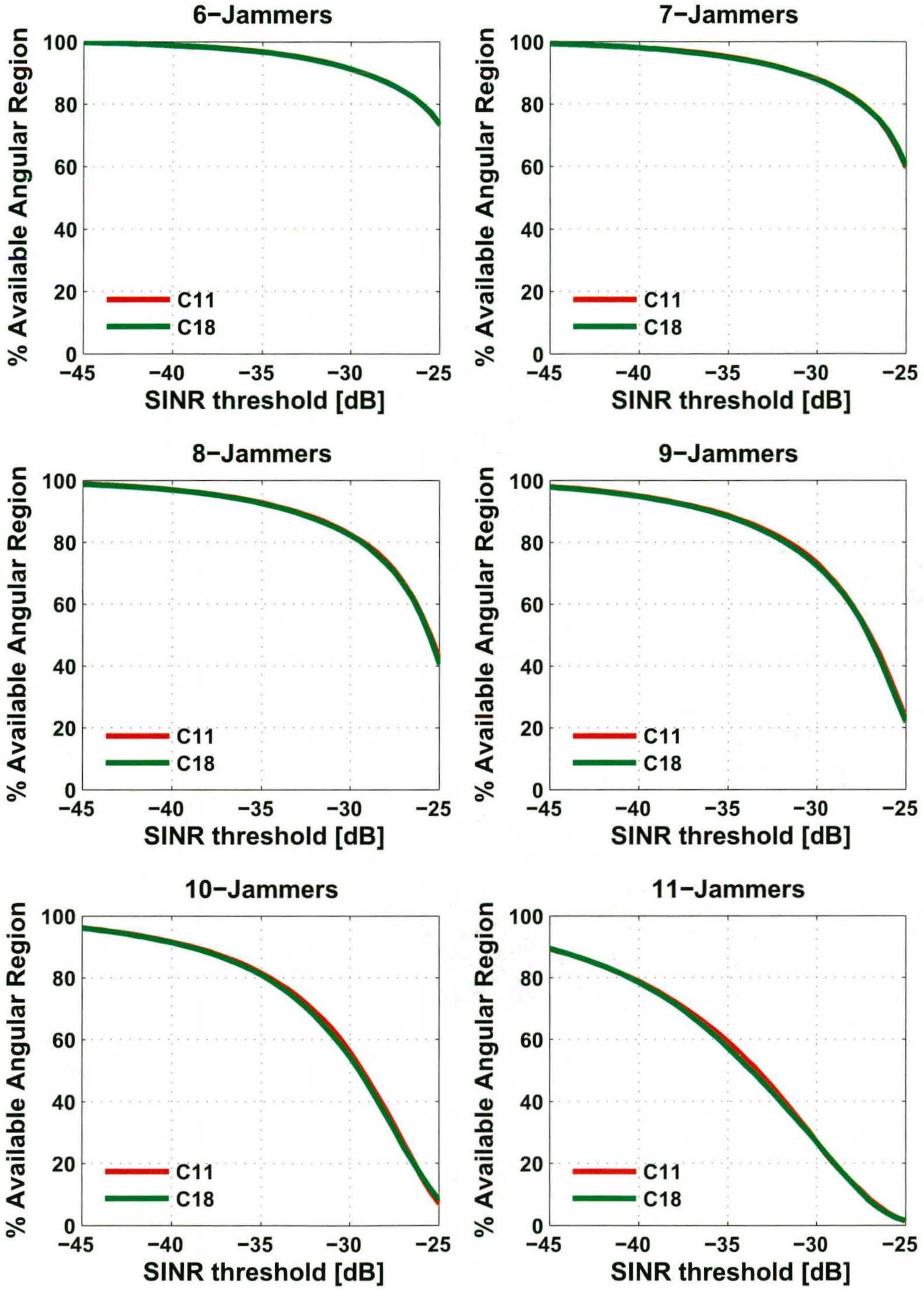


Figure 5.44: Performance of twelve element antenna arrays in the presence of six to eleven interfering signals. AE is operating in beam forming / null steering mode. L1 frequency band.

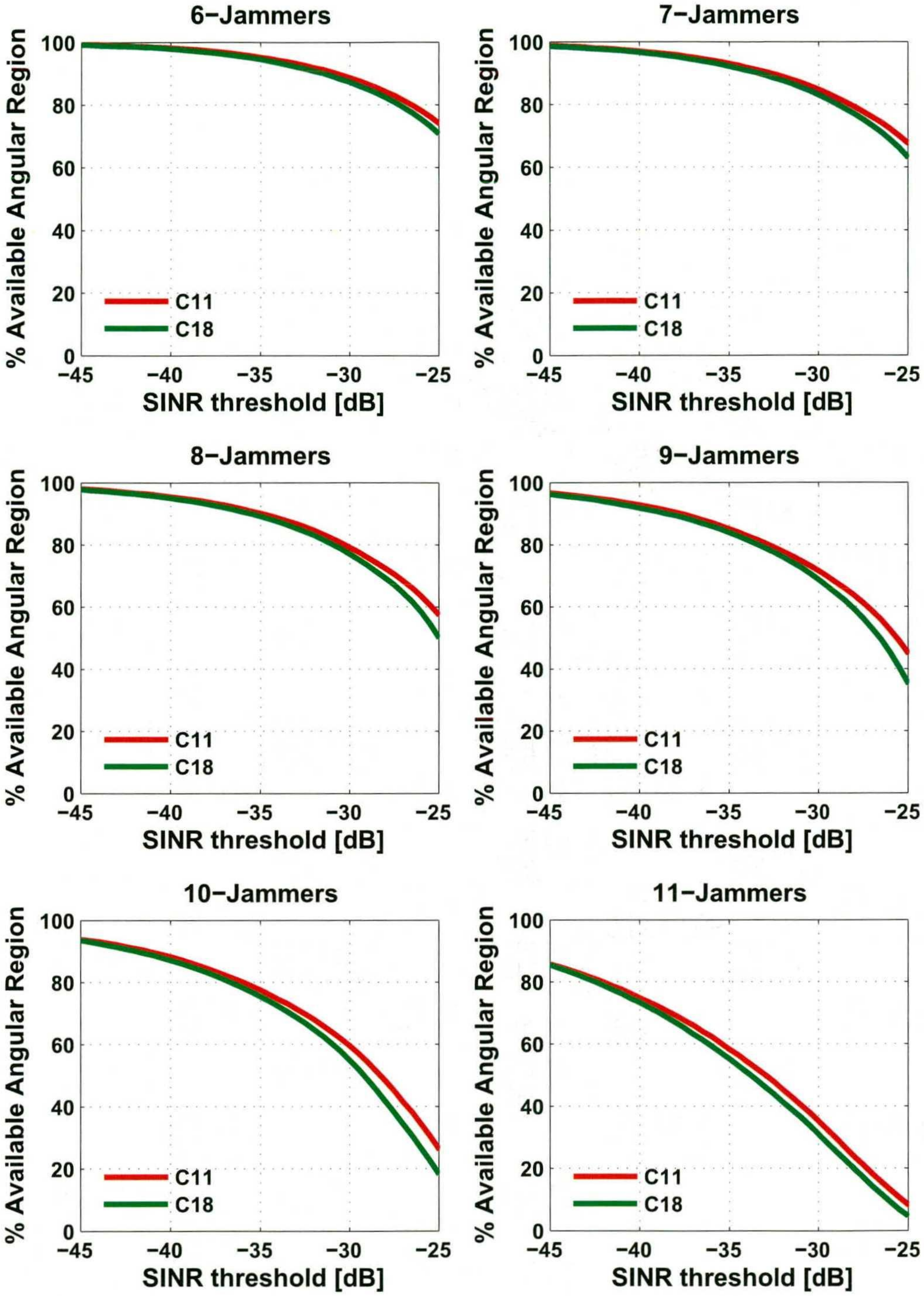


Figure 5.45: Performance of twelve element antenna arrays in the presence of six to eleven interfering signals. AE is operating in beam forming / null steering mode. L2 frequency band.

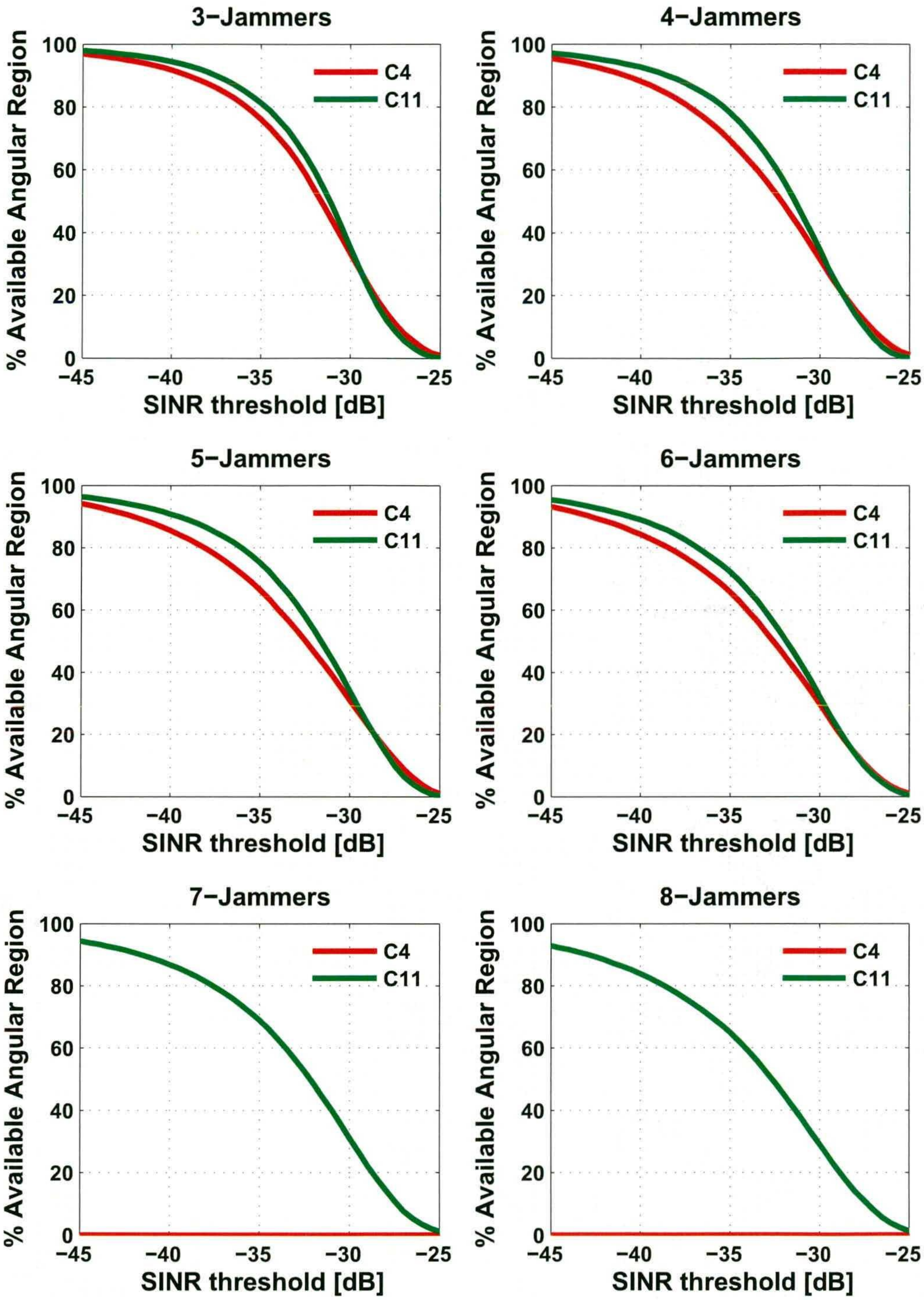


Figure 5.46: Performance of seven and twelve element antenna arrays in the presence of three to eight interfering signals. AE is operating in simple power minimization mode. L1 frequency band.

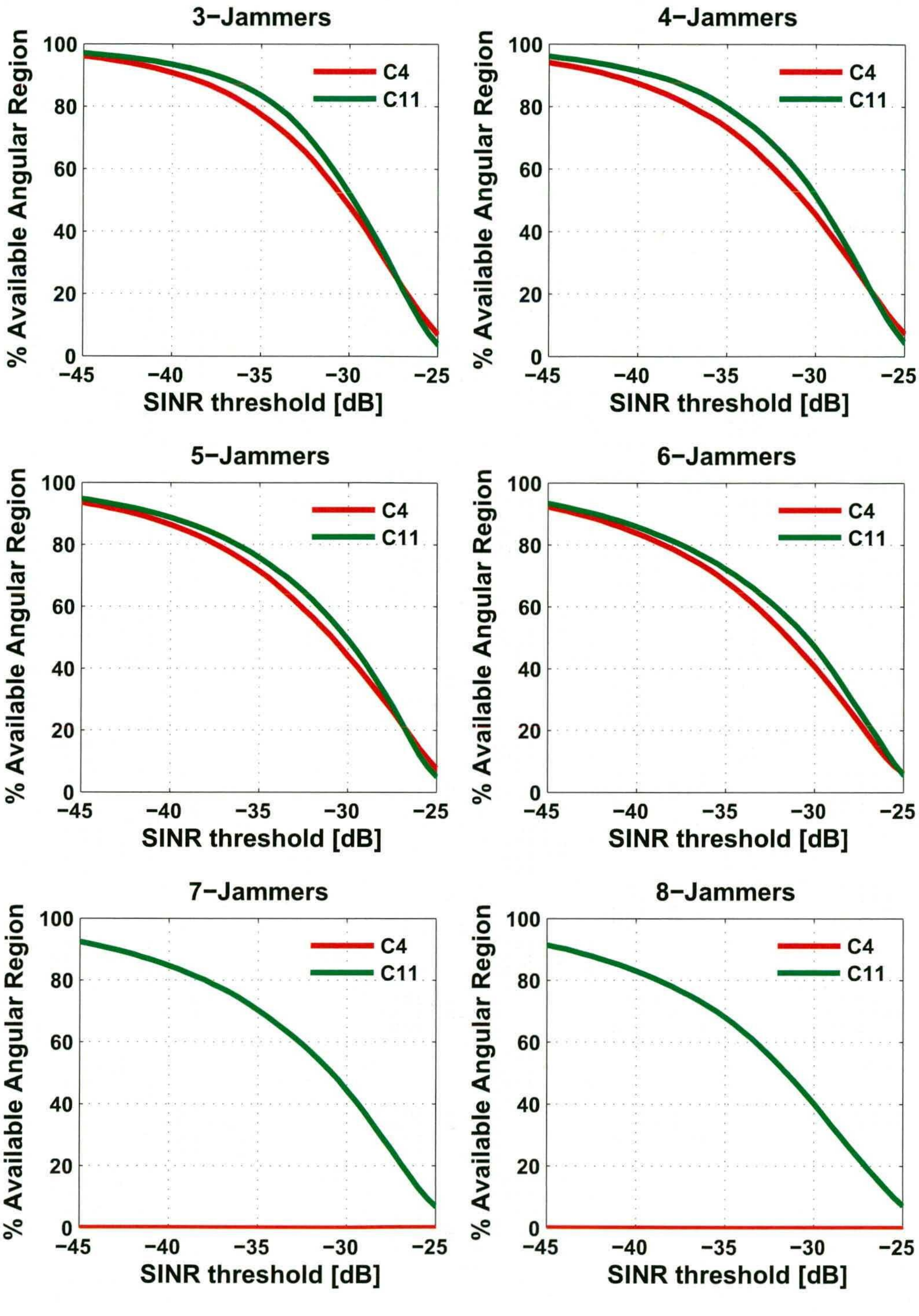


Figure 5.47: Performance of seven and twelve element antenna arrays in the presence of three to eight interfering signals. AE is operating in simple power minimization mode. L2 frequency band.

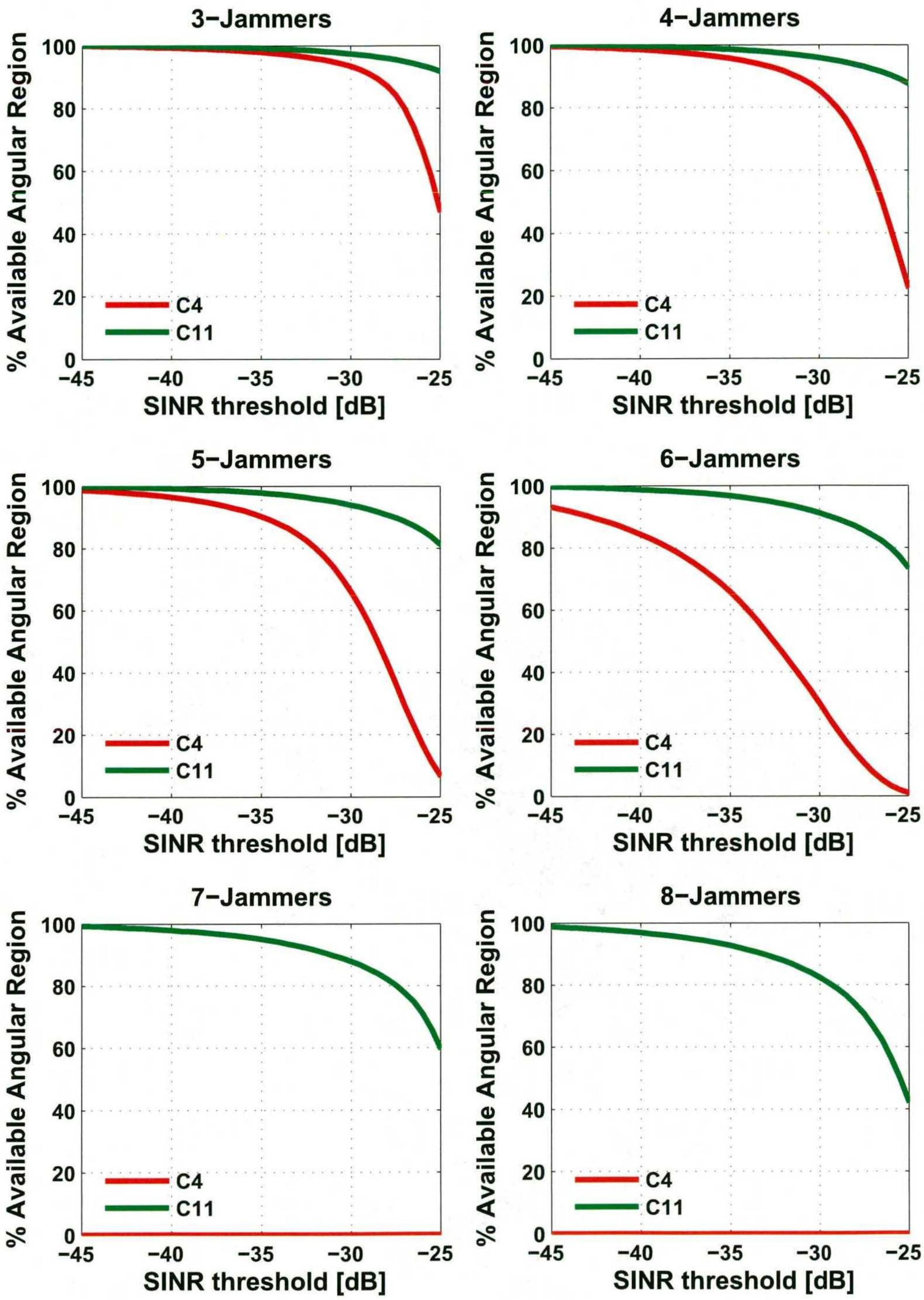


Figure 5.48: Performance of seven and twelve element antenna arrays in the presence of three to eight interfering signals. AE is operating in beam forming / null steering mode. L1 frequency band.

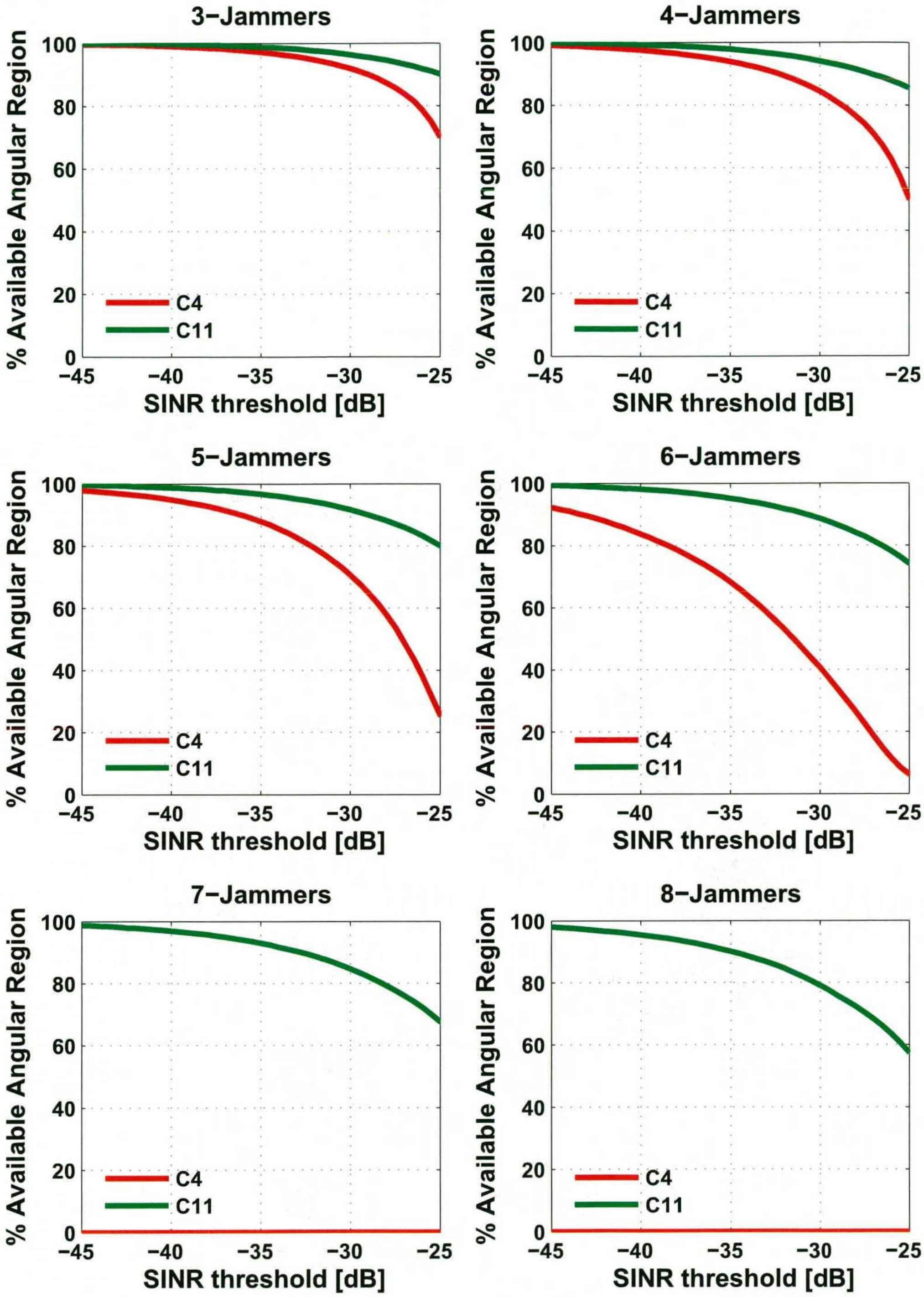


Figure 5.49: Performance of seven and twelve element antenna arrays in the presence of three to eight interfering signals. AE is operating in beam forming / null steering mode. L2 frequency band.

| No. of interfering signals | Antenna Array | | | | |
|---|---|---|---|---|---|
| | B4 | C1 | C2 | C3 | C4 |
| **0** | 96.38 | 96.29 | 93.77 | 95.34 | 95.46 |
| **1** | 90.04 | 89.73 | 84.98 | 85.96 | 85.78 |
| **2** | 83.40 | 83.53 | 78.46 | 78.02 | 78.96 |
| **3** | 78.69 | 78.79 | 72.91 | 73.81 | 75.92 |
| **4** | 73.74 | 75.31 | 66.94 | 68.33 | 69.13 |
| **5** | 68.08 | 66.94 | 63.28 | 66.53 | 66.24 |
| **6** | 63.60 | 60.15 | 59.81 | 65.60 | 65.69 |

Table 5.1: Seven element antenna arrays. Percentage of available angular region when SINR threshold is greater than -35 dB. AE is operating in simple power minimization mode. L1 frequency band.

| No. of interfering signals | Antenna Array | | | | |
|---|---|---|---|---|---|
| | B4 | C1 | C2 | C3 | C4 |
| **0** | 98.57 | 98.15 | 95.92 | 96.76 | 96.76 |
| **1** | 92.41 | 91.88 | 87.47 | 87.50 | 87.62 |
| **2** | 86.80 | 86.96 | 82.25 | 79.91 | 81.01 |
| **3** | 82.69 | 83.59 | 76.83 | 77.44 | 77.31 |
| **4** | 78.29 | 80.65 | 71.26 | 73.15 | 73.20 |
| **5** | 72.16 | 72.35 | 65.74 | 68.96 | 71.32 |
| **6** | 66.52 | 64.22 | 62.45 | 66.83 | 68.11 |

Table 5.2: Seven element antenna arrays. Percentage of available angular region when SINR threshold is greater than -35 dB. AE is operating in simple power minimization mode. L2 frequency band.

| No. of interfering signals | Antenna Array | | | | |
|---|---|---|---|---|---|
| | B4 | C1 | C2 | C3 | C4 |
| **0** | 100.00 | 100.00 | 100.00 | 100.00 | 100.00 |
| **1** | 99.64 | 99.61 | 99.63 | 99.64 | 99.63 |
| **2** | 99.08 | 99.02 | 98.86 | 98.99 | 98.98 |
| **3** | 98.18 | 98.04 | 97.46 | 97.88 | 97.86 |
| **4** | 95.89 | 95.69 | 94.20 | 95.69 | 95.65 |
| **5** | 89.49 | 87.60 | 86.61 | 89.84 | 90.16 |
| **6** | 63.64 | 60.18 | 59.83 | 65.62 | 65.71 |

Table 5.3: Seven element antenna arrays. Percentage of available angular region when SINR threshold is greater than -35 dB. AE is operating in beam forming / null steering mode. L1 frequency band.

| No. of interfering signals | Antenna Array | | | | |
|---|---|---|---|---|---|
| | B4 | C1 | C2 | C3 | C4 |
| **0** | 100.00 | 100.00 | 100.00 | 100.00 | 100.00 |
| **1** | 99.48 | 99.43 | 99.50 | 99.48 | 99.45 |
| **2** | 98.51 | 98.47 | 98.31 | 98.53 | 98.49 |
| **3** | 97.19 | 97.12 | 96.38 | 96.98 | 97.08 |
| **4** | 94.10 | 93.95 | 92.75 | 93.94 | 93.77 |
| **5** | 88.72 | 87.44 | 85.30 | 88.05 | 87.83 |
| **6** | 66.54 | 64.26 | 62.47 | 66.85 | 68.11 |

Table 5.4: Seven element antenna arrays. Percentage of available angular region when SINR threshold is greater than -35 dB. AE is operating in beam forming / null steering mode. L2 frequency band.

| No. of interfering signals | Antenna Array | | | | |
|---|---|---|---|---|---|
| | B4 | C5 | C6 | C7 | C8 |
| **0** | 96.38 | 96.59 | 96.25 | 96.50 | 96.59 |
| **1** | 90.04 | 90.55 | 91.37 | 92.39 | 93.05 |
| **2** | 83.40 | 85.33 | 85.70 | 87.13 | 88.03 |
| **3** | 78.69 | 80.36 | 81.08 | 82.59 | 84.44 |
| **4** | 73.74 | 76.71 | 77.90 | 78.80 | 80.42 |
| **5** | 68.08 | 69.83 | 72.26 | 74.27 | 76.36 |
| **6** | 63.60 | 66.23 | 69.95 | 71.41 | 73.79 |
| **7** | 0.00 | 58.79 | 62.30 | 66.99 | 69.77 |
| **8** | 0.00 | 0.00 | 56.88 | 60.54 | 66.66 |
| **9** | 0.00 | 0.00 | 0.00 | 52.71 | 61.22 |
| **10** | 0.00 | 0.00 | 0.00 | 0.00 | 49.35 |

Table 5.5: One ring uniform distribution. Percentage of available angular region when SINR threshold is greater than -35 dB. AE is operating in simple power minimization mode. L1 frequency band.

| No. of interfering signals | Antenna Array | | | | |
|---|---|---|---|---|---|
| | B4 | C5 | C6 | C7 | C8 |
| **0** | 98.57 | 98.52 | 98.48 | 98.40 | 98.27 |
| **1** | 92.41 | 92.76 | 93.45 | 94.16 | 94.25 |
| **2** | 86.80 | 88.08 | 89.13 | 90.02 | 90.13 |
| **3** | 82.69 | 84.62 | 85.66 | 86.59 | 87.26 |
| **4** | 78.29 | 80.45 | 81.84 | 83.50 | 84.90 |
| **5** | 72.16 | 74.10 | 76.14 | 77.83 | 80.01 |
| **6** | 66.52 | 70.15 | 72.37 | 75.02 | 77.15 |
| **7** | 0.00 | 63.27 | 66.84 | 70.25 | 73.13 |
| **8** | 0.00 | 0.00 | 57.61 | 63.28 | 67.67 |
| **9** | 0.00 | 0.00 | 0.00 | 52.84 | 57.63 |
| **10** | 0.00 | 0.00 | 0.00 | 0.00 | 49.79 |

Table 5.6: One ring uniform distribution. Percentage of available angular region when SINR threshold is greater than -35 dB. AE is operating in simple power minimization mode. L2 frequency band.

| No. of interfering signals | Antenna Array | | | | |
|---|---|---|---|---|---|
| | B4 | C5 | C6 | C7 | C8 |
| **0** | 100.00 | 100.00 | 100.00 | 100.00 | 100.00 |
| **1** | 99.64 | 99.66 | 99.68 | 99.70 | 99.71 |
| **2** | 99.08 | 99.16 | 99.18 | 99.21 | 99.26 |
| **3** | 98.18 | 98.45 | 98.55 | 98.59 | 98.69 |
| **4** | 95.89 | 97.24 | 97.50 | 97.75 | 97.87 |
| **5** | 89.49 | 94.61 | 96.03 | 96.52 | 96.84 |
| **6** | 63.64 | 87.33 | 93.11 | 94.70 | 95.50 |
| **7** | 0.00 | 58.81 | 83.18 | 90.32 | 92.85 |
| **8** | 0.00 | 0.00 | 56.90 | 79.41 | 88.35 |
| **9** | 0.00 | 0.00 | 0.00 | 52.74 | 76.91 |
| **10** | 0.00 | 0.00 | 0.00 | 0.00 | 49.45 |

Table 5.7: One ring uniform distribution. Percentage of available angular region when SINR threshold is greater than -35 dB. AE is operating in beam forming / null steering mode. L1 frequency band.

| No. of interfering signals | Antenna Array | | | | |
|---|---|---|---|---|---|
| | B4 | C5 | C6 | C7 | C8 |
| **0** | 100.00 | 100.00 | 100.00 | 100.00 | 100.00 |
| **1** | 99.48 | 99.53 | 99.57 | 99.61 | 99.64 |
| **2** | 98.51 | 98.69 | 98.82 | 98.98 | 99.08 |
| **3** | 97.19 | 97.52 | 97.78 | 98.12 | 98.39 |
| **4** | 94.10 | 95.50 | 96.07 | 96.70 | 97.27 |
| **5** | 88.72 | 92.86 | 94.06 | 95.15 | 96.09 |
| **6** | 66.54 | 86.65 | 90.42 | 92.89 | 94.41 |
| **7** | 0.00 | 63.31 | 81.52 | 88.22 | 91.11 |
| **8** | 0.00 | 0.00 | 57.66 | 79.50 | 86.13 |
| **9** | 0.00 | 0.00 | 0.00 | 52.90 | 74.07 |
| **10** | 0.00 | 0.00 | 0.00 | 0.00 | 49.85 |

Table 5.8: One ring uniform distribution. Percentage of available angular region when SINR threshold is greater than -35 dB. AE is operating in beam forming / null steering mode. L2 frequency band.

| No. of interfering signals | Antenna Array | | | | | |
|---|---|---|---|---|---|---|
| | C6 | C7 | C8 | C9 | B8 | C10 |
| **0** | 96.25 | 96.50 | 96.59 | 95.62 | 94.66 | 95.37 |
| **1** | 91.37 | 92.39 | 93.05 | 87.95 | 88.80 | 89.32 |
| **2** | 85.70 | 87.13 | 88.03 | 81.47 | 82.81 | 84.08 |
| **3** | 81.08 | 82.59 | 84.44 | 77.24 | 78.52 | 81.50 |
| **4** | 77.90 | 78.80 | 80.42 | 72.26 | 74.77 | 78.04 |
| **5** | 72.26 | 74.27 | 76.36 | 69.24 | 70.87 | 73.91 |
| **6** | 69.95 | 71.41 | 73.79 | 67.61 | 68.03 | 70.08 |
| **7** | 62.30 | 66.99 | 69.77 | 64.75 | 65.28 | 67.32 |
| **8** | 56.88 | 60.54 | 66.66 | 59.79 | 63.37 | 64.54 |
| **9** | 0.00 | 52.71 | 61.22 | 0.00 | 58.80 | 62.57 |
| **10** | 0.00 | 0.00 | 49.35 | 0.00 | 0.00 | 60.72 |

Table 5.9: Comparison of one and two ring distributions. Percentage of available angular region when SINR threshold is greater than -35 dB. AE is operating in simple power minimization mode. L1 frequency band.

| No. of interfering signals | Antenna Array | | | | | |
|---|---|---|---|---|---|---|
| | C6 | C7 | C8 | C9 | B8 | C10 |
| **0** | 98.48 | 98.40 | 98.27 | 97.43 | 96.29 | 95.00 |
| **1** | 93.45 | 94.16 | 94.25 | 90.40 | 90.70 | 88.69 |
| **2** | 89.13 | 90.02 | 90.13 | 83.99 | 85.28 | 83.88 |
| **3** | 85.66 | 86.59 | 87.26 | 80.63 | 81.55 | 81.21 |
| **4** | 81.84 | 83.50 | 84.90 | 76.59 | 79.31 | 77.88 |
| **5** | 76.14 | 77.83 | 80.01 | 71.78 | 75.56 | 73.85 |
| **6** | 72.37 | 75.02 | 77.15 | 69.28 | 73.48 | 69.68 |
| **7** | 66.84 | 70.25 | 73.13 | 66.55 | 70.56 | 66.39 |
| **8** | 57.61 | 63.28 | 67.67 | 61.72 | 66.36 | 64.11 |
| **9** | 0.00 | 52.84 | 57.63 | 0.02 | 62.02 | 62.26 |
| **10** | 0.00 | 0.00 | 49.79 | 0.00 | 0.00 | 56.85 |

Table 5.10: Comparison of one and two ring distributions. Percentage of available angular region when SINR threshold is greater than -35 dB. AE is operating in simple power minimization mode. L2 frequency band.

| No. of interfering signals | Antenna Array | | | | | |
|---|---|---|---|---|---|---|
| | C6 | C7 | C8 | C9 | B8 | C10 |
| **0** | 100.00 | 100.00 | 100.00 | 100.00 | 100.00 | 100.00 |
| **1** | 99.68 | 99.70 | 99.71 | 99.73 | 99.76 | 99.79 |
| **2** | 99.18 | 99.21 | 99.26 | 99.36 | 99.42 | 99.46 |
| **3** | 98.55 | 98.59 | 98.69 | 98.78 | 98.92 | 99.05 |
| **4** | 97.50 | 97.75 | 97.87 | 97.85 | 98.11 | 98.42 |
| **5** | 96.03 | 96.52 | 96.84 | 96.42 | 96.99 | 97.61 |
| **6** | 93.11 | 94.70 | 95.50 | 93.85 | 95.50 | 96.38 |
| **7** | 83.18 | 90.32 | 92.85 | 86.35 | 92.25 | 94.26 |
| **8** | 56.90 | 79.41 | 88.35 | 62.07 | 84.80 | 91.10 |
| **9** | 0.00 | 52.74 | 76.91 | 1.29 | 58.83 | 84.01 |
| **10** | 0.00 | 0.00 | 49.45 | 0.05 | 0.00 | 62.25 |

Table 5.11: Comparison of one and two ring distributions. Percentage of available angular region when SINR threshold is greater than -35 dB. AE is operating in beam forming / null steering mode. L1 frequency band.

| No. of interfering signals | Antenna Array | | | | | |
|---|---|---|---|---|---|---|
| | C6 | C7 | C8 | C9 | B8 | C10 |
| **0** | 100.00 | 100.00 | 100.00 | 100.00 | 100.00 | 100.00 |
| **1** | 99.57 | 99.61 | 99.64 | 99.63 | 99.69 | 99.66 |
| **2** | 98.82 | 98.98 | 99.08 | 99.07 | 99.14 | 99.17 |
| **3** | 97.78 | 98.12 | 98.39 | 98.15 | 98.37 | 98.49 |
| **4** | 96.07 | 96.70 | 97.27 | 96.57 | 96.94 | 97.29 |
| **5** | 94.06 | 95.15 | 96.09 | 94.40 | 95.34 | 96.00 |
| **6** | 90.42 | 92.89 | 94.41 | 91.53 | 93.15 | 94.02 |
| **7** | 81.52 | 88.22 | 91.11 | 84.45 | 89.19 | 91.33 |
| **8** | 57.66 | 79.50 | 86.13 | 62.74 | 81.99 | 87.20 |
| **9** | 0.00 | 52.90 | 74.07 | 0.02 | 62.05 | 79.12 |
| **10** | 0.00 | 0.00 | 49.85 | 0.00 | 0.00 | 57.64 |

Table 5.12: Comparison of one and two ring distributions. Percentage of available angular region when SINR threshold is greater than -35 dB. AE is operating in beam forming / null steering mode. L2 frequency band.

| No. of interfering signals | Antenna Array | | | | | | |
|---|---|---|---|---|---|---|---|
| | C9 | B8 | C10 | C11 | C12 | C13 | C14 |
| **0** | 95.62 | 94.66 | 95.37 | 94.07 | 94.40 | 94.49 | 94.36 |
| **1** | 87.95 | 88.80 | 89.32 | 89.42 | 88.82 | 88.69 | 88.12 |
| **2** | 81.47 | 82.81 | 84.08 | 84.36 | 82.90 | 82.46 | 82.45 |
| **3** | 77.24 | 78.52 | 81.50 | 81.17 | 79.31 | 79.79 | 78.49 |
| **4** | 72.26 | 74.77 | 78.04 | 77.97 | 76.52 | 76.07 | 74.93 |
| **5** | 69.24 | 70.87 | 73.91 | 75.07 | 72.56 | 73.10 | 71.13 |
| **6** | 67.61 | 68.03 | 70.08 | 72.27 | 70.41 | 69.43 | 67.61 |
| **7** | 64.75 | 65.28 | 67.32 | 68.94 | 67.16 | 66.46 | 65.03 |
| **8** | 59.79 | 63.37 | 64.54 | 65.04 | 63.83 | 63.14 | 62.66 |
| **9** | 0.00 | 58.80 | 62.57 | 63.64 | 63.19 | 60.95 | 59.82 |
| **10** | 0.00 | 0.00 | 60.72 | 60.29 | 60.43 | 57.98 | 56.15 |
| **11** | 0.00 | 0.00 | 0.00 | 58.08 | 58.16 | 56.94 | 53.07 |
| **12** | 0.00 | 0.00 | 0.00 | 0.00 | 56.67 | 53.80 | 48.69 |
| **13** | 0.00 | 0.00 | 0.00 | 0.00 | 0.00 | 50.56 | 47.53 |
| **14** | 0.00 | 0.00 | 0.00 | 0.00 | 0.00 | 0.00 | 46.60 |

Table 5.13: Two ring distribution with an inner ring height of 4.24 inches. Percentage of available angular region when SINR threshold is greater than -35 dB. AE is operating in simple power minimization mode. L1 frequency band.

| No. of interfering signals | Antenna Array | | | | | | |
|---|---|---|---|---|---|---|---|
| | C9 | B8 | C10 | C11 | C12 | C13 | C14 |
| **0** | 97.43 | 96.29 | 95.00 | 96.29 | 95.08 | 94.74 | 92.69 |
| **1** | 90.40 | 90.70 | 88.69 | 91.09 | 88.77 | 88.96 | 87.16 |
| **2** | 83.99 | 85.28 | 83.88 | 86.29 | 83.38 | 83.64 | 82.33 |
| **3** | 80.63 | 81.55 | 81.21 | 83.42 | 79.95 | 80.20 | 79.01 |
| **4** | 76.59 | 79.31 | 77.88 | 79.53 | 76.67 | 76.61 | 76.23 |
| **5** | 71.78 | 75.56 | 73.85 | 75.68 | 71.76 | 72.18 | 71.20 |
| **6** | 69.28 | 73.48 | 69.68 | 72.09 | 68.30 | 68.57 | 67.24 |
| **7** | 66.55 | 70.56 | 66.39 | 70.32 | 65.69 | 66.14 | 64.66 |
| **8** | 61.72 | 66.36 | 64.11 | 68.01 | 63.74 | 64.63 | 62.49 |
| **9** | 0.02 | 62.02 | 62.26 | 64.48 | 62.14 | 61.59 | 59.98 |
| **10** | 0.00 | 0.00 | 56.85 | 60.47 | 60.50 | 59.24 | 58.09 |
| **11** | 0.00 | 0.00 | 5.34 | 56.99 | 56.13 | 56.47 | 55.51 |
| **12** | 0.00 | 0.00 | 0.00 | 3.65 | 54.98 | 53.29 | 51.41 |
| **13** | 0.00 | 0.00 | 0.00 | 2.51 | 4.79 | 50.35 | 49.03 |
| **14** | 0.00 | 0.00 | 0.00 | 0.00 | 2.37 | 7.18 | 45.01 |

Table 5.14: Two ring distribution with an inner ring height of 4.24 inches. Percentage of available angular region when SINR threshold is greater than -35 dB. AE is operating in simple power minimization mode. L2 frequency band.

| No. of interfering signals | Antenna Array | | | | | | |
|---|---|---|---|---|---|---|---|
| | C9 | B8 | C10 | C11 | C12 | C13 | C14 |
| **0** | 100.00 | 100.00 | 100.00 | 100.00 | 100.00 | 100.00 | 100.00 |
| **1** | 99.73 | 99.76 | 99.79 | 99.79 | 99.80 | 99.82 | 99.82 |
| **2** | 99.36 | 99.42 | 99.46 | 99.48 | 99.53 | 99.58 | 99.58 |
| **3** | 98.78 | 98.92 | 99.05 | 99.05 | 99.15 | 99.21 | 99.26 |
| **4** | 97.85 | 98.11 | 98.42 | 98.48 | 98.62 | 98.75 | 98.78 |
| **5** | 96.42 | 96.99 | 97.61 | 97.73 | 98.04 | 98.18 | 98.24 |
| **6** | 93.85 | 95.50 | 96.38 | 96.65 | 97.18 | 97.36 | 97.48 |
| **7** | 86.35 | 92.25 | 94.26 | 95.00 | 95.81 | 96.12 | 96.36 |
| **8** | 62.07 | 84.80 | 91.10 | 92.61 | 93.93 | 94.54 | 94.91 |
| **9** | 1.29 | 58.83 | 84.01 | 88.51 | 91.32 | 92.28 | 92.69 |
| **10** | 0.05 | 0.00 | 62.25 | 81.40 | 87.67 | 89.45 | 90.27 |
| **11** | 0.00 | 0.00 | 4.15 | 59.17 | 80.47 | 85.25 | 87.31 |
| **12** | 0.00 | 0.00 | 0.10 | 3.23 | 58.37 | 76.53 | 80.71 |
| **13** | 0.00 | 0.00 | 0.00 | 0.00 | 3.34 | 54.12 | 70.32 |
| **14** | 0.00 | 0.00 | 0.00 | 0.00 | 0.00 | 3.34 | 49.64 |

Table 5.15: Two ring distribution with an inner ring height of 4.24 inches. Percentage of available angular region when SINR threshold is greater than -35 dB. AE is operating in beam forming / null steering mode. L1 frequency band.

| No. of interfering signals | Antenna Array | | | | | | |
|---|---|---|---|---|---|---|---|
| | C9 | B8 | C10 | C11 | C12 | C13 | C14 |
| **0** | 100.00 | 100.00 | 100.00 | 100.00 | 100.00 | 100.00 | 100.00 |
| **1** | 99.63 | 99.69 | 99.66 | 99.71 | 99.73 | 99.74 | 99.75 |
| **2** | 99.07 | 99.14 | 99.17 | 99.28 | 99.32 | 99.36 | 99.38 |
| **3** | 98.15 | 98.37 | 98.49 | 98.69 | 98.76 | 98.86 | 98.89 |
| **4** | 96.57 | 96.94 | 97.29 | 97.75 | 97.93 | 98.06 | 98.12 |
| **5** | 94.40 | 95.34 | 96.00 | 96.64 | 97.04 | 97.19 | 97.31 |
| **6** | 91.53 | 93.15 | 94.02 | 95.09 | 95.62 | 95.88 | 96.18 |
| **7** | 84.45 | 89.19 | 91.33 | 92.92 | 93.61 | 94.04 | 94.50 |
| **8** | 62.74 | 81.99 | 87.20 | 90.07 | 91.11 | 91.85 | 92.51 |
| **9** | 0.02 | 62.05 | 79.12 | 84.92 | 87.46 | 88.36 | 89.55 |
| **10** | 0.00 | 0.00 | 57.64 | 77.43 | 82.92 | 84.66 | 86.73 |
| **11** | 0.00 | 0.00 | 5.55 | 58.19 | 74.73 | 79.10 | 82.81 |
| **12** | 0.00 | 0.00 | 0.00 | 4.03 | 55.98 | 69.92 | 76.31 |
| **13** | 0.00 | 0.00 | 0.00 | 2.64 | 5.36 | 53.01 | 65.39 |
| **14** | 0.00 | 0.00 | 0.00 | 0.00 | 2.41 | 8.72 | 49.04 |

Table 5.16: Two ring distribution with an inner ring height of 4.24 inches. Percentage of available angular region when SINR threshold is greater than -35 dB. AE is operating in beam forming / null steering mode. L2 frequency band.

| No. of interfering signals | Antenna Array | | | | |
|---|---|---|---|---|---|
| | C15 | C16 | C17 | C18 | C19 |
| **0** | 96.42 | 96.17 | 96.21 | 96.25 | 96.00 |
| **1** | 90.80 | 91.61 | 91.20 | 91.90 | 92.12 |
| **2** | 85.21 | 86.51 | 86.59 | 87.38 | 87.70 |
| **3** | 81.59 | 82.09 | 84.13 | 84.66 | 84.46 |
| **4** | 76.99 | 77.91 | 80.84 | 81.44 | 81.45 |
| **5** | 72.93 | 74.02 | 76.42 | 77.62 | 77.68 |
| **6** | 69.44 | 71.09 | 72.26 | 74.75 | 74.59 |
| **7** | 66.93 | 68.55 | 69.07 | 71.26 | 71.10 |
| **8** | 60.71 | 63.78 | 64.23 | 66.28 | 66.95 |
| **9** | 0.00 | 61.29 | 61.47 | 63.26 | 64.61 |
| **10** | 0.00 | 0.00 | 57.42 | 61.15 | 60.36 |
| **11** | 0.00 | 0.00 | 0.00 | 55.74 | 58.35 |
| **12** | 0.00 | 0.00 | 0.00 | 0.00 | 54.31 |

Table 5.17: Two ring distribution with an inner ring height of three inches. Percentage of available angular region when SINR threshold is greater than -35 dB. AE is operating in simple power minimization mode. L1 frequency band.

| No. of interfering signals | Antenna Array | | | | |
|---|---|---|---|---|---|
| | C15 | C16 | C17 | C18 | C19 |
| **0** | 96.21 | 95.41 | 96.26 | 95.46 | 95.62 |
| **1** | 90.47 | 90.85 | 90.83 | 90.78 | 90.10 |
| **2** | 84.02 | 85.06 | 86.18 | 86.04 | 85.56 |
| **3** | 79.93 | 81.24 | 83.17 | 83.40 | 81.96 |
| **4** | 76.62 | 78.28 | 80.40 | 79.77 | 78.85 |
| **5** | 70.10 | 73.26 | 74.79 | 74.66 | 73.44 |
| **6** | 68.18 | 70.06 | 70.11 | 70.83 | 68.72 |
| **7** | 65.30 | 67.61 | 66.08 | 67.57 | 67.13 |
| **8** | 60.41 | 63.16 | 63.11 | 64.66 | 64.56 |
| **9** | 0.00 | 58.56 | 60.12 | 61.51 | 61.72 |
| **10** | 0.00 | 1.39 | 55.01 | 59.10 | 59.87 |
| **11** | 0.00 | 0.00 | 4.58 | 54.06 | 55.64 |
| **12** | 0.00 | 0.00 | 0.00 | 4.03 | 52.74 |

Table 5.18: Two ring distribution with an inner ring height of three inches. Percentage of available angular region when SINR threshold is greater than -35 dB. AE is operating in simple power minimization mode. L2 frequency band.

| No. of interfering signals | Antenna Array | | | | |
|---|---|---|---|---|---|
| | C15 | C16 | C17 | C18 | C19 |
| **0** | 100.00 | 100.00 | 100.00 | 100.00 | 100.00 |
| **1** | 99.71 | 99.73 | 99.74 | 99.76 | 99.78 |
| **2** | 99.31 | 99.37 | 99.41 | 99.43 | 99.50 |
| **3** | 98.68 | 98.83 | 98.95 | 98.99 | 99.08 |
| **4** | 97.70 | 98.01 | 98.24 | 98.37 | 98.50 |
| **5** | 96.24 | 97.02 | 97.41 | 97.65 | 97.86 |
| **6** | 93.56 | 95.24 | 96.06 | 96.60 | 96.94 |
| **7** | 86.21 | 92.01 | 93.73 | 94.85 | 95.55 |
| **8** | 61.32 | 84.16 | 90.35 | 92.39 | 93.75 |
| **9** | 0.06 | 58.35 | 82.41 | 88.27 | 91.09 |
| **10** | 0.00 | 0.93 | 58.46 | 80.89 | 87.33 |
| **11** | 0.00 | 0.00 | 2.47 | 57.33 | 79.91 |
| **12** | 0.00 | 0.00 | 0.00 | 2.09 | 57.15 |

Table 5.19: Two ring distribution with an inner ring height of three inches. Percentage of available angular region when SINR threshold is greater than -35 dB. AE is operating in beam forming / null steering mode. L1 frequency band.

| No. of interfering signals | Antenna Array | | | | |
|---|---|---|---|---|---|
| | C15 | C16 | C17 | C18 | C19 |
| **0** | 100.00 | 100.00 | 100.00 | 100.00 | 100.00 |
| **1** | 99.59 | 99.63 | 99.64 | 99.67 | 99.69 |
| **2** | 98.91 | 99.02 | 99.10 | 99.19 | 99.21 |
| **3** | 97.94 | 98.18 | 98.38 | 98.49 | 98.59 |
| **4** | 96.17 | 96.81 | 97.12 | 97.42 | 97.65 |
| **5** | 93.88 | 95.14 | 95.77 | 96.17 | 96.63 |
| **6** | 90.63 | 92.63 | 93.80 | 94.50 | 95.16 |
| **7** | 82.46 | 88.43 | 90.89 | 92.14 | 93.02 |
| **8** | 60.61 | 80.13 | 86.72 | 89.13 | 90.36 |
| **9** | 0.01 | 58.68 | 78.00 | 83.79 | 86.48 |
| **10** | 0.00 | 1.45 | 55.80 | 75.44 | 82.04 |
| **11** | 0.00 | 0.00 | 4.78 | 55.19 | 72.98 |
| **12** | 0.00 | 0.00 | 0.00 | 4.39 | 53.93 |

Table 5.20: Two ring distribution with an inner ring height of three inches. Percentage of available angular region when SINR threshold is greater than -35 dB. AE is operating in beam forming / null steering mode. L2 frequency band.

| No. of interfering signals | Antenna Array | |
|---|---|---|
| | C11 | C18 |
| **0** | 94.07 | 96.25 |
| **1** | 89.42 | 91.90 |
| **2** | 84.36 | 87.38 |
| **3** | 81.17 | 84.66 |
| **4** | 77.97 | 81.44 |
| **5** | 75.07 | 77.62 |
| **6** | 72.27 | 74.75 |
| **7** | 68.94 | 71.26 |
| **8** | 65.04 | 66.28 |
| **9** | 63.64 | 63.26 |
| **10** | 60.29 | 61.15 |
| **11** | 58.08 | 55.74 |

Table 5.21: Twelve Element Antenna Arrays. Percentage of available angular region when SINR threshold is greater than -35 dB. AE is operating in simple power minimization mode. L1 frequency band.

| No. of interfering signals | Antenna Array | |
|---|---|---|
| | C11 | C18 |
| **0** | 96.29 | 95.46 |
| **1** | 91.09 | 90.78 |
| **2** | 86.29 | 86.04 |
| **3** | 83.42 | 83.40 |
| **4** | 79.53 | 79.77 |
| **5** | 75.68 | 74.66 |
| **6** | 72.09 | 70.83 |
| **7** | 70.32 | 67.57 |
| **8** | 68.01 | 64.66 |
| **9** | 64.48 | 61.51 |
| **10** | 60.47 | 59.10 |
| **11** | 56.99 | 54.06 |

Table 5.22: Twelve Element Antenna Arrays. Percentage of available angular region when SINR threshold is greater than -35 dB. AE is operating in simple power minimization mode. L2 frequency band.

| No. of interfering signals | Antenna Array | |
|---|---|---|
| | C11 | C18 |
| **0** | 100.00 | 100.00 |
| **1** | 99.79 | 99.76 |
| **2** | 99.48 | 99.43 |
| **3** | 99.05 | 98.99 |
| **4** | 98.48 | 98.37 |
| **5** | 97.73 | 97.65 |
| **6** | 96.65 | 96.60 |
| **7** | 95.00 | 94.85 |
| **8** | 92.61 | 92.39 |
| **9** | 88.51 | 88.27 |
| **10** | 81.40 | 80.89 |
| **11** | 59.17 | 57.33 |

Table 5.23: Twelve Element Antenna Arrays. Percentage of available angular region when SINR threshold is greater than -35 dB. AE is operating in beam forming / null steering mode. L1 frequency band.

| No. of interfering signals | Antenna Array | |
|---|---|---|
| | C11 | C18 |
| **0** | 100.00 | 100.00 |
| **1** | 99.71 | 99.67 |
| **2** | 99.28 | 99.19 |
| **3** | 98.69 | 98.49 |
| **4** | 97.75 | 97.42 |
| **5** | 96.64 | 96.17 |
| **6** | 95.09 | 94.50 |
| **7** | 92.92 | 92.14 |
| **8** | 90.07 | 89.13 |
| **9** | 84.92 | 83.79 |
| **10** | 77.43 | 75.44 |
| **11** | 58.19 | 55.19 |

Table 5.24: Twelve Element Antenna Arrays. Percentage of available angular region when SINR threshold is greater than -35 dB. AE is operating in beam forming / null steering mode. L2 frequency band.

| No. of interfering signals | Antenna Array | |
|---|---|---|
| | C4 | C11 |
| **0** | 95.46 | 94.07 |
| **1** | 85.78 | 89.42 |
| **2** | 78.96 | 84.36 |
| **3** | 75.92 | 81.17 |
| **4** | 69.13 | 77.97 |
| **5** | 66.24 | 75.07 |
| **6** | 65.69 | 72.27 |
| **7** | 0.00 | 68.94 |
| **8** | 0.00 | 65.04 |
| **9** | 0.00 | 63.64 |
| **10** | 0.00 | 60.29 |
| **11** | 0.00 | 58.08 |

Table 5.25: Comparison of seven and twelve element antenna arrays. Percentage of available angular region when SINR threshold is greater than -35 dB. AE is operating in simple power minimization mode. L1 frequency band.

| No. of interfering signals | Antenna Array | |
|---|---|---|
| | C4 | C11 |
| **0** | 96.76 | 96.29 |
| **1** | 87.62 | 91.09 |
| **2** | 81.01 | 86.29 |
| **3** | 77.31 | 83.42 |
| **4** | 73.20 | 79.53 |
| **5** | 71.32 | 75.68 |
| **6** | 68.11 | 72.09 |
| **7** | 0.00 | 70.32 |
| **8** | 0.00 | 68.01 |
| **9** | 0.00 | 64.48 |
| **10** | 0.00 | 60.47 |
| **11** | 0.00 | 56.99 |

Table 5.26: Comparison of seven and twelve element antenna arrays. Percentage of available angular region when SINR threshold is greater than -35 dB. AE is operating in simple power minimization mode. L2 frequency band.

| No. of interfering signals | Antenna Array | |
|---|---|---|
| | C4 | C11 |
| **0** | 100.00 | 100.00 |
| **1** | 99.63 | 99.79 |
| **2** | 98.98 | 99.48 |
| **3** | 97.86 | 99.05 |
| **4** | 95.65 | 98.48 |
| **5** | 90.16 | 97.73 |
| **6** | 65.71 | 96.65 |
| **7** | 0.00 | 95.00 |
| **8** | 0.00 | 92.61 |
| **9** | 0.00 | 88.51 |
| **10** | 0.00 | 81.40 |
| **11** | 0.00 | 59.17 |

Table 5.27: Comparison of seven and twelve element antenna arrays. Percentage of available angular region when SINR threshold is greater than -35 dB. AE is operating in beam forming / null steering mode. L1 frequency band.

| No. of interfering signals | Antenna Array | |
|---|---|---|
| | C4 | C11 |
| **0** | 100.00 | 100.00 |
| **1** | 99.45 | 99.71 |
| **2** | 98.49 | 99.28 |
| **3** | 97.08 | 98.69 |
| **4** | 93.77 | 97.75 |
| **5** | 87.83 | 96.64 |
| **6** | 68.11 | 95.09 |
| **7** | 0.00 | 92.92 |
| **8** | 0.00 | 90.07 |
| **9** | 0.00 | 84.92 |
| **10** | 0.00 | 77.43 |
| **11** | 0.00 | 58.19 |

Table 5.28: Comparison of seven and twelve element antenna arrays. Percentage of available angular region when SINR threshold is greater than -35 dB. AE is operating in beam forming / null steering mode. L2 frequency band.

# CHAPTER 6

# TWO INCH HIGH GEOMETRIES

Previously, we have studied the six inch spherical surface, which is a possibility for ship-board application; however, it would not be desirable to the aerodynamic profile of an aircraft due to its physical size. Therefore, we are studying a two inch high surface, which maintains a curvature relative to a spherical surface of radius ten inches. As we have seen previously, this surface will not yield the performance of a six inch high geometry; however, it will still yield better performance than a planar geometry. In this chapter, we will investigate the best distribution for a two inch high surface. Three types of geometry distributions have been studied. The first type of geometry has a reference element located at the apex of the surface, where the remaining elements are distributed uniformly at the bottom of the surface. The second type of geometry has a two ring distribution, with one element located at the top of the surface, some elements distributed on an inner ring height of 1.46 inches, and the remaining elements distributed along the bottom of the surface. The third type of geometry has one element at the top and the remaining elements distributed non-uniformly at the bottom of the surface. First, we will set a baseline using seven element arrays. Then, we will study the effect of the addition of elements to AJ performance for each individual brand of antenna geometry. We will then compare the results of the best antenna arrays regarding AJ performance, and direct comparison to the seven element array to see the result of attainable performance improvement. It will be shown that the one ring distribution achieve better AJ performance than the two ring distribution. Furthermore, as the antenna aperture becomes filled with antenna elements there is not much difference between distributing the auxiliary elements uniformly or non-uniformly.

## 6.1 Seven Element Antenna Arrays

We will set a baseline using the seven element antenna arrays, with the three types of distributions mentioned above, and compare their respective AJ performances. Antenna array B2 (Figure 6.1), introduced in Chapter 4 has seven elements with the reference element located at the top of the surface and the remaining elements distributed uniformly around the bottom of the surface. Antenna array D1 (Figure 6.2) has one element at the top, three elements distributed on an inner ring height of 1.46 inches, and the remaining three elements distributed along the bottom of the surface. Antenna array D2 (Figure 6.3) has one element at the top of the surface, and the remaining six elements distributed non-uniformly around the bottom of the hemisphere.

Figures 6.16 and 6.17 show the percentage available angular region for the L1 and L2 bands, respectively, while the antenna is operating in the presence of one to six interfering signals. The AE is operating in simple power minimization mode. For the L1 band (Figure 6.16), it is shown that all three antenna arrays have similar performance. However, for six interfering signals the two one ring distributions (antenna arrays B2 and D2) outperform the two ring distribution (antenna array D1) and antenna array D2 has slightly better performance than antenna array B2. In the L2 band (Figure 6.17), there are similar results as the L1 band. All three antenna arrays have similar performance and for six interfering signals antenna array D2 exhibits slightly better performance. Note that antenna array D1 has slightly better performance than antenna array D2 for a lower number of interfering signals; however, we are interested in how the antenna arrays perform in severe interference environments.

These results are further supported by Tables 6.1 and 6.2, which display the percentage available angular region when the output SINR exceeds -35 dB in the presence of zero to six interfering signals. The antenna electronics is operating in the simple power minimization mode. In Table 6.1, one observes that antenna array D2 exhibits the best AJ performance for any given number of interfering signals. In the

L2 band (Table 6.2), one observes that antenna array D1 yields the best performance for 5 or less interfering signals; however, in the presence of six interfering signals, it is seen that antenna array D2 has the best performance. Therefore, antenna array D2 has the best overall performance of the three antenna arrays for the interference signal scenarios of interest while the AE is operating in simple power minimization mode.

Figures 6.18 and 6.19 show the performance of the three antenna arrays when the AE is operating in the beam forming / null steering mode. All other parameters are the same as in Figures and 6.16 and 6.17, respectively. One observes similar results for the simple power minimization mode. In the L1 band, the one ring distributions outperform the two ring distribution with antenna array D2 performing slightly better than B2 for a high number of interfering signals. In the L2 band, one notices that all three antenna arrays have similar performance; however, antenna array D2 has better performance than the other two antenna arrays B2 and D1 for any given number of interfering signals.

This conclusion can be seen in Tables 6.3 and 6.4, which show the percentage available angular region for which the output SINR is greater than -35 dB in the presence of zero to six interfering signals while the AE is operating in simple power minimization mode. From Table 6.3, one observes that antenna arrays B2 and D2 have similar performance and are performing better than antenna array D1. Also, antenna array D2 has slightly better performance than antenna array B1 in the presence of six interfering signals. The same can be seen in Table 6.4. Therefore, one can again conclude that antenna array D2 has the best overall performance and is selected as the best seven element antenna array for further studies. Another observation to be made from comparing Tables 6.3 and 6.4 with Tables 6.1 and 6.2, is that the antenna arrays perform significantly better in the beam forming / null steering mode, as expected. It has been shown for the seven element antenna arrays that the one ring non-uniform distribution of antenna array D2 performed the best; however, this may not be true with the increase of the number of elements. Therefore, we will investigate the addition of elements to the three types of geometries and compare their performances.

## 6.2 Distribution of Elements Uniformly on One Ring

The antenna arrays studied in this section all have the same distribution with one element at the top of the surface and the remaining elements uniformly distributed along an outer ring at the bottom of the surface. Antenna array B2 will be included from above. Antenna arrays D3 (Figure 6.4), D4 (Figure 6.5), D5 (Figure 6.6), and D6 (Figure 6.7) have nine, ten, eleven, and twelve elements, respectively. The AJ performance of the five antenna arrays will be shown in the presence of four to eleven interfering signals while the antenna electronics is operating in both simple power minimization and beam forming / null steering mode.

Figures 6.20 and 6.21 show the AJ performance while the AE is operating in simple power minimization mode for the L1 and L2 band, respectively. For both the L1 and L2 bands, one observes that for a low number of jammers, antenna arrays with a larger number of elements exhibit slightly better performance; however, as the number of interfering signals increase and one maintains at least N+1 antenna elements in the presence of N jammers, all antenna arrays maintain similar performance.

Tables 6.5 and 6.6 display the percentage available angular region where the output SINR exceeds -35 dB while the AE is operating in the simple power minimization mode for the L1 and L2 bands, respectively. The results are shown for the antenna arrays operating in the presence of zero to eleven interfering signals. In the tables, one observes that AJ performance degrades as the number of interfering signals increase, as expected. In the L1 band (Table 6.5), one observes that the performance consistently improves as the number of antenna elements increases for five or less interfering signals. It is noted that the twelve element array (antenna array D6), has the best performance up to ten interfering signals, where antenna array D5 has better performance. However, antenna array D6 possesses the capability to null more interfering signals. In Table 6.6, it shows that the AJ performance improves constantly as the number of antenna elements is increased up to four interfering signals. Furthermore, it is seen that antenna array D6 has the best performance for any given number of interfering signals. Comparing 6.5 and 6.6, one observes that there is much better AJ performance in the L1 band than in the L2 band. This result is due to the antenna array aperture being electrically larger in the L1 band and a larger amount of mutual coupling between the reference element and the auxiliary elements in the L2 band.

Figures 6.22 and 6.23 show the AJ performance for the L1 and L2 bands, respectively, while the AE is operating in beam forming / null steering mode. All other parameters are the same as in Figures 6.20 and 6.21. For both the L1 and L2 bands, one observes that there is a consistent performance improvement as the number of antenna elements are increased. Also, comparing Figures 6.22 and 6.23 with Figures 6.20 and 6.21, it is easily observed that the AE operating in the beam forming / null steering mode has a significant advantage over the AE operating in the simple power minimization mode.

Tables 6.7 and 6.8 display the percentage available angular region while the AE is operating in the beam forming / null steering mode for L1 and L2 bands, respectively. All other parameters are the same as in Tables 6.5 and 6.6. It is observed in both tables that one requires N+1 antenna elements to effectively operate in the presence of N interfering signals. Also, it is seen again that increasing the number of antenna elements results in better AJ performance. Furthermore, it is seen that there is better AJ performance in the L1 band than in the L2 band.

## 6.3 Distribution of Elements on Two Rings

The antenna elements are now distributed on two rings, with a reference element at the top of the surface, and some elements distributed on an inner ring height of 1.46 inches, as well as along the outer ring on the bottom of the surface. Antenna array D1 is also included in this section. Antenna array D7 (Figure 6.8) has nine elements with one element distributed at the top, two elements distributed on the 1.46 inch high inner ring and six elements distributed at the bottom on of the surface. Antenna array B6 (Figure 6.9), introduced in Chapter 4, has ten elements overall with three elements along the inner ring, one element at the top, and six elements along the outer ring. Antenna array D8 (Figure 6.10) has eleven total elements with one element located at the top of the surface, three elements located on the inner ring and twelve elements distributed on the outer ring. Finally, antenna array D9 (Figure 6.11) has twelve elements where the reference element is located at the top, three elements are placed on an inner ring with height equal to 1.46 inches, and eight elements along an outer ring at the bottom of the surface.

Figures 6.24 and 6.25 show the AJ performance for the L1 and L2 bands, respectively, of the five antenna arrays while the antenna electronics is operating in simple power minimization mode. The antenna arrays are operating in the presence of four to eleven interfering signals. In the L1 band, as the number of jammers grows the performance begins to degrade, and the antenna arrays exhibit similar AJ performance. Also, for this particular distribution an increase in the number of elements does not guarantee an improvement in AJ performance. One can easily observe this effect for ten interfering signals and that fully constrained antenna array D8 is performing better than antenna array D9. This is especially true for the L2 band. Even though the antenna arrays are fully constrained in the case of a high number of jammers, they are performing better than antenna arrays with more elements. As one can see with antenna array D7 in the presence of eight jammers, antenna array B6 in the presence of nine jammers, and again antenna array D8 in the presence of ten interfering signals. Also, note that the AJ performance at the L2 band is significantly decreased compared to the L1 band. This effect is caused due to the larger amount of mutual coupling at the L2 band between the reference element and the inner ring antenna elements of the arrays.

This can also be more directly observed in comparing Tables 6.9 and 6.10, which is the percentage available region for the L1 and L2 bands, respectively, for which the output SINR exceeds a -35 dB threshold when the antenna arrays are operating in the presence of zero to eleven interfering signals. The AE is operating in simple power minimization mode. In Table 6.9, one observes that for a large number of interfering signals the AJ performance is actually worse for a large number of antenna elements than the fully constrained antenna arrays. One observes antenna array D7 has the best performance for eight interfering signals, antenna array B6 has the best performance for nine interfering signals, and antenna array D8 has the best performance for ten interfering signals. In Table 6.10, one observes that similar results in the L1 band. Antenna array B6 has the best performance for nine interfering signals and antenna array D8 has the best performance for ten interfering signals. Also note that the AJ performance consistently degrades as one increases the number of elements from ten to twelve. This is again possible due to the larger amount of mutual coupling at the L2 band. Also, comparing Tables 6.9 and 6.10 with Tables 6.5 and 6.6, one notices a performance degradation for the two ring distribution when compared with the one ring distribution.

On the contrary, again, one observes the AJ performance improves as the number of antenna elements when the AE is operating in the beam forming / null steering mode. Also, the AJ performance is much better when the AE is operating in the beam forming / null steering mode than in the case of the simple power minimization mode. These results can be viewed in Figures 6.26 and 6.27 for the L1 and L2 band, respectively. One also observes that there is also sufficient performance degradation for the L2 band compared with the L1 band due electric size of the aperture.

This information is further supported by Tables 6.11 and 6.12, which display the percentage available angular region for the L1 and L2 bands, respectively, for which the output SINR exceeds -35 dB while the antenna electronics is operating in the beam forming / null steering mode. All other parameters are the same as in Tables 6.9 and 6.10. One observes a consistent improvement in AJ performance with an increase in the number of antenna elements in both the L1 and L2 bands. Also, comparing Table 6.11 with Table 6.12, one observes that there the performance is somewhat better in the L1 band. Comparing Tables 6.11 and 6.12 with Tables 6.7 and 6.8 one sees that there is better performance exhibited by the one ring distribution antenna arrays. Therefore, the two ring distribution does not seem like it would be the best antenna array distribution due to this degradation.

## 6.4 Distribution of Elements Non-Uniformly on One Ring

It has been shown that distributing antenna elements non-uniformly along the periphery of a surface can yield improved AJ performance [14]. This result was confirmed with bi-conical antenna elements for a planar surface; however, we will use patch antenna elements and a non-planar convex surface. All antenna arrays studied in this section will have a reference element at the top of the surface and the remaining elements located non-uniformly along the outer ring at the bottom of the surface. Antenna array D2 from section 6.1 will also be included in this study. The antenna arrays have nine, ten, eleven, and twelve elements associated to D10 (Figure 6.12), D11 (Figure 6.13), D12 (Figure 6.14), and D13 (Figure 6.15), respectively.

Figures 6.28 and 6.29 show the performance of the five antenna arrays when the AE is operating in a simple power minimization mode. Interference signal scenarios containing four to eleven interfering signals are considered. For the one ring non-uniformly distributed antenna arrays, one can see that the same conclusions hold true as the one ring uniformly distributed antenna arrays. Again, as expected, one can see that in the presence of N interfering signals, one requires at least N+1 antenna elements for AJ performance. The performance of the antenna arrays degrades with an increase in the number of interfering signals. In both the L1 and L2 bands, it is seen that there is a slight advantage of the twelve element antenna array for a low number of interfering signals, and as long as one contains N+1 antenna elements for N interfering signals, all antenna array have fairly similar AJ performance.

Tables 6.13 and 6.14 show the percentage available angular region for the L1 and L2 bands, respectively, where the output SINR is greater than -35 dB in the presence of zero to eleven interfering signals. The AE is operating in the simple power minimization mode. In both the L1 and L2 bands, one observes that antenna array D13 has the best performance for any given number of interfering signals except for ten interfering signals where antenna array D12 has better performance. However, antenna array D13 can null the most interfering signals. Also, it is important to note that in comparing the two tables there is better performance exhibited in the L1 band.

The plots of the antenna electronics operating in beam forming / null steering are given below in Figures 6.30 and 6.31 below. All other parameters are the same as Figures 6.28 and 6.29. Also, the same conclusions drawn here are the same for the uniformly distributed antennas. Beam forming / null steering performs significantly better as one increases the number of elements, and it performs much better as compared to simple power minimization mode. Comparing the performance of non-uniformly distributed antennas with those of the uniformly distributed antennas (see Figures 6.20 and 6.21 for simple power minimization and Figures 6.22 and 6.23 for beam forming / null steering), one can see that the two groups of antennas have almost similar performance. Thus, distributing the elements uniformly or non-uniformly on the outer ring does not make much of a difference.

Tables 6.15 and 6.16 refer to the available angular region for which the output SINR exceeds -35 dB while the AE is operating in the beam forming / null steering mode for the L1 and L2 bands, respectively. All other parameters are the same as in Tables 6.13 and 6.14. One again sees that in both the L1 and L2, a larger number of antenna elements leads to an enhancement in AJ performance. Furthermore, comparing Tables 6.15 and 6.16 with Tables 6.13 and 6.14, one observes a significant performance improvement operating in the beam forming / null steering mode. Therefore, it is recommended to operate in the beam forming / null steering mode with as many elements as possible to achieve the best possible performance. As a result, we will compare the performance of the twelve element antenna arrays for the two inch high geometries.

## 6.5 Comparison of 12 Element Antenna Arrays

We will now examine the three distributions with twelve elements. The selected three twelve element antenna arrays D6, D9, and D13 will be evaluated with respect to AJ performance and we will conclude the best distribution for the two inch high antenna geometry.

Figures 6.32 and 6.33 compare the performance of the antenna arrays at L1 and L2 carrier frequencies, respectively with the number of jammers ranging from four to eleven. The AE is operating in simple power minimization mode. Note that at the L1 and L2 and carrier frequencies, antenna arrays D6 and D13, have similar performance; whereas, antenna array D9 has degraded performance due to mutual coupling effects between the inner ring elements and the reference element, with a more significant degradation observed in the L2 band. Therefore, it is better to distribute the elements in a one ring distribution with the auxiliary elements placed on the bottom of the two inch high surface. Furthermore, from these results it is shown that as one begins to fill the antenna aperture there is not an advantage between distributing the antenna elements uniformly or non-uniformly on the bottom of the surface.

Tables 6.17 and 6.18 show the percentage available angular region for which the output SINR exceeds -35 dB for the L1 and L2 bands, respectively, in the presence of zero to eleven interfering signals. The antenna electronics is operating in the simple power minimization mode. In the L1 band (Table 6.17), one observes that the one ring distributions perform better than the two ring distribution for seven or more interfering signals. Also, when the antenna arrays are fully constrained, antenna array D13 barely exhibits the best performance over antenna array D6($< 2\%$). In Table 6.18 (L2 band), one notices that in the presence of any interference the one ring distribution antenna arrays are outperforming the two ring distribution antenna array. For eleven interfering signals, antenna array D6 has a minimal advantage over antenna array D13 ($< 1\%$). Also, note the antenna arrays yield better AJ performance in the L1 band than in the L2 band.

Figures 6.34 and 6.35 show the performance of antenna arrays D6, D9, and D13 when the AE is operating is the beam forming / null steering mode. All other parameters are the same as in Figures 6.32 and 6.33, respectively. From the results, one can see that at the L1 and L2 carrier frequencies antenna arrays D6 and D13 have similar performance and out perform antenna array D9. Also, it is noted that antenna array D13 has slightly better performance in the L1 band; however, it is by no means significant. Another observation to be made from the plots in Figures 6.32 and 6.35 is that in the beam forming / null steering mode, as expected, the antenna arrays perform extremely better. Therefore, it is definitely advised to operate in beam forming / null steering based AE, if one can afford to do so.

Tables 6.19 and 6.20 show the percentage available angular region for which the output SINR exceeds -35 dB while the AE is operating in the beam forming / null steering mode. All parameters are the same as in 6.17 and 6.18. In both the L1 and L2 bands, the antenna arrays with the one ring distribution outperform the antenna array with the two ring distribution. For eleven interfering signals, antenna array D13 has a slight advantage in AJ performance ($< 2\%$) in the L1 band, and antenna array D6 has a slight advantage in the L2 band ($< 2\%$). Therefore, it does not make a difference how one distributes the elements in one ring as the aperture becomes filled.

Antenna array D13 will be the selected twelve element geometry and compared with seven element antenna array D2.

## 6.6 Comparison of 7 and 12 Element Antenna Arrays

In this section, we will compare the seven element antenna array D2 against the twelve element antenna array D13 to show the amount of performance advantage one will yield by increasing the number of elements. It is noted that both antenna arrays being compared have the non-uniform distribution of the outer ring elements along the bottom of the surface. They performed slightly better than their uniformly distributed counterparts; however, it was by no means significant. Antenna arrays D2 and D13 are compared in the figures below.

Figures 6.36 and 6.37 compare the AJ performance of antenna arrays operating in the simple power minimization mode in the presence of three to eight interfering signals at L1 and L2 frequency bands, respectively. From the figures, as expected, one can see that antenna array D13 outperforms antenna array D2. This is especially true in the presence of seven or more interfering signals. However, it should be noted that antenna array D2 only has seven elements yielding the capability to null six interfering signals; whereas, antenna array D13 has twelve elements. Taking this into account, the performance improvement when the antenna is operating in simple power minimization mode is not very significant unless one is operating in a severe interference environment. Note that the antenna performance of the two antenna arrays is almost similar in the presence of six interfering signals at the L2 carrier frequency.

Tables 6.21 and 6.22 show the percentage available angular region for the L1 and L2 bands, respectively, for which the output SINR exceeds -35 dB in the presence of zero to eleven interfering signals. The AE is operating in simple power minimization mode. One can observe that there is not a significant performance advantage in moving from seven to twelve elements while the antenna electronics is operating in the simple power minimization mode. In fact, for six interfering signals, there is only less than 3% advantage in the L1 band and less than 1% in the L2 band.

Figures 6.36 and 6.37 show the AJ performance of the two antenna arrays when the antenna is operating in the beam forming / null steering mode. All other parameters are the same as in Figures 6.36 and 6.37. Now, one can see that antenna array D13 has significantly better performance than antenna array D2. In fact, D13 shows approximately 30% and 35% performance improvement over D2 in the presence of six interfering signals for the L1 and L2 bands, respectively. Thus, to obtain the best performance as the number of elements is increased, the antenna array should be used with beam forming / null steering based AE. It leads to increase in the number of interfering signals the antenna can null as well as significant improvement in the available angular region in the presence of interfering signals.

Tables 6.23 and 6.24 show the percentage available angular region for the L1 and L2 bands, respectively, while the AE is operating in the beam forming / null steering mode. All other parameters are the same as in Tables 6.21 and 6.22. One can clearly see a significant performance advantage from moving from seven to twelve elements in the presence of a large number of interfering signals. As the seven element antenna array becomes fully constrained, the twelve element antenna array significantly outperforms it with a 32.54% advantage in the L1 band and 36.3% better performance in the L2 band.

## 6.7 Chapter Summary

It was shown that the best distribution for a two inch high geometry with the given dimensions is not a two ring distribution, but a one ring distribution with the auxiliary elements distributed uniformly or non-uniformly along an outer ring at the bottom of the surface. It was also reinforced that the performance does in fact increase as the number of antenna elements increase. However, when the antenna arrays were operating in the simple power minimization mode, there was not a significant increase in AJ performance observed with the addition of more elements. Furthermore, it was shown that when the antenna arrays were operating in the simple power minimization mode, they were able to yield better AJ performance in the L1 band than in the L2 band, which has to do with the antenna array being electrically larger in the L1 band. It has been shown again that one should take extreme consideration into antenna electronics operating in beam forming / null steering mode as the AJ performance is far superior to simple power minimization, and the addition of more elements allows one to null more jammers. Also, it has been suggested that out of the antenna arrays studied for the two inch high geometry, D13 yielded the best overall performance. In the next chapter we will examine the performance advantage one can achieve moving from a planar antenna array to a two inch convex non planar or a six inch convex non planar antenna array.

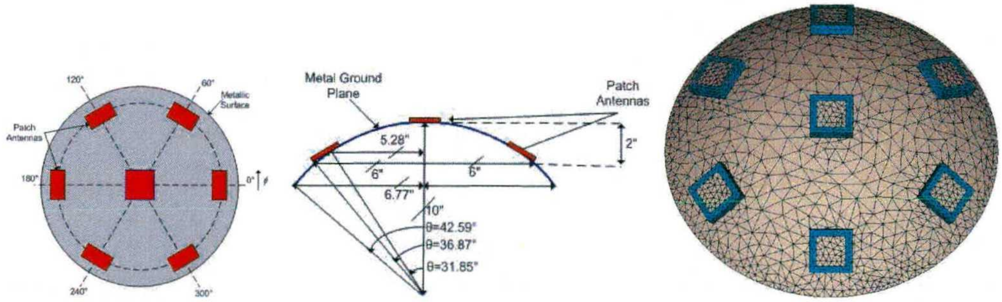


(a) Top Down View (b) Side View (c) Gridded Surface

Figure 6.1: Antenna Array B2.

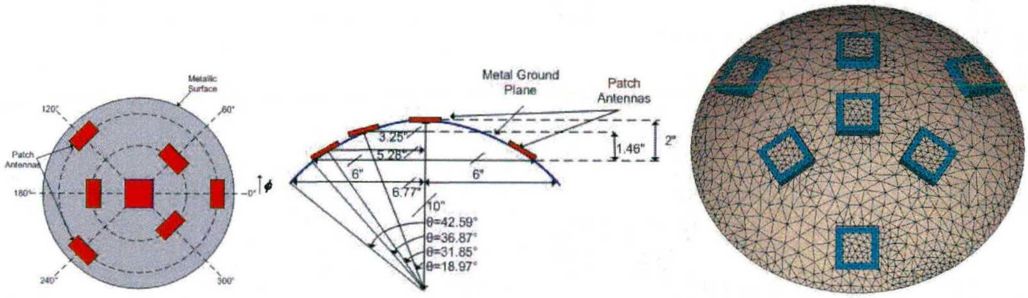


(a) Top Down View (b) Side View (c) Gridded Surface

Figure 6.2: Antenna Array D1.

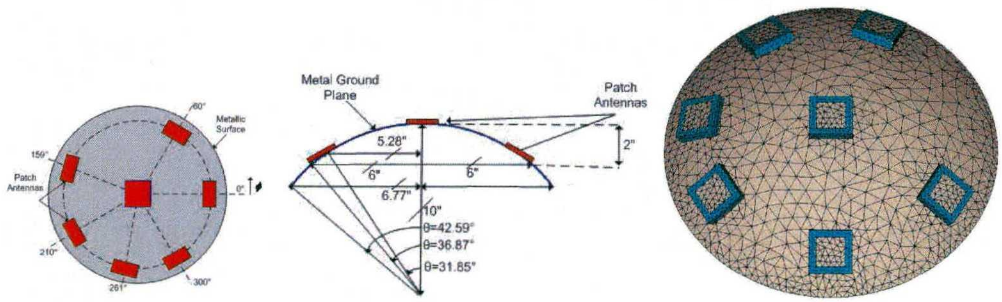


(a) Top Down View (b) Side View (c) Gridded Surface

Figure 6.3: Antenna Array D2.

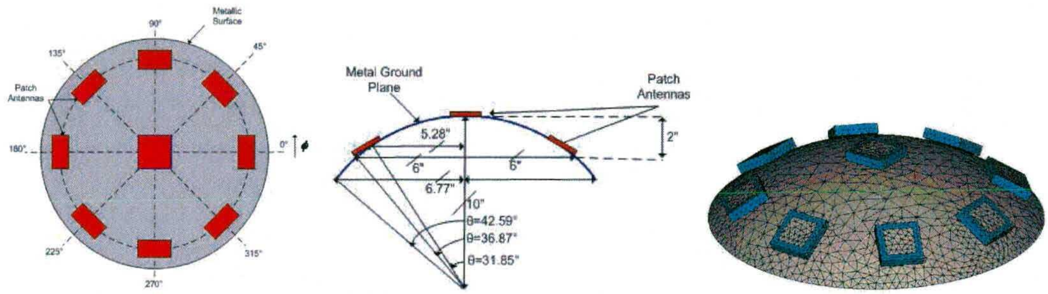


(a) Top Down View (b) Side View (c) Gridded Surface

Figure 6.4: Antenna Array D3.

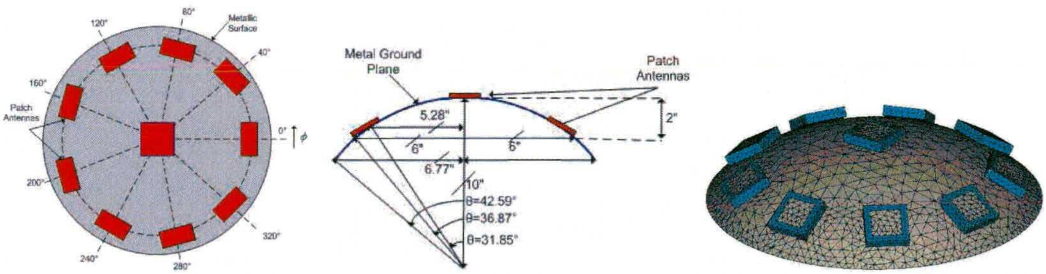


(a) Top Down View (b) Side View (c) Gridded Surface

Figure 6.5: Antenna Array D4.

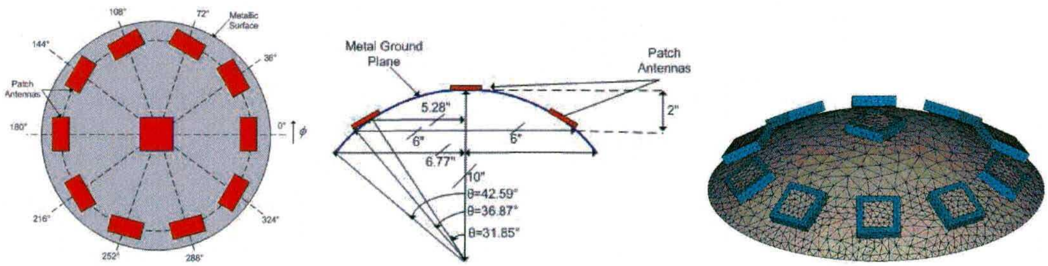


(a) Top Down View (b) Side View (c) Gridded Surface

Figure 6.6: Antenna Array D5.

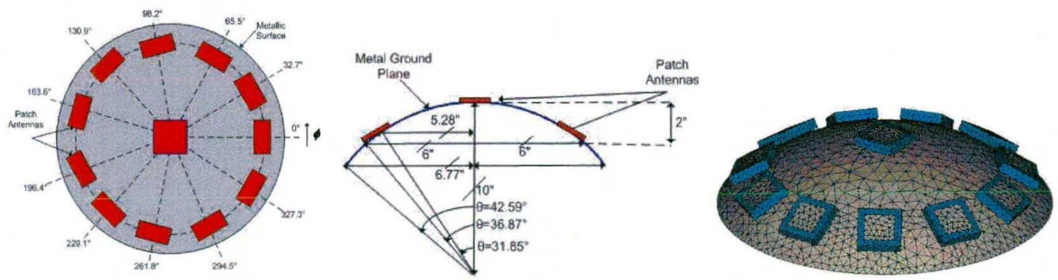


(a) Top Down View (b) Side View (c) Gridded Surface

Figure 6.7: Antenna Array D6.

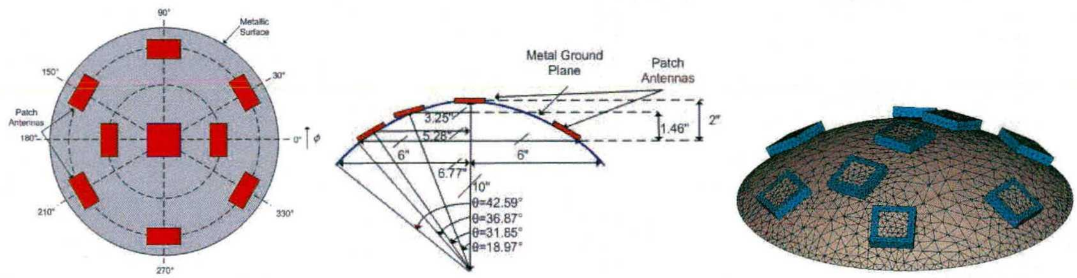


(a) Top Down View (b) Side View (c) Gridded Surface

Figure 6.8: Antenna Array D7.

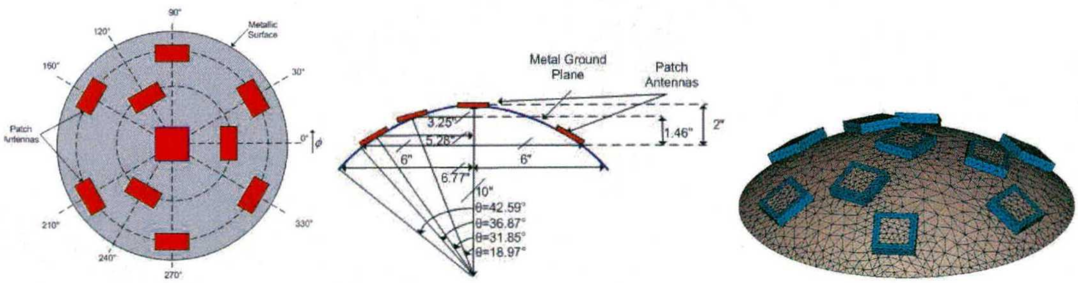


(a) Top Down View (b) Side View (c) Gridded Surface

Figure 6.9: Antenna Array B6.

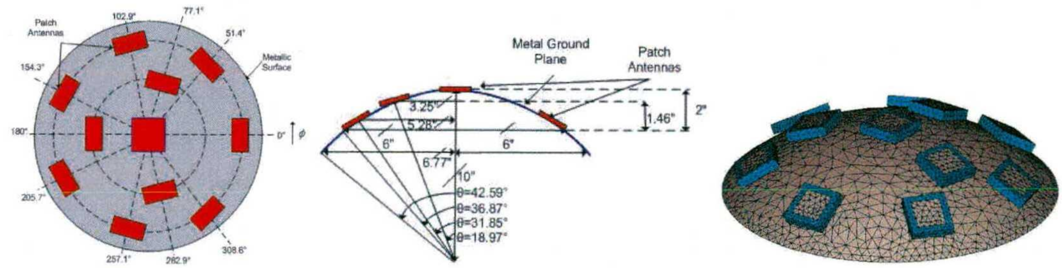


(a) Top Down View (b) Side View (c) Gridded Surface

Figure 6.10: Antenna Array D8.

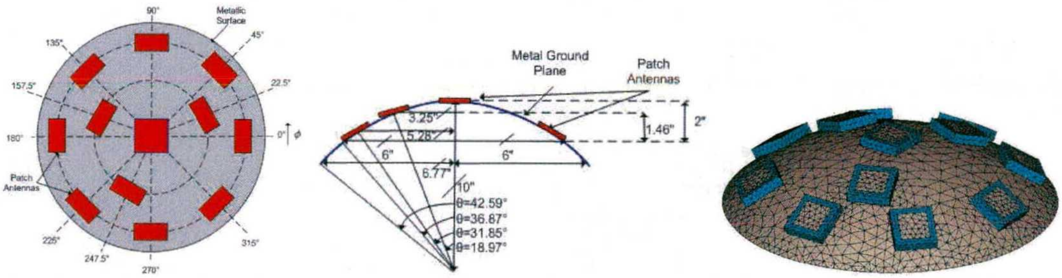


(a) Top Down View (b) Side View (c) Gridded Surface

Figure 6.11: Antenna Array D9.

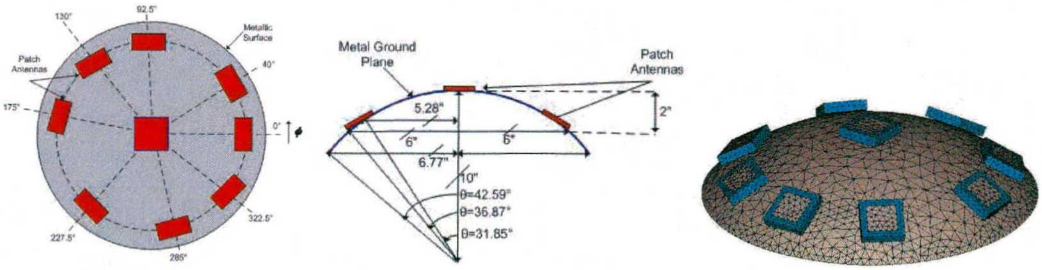


(a) Top Down View (b) Side View (c) Gridded Surface

Figure 6.12: Antenna Array D10.

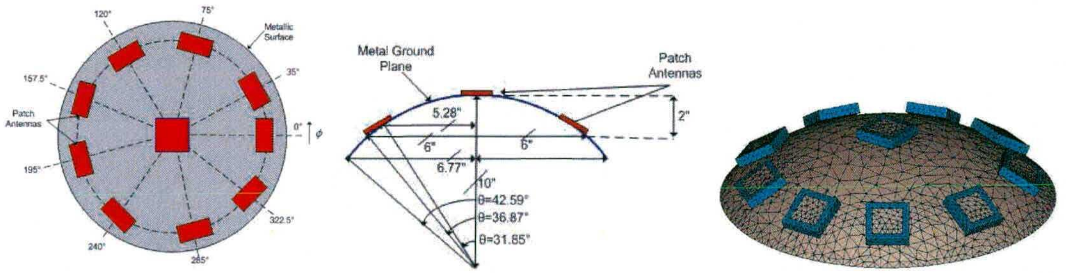


(a) Top Down View (b) Side View (c) Gridded Surface

Figure 6.13: Antenna Array D11.

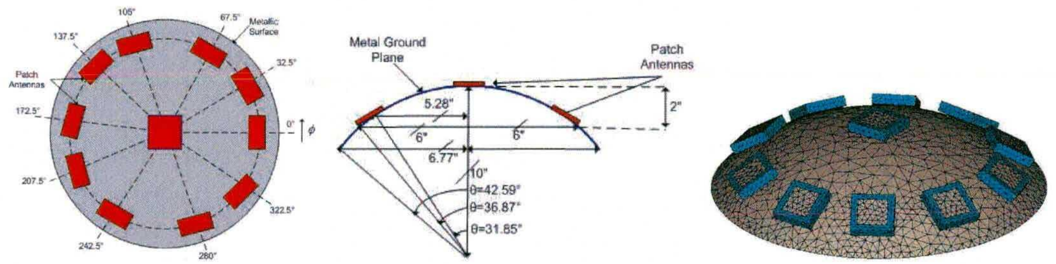


(a) Top Down View (b) Side View (c) Gridded Surface

Figure 6.14: Antenna Array D12.

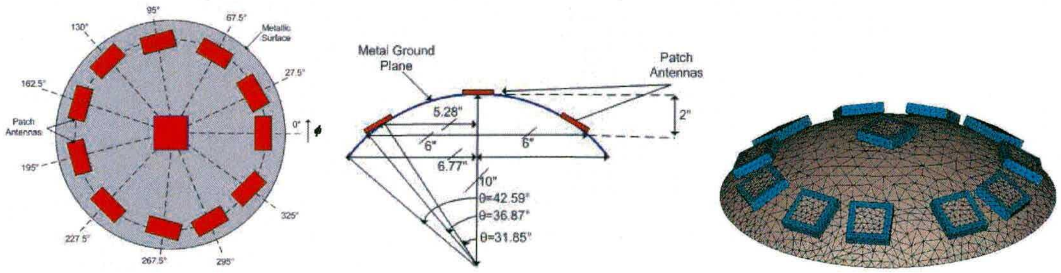


(a) Top Down View (b) Side View (c) Gridded Surface

Figure 6.15: Antenna Array D13.

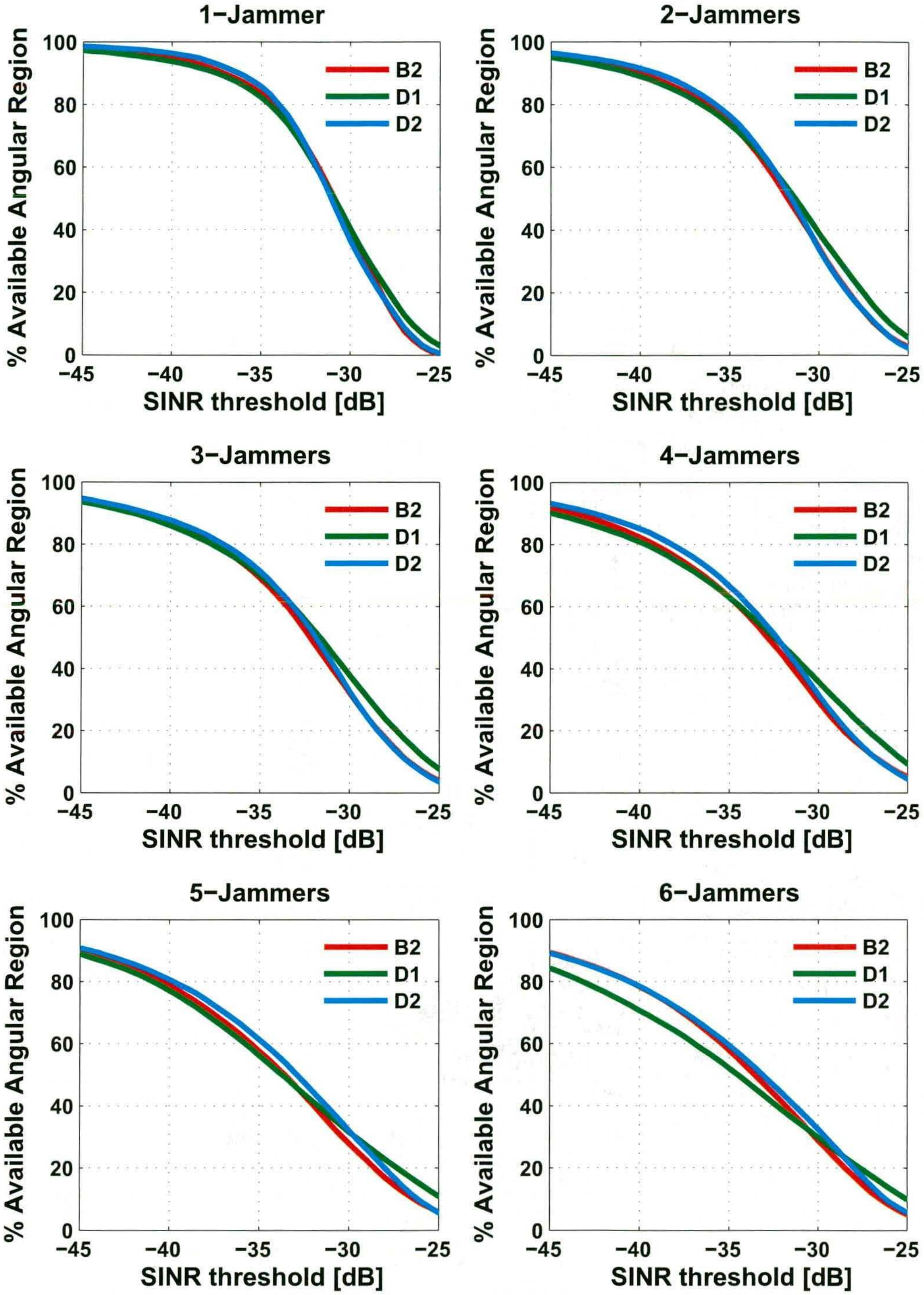


Figure 6.16: Performance of seven element antenna arrays in the presence of one to six interfering signals. AE is operating in simple power minimization mode. L1 frequency band.

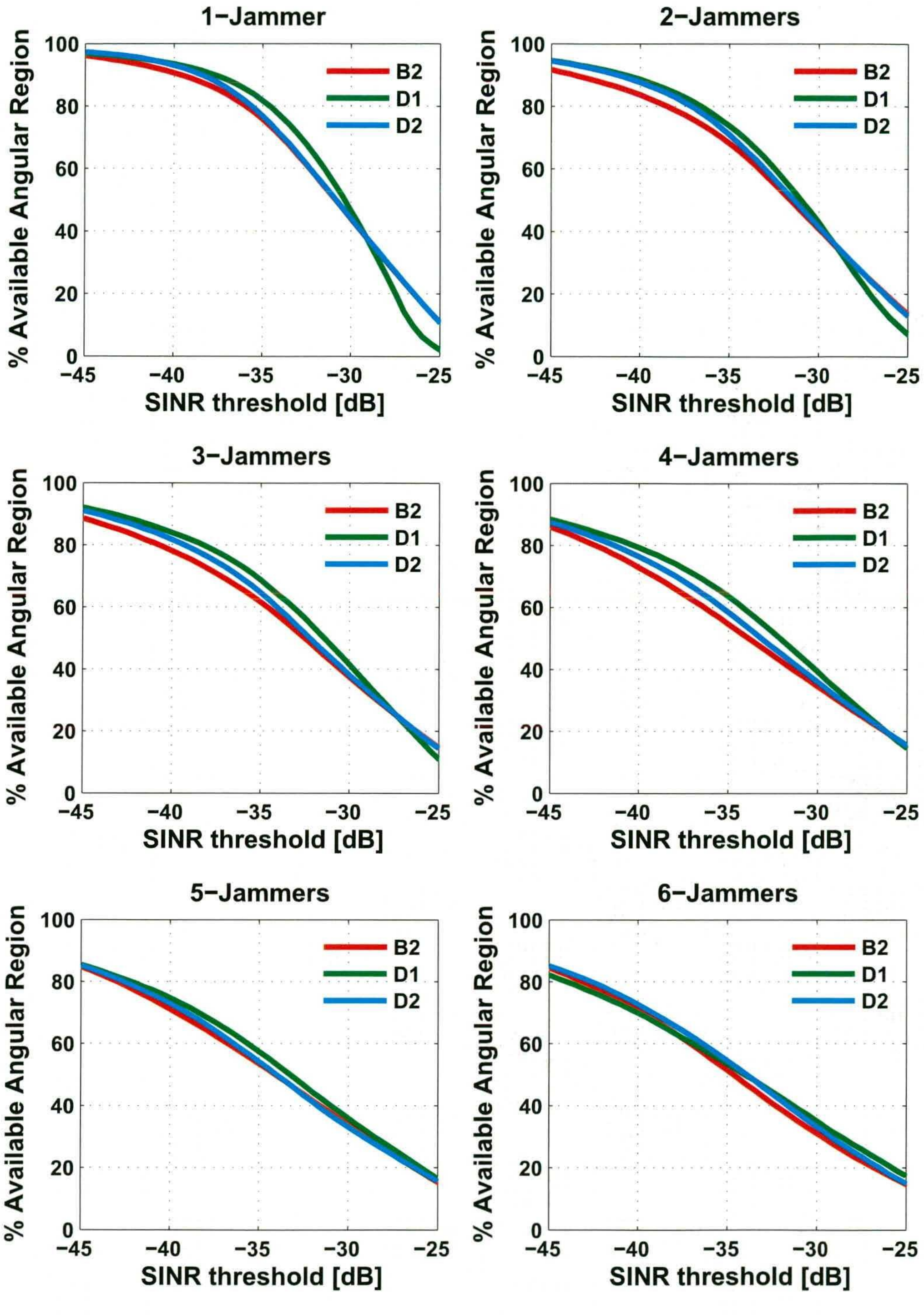


Figure 6.17: Performance of seven element antenna arrays in the presence of one to six interfering signals. AE is operating in simple power minimization mode. L2 frequency band.

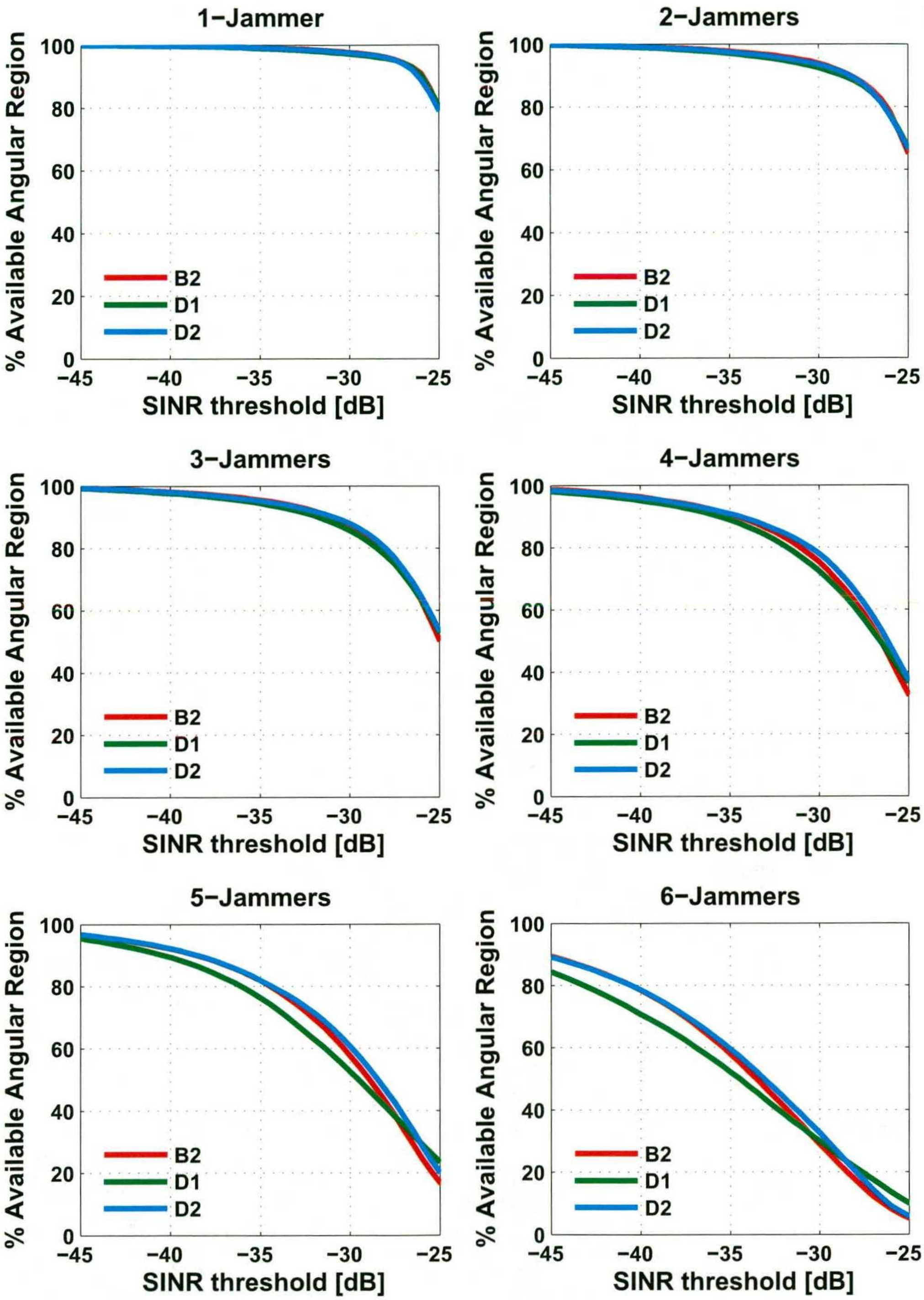


Figure 6.18: Performance of seven element antenna arrays in the presence of one to six interfering signals. AE is operating in beam forming / null steering mode. L1 frequency band.

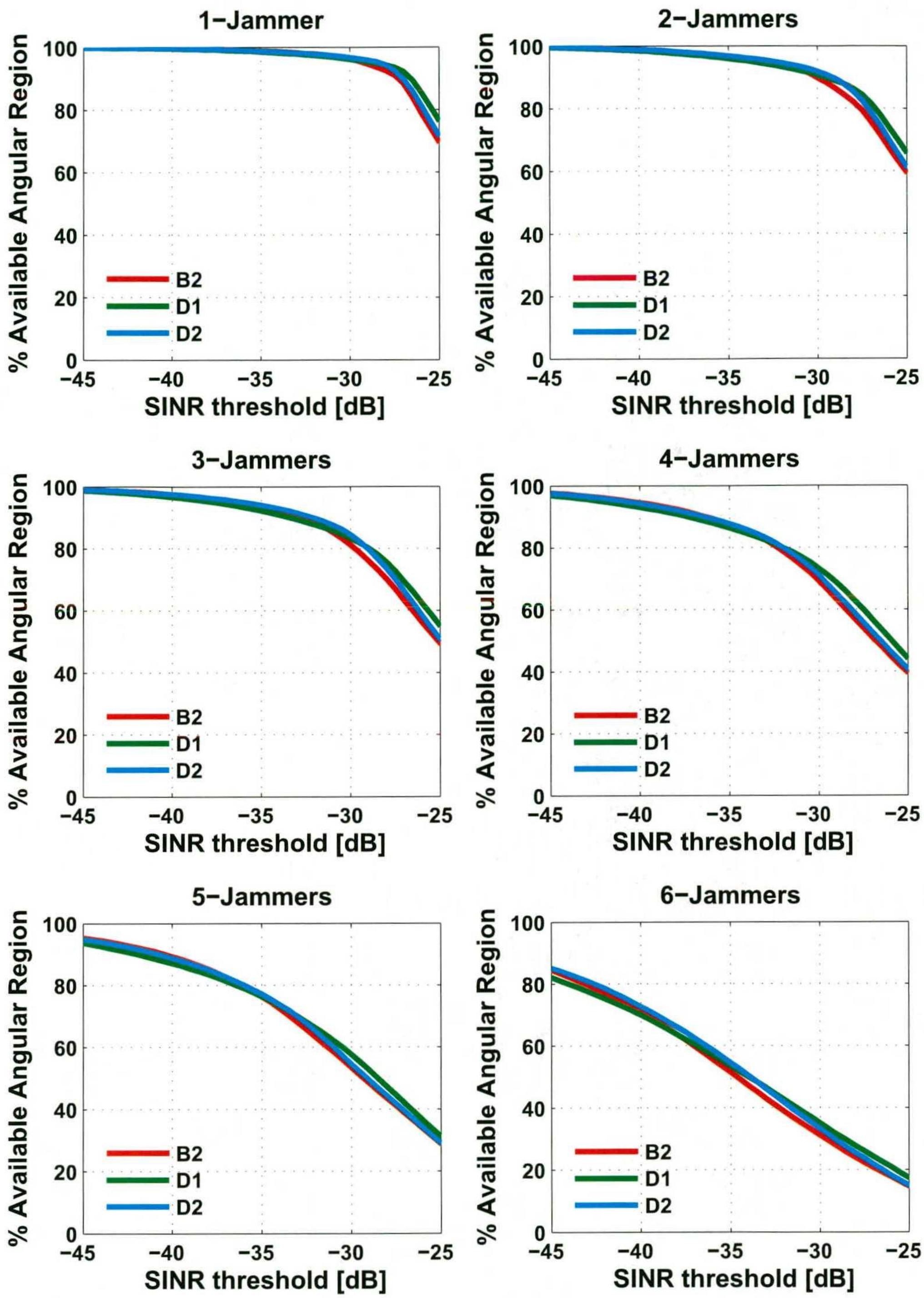


Figure 6.19: Performance of seven element antenna arrays in the presence of one to six interfering signals. AE is operating in beam forming / null steering mode. L2 frequency band.

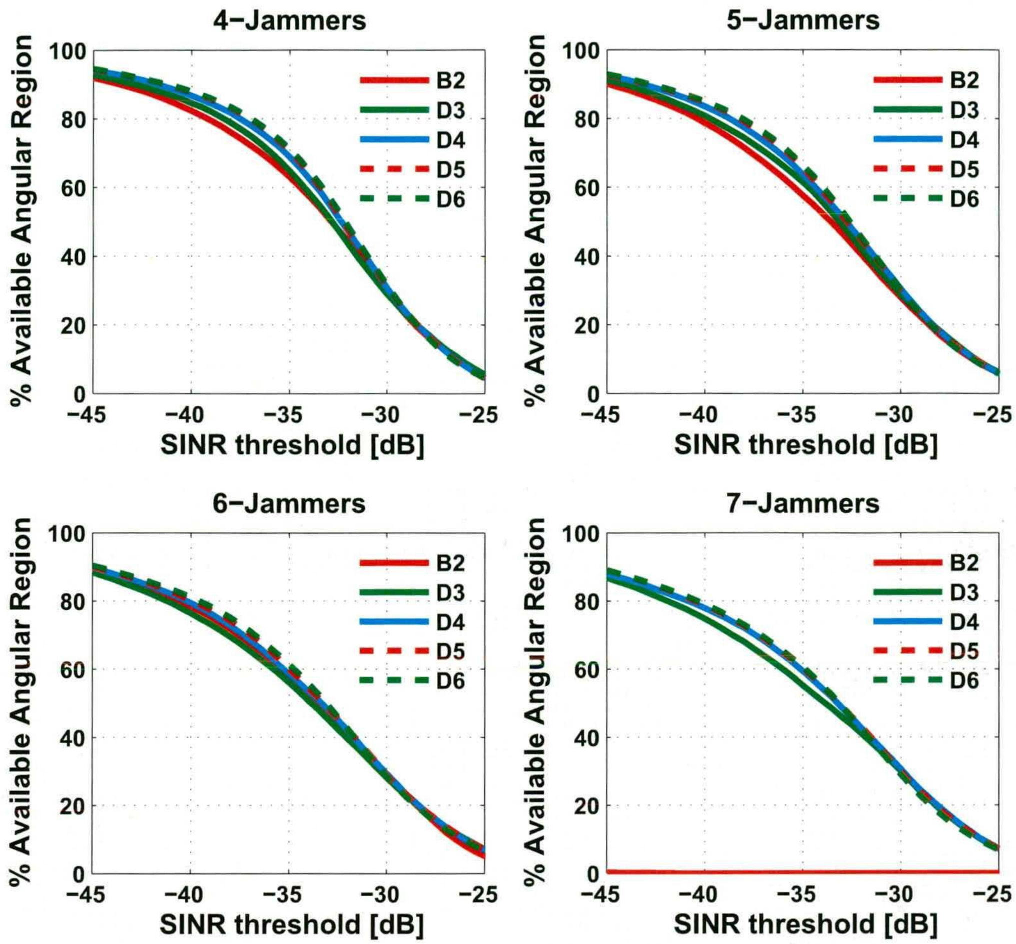


Figure 6.20: Performance of antenna arrays with elements distributed uniformly on one ring in the presence of four to eleven interfering signals. AE is operating in simple power minimization mode. L1 frequency band. (Continued on the following page).

Figure 6.20 continued.

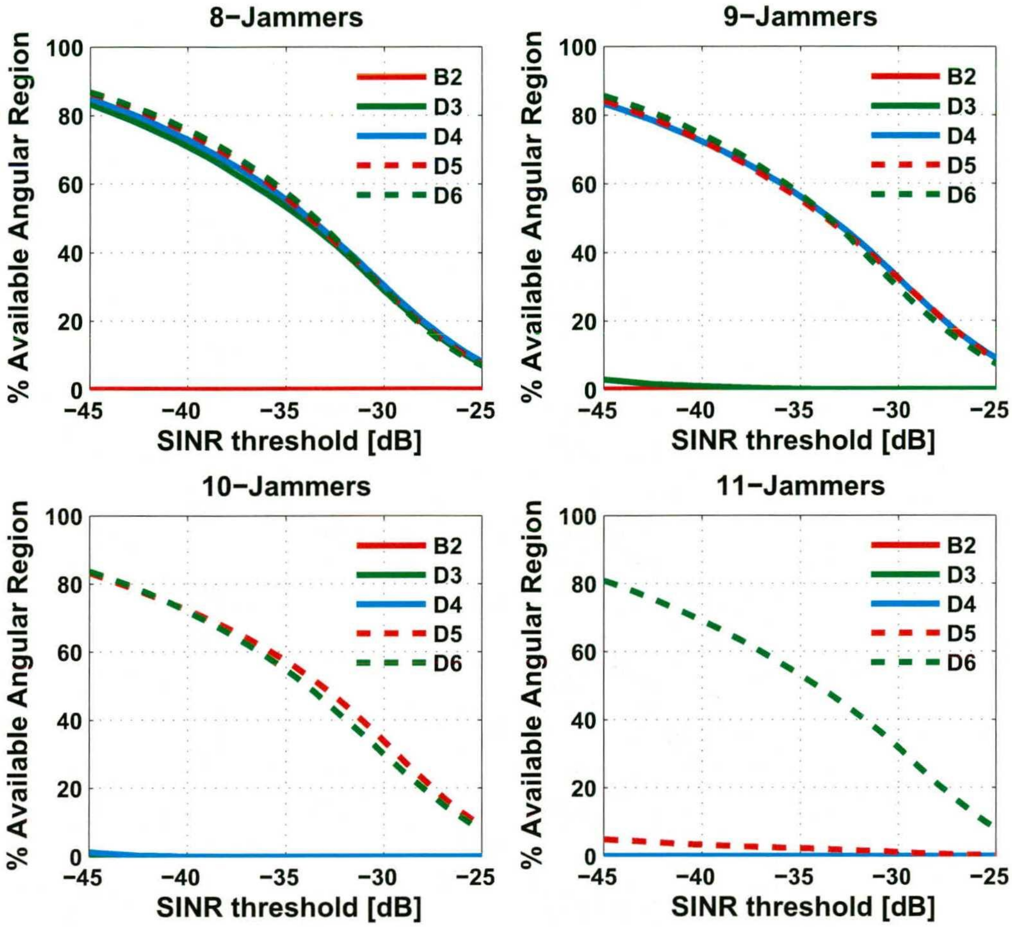

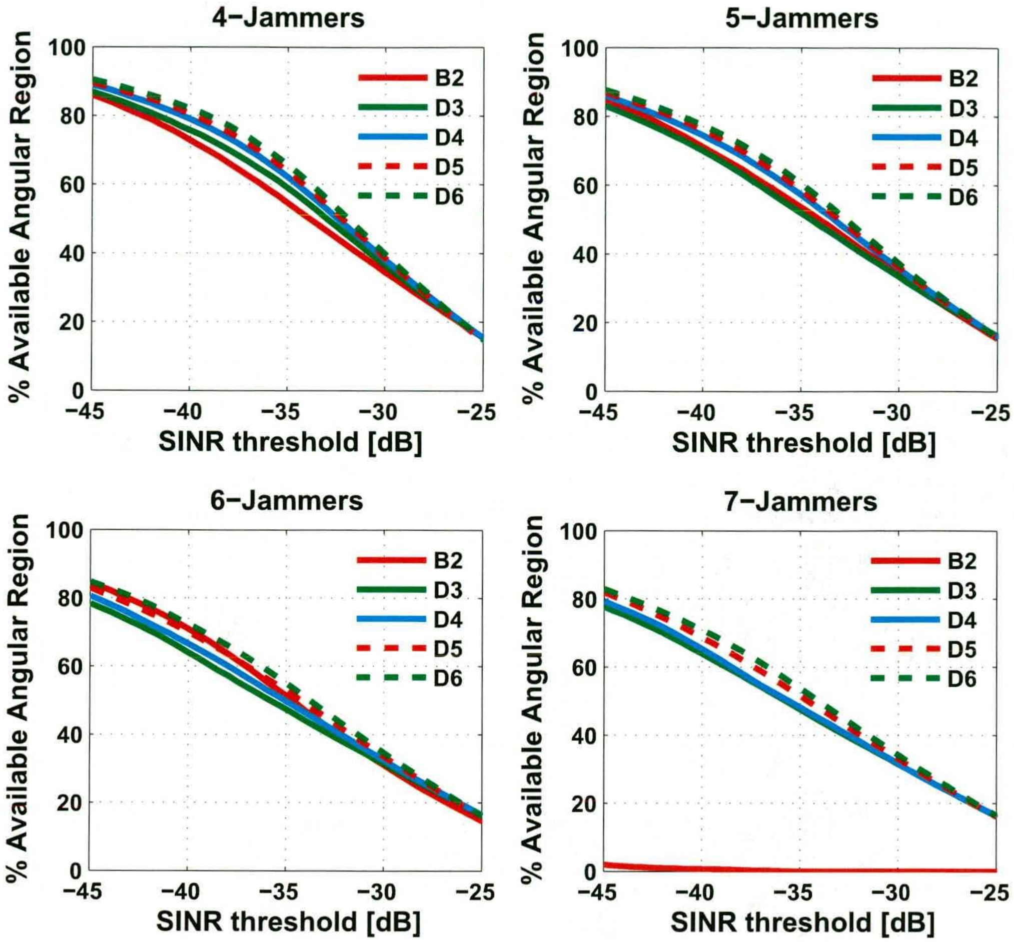


Figure 6.21: Performance of antenna arrays with elements distributed uniformly on one ring in the presence of four to eleven interfering signals. AE is operating in simple power minimization mode. L2 frequency band. (Continued on the following page).

Figure 6.21 continued.

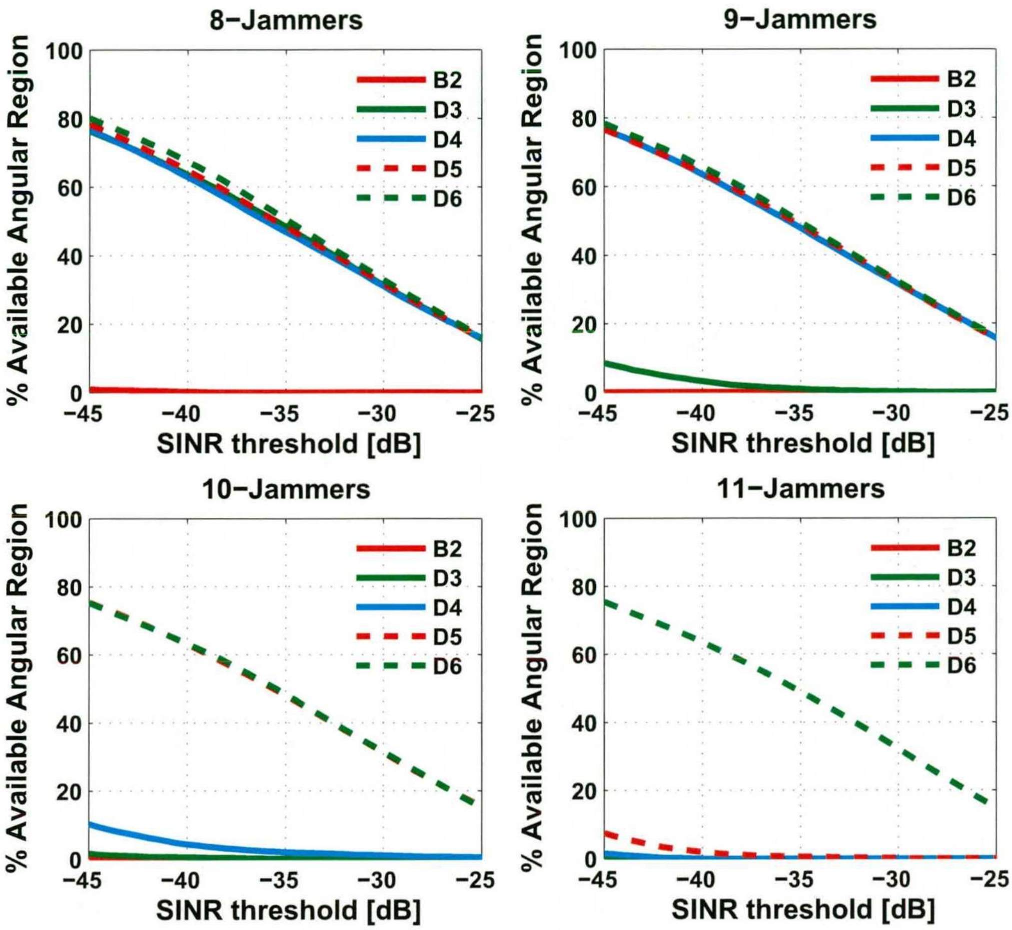

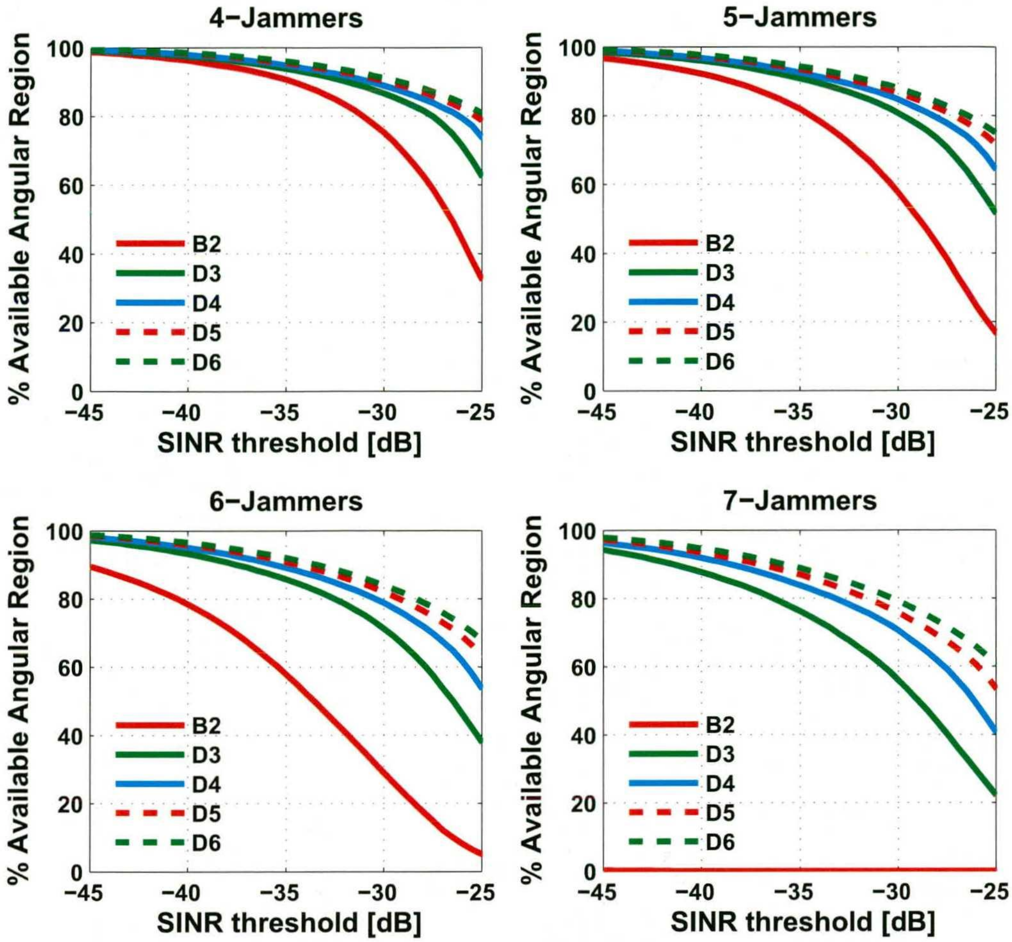


Figure 6.22: Performance of antenna arrays with elements distributed uniformly on one ring in the presence of four to eleven interfering signals. AE is operating in beam forming / null steering mode. L1 frequency band. (Continued on the following page).

Figure 6.22 continued.

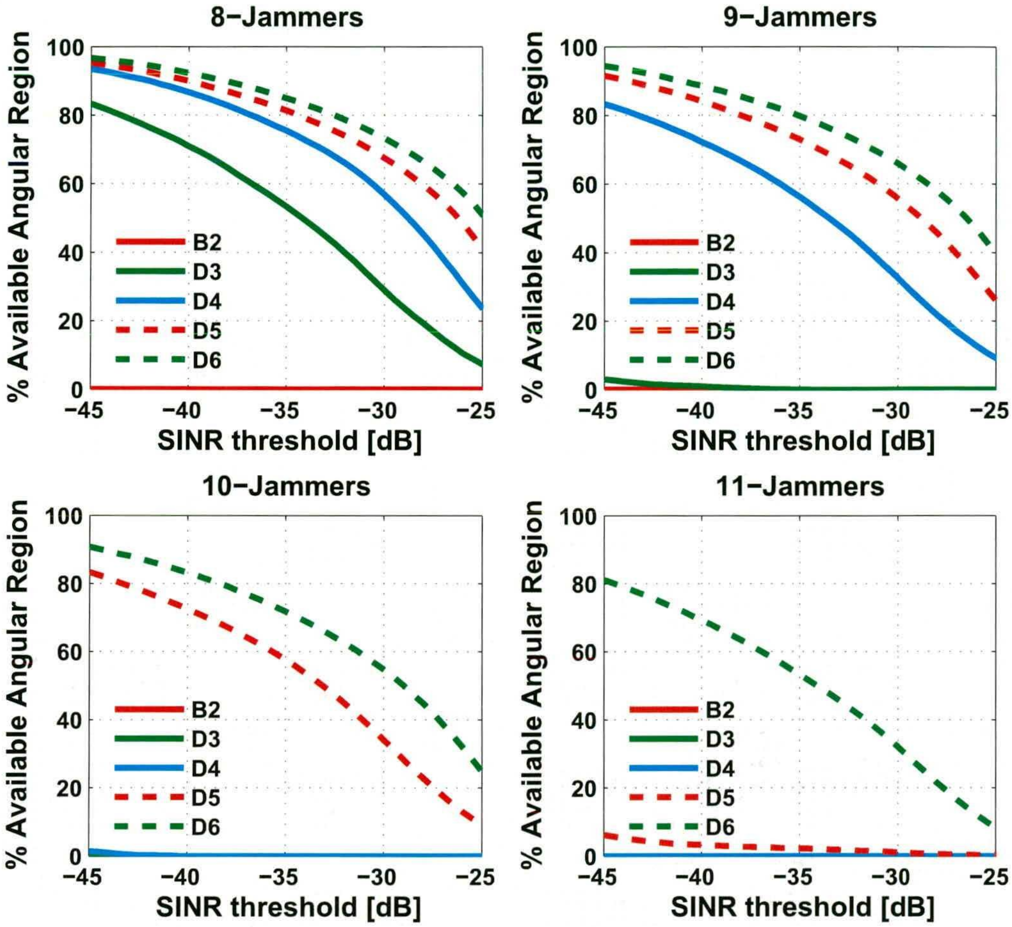

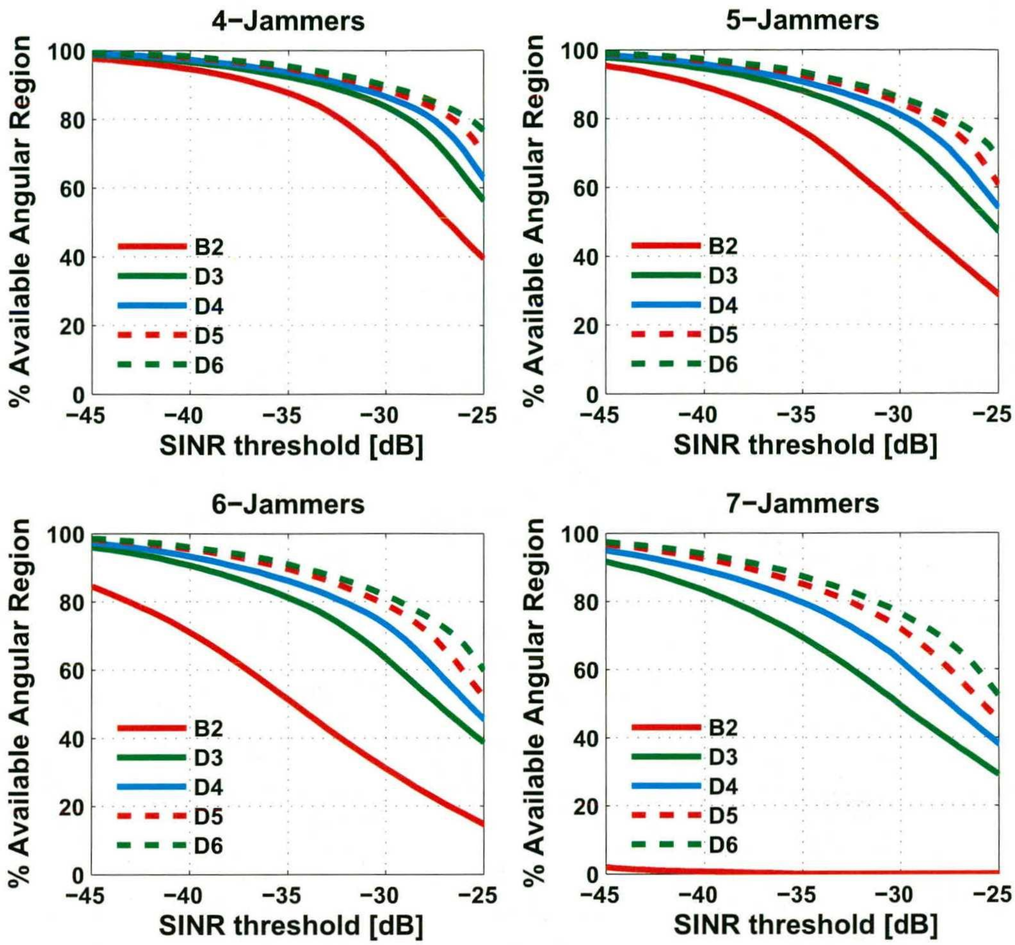


Figure 6.23: Performance of antenna arrays with elements distributed uniformly on one ring in the presence of four to eleven interfering signals. AE is operating in beam forming / null steering mode. L2 frequency band. (Continued on the following page).

Figure 6.23 continued.

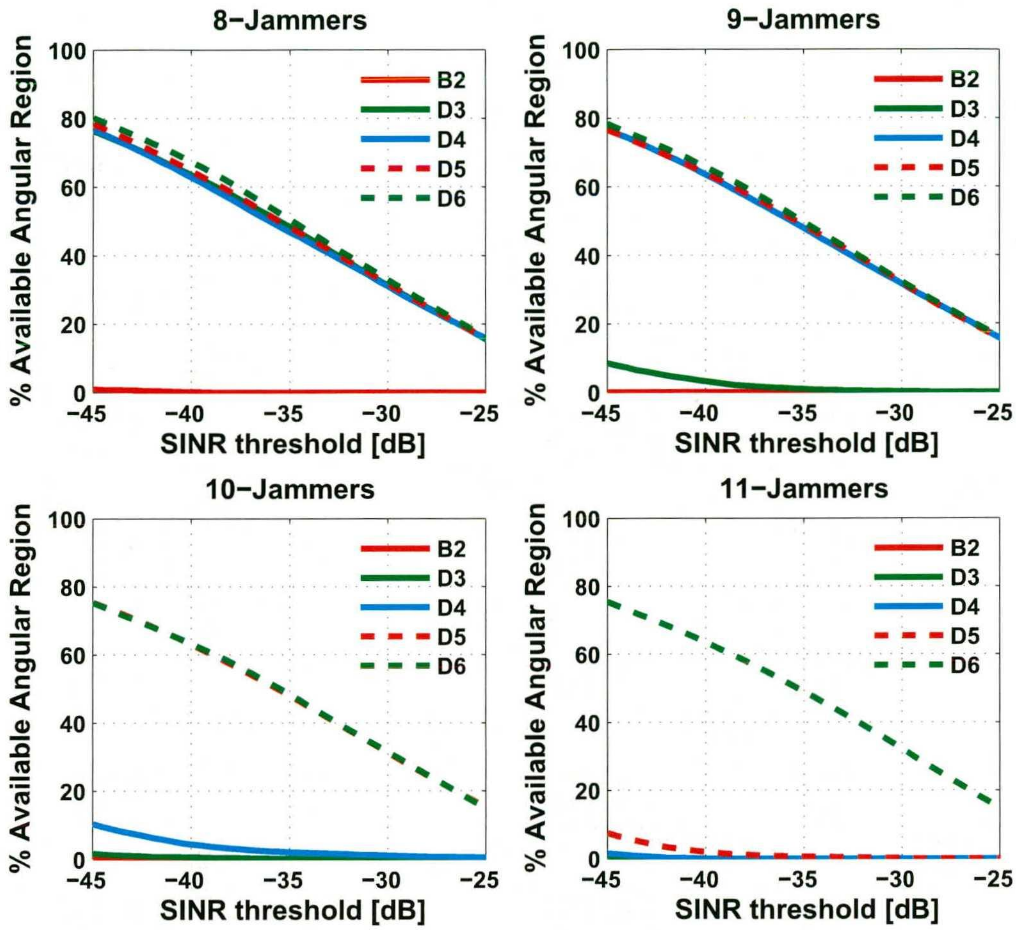

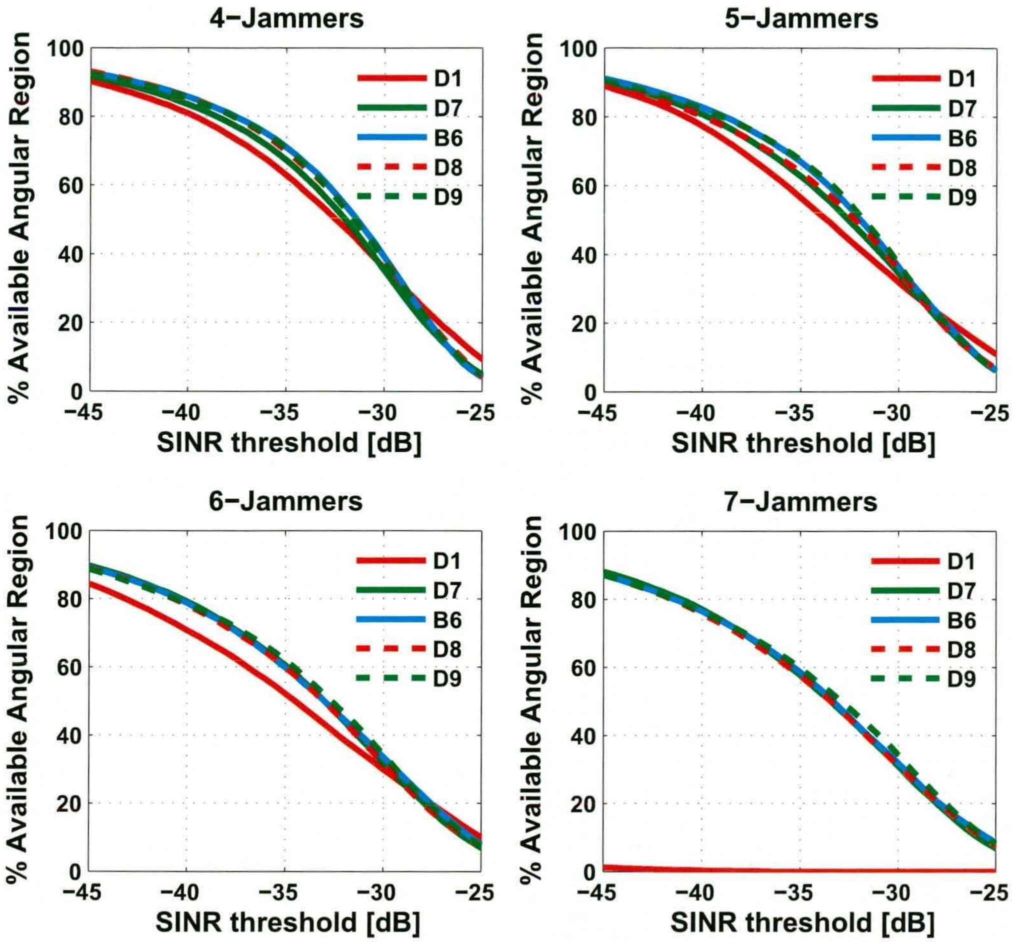


Figure 6.24: Performance of antenna arrays with elements distributed on two rings in the presence of four to eleven interfering signals. AE is operating in simple power minimization mode. L1 frequency band. (Continued on the following page).

Figure 6.24 continued.

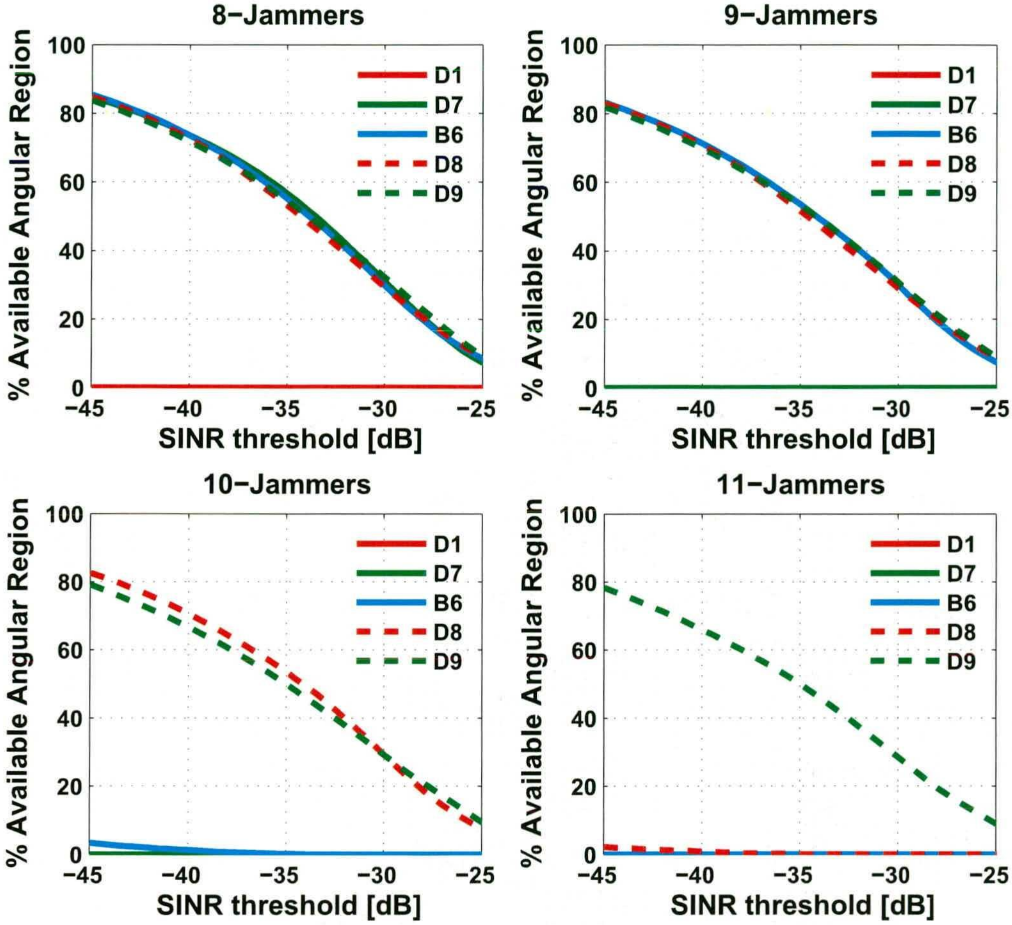

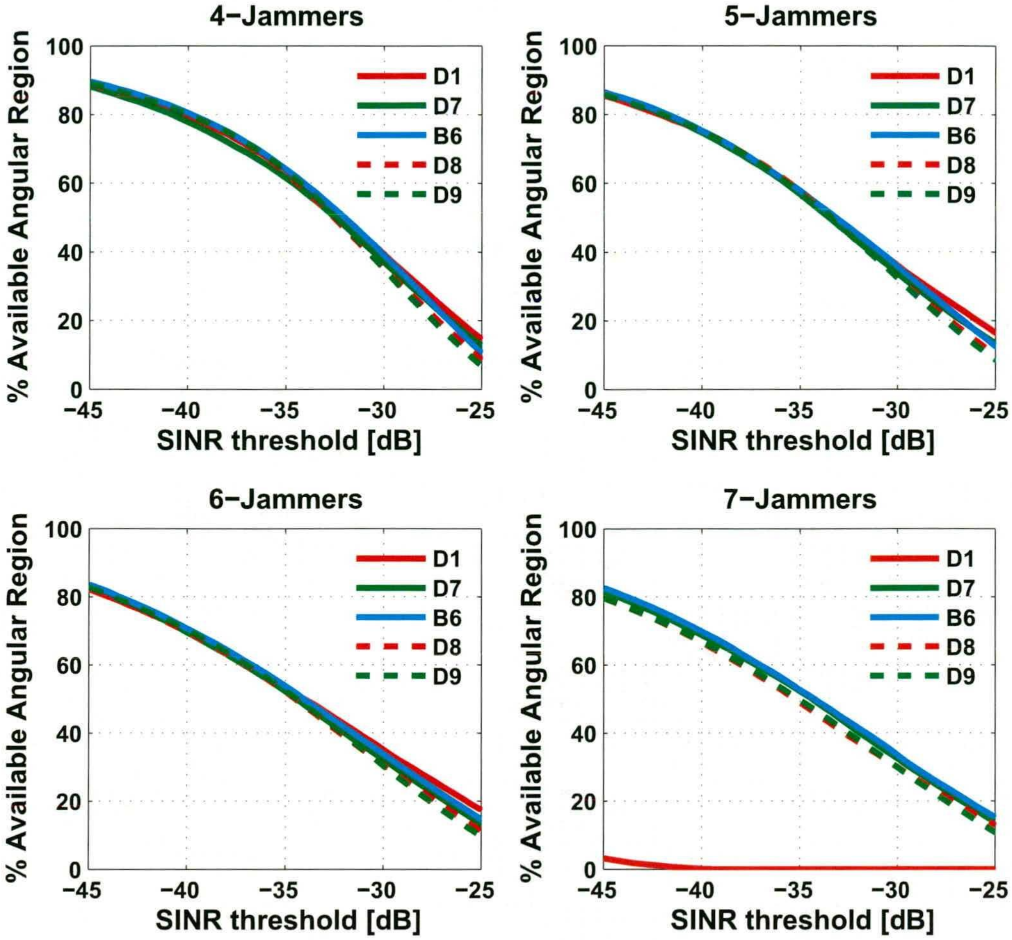


Figure 6.25: Performance of antenna arrays with elements distributed on two rings in the presence of four to eleven interfering signals. AE is operating in simple power minimization mode. L2 frequency band. (Continued on the following page).

Figure 6.25 continued.

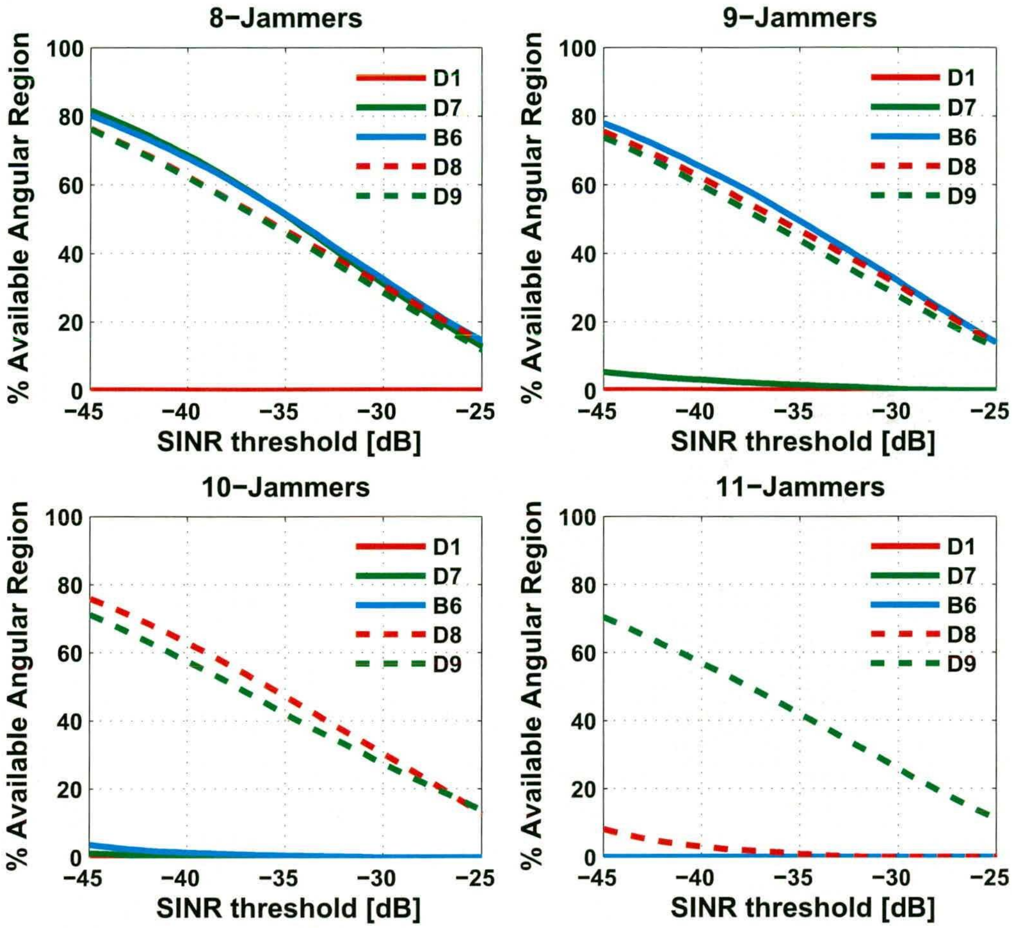

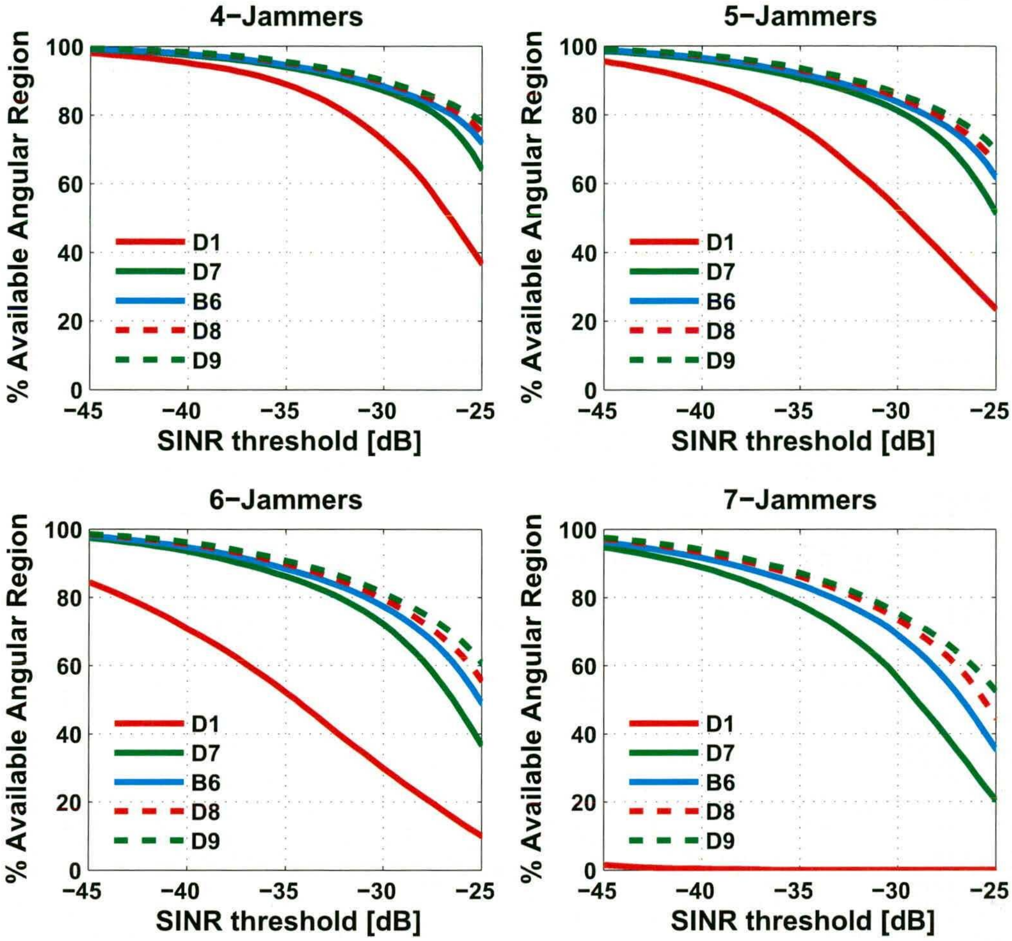


Figure 6.26: Performance of antenna arrays with elements distributed on two rings in the presence of four to eleven interfering signals. AE is operating in beam forming / null steering mode. L1 frequency band. (Continued on the following page).

Figure 6.26 continued.

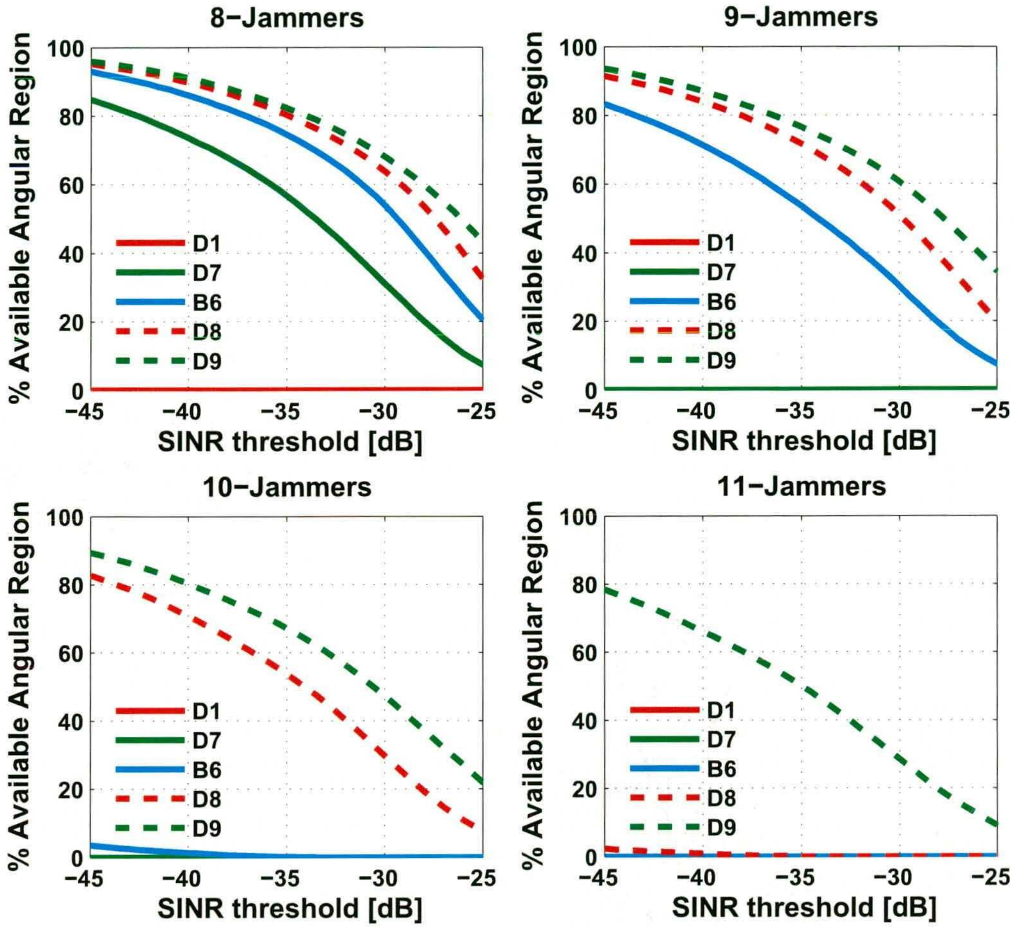

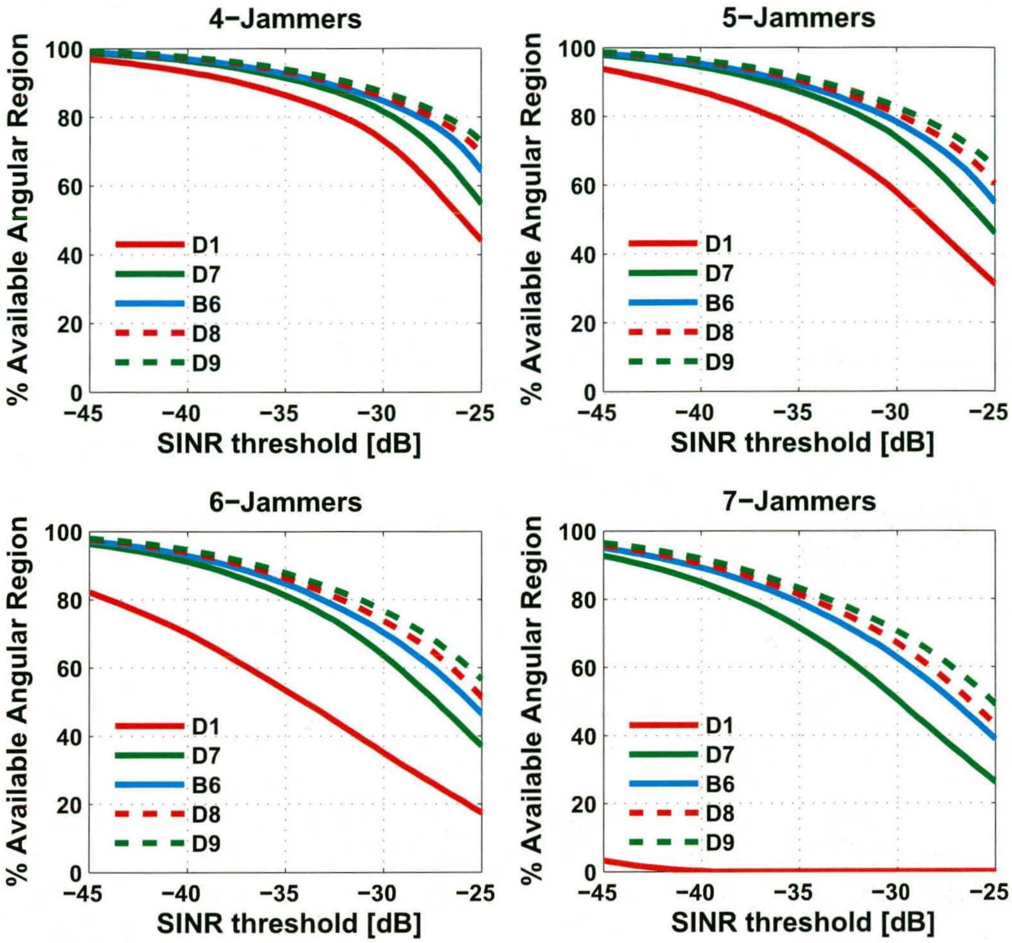


Figure 6.27: Performance of antenna arrays with elements distributed on two rings in the presence of four to eleven interfering signals. AE is operating in beam forming / null steering mode. L2 frequency band. (Continued on the following page).

Figure 6.27 continued.

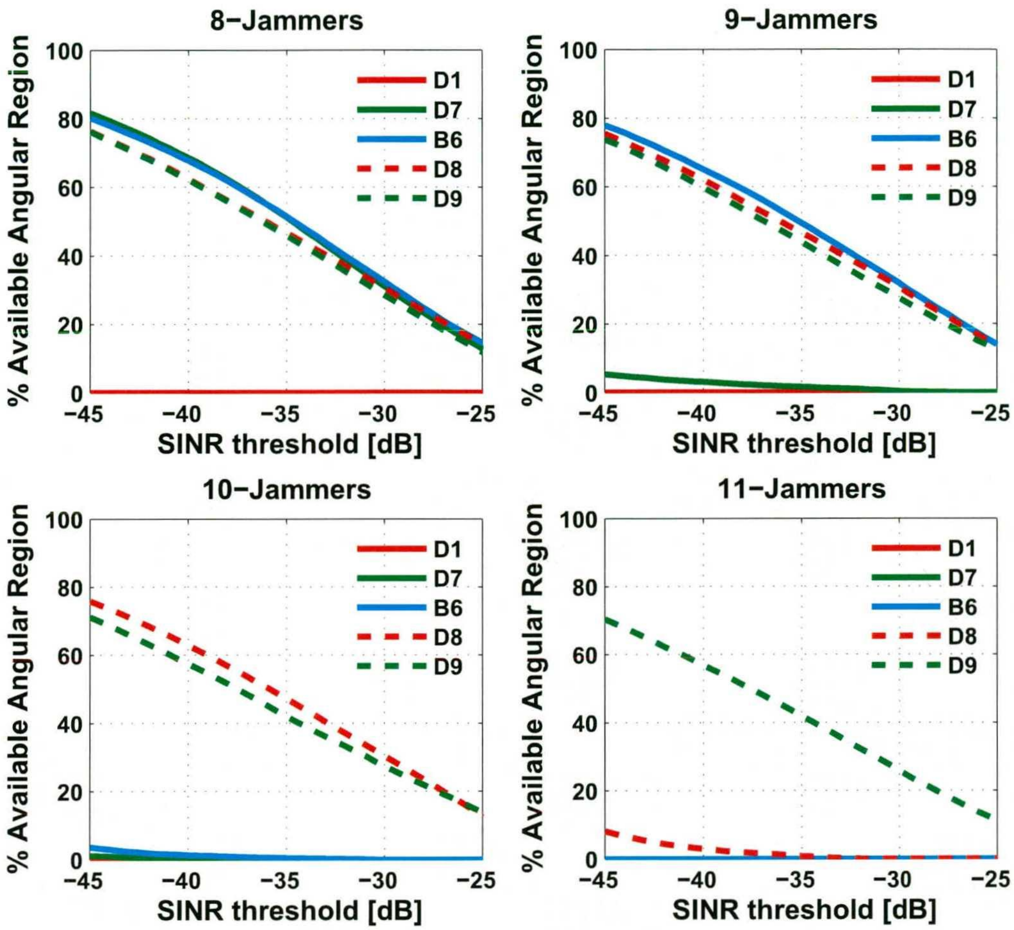

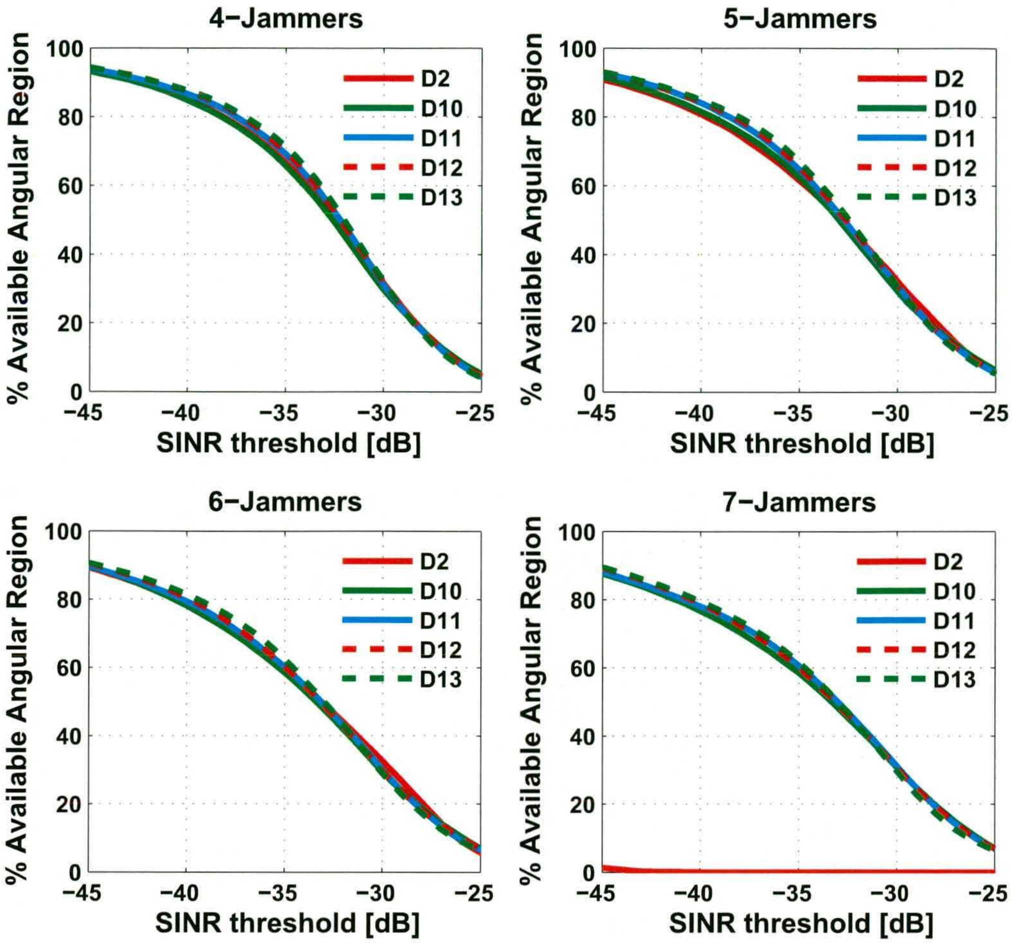


Figure 6.28: Performance of antenna arrays with elements distributed non-uniformly on one ring in the presence of four to eleven interfering signals. AE is operating in simple power minimization mode. L1 frequency band. (Continued on the following page).

Figure 6.28 continued.

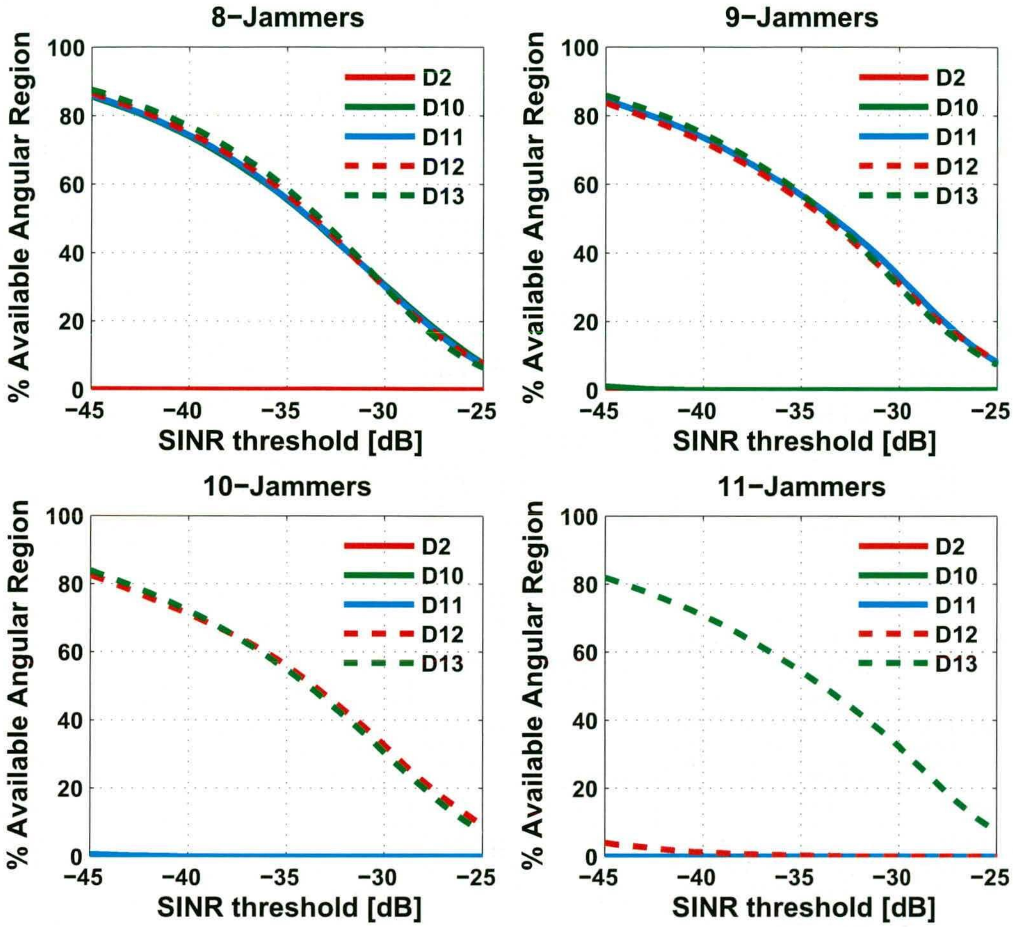

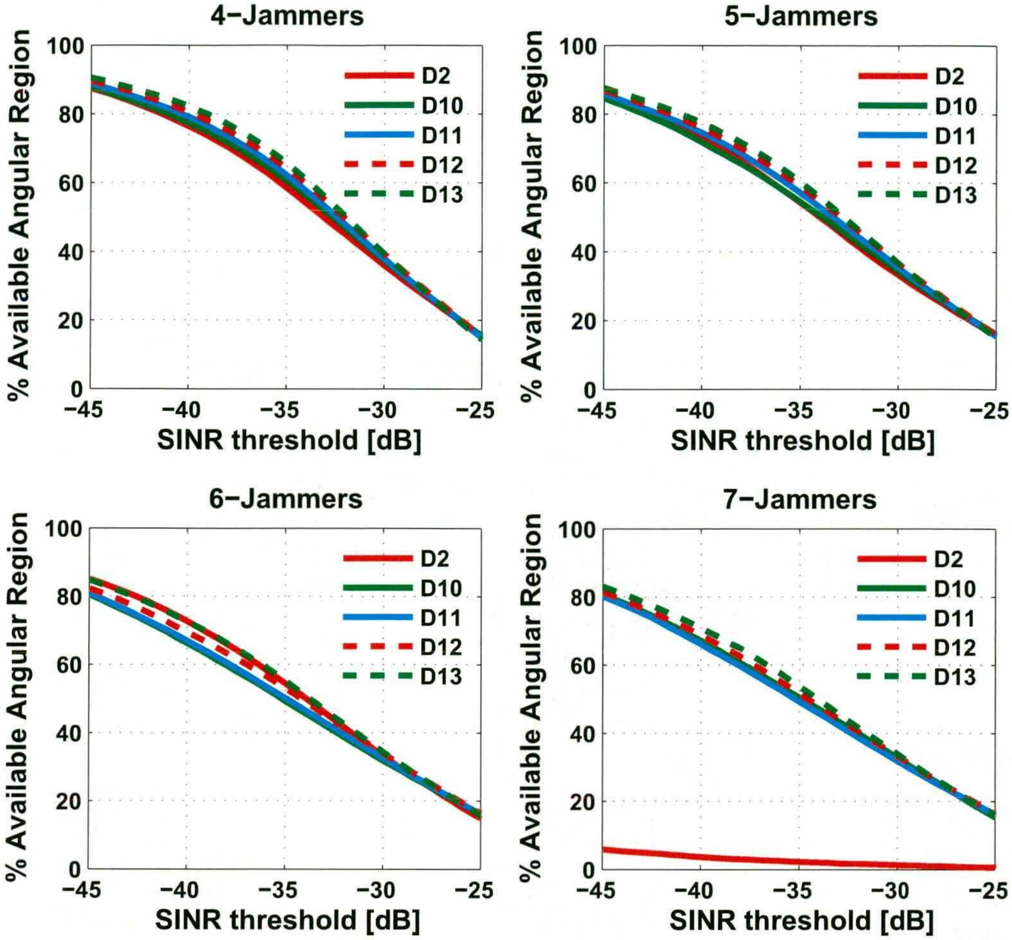


Figure 6.29: Performance of antenna arrays with elements distributed non-uniformly on one ring in the presence of four to eleven interfering signals. AE is operating in simple power minimization mode. L2 frequency band. (Continued on the following page).

Figure 6.29 continued.

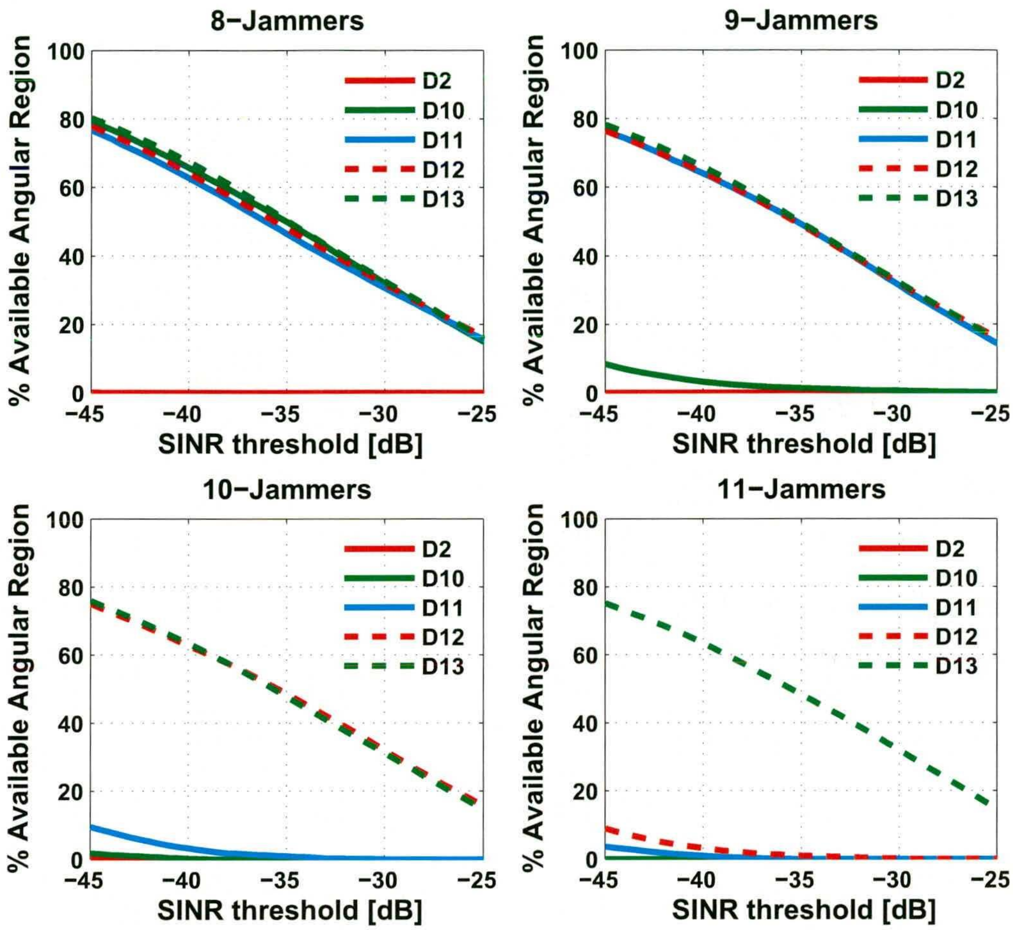

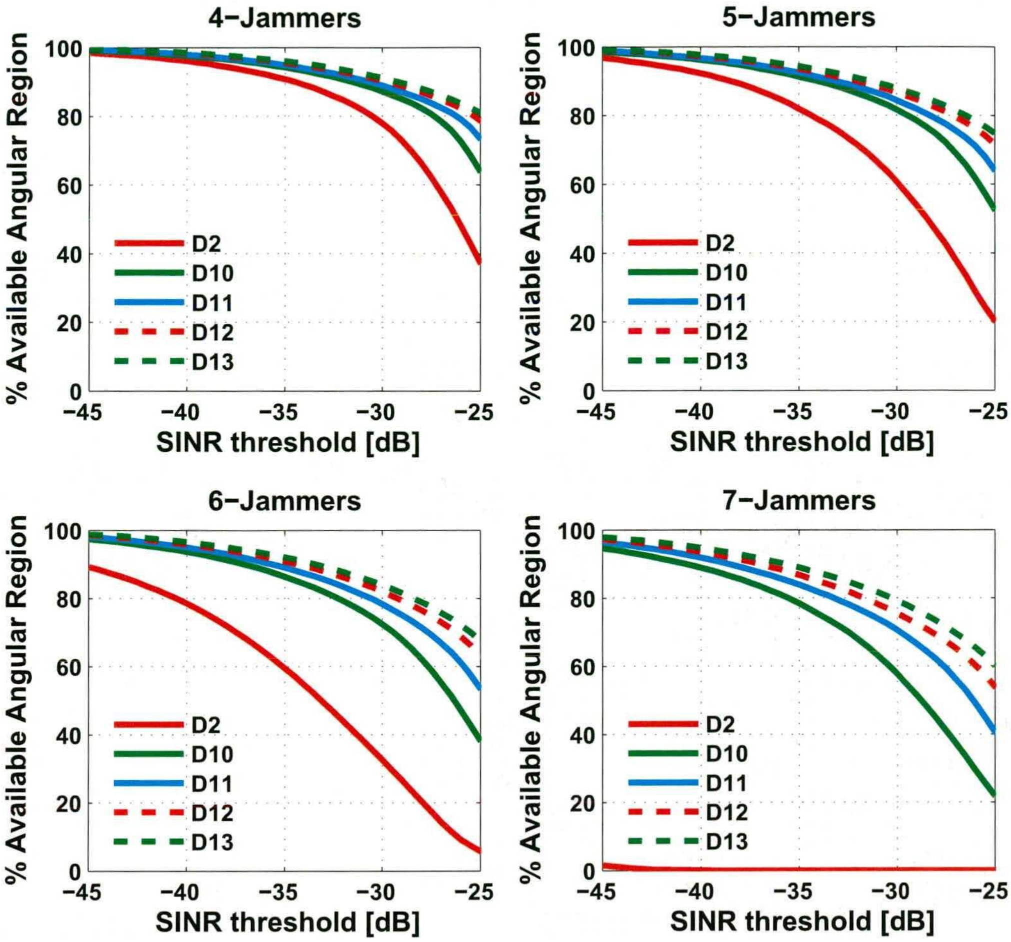


Figure 6.30: Performance of antenna arrays with elements distributed non-uniformly on one ring in the presence of four to eleven interfering signals. AE is operating in beam forming / null steering mode. L1 frequency band. (Continued on the following page).

Figure 6.30 continued.

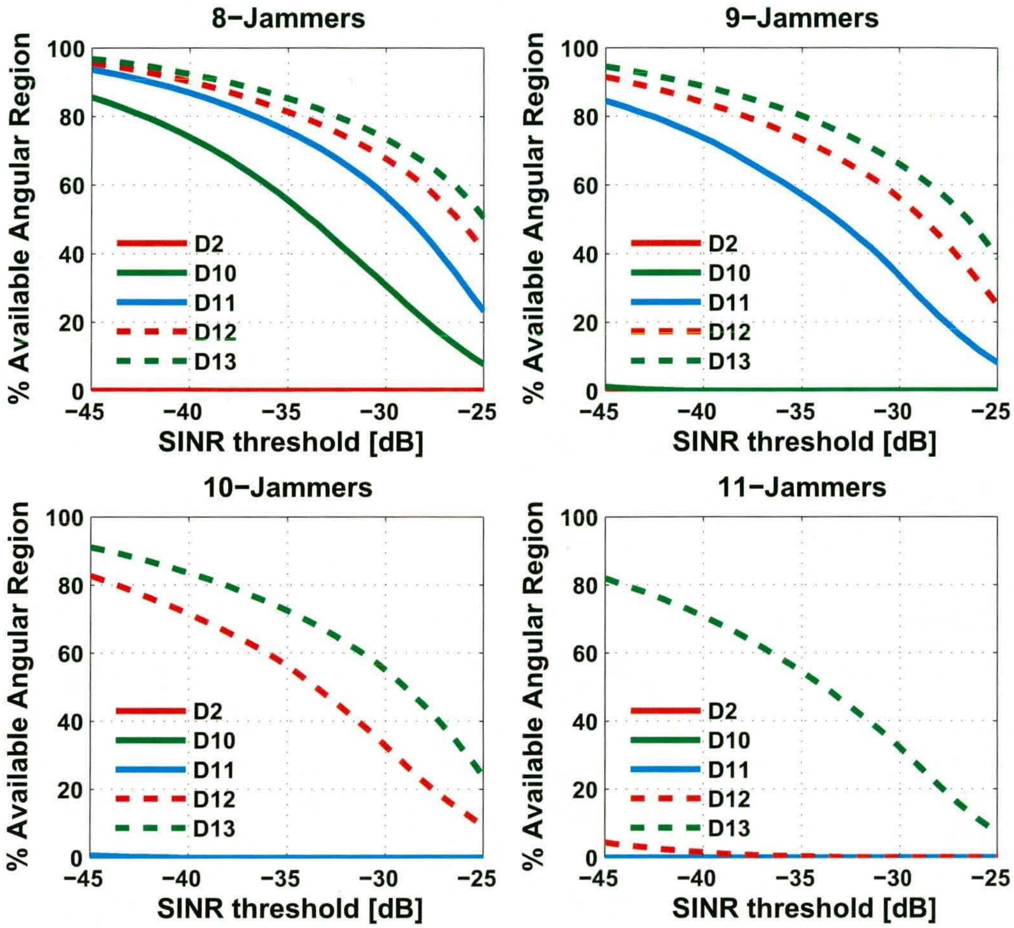

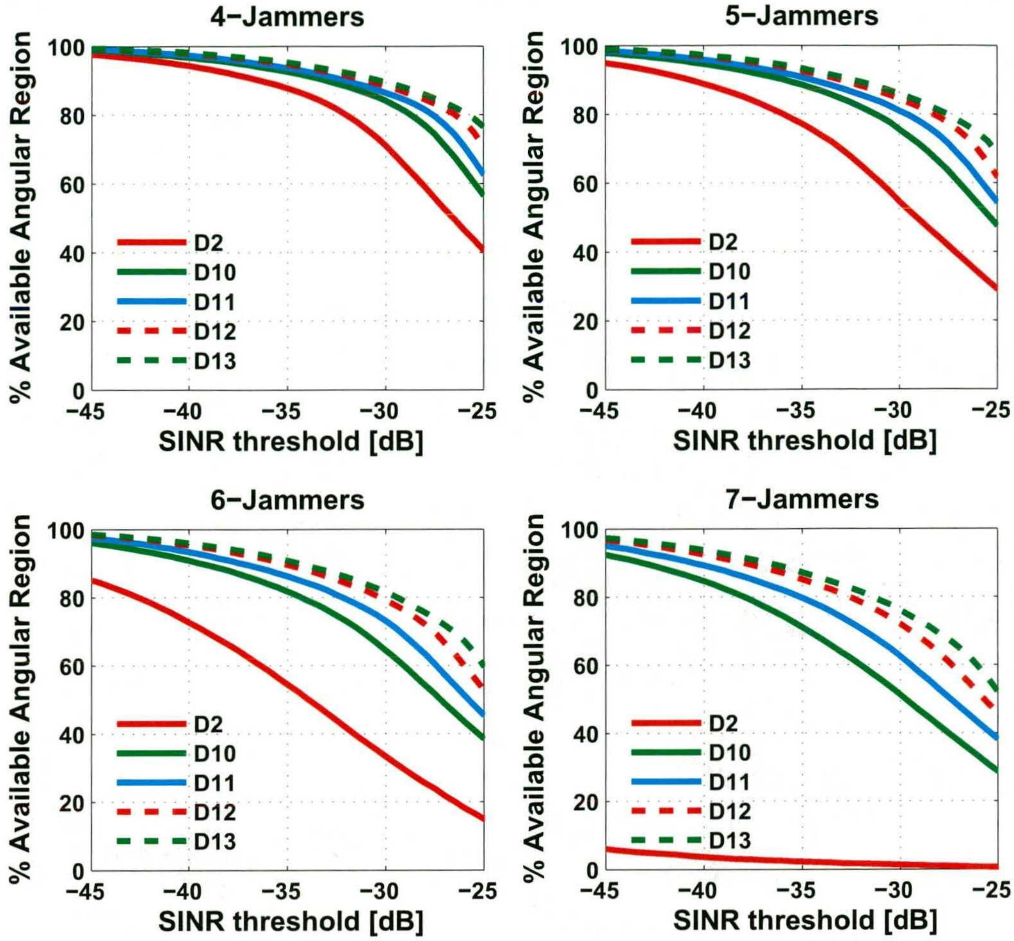


Figure 6.31: Performance of antenna arrays with elements distributed non-uniformly on one ring in the presence of four to eleven interfering signals. AE is operating in beam forming / null steering mode. L2 frequency band. (Continued on the following page).

Figure 6.31 continued.

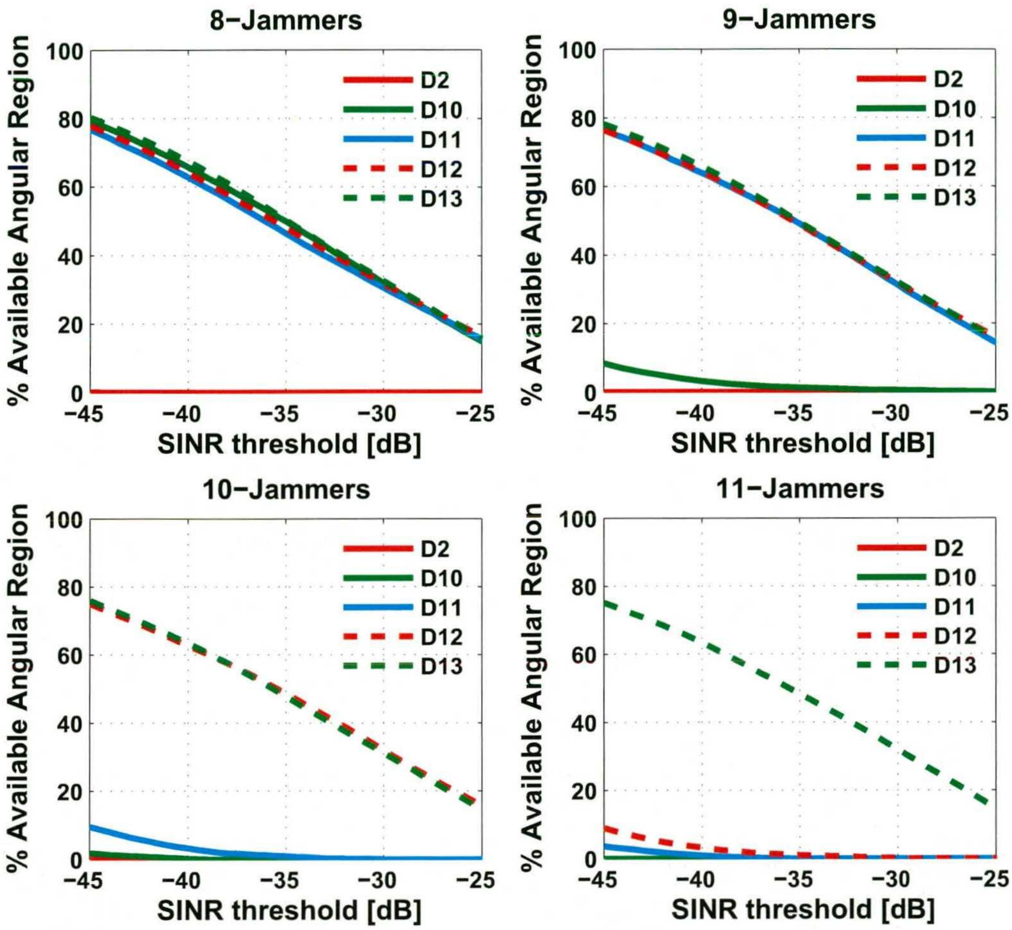

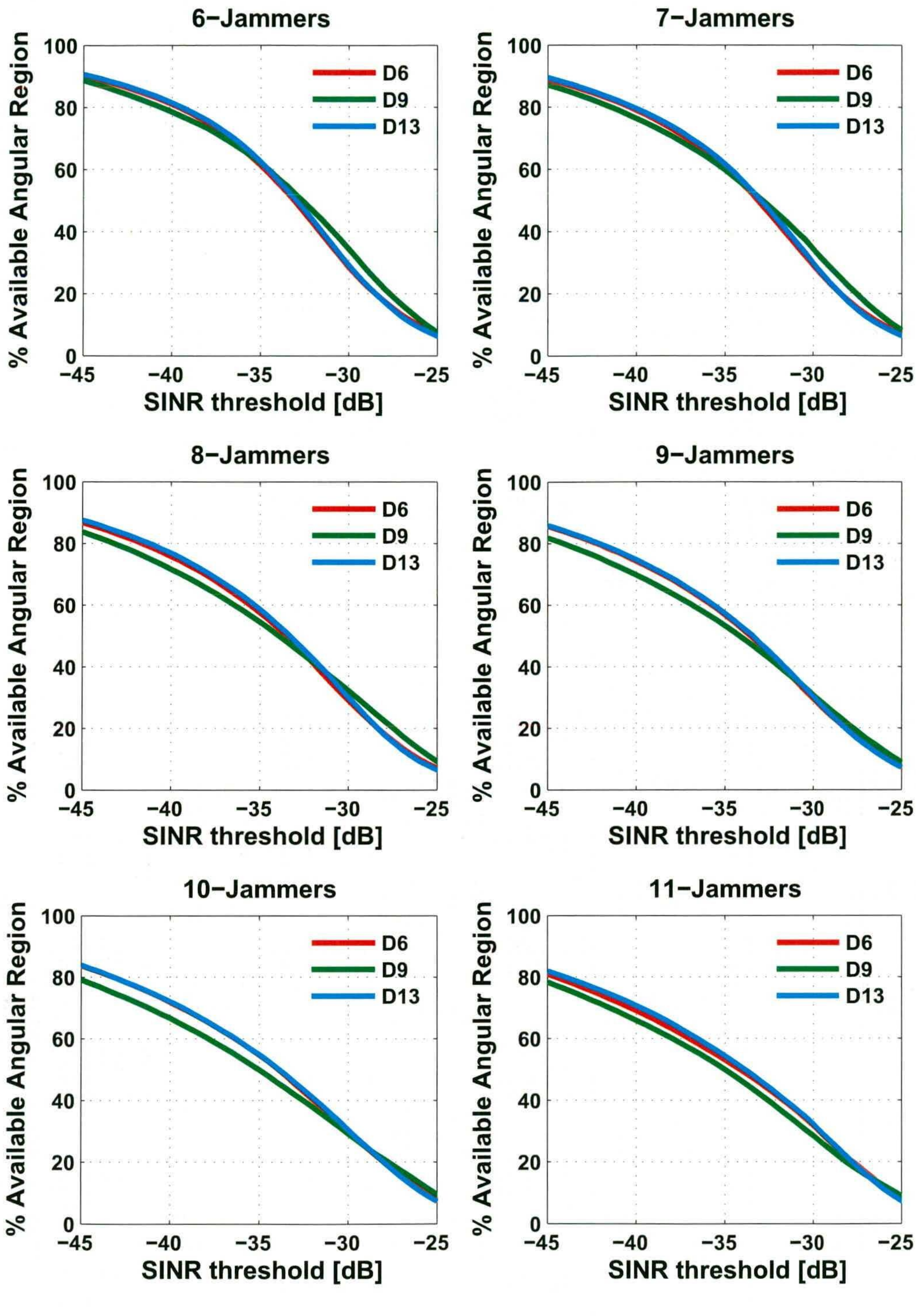


Figure 6.32: Performance of twelve element antenna arrays in the presence of six to eleven interfering signals. AE is operating in simple power minimization mode. L1 frequency band.

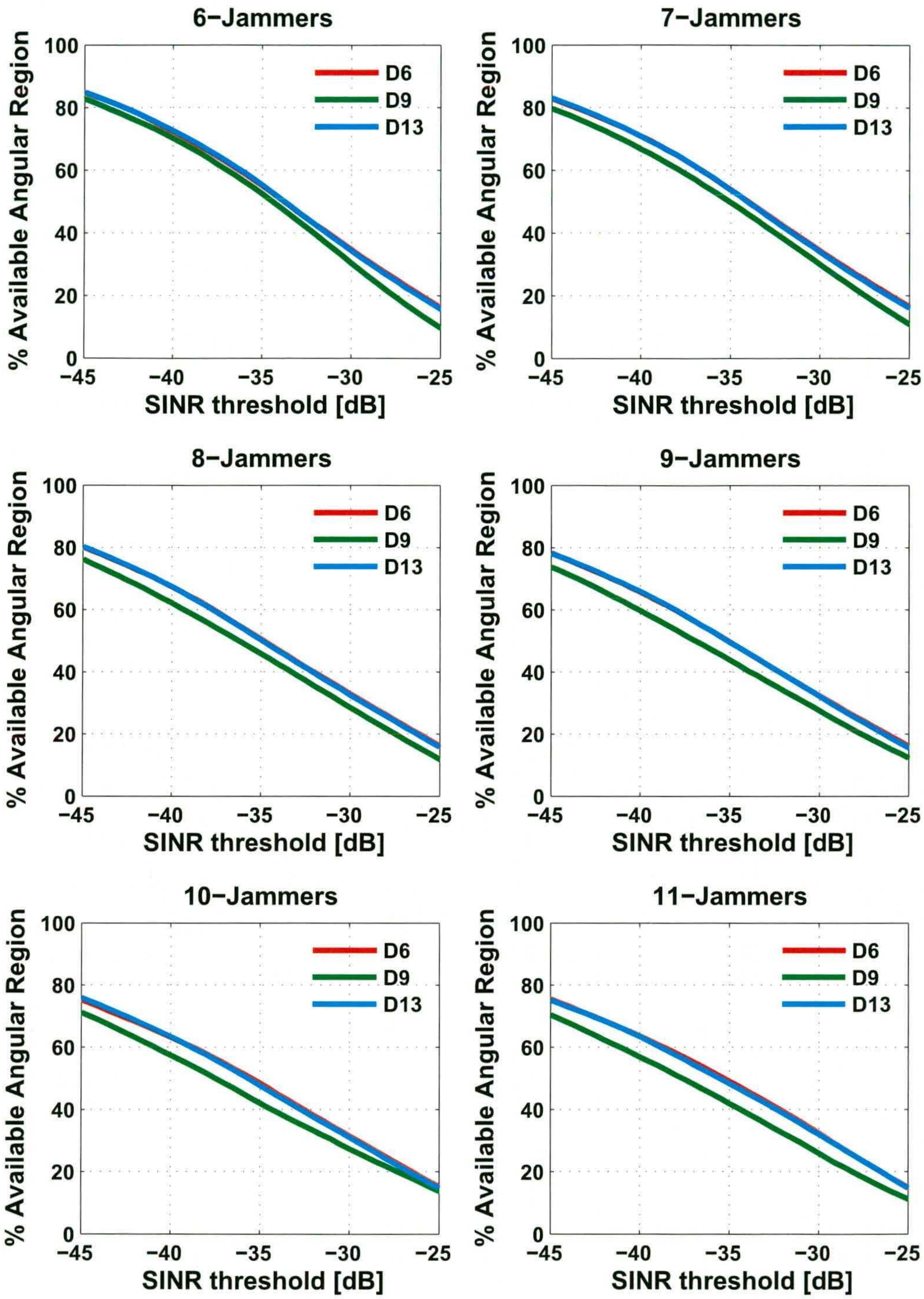


Figure 6.33: Performance of twelve element antenna arrays in the presence of six to eleven interfering signals. AE is operating in simple power minimization mode. L2 frequency band.

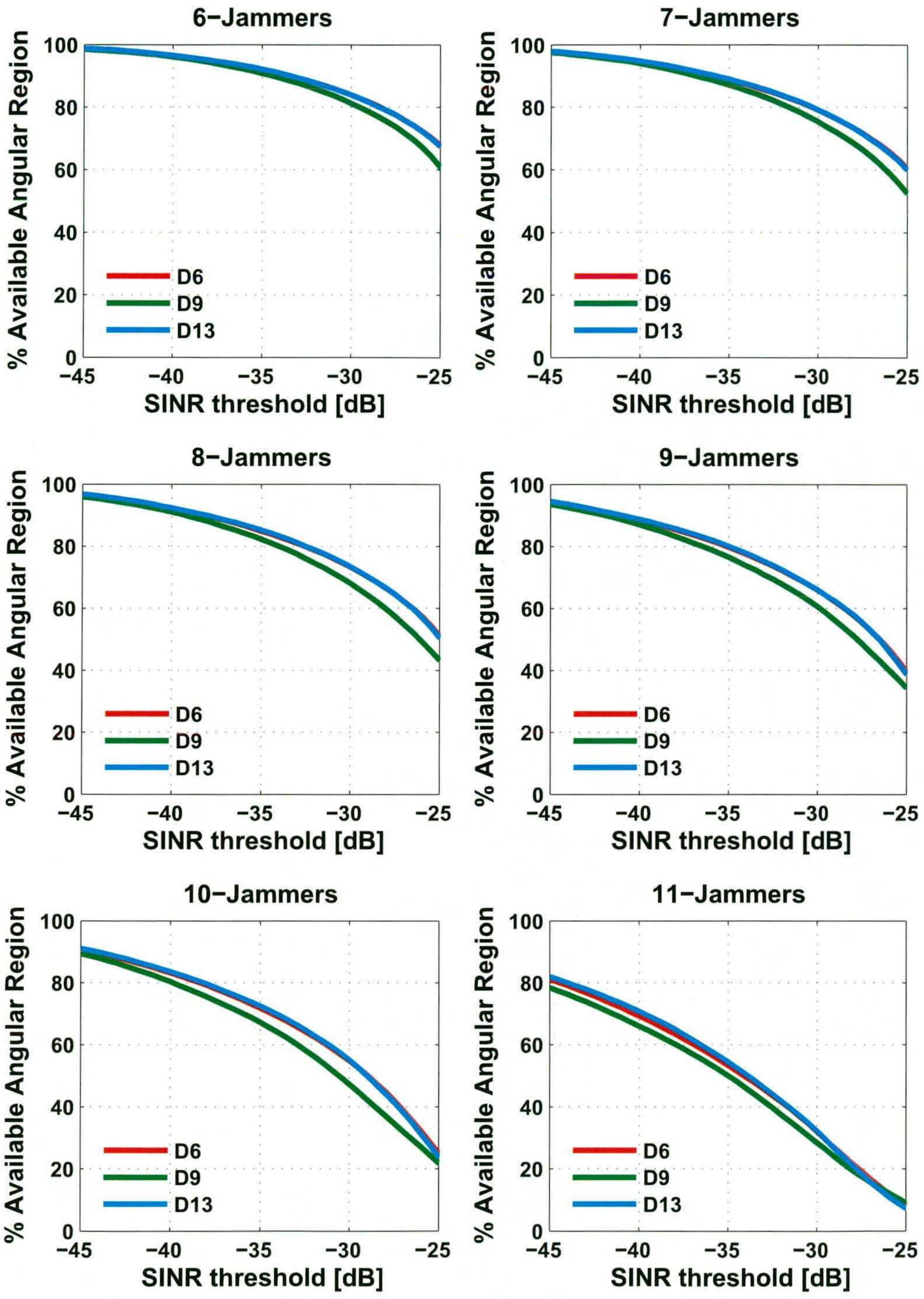


Figure 6.34: Performance of twelve element antenna arrays in the presence of six to eleven interfering signals. AE is operating in beam forming / null steering mode. L1 frequency band.

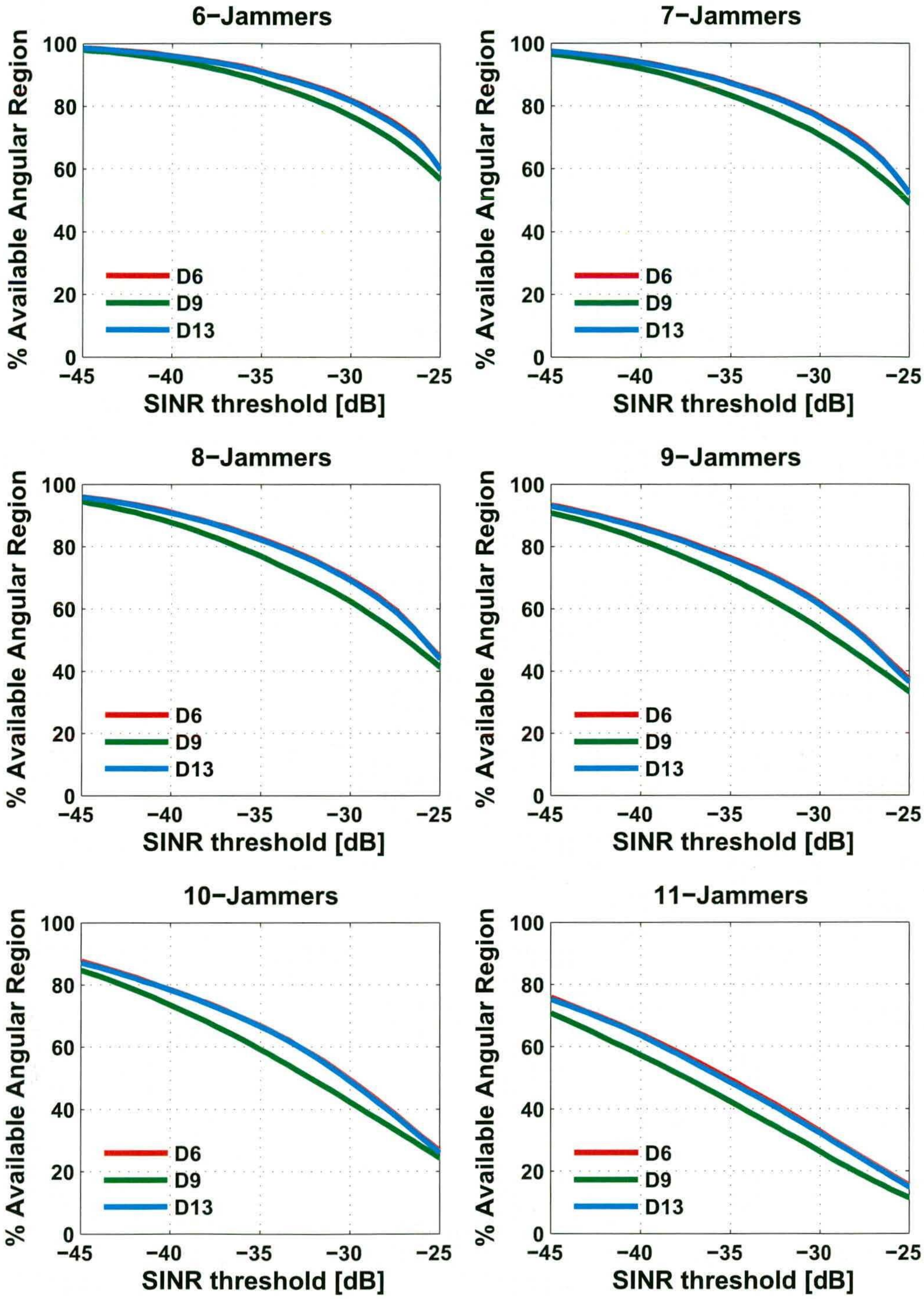


Figure 6.35: Performance of twelve element antenna arrays in the presence of six to eleven interfering signals. AE is operating in beam forming / null steering mode. L2 frequency band.

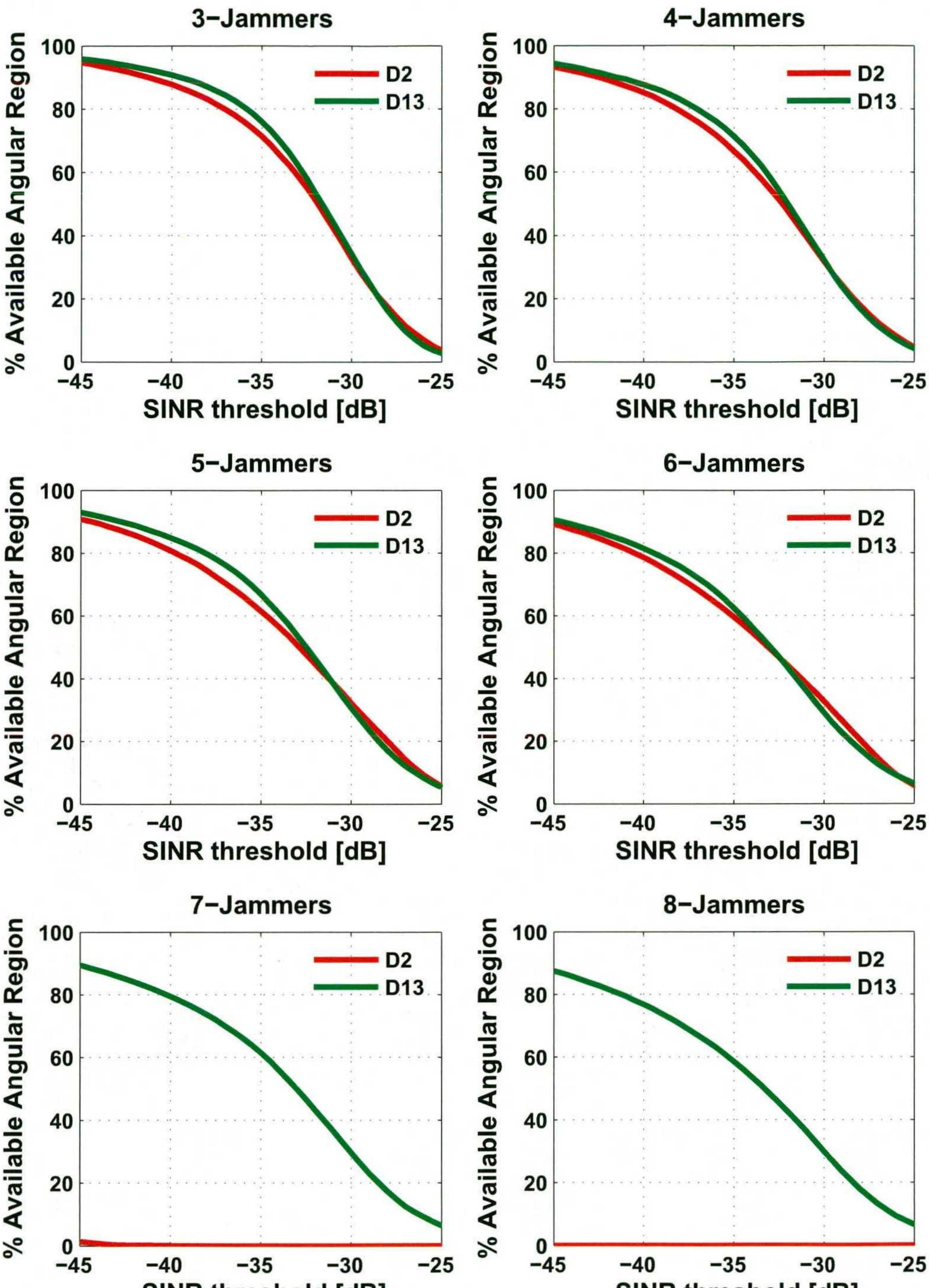


Figure 6.36: Performance of seven and twelve element antenna arrays in the presence of three to eight interfering signals. AE is operating in simple power minimization mode. L1 frequency band.

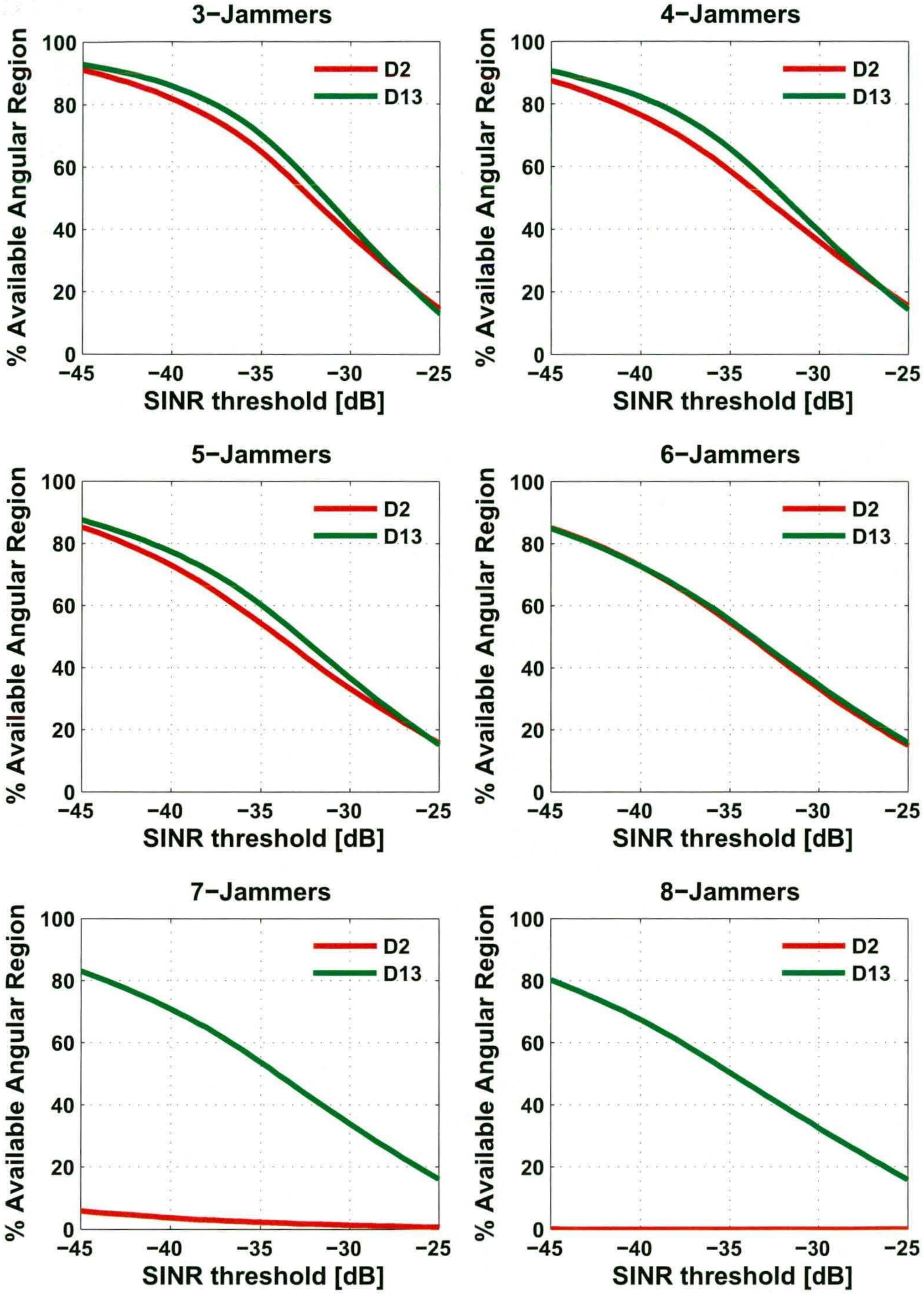


Figure 6.37: Performance of seven and twelve element antenna arrays in the presence of three to eight interfering signals. AE is operating in simple power minimization mode. L2 frequency band.

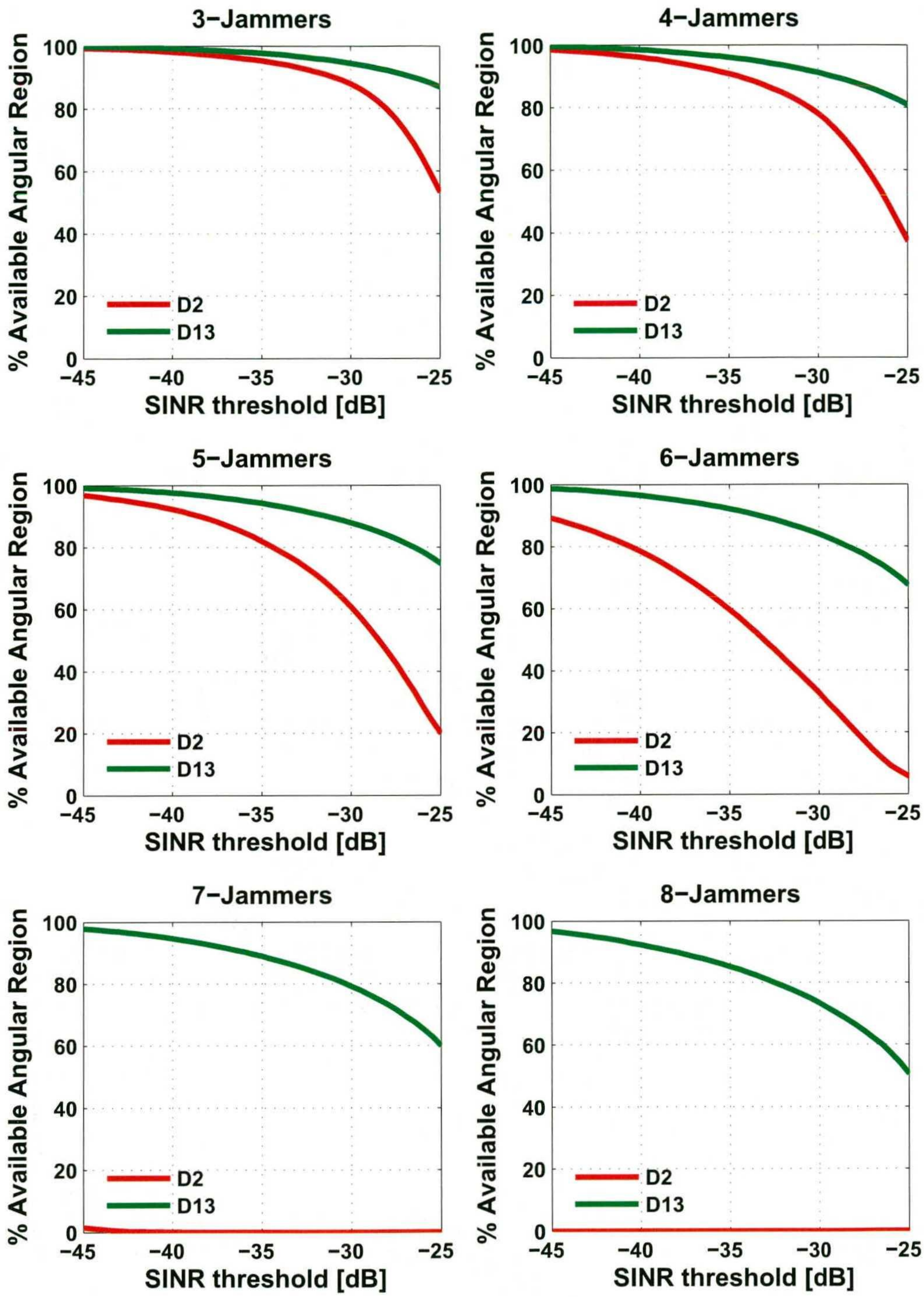


Figure 6.38: Performance of seven and twelve element antenna arrays in the presence of three to eight interfering signals. AE is operating in beam forming / null steering mode. L1 frequency band.

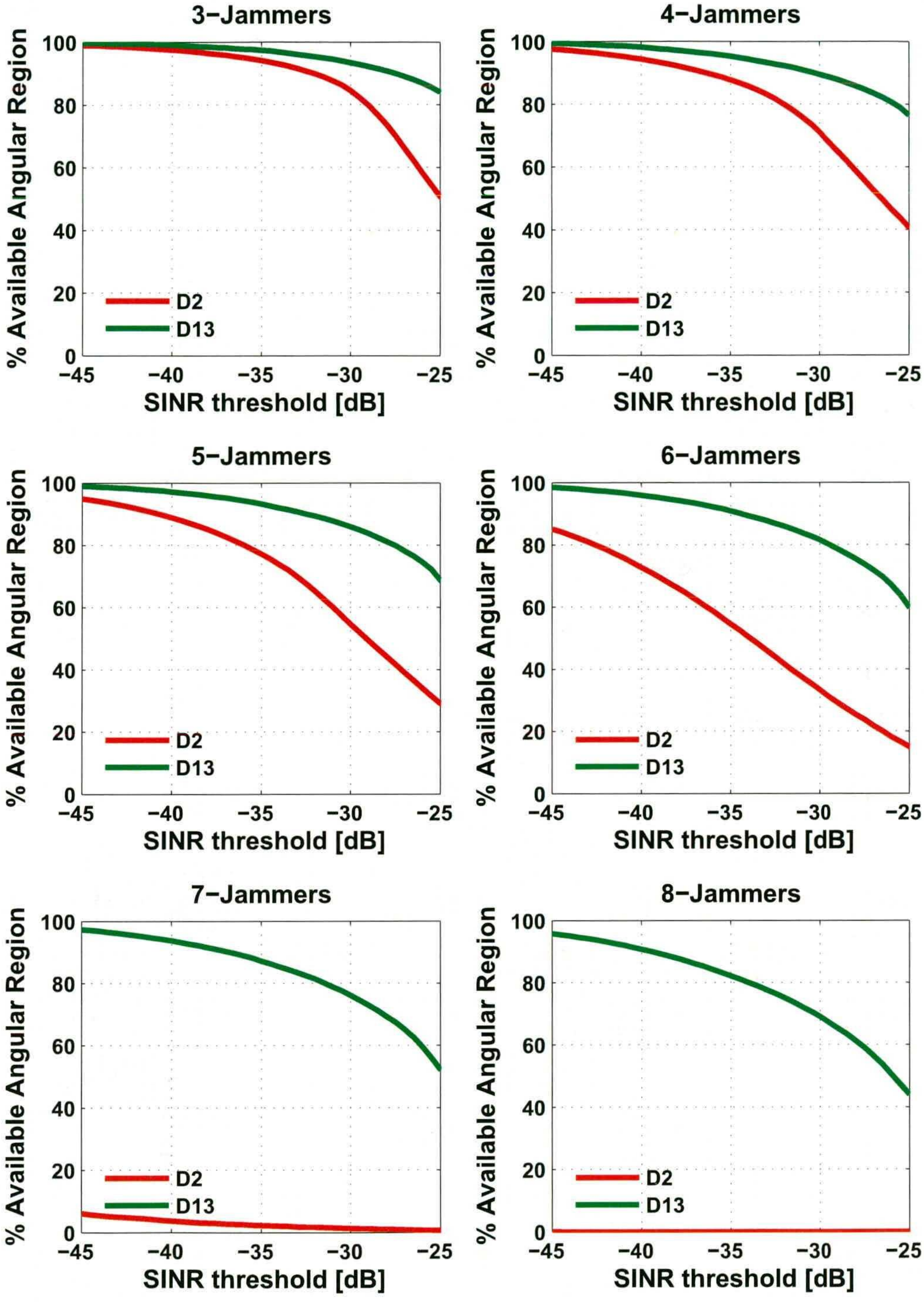


Figure 6.39: Performance of seven and twelve element antenna arrays in the presence of three to eight interfering signals. AE is operating in beam forming / null steering mode. L2 frequency band.

| No. of interfering signals | Antenna Array | | |
|---|---|---|---|
| | B2 | D1 | D2 |
| **0** | 97.22 | 93.01 | 97.51 |
| **1** | 83.46 | 82.19 | 85.60 |
| **2** | 74.09 | 73.43 | 76.12 |
| **3** | 68.96 | 70.02 | 71.28 |
| **4** | 62.94 | 62.85 | 66.49 |
| **5** | 57.53 | 56.18 | 61.38 |
| **6** | 57.82 | 52.10 | 59.41 |

Table 6.1: Seven Element Antenna Arrays. Percentage of available angular region when SINR threshold is greater than -35 dB. AE is operating in simple power minimization mode. L1 frequency band.

| No. of interfering signals | Antenna Array | | |
|---|---|---|---|
| | B2 | D1 | D2 |
| **0** | 88.09 | 93.82 | 88.71 |
| **1** | 75.74 | 81.72 | 76.72 |
| **2** | 68.16 | 73.70 | 70.92 |
| **3** | 61.54 | 68.73 | 64.61 |
| **4** | 54.55 | 63.61 | 58.43 |
| **5** | 53.50 | 57.46 | 54.20 |
| **6** | 51.32 | 53.44 | 54.45 |

Table 6.2: Seven Element Antenna Arrays. Percentage of available angular region when SINR threshold is greater than -35 dB. AE is operating in simple power minimization mode. L2 frequency band.

| No. of interfering signals | Antenna Array | | |
|---|---|---|---|
| | B2 | D1 | D2 |
| **0** | 100.00 | 100.00 | 100.00 |
| **1** | 99.04 | 98.84 | 98.98 |
| **2** | 97.60 | 96.96 | 97.38 |
| **3** | 95.37 | 94.39 | 95.11 |
| **4** | 90.58 | 88.69 | 90.71 |
| **5** | 81.84 | 76.29 | 81.86 |
| **6** | 57.85 | 52.13 | 59.48 |

Table 6.3: Seven Element Antenna Arrays. Percentage of available angular region when SINR threshold is greater than -35 dB. AE is operating in beam forming / null steering mode. L1 frequency band.

| No. of interfering signals | Antenna Array | | |
|---|---|---|---|
| | B2 | D1 | D2 |
| **0** | 100.00 | 100.00 | 100.00 |
| **1** | 98.73 | 98.45 | 98.68 |
| **2** | 96.53 | 95.85 | 96.68 |
| **3** | 93.56 | 92.20 | 93.96 |
| **4** | 87.54 | 86.36 | 87.60 |
| **5** | 76.22 | 76.34 | 77.12 |
| **6** | 51.36 | 53.46 | 54.48 |

Table 6.4: Seven Element Antenna Arrays. Percentage of available angular region when SINR threshold is greater than -35 dB. AE is operating in beam forming / null steering mode. L2 frequency band.

| No. of interfering signals | Antenna Array | | | | |
|---|---|---|---|---|---|
| | B2 | D3 | D4 | D5 | D6 |
| **0** | 97.22 | 97.26 | 97.22 | 97.18 | 97.05 |
| **1** | 83.46 | 84.91 | 88.11 | 87.61 | 88.08 |
| **2** | 74.09 | 76.13 | 78.91 | 79.39 | 80.08 |
| **3** | 68.96 | 70.91 | 73.89 | 75.13 | 75.94 |
| **4** | 62.94 | 64.67 | 68.73 | 70.48 | 70.94 |
| **5** | 57.53 | 61.43 | 63.58 | 65.51 | 66.32 |
| **6** | 57.82 | 56.01 | 58.56 | 59.93 | 61.33 |
| **7** | 0.00 | 55.23 | 59.38 | 60.08 | 60.56 |
| **8** | 0.00 | 53.31 | 55.30 | 55.99 | 57.47 |
| **9** | 0.00 | 0.06 | 56.15 | 55.16 | 56.72 |
| **10** | 0.00 | 0.00 | 0.00 | 57.36 | 54.72 |
| **11** | 0.00 | 0.00 | 0.00 | 2.18 | 53.02 |

Table 6.5: One ring uniform distribution. Percentage of available angular region when SINR threshold is greater than -35 dB. AE is operating in simple power minimization mode. L1 frequency band.

| No. of interfering signals | Antenna Array | | | | |
|---|---|---|---|---|---|
| | B2 | D3 | D4 | D5 | D6 |
| **0** | 88.09 | 86.76 | 86.63 | 85.47 | 86.05 |
| **1** | 75.74 | 76.79 | 78.23 | 78.35 | 79.59 |
| **2** | 68.16 | 70.64 | 72.30 | 72.84 | 74.40 |
| **3** | 61.54 | 65.49 | 67.24 | 68.61 | 70.16 |
| **4** | 54.55 | 58.91 | 62.12 | 63.66 | 65.62 |
| **5** | 53.50 | 51.77 | 57.14 | 58.39 | 60.28 |
| **6** | 51.32 | 47.41 | 49.82 | 52.87 | 55.11 |
| **7** | 0.00 | 47.62 | 48.23 | 51.52 | 53.81 |
| **8** | 0.00 | 48.25 | 46.80 | 48.12 | 50.49 |
| **9** | 0.00 | 0.88 | 47.90 | 48.62 | 49.63 |
| **10** | 0.00 | 0.12 | 2.04 | 47.96 | 48.36 |
| **11** | 0.00 | 0.00 | 0.00 | 0.53 | 48.97 |

Table 6.6: One ring uniform distribution. Percentage of available angular region when SINR threshold is greater than -35 dB. AE is operating in simple power minimization mode. L2 frequency band.

| No. of interfering signals | Antenna Array | | | | |
|---|---|---|---|---|---|
| | B2 | D3 | D4 | D5 | D6 |
| **0** | 100.00 | 100.00 | 100.00 | 100.00 | 100.00 |
| **1** | 99.04 | 99.22 | 99.32 | 99.38 | 99.43 |
| **2** | 97.60 | 98.00 | 98.26 | 98.49 | 98.58 |
| **3** | 95.37 | 96.47 | 96.97 | 97.35 | 97.59 |
| **4** | 90.58 | 93.80 | 94.72 | 95.39 | 95.91 |
| **5** | 81.84 | 90.67 | 92.39 | 93.41 | 94.17 |
| **6** | 57.85 | 85.78 | 89.14 | 90.74 | 92.01 |
| **7** | 0.00 | 76.19 | 83.74 | 86.86 | 88.80 |
| **8** | 0.00 | 53.35 | 75.37 | 81.27 | 84.83 |
| **9** | 0.00 | 0.06 | 56.21 | 72.86 | 79.70 |
| **10** | 0.00 | 0.00 | 0.00 | 57.59 | 71.76 |
| **11** | 0.00 | 0.00 | 0.00 | 2.18 | 53.27 |

Table 6.7: One ring uniform distribution. Percentage of available angular region when SINR threshold is greater than -35 dB. AE is operating in beam forming / null steering mode. L1 frequency band.

| No. of interfering signals | Antenna Array | | | | |
|---|---|---|---|---|---|
| | B2 | D3 | D4 | D5 | D6 |
| **0** | 100.00 | 100.00 | 100.00 | 100.00 | 100.00 |
| **1** | 98.73 | 99.06 | 99.24 | 99.37 | 99.38 |
| **2** | 96.53 | 97.57 | 97.95 | 98.35 | 98.44 |
| **3** | 93.56 | 95.65 | 96.35 | 96.93 | 97.30 |
| **4** | 87.54 | 92.17 | 93.46 | 94.65 | 95.32 |
| **5** | 76.22 | 87.94 | 90.56 | 92.44 | 93.42 |
| **6** | 51.36 | 81.19 | 86.14 | 89.55 | 91.00 |
| **7** | 0.00 | 69.33 | 79.52 | 84.87 | 87.26 |
| **8** | 0.00 | 48.38 | 68.61 | 77.92 | 82.38 |
| **9** | 0.00 | 0.94 | 48.08 | 67.98 | 76.14 |
| **10** | 0.00 | 0.12 | 2.05 | 48.08 | 66.79 |
| **11** | 0.00 | 0.00 | 0.00 | 0.53 | 49.30 |

Table 6.8: One ring uniform distribution. Percentage of available angular region when SINR threshold is greater than -35 dB. AE is operating in beam forming / null steering mode. L2 frequency band.

| No. of interfering signals | Antenna Array | | | | |
|---|---|---|---|---|---|
| | D1 | D7 | B6 | D8 | D9 |
| **0** | 93.01 | 95.38 | 93.68 | 94.20 | 93.55 |
| **1** | 82.19 | 85.07 | 84.96 | 85.13 | 84.87 |
| **2** | 73.43 | 76.87 | 78.07 | 78.71 | 78.58 |
| **3** | 70.02 | 71.02 | 74.21 | 73.68 | 74.77 |
| **4** | 62.85 | 67.24 | 70.92 | 69.82 | 70.62 |
| **5** | 56.18 | 62.53 | 66.71 | 63.56 | 67.22 |
| **6** | 52.10 | 60.52 | 59.87 | 59.79 | 62.00 |
| **7** | 0.00 | 57.66 | 58.54 | 57.35 | 59.73 |
| **8** | 0.00 | 56.56 | 55.12 | 53.14 | 54.51 |
| **9** | 0.00 | 0.00 | 53.49 | 51.56 | 53.20 |
| **10** | 0.00 | 0.00 | 0.13 | 53.48 | 49.93 |
| **11** | 0.00 | 0.00 | 0.00 | 0.04 | 49.94 |

Table 6.9: Two ring distribution. Percentage of available angular region when SINR threshold is greater than -35 dB. AE is operating in simple power minimization mode. L1 frequency band.

| No. of interfering signals | Antenna Array | | | | |
|---|---|---|---|---|---|
| | D1 | D7 | B6 | D8 | D9 |
| **0** | 93.82 | 88.97 | 91.28 | 85.31 | 86.12 |
| **1** | 81.72 | 78.41 | 81.71 | 77.87 | 78.90 |
| **2** | 73.70 | 72.41 | 73.54 | 72.90 | 72.49 |
| **3** | 68.73 | 66.06 | 68.80 | 67.53 | 67.86 |
| **4** | 63.61 | 61.30 | 63.89 | 62.73 | 63.34 |
| **5** | 57.46 | 56.61 | 57.65 | 57.49 | 57.05 |
| **6** | 53.44 | 52.19 | 53.76 | 52.07 | 52.47 |
| **7** | 0.00 | 52.28 | 52.69 | 48.91 | 49.66 |
| **8** | 0.00 | 51.24 | 51.46 | 46.60 | 45.87 |
| **9** | 0.00 | 1.58 | 49.42 | 46.57 | 43.77 |
| **10** | 0.00 | 0.00 | 0.50 | 47.18 | 42.05 |
| **11** | 0.00 | 0.00 | 0.00 | 0.80 | 41.90 |

Table 6.10: Two ring distribution. Percentage of available angular region when SINR threshold is greater than -35 dB. AE is operating in simple power minimization mode. L2 frequency band.

| No. of interfering signals | Antenna Array | | | | |
|---|---|---|---|---|---|
| | D1 | D7 | B6 | D8 | D9 |
| **0** | 100.00 | 100.00 | 100.00 | 100.00 | 100.00 |
| **1** | 98.84 | 99.17 | 99.25 | 99.32 | 99.40 |
| **2** | 96.96 | 97.97 | 98.16 | 98.36 | 98.49 |
| **3** | 94.39 | 96.51 | 96.78 | 97.07 | 97.32 |
| **4** | 88.69 | 93.84 | 94.36 | 95.00 | 95.33 |
| **5** | 76.29 | 90.48 | 91.73 | 92.87 | 93.38 |
| **6** | 52.13 | 86.12 | 88.32 | 89.78 | 90.77 |
| **7** | 0.00 | 77.72 | 83.63 | 86.09 | 87.09 |
| **8** | 0.00 | 56.61 | 74.49 | 80.13 | 82.25 |
| **9** | 0.00 | 0.00 | 53.59 | 71.54 | 76.49 |
| **10** | 0.00 | 0.00 | 0.14 | 53.67 | 67.19 |
| **11** | 0.00 | 0.00 | 0.00 | 0.05 | 50.04 |

Table 6.11: Two ring distribution. Percentage of available angular region when SINR threshold is greater than -35 dB. AE is operating in beam forming / null steering mode. L1 frequency band.

| No. of interfering signals | Antenna Array | | | | |
|---|---|---|---|---|---|
| | D1 | D7 | B6 | D8 | D9 |
| **0** | 100.00 | 100.00 | 100.00 | 100.00 | 100.00 |
| **1** | 98.45 | 98.88 | 99.01 | 99.09 | 99.21 |
| **2** | 95.85 | 97.16 | 97.50 | 97.75 | 98.00 |
| **3** | 92.20 | 95.16 | 95.70 | 96.10 | 96.47 |
| **4** | 86.36 | 91.38 | 92.53 | 93.18 | 93.83 |
| **5** | 76.34 | 87.21 | 89.29 | 90.50 | 91.38 |
| **6** | 53.46 | 81.23 | 84.63 | 86.36 | 87.80 |
| **7** | 0.00 | 71.55 | 78.93 | 81.23 | 83.19 |
| **8** | 0.00 | 51.54 | 68.21 | 73.04 | 76.93 |
| **9** | 0.00 | 1.58 | 49.47 | 64.23 | 69.68 |
| **10** | 0.00 | 0.00 | 0.54 | 47.35 | 59.21 |
| **11** | 0.00 | 0.00 | 0.00 | 0.83 | 42.29 |

Table 6.12: Two ring distribution. Percentage of available angular region when SINR threshold is greater than -35 dB. AE is operating in beam forming / null steering mode. L2 frequency band.

| No. of interfering signals | Antenna Array | | | | |
|---|---|---|---|---|---|
| | D2 | D10 | D11 | D12 | D13 |
| **0** | 97.51 | 97.56 | 97.26 | 97.18 | 97.14 |
| **1** | 85.60 | 86.87 | 87.47 | 87.36 | 88.12 |
| **2** | 76.12 | 78.67 | 78.47 | 79.61 | 80.15 |
| **3** | 71.28 | 71.30 | 74.35 | 75.08 | 75.89 |
| **4** | 66.49 | 65.69 | 69.09 | 69.63 | 71.19 |
| **5** | 61.38 | 62.15 | 64.40 | 65.25 | 66.75 |
| **6** | 59.41 | 58.50 | 60.09 | 60.19 | 62.41 |
| **7** | 0.00 | 58.49 | 60.63 | 59.99 | 61.53 |
| **8** | 0.00 | 55.40 | 55.60 | 56.82 | 58.52 |
| **9** | 0.00 | 0.00 | 56.82 | 55.21 | 57.13 |
| **10** | 0.00 | 0.00 | 0.00 | 55.94 | 54.87 |
| **11** | 0.00 | 0.00 | 0.00 | 0.24 | 54.36 |

Table 6.13: One ring non-uniform distribution. Percentage of available angular region when SINR threshold is greater than -35 dB. AE is operating in simple power minimization mode. L1 frequency band.

| No. of interfering signals | Antenna Array | | | | |
|---|---|---|---|---|---|
| | D2 | D10 | D11 | D12 | D13 |
| **0** | 88.71 | 87.26 | 85.63 | 86.30 | 85.26 |
| **1** | 76.72 | 77.59 | 77.51 | 79.01 | 79.29 |
| **2** | 70.92 | 71.25 | 71.88 | 73.28 | 74.14 |
| **3** | 64.61 | 65.86 | 67.02 | 68.91 | 70.04 |
| **4** | 58.43 | 60.45 | 62.11 | 64.06 | 65.58 |
| **5** | 54.20 | 54.44 | 57.02 | 58.95 | 60.22 |
| **6** | 54.45 | 49.35 | 50.20 | 53.02 | 55.29 |
| **7** | 2.22 | 50.40 | 49.23 | 51.64 | 53.68 |
| **8** | 0.00 | 49.94 | 46.47 | 47.92 | 50.37 |
| **9** | 0.00 | 1.28 | 49.12 | 48.77 | 49.49 |
| **10** | 0.00 | 0.00 | 0.87 | 48.56 | 47.76 |
| **11** | 0.00 | 0.00 | 0.01 | 0.93 | 48.28 |

Table 6.14: One ring non-uniform distribution. Percentage of available angular region when SINR threshold is greater than -35 dB. AE is operating in simple power minimization mode. L2 frequency band.

| No. of interfering signals | Antenna Array | | | | |
|---|---|---|---|---|---|
| | D2 | D10 | D11 | D12 | D13 |
| **0** | 100.00 | 100.00 | 100.00 | 100.00 | 100.00 |
| **1** | 98.98 | 99.21 | 99.32 | 99.39 | 99.43 |
| **2** | 97.38 | 98.06 | 98.28 | 98.49 | 98.58 |
| **3** | 95.11 | 96.61 | 97.04 | 97.37 | 97.59 |
| **4** | 90.71 | 94.09 | 94.74 | 95.45 | 95.91 |
| **5** | 81.86 | 91.21 | 92.32 | 93.48 | 94.19 |
| **6** | 59.48 | 86.36 | 89.03 | 90.81 | 92.02 |
| **7** | 0.00 | 78.36 | 83.86 | 86.67 | 88.91 |
| **8** | 0.00 | 55.45 | 75.51 | 81.23 | 85.10 |
| **9** | 0.00 | 0.00 | 57.07 | 73.08 | 79.96 |
| **10** | 0.00 | 0.00 | 0.00 | 56.12 | 72.44 |
| **11** | 0.00 | 0.00 | 0.00 | 0.28 | 54.43 |

Table 6.15: One ring non-uniform distribution. Percentage of available angular region when SINR threshold is greater than -35 dB. AE is operating in beam forming / null steering mode. L1 frequency band.

| No. of interfering signals | Antenna Array | | | | |
|---|---|---|---|---|---|
| | D2 | D10 | D11 | D12 | D13 |
| **0** | 100.00 | 100.00 | 100.00 | 100.00 | 100.00 |
| **1** | 98.68 | 99.05 | 99.20 | 99.36 | 99.37 |
| **2** | 96.68 | 97.55 | 97.94 | 98.33 | 98.43 |
| **3** | 93.96 | 95.71 | 96.33 | 96.90 | 97.24 |
| **4** | 87.60 | 92.49 | 93.50 | 94.60 | 95.18 |
| **5** | 77.12 | 88.44 | 90.65 | 92.44 | 93.23 |
| **6** | 54.48 | 81.74 | 86.26 | 89.49 | 90.78 |
| **7** | 2.23 | 71.03 | 79.61 | 84.99 | 87.13 |
| **8** | 0.00 | 50.08 | 68.79 | 77.73 | 82.12 |
| **9** | 0.00 | 1.28 | 49.17 | 68.08 | 75.74 |
| **10** | 0.00 | 0.00 | 0.88 | 48.67 | 66.59 |
| **11** | 0.00 | 0.00 | 0.01 | 0.93 | 48.43 |

Table 6.16: One ring non-uniform distribution. Percentage of available angular region when SINR threshold is greater than -35 dB. AE is operating in beam forming / null steering mode. L2 frequency band.

| No. of interfering signals | Antenna Array | | |
|---|---|---|---|
| | D6 | D9 | D13 |
| **0** | 97.05 | 93.55 | 97.14 |
| **1** | 88.08 | 84.87 | 88.12 |
| **2** | 80.08 | 78.58 | 80.15 |
| **3** | 75.94 | 74.77 | 75.89 |
| **4** | 70.94 | 70.62 | 71.19 |
| **5** | 66.32 | 67.22 | 66.75 |
| **6** | 61.33 | 62.00 | 62.41 |
| **7** | 60.56 | 59.73 | 61.53 |
| **8** | 57.47 | 54.51 | 58.52 |
| **9** | 56.72 | 53.20 | 57.13 |
| **10** | 54.72 | 49.93 | 54.87 |
| **11** | 53.02 | 49.94 | 54.36 |

Table 6.17: Comparison of 12 element distributions. Percentage of available angular region when SINR threshold is greater than -35 dB. AE is operating in simple power minimization mode. L1 frequency band.

| No. of interfering signals | Antenna Array | | |
|---|---|---|---|
| | D6 | D9 | D13 |
| **0** | 86.05 | 86.12 | 85.26 |
| **1** | 79.59 | 78.90 | 79.29 |
| **2** | 74.40 | 72.49 | 74.14 |
| **3** | 70.16 | 67.86 | 70.04 |
| **4** | 65.62 | 63.34 | 65.58 |
| **5** | 60.28 | 57.05 | 60.22 |
| **6** | 55.11 | 52.47 | 55.29 |
| **7** | 53.81 | 49.66 | 53.68 |
| **8** | 50.49 | 45.87 | 50.37 |
| **9** | 49.63 | 43.77 | 49.49 |
| **10** | 48.36 | 42.05 | 47.76 |
| **11** | 48.97 | 41.90 | 48.28 |

Table 6.18: Comparison of 12 element distributions. Percentage of available angular region when SINR threshold is greater than -35 dB. AE is operating in simple power minimization mode. L2 frequency band.

| No. of interfering signals | Antenna Array | | |
|---|---|---|---|
| | D6 | D9 | D13 |
| **0** | 100.00 | 100.00 | 100.00 |
| **1** | 99.43 | 99.40 | 99.43 |
| **2** | 98.58 | 98.49 | 98.58 |
| **3** | 97.59 | 97.32 | 97.59 |
| **4** | 95.91 | 95.33 | 95.91 |
| **5** | 94.17 | 93.38 | 94.19 |
| **6** | 92.01 | 90.77 | 92.02 |
| **7** | 88.80 | 87.09 | 88.91 |
| **8** | 84.83 | 82.25 | 85.10 |
| **9** | 79.70 | 76.49 | 79.96 |
| **10** | 71.76 | 67.19 | 72.44 |
| **11** | 53.27 | 50.04 | 54.43 |

Table 6.19: Comparison of 12 element distributions. Percentage of available angular region when SINR threshold is greater than -35 dB. AE is operating in beam forming / null steering mode. L1 frequency band.

| No. of interfering signals | Antenna Array | | |
|---|---|---|---|
| | D6 | D9 | D13 |
| **0** | 100.00 | 100.00 | 100.00 |
| **1** | 99.38 | 99.21 | 99.37 |
| **2** | 98.44 | 98.00 | 98.43 |
| **3** | 97.30 | 96.47 | 97.24 |
| **4** | 95.32 | 93.83 | 95.18 |
| **5** | 93.42 | 91.38 | 93.23 |
| **6** | 91.00 | 87.80 | 90.78 |
| **7** | 87.26 | 83.19 | 87.13 |
| **8** | 82.38 | 76.93 | 82.12 |
| **9** | 76.14 | 69.68 | 75.74 |
| **10** | 66.79 | 59.21 | 66.59 |
| **11** | 49.30 | 42.29 | 48.43 |

Table 6.20: Comparison of 12 element distributions. Percentage of available angular region when SINR threshold is greater than -35 dB. AE is operating in beam forming / null steering mode. L2 frequency band.

| No. of interfering signals | Antenna Array | |
|---|---|---|
| | D2 | D13 |
| **0** | 97.51 | 97.14 |
| **1** | 85.60 | 88.12 |
| **2** | 76.12 | 80.15 |
| **3** | 71.28 | 75.89 |
| **4** | 66.49 | 71.19 |
| **5** | 61.38 | 66.75 |
| **6** | 59.41 | 62.41 |
| **7** | 0.00 | 61.53 |
| **8** | 0.00 | 58.52 |
| **9** | 0.00 | 57.13 |
| **10** | 0.00 | 54.87 |
| **11** | 0.00 | 54.36 |

Table 6.21: Comparison of 7 and 12 element distributions. Percentage of available angular region when SINR threshold is greater than -35 dB. AE is operating in simple power minimization mode. L1 frequency band.

| No. of interfering signals | Antenna Array | |
|---|---|---|
| | D2 | D13 |
| **0** | 88.71 | 85.26 |
| **1** | 76.72 | 79.29 |
| **2** | 70.92 | 74.14 |
| **3** | 64.61 | 70.04 |
| **4** | 58.43 | 65.58 |
| **5** | 54.20 | 60.22 |
| **6** | 54.45 | 55.29 |
| **7** | 2.22 | 53.68 |
| **8** | 0.00 | 50.37 |
| **9** | 0.00 | 49.49 |
| **10** | 0.00 | 47.76 |
| **11** | 0.00 | 48.28 |

Table 6.22: Comparison of 7 and 12 element distributions. Percentage of available angular region when SINR threshold is greater than -35 dB. AE is operating in simple power minimization mode. L2 frequency band.

| No. of interfering signals | Antenna Array | |
|---|---|---|
| | D2 | D13 |
| **0** | 100.00 | 100.00 |
| **1** | 98.98 | 99.43 |
| **2** | 97.38 | 98.58 |
| **3** | 95.11 | 97.59 |
| **4** | 90.71 | 95.91 |
| **5** | 81.86 | 94.19 |
| **6** | 59.48 | 92.02 |
| **7** | 0.00 | 88.91 |
| **8** | 0.00 | 85.10 |
| **9** | 0.00 | 79.96 |
| **10** | 0.00 | 72.44 |
| **11** | 0.00 | 54.43 |

Table 6.23: Comparison of 7 and 12 element distributions. Percentage of available angular region when SINR threshold is greater than -35 dB. AE is operating in beam forming / null steering mode. L1 frequency band.

| No. of interfering signals | Antenna Array | |
|---|---|---|
| | D2 | D13 |
| **0** | 100.00 | 100.00 |
| **1** | 98.68 | 99.37 |
| **2** | 96.68 | 98.43 |
| **3** | 93.96 | 97.24 |
| **4** | 87.60 | 95.18 |
| **5** | 77.12 | 93.23 |
| **6** | 54.48 | 90.78 |
| **7** | 2.23 | 87.13 |
| **8** | 0.00 | 82.12 |
| **9** | 0.00 | 75.74 |
| **10** | 0.00 | 66.59 |
| **11** | 0.00 | 48.43 |

Table 6.24: Comparison of 7 and 12 element distributions. Percentage of available angular region when SINR threshold is greater than -35 dB. AE is operating in beam forming / null steering mode. L2 frequency band.

# CHAPTER 7

# COMPARISON OF SELECTED GEOMETRIES

This purpose of this chapter is to show the performance improvement one would obtain from moving from a planar surface (zero curvature), to a two inch high geometry (curvature relative to a sphere of radius ten inches), on up to a six inch high geometry (curvature relative to a sphere of six inches).

## 7.1 Performance of 12 Element Antenna Arrays

All antenna arrays investigated in this chapter contain twelve elements. Antenna array E1 (Figure 7.1) is a planar geometry with the reference element located at the center of the aperture, and the remaining eleven elements distributed non-uniformly along the periphery. It is noted that a twelve element planar antenna array with the auxiliary elements distributed uniformly was also examined. The same conclusion was drawn as for the two inch high geometry. As the antenna aperture becomes filled it does not make much difference between distributing the antenna elements uniformly or non-uniformly. Antenna Array D13 (Figure 7.2) is the best selection from Chapter 6 and has one element located at the the top of the two inch high surface, and the other eleven elements are distributed non-uniformly along the outer ring at the bottom of the surface. Antenna array C11 (Figure 7.3) was selected as the best choice from Chapter 5 and has the reference element located at the apex of the six inch high surface, three elements along an inner ring that is 4.24 inches high, and the remaining eight elements located along the outer ring around the bottom of the hemisphere.

Figures 7.4 and 7.5 show the AJ performance of the three antenna arrays for the L1 and L2 bands, respectively, in the presence of six to eleven interfering signals. The antenna electronics is operating in the simple power minimization mode. In the L1 band, one observes that antenna array C11 and D13 drastically outperform the planar antenna array E1, with antenna array C11 having the best AJ performance. Similar results are also seen in the L2 band. Antenna array C11 has the best performance followed in sequential order by antenna arrays D13 and E1. Therefore, one should utilize the six inch high geometry of antenna array C11 if the platform allows.

Tables 7.1 and 7.2 show the percentage available angular region for which the output SINR exceeds -35 dB for the L1 and L2 bands, respectively. The AE is operating in simple power minimization mode. For eleven incident interfering signals one observes antenna array D13 outperforms antenna array E1 by approximately 23% in the L1 band and approximately 5% in the L2 band. Furthermore, antenna array C11 outperforms antenna array E1 by approximately 27% at L1 band, and 14% at L2 band for eleven incident interfering signals. Also, it is seen in directly comparing antenna array C11 and D13, that antenna array C11 outperforms antenna array D13 by approximately 4% in the L1 band and 9% in the L2 band. It is shown that there is an advantage in moving from a planar surface to a non planar convex surface. Also, the larger the surface curvature the better AJ performance that can be achieved. This will allow a significant advantage in maintaining reception of low elevation angle satellites.

Figures 7.6 and 7.7 display the performance while the AE is operating in beam forming / null steering mode for the L1 and L2 band, respectively. All other parameters are the same as in Figures 7.4 and 7.5. For the both the L1 and L2 bands, one notices that the same results hold true as for simple power minimization. Antenna array C11 performs the best followed by antenna arrays D13 and E1, in the given order, as expected.

One can further refer to Tables 7.3 and 7.4 for the AE operating in beam forming / null steering mode to yield a better idea of the exact percentage improvement of available angular region for which the output SINR exceeds -35 dB moving from antenna array E1 to antenna array C11. One notices that the performance does in fact increase as one moves from a planar geometry up to a convex non planar two inch high geometry and even more so for the six inch high geometry. In fact, for the signal scenario where the antenna arrays are fully constrained, antenna array D13 yields a 22.54% improvement in the L1 band and a 5.02% improvement in the L2 band when compared against antenna array E1. It is also seen that one can achieve an even greater performance increase for the six inch high geometry. Antenna array C11 outperforms antenna array E1 by 27.28% in the L1 band and 14.78% in the L2 band. It is seen that antenna array C11 outperforms antenna array D13 by 4.74% in the L1 band and 9.76% in the L2 band. Also, comparing Tables 7.3 and 7.4 with Tables 7.1 and 7.2 one sees significant performance improvement when the antenna electronics is operating in the beam forming / null steering mode. Therefore, it is strongly advised to operate in the beam forming / null steering mode.

## 7.2 Chapter Summary

It was shown that a significant performance improvement could be achieved by moving from a planar geometry up to a convex non planar antenna geometry with larger curvature. Therefore, if the platform allows, one should select the six inch high geometry. It is strongly advised that the AE operates in the beam forming / null steering mode to yield better AJ performance. As a result, there is a trade off between attainable performance and hardware cost (antenna and antenna electronics).

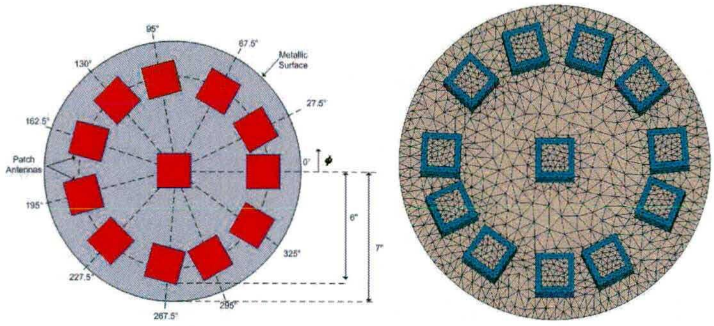


(a) Top Down View (b) Gridded Surface

Figure 7.1: Antenna Array E1.

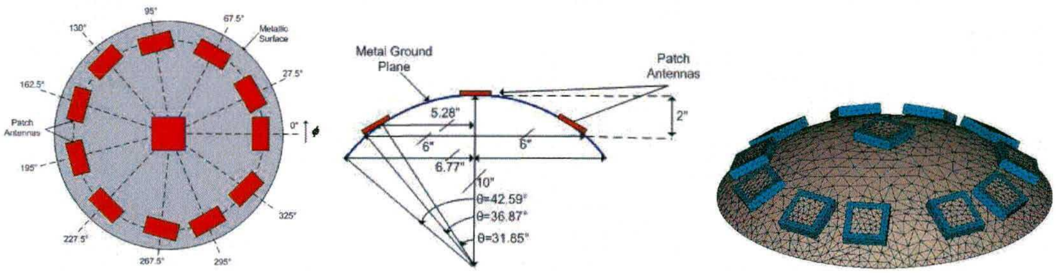


(a) Top Down View (b) Side View (c) Gridded Surface

Figure 7.2: Antenna Array D13.

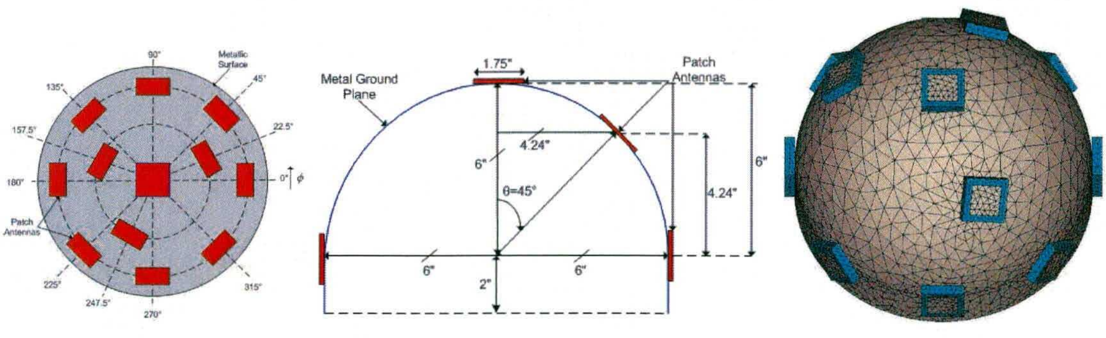


(a) Top Down View (b) Side View (c) Gridded Surface

Figure 7.3: Antenna Array C11.

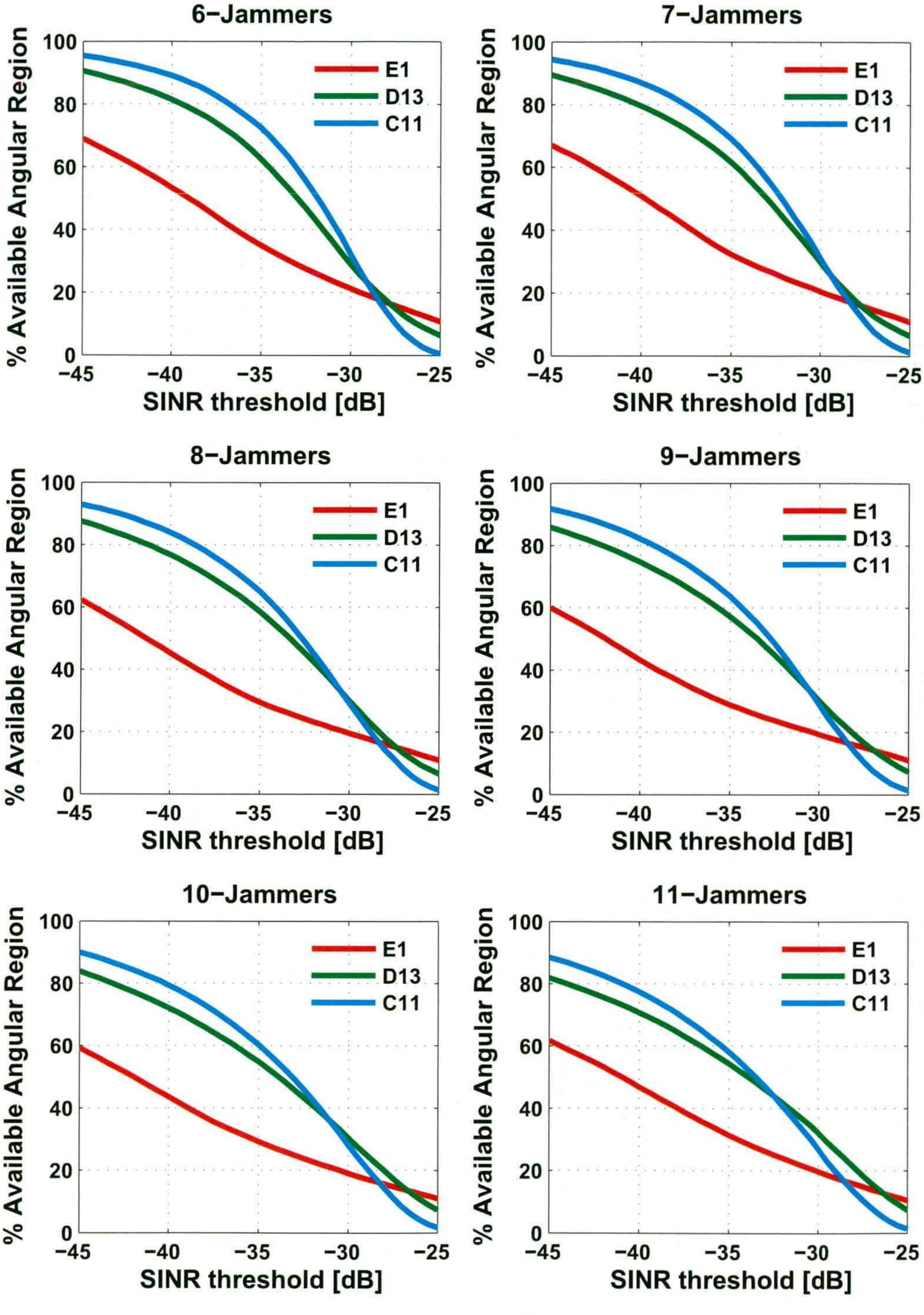


Figure 7.4: Performance of twelve element antenna arrays in the presence of six to eleven interfering signals. AE is operating in simple power minimization mode. L1 frequency band.

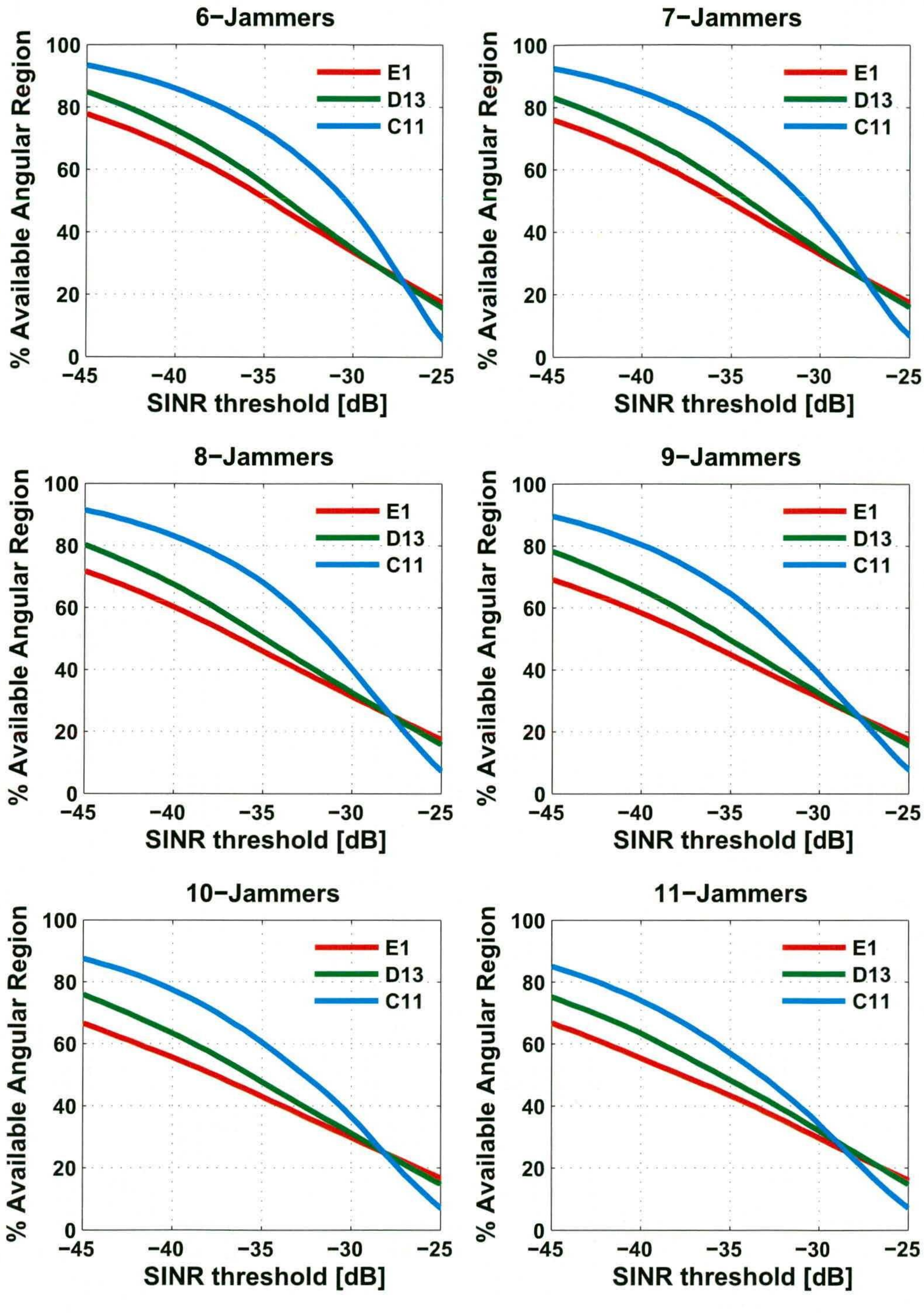


Figure 7.5: Performance of twelve element antenna arrays in the presence of six to eleven interfering signals. AE is operating in simple power minimization mode. L2 frequency band.

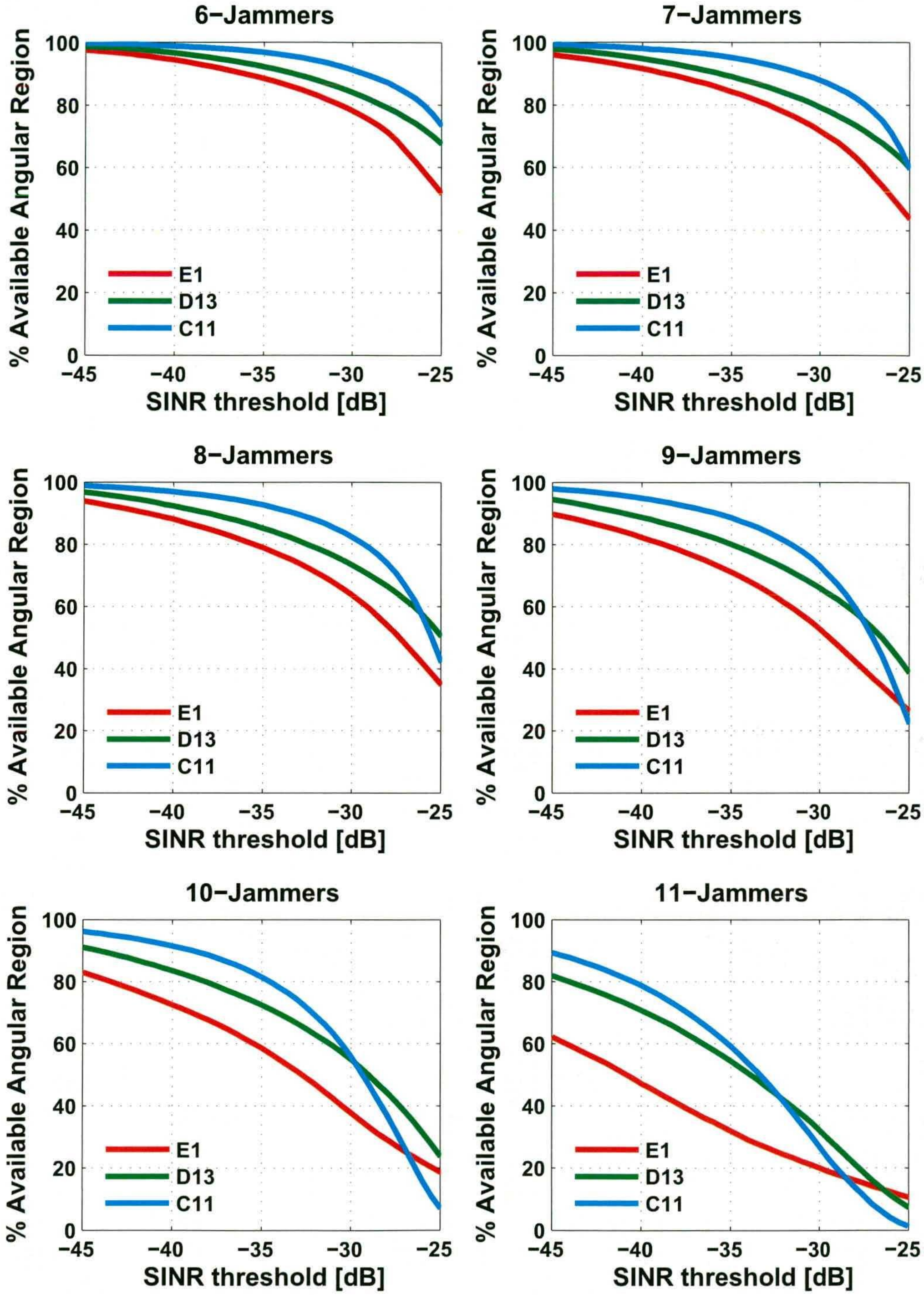


Figure 7.6: Performance of twelve element antenna arrays in the presence of six to eleven interfering signals. AE is operating in beam forming / null steering mode. L1 frequency band.

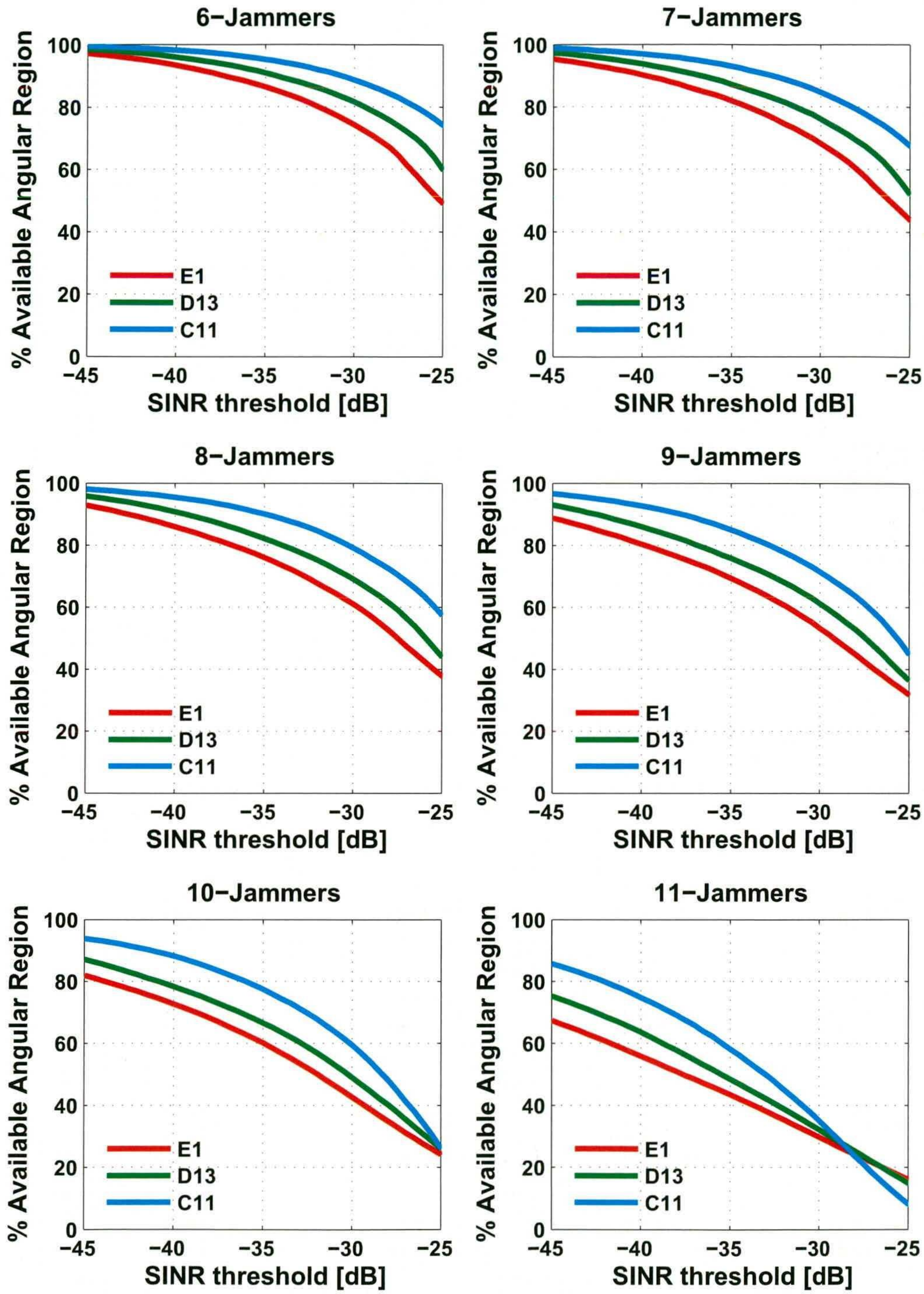


Figure 7.7: Performance of twelve element antenna arrays in the presence of six to eleven interfering signals. AE is operating in beam forming / null steering mode. L2 frequency band.

| No. of interfering signals | Antenna Array | | |
|---|---|---|---|
| | E1 | D13 | C11 |
| **0** | 73.02 | 97.14 | 94.07 |
| **1** | 65.94 | 88.12 | 89.42 |
| **2** | 58.81 | 80.15 | 84.36 |
| **3** | 53.06 | 75.89 | 81.17 |
| **4** | 46.33 | 71.19 | 77.97 |
| **5** | 40.95 | 66.75 | 75.07 |
| **6** | 34.96 | 62.41 | 72.27 |
| **7** | 32.27 | 61.53 | 68.94 |
| **8** | 29.46 | 58.52 | 65.04 |
| **9** | 28.80 | 57.13 | 63.64 |
| **10** | 29.17 | 54.87 | 60.29 |
| **11** | 31.34 | 54.36 | 58.08 |

Table 7.1: Comparison of 12 element distributions. Percentage of available angular region when SINR threshold is -35 dB. AE is operating in simple power minimization mode. L1 frequency band.

| No. of interfering signals | Antenna Array | | |
|---|---|---|---|
| | E1 | D13 | C11 |
| **0** | 80.36 | 85.26 | 96.29 |
| **1** | 74.86 | 79.29 | 91.09 |
| **2** | 70.57 | 74.14 | 86.29 |
| **3** | 65.90 | 70.04 | 83.42 |
| **4** | 61.36 | 65.58 | 79.53 |
| **5** | 55.89 | 60.22 | 75.68 |
| **6** | 50.82 | 55.29 | 72.09 |
| **7** | 49.17 | 53.68 | 70.32 |
| **8** | 45.89 | 50.37 | 68.01 |
| **9** | 44.83 | 49.49 | 64.48 |
| **10** | 42.95 | 47.76 | 60.47 |
| **11** | 43.26 | 48.28 | 56.99 |

Table 7.2: Comparison of 12 element distributions. Percentage of available angular region when SINR threshold is -35 dB. AE is operating in simple power minimization mode. L2 frequency band.

| No. of interfering signals | Antenna Array | | |
|---|---|---|---|
| | E1 | D13 | C11 |
| **0** | 100.00 | 100.00 | 100.00 |
| **1** | 99.15 | 99.43 | 99.79 |
| **2** | 97.92 | 98.58 | 99.48 |
| **3** | 96.38 | 97.59 | 99.05 |
| **4** | 93.75 | 95.91 | 98.48 |
| **5** | 91.26 | 94.19 | 97.73 |
| **6** | 88.29 | 92.02 | 96.65 |
| **7** | 84.11 | 88.91 | 95.00 |
| **8** | 78.83 | 85.10 | 92.61 |
| **9** | 70.96 | 79.96 | 88.51 |
| **10** | 58.49 | 72.44 | 81.40 |
| **11** | 31.89 | 54.43 | 59.17 |

Table 7.3: Comparison of 12 element distributions. Percentage of available angular region when SINR threshold is -35 dB. AE is operating in beam forming / null steering mode. L1 frequency band.

| No. of interfering signals | Antenna Array | | |
|---|---|---|---|
| | E1 | D13 | C11 |
| **0** | 100.00 | 100.00 | 100.00 |
| **1** | 98.98 | 99.37 | 99.71 |
| **2** | 97.43 | 98.43 | 99.28 |
| **3** | 95.57 | 97.24 | 98.69 |
| **4** | 92.55 | 95.18 | 97.75 |
| **5** | 89.73 | 93.23 | 96.64 |
| **6** | 86.35 | 90.78 | 95.09 |
| **7** | 81.87 | 87.13 | 92.92 |
| **8** | 75.99 | 82.12 | 90.07 |
| **9** | 69.28 | 75.74 | 84.92 |
| **10** | 60.09 | 66.59 | 77.43 |
| **11** | 43.41 | 48.43 | 58.19 |

Table 7.4: Comparison of 12 element distributions. Percentage of available angular region when SINR threshold is -35 dB. AE is operating in beam forming / null steering mode. L2 frequency band.

# CHAPTER 8

# SUMMARY, CONCLUSIONS AND FUTURE WORK

## 8.1 Summary and Conclusions

In this thesis, the performance of planar and non-planar adaptive antenna arrays operating at GPS frequencies in harsh interference environments consisting of multiple low elevation jammers was investigated. The main purpose of the antenna array design is to enhance their performance for improving reception of low elevation GPS satellites. All antenna array apertures studied in this work had similar projected area (looking from the top) of twelve inches. The selected individual antenna element was a RHCP dual band stacked microstrip patch antenna designed to operate at L1 (1575.42 MHz) and L2 (1227.6 MHz) bands with physical dimensions of 1.75" x 1.75" x 0.4". Rigorous electromagnetic modeling was carried out to include mutual coupling between the individual antenna elements as well as structure effects. A numerical EM code, FEKO, was utilized to calculate the *in situ* volumetric patterns of the various antenna elements used for this study. Furthermore, all incident signals (desired as well as interference) on the antenna arrays were assumed to be CW signals and the AE was assumed to be based on space-only processing. However, it has been shown in [14] that the performance of multi-tap STAP based AE in the presence of wideband signals is almost identical to the performance of space-only processing in the presence of CW signals. Therefore, the conclusions of this thesis are also applicable to STAP based AE. Furthermore, the performance was examined using two adaptive algorithms constrained to minimize the total output power. The two adaptive algorithms are simple power minimization and beam forming / null steering. Also, the performance metric of choice used to evaluate the antenna array performance is available angular region, which is defined as the percentage over the entire upper hemisphere for which the output SINR exceeds a selected value. This was calculated as the mean value over twenty-five independent trials for a given number of interfering signals. The interfering signals angle of arrival varied randomly from one trial to the next ranging from $-10°$ to $+20°$ in elevation with at least $15°$ separation in azimuth.

In Chapter 3, it was shown that distributing the elements on a convex non-planar surface will lead to improved AJ performance over planar as well as concave non-planar surface. In fact, the concave non-planar antenna arrays do not even perform as well as the planar antenna arrays. Also, since non-planar antenna arrays have larger surface area, one can add more elements to these antenna arrays for further performance improvement and this was shown for an increase of seven to ten antenna elements. This was true for both the L1 and L2 GPS frequencies while the AE was operating in both simple power minimization and beam forming / null steering mode. Furthermore, an antenna array requires N+1 antenna elements to null N interfering signals, and AJ performance always degrades with an increase of interfering signals incident upon the antenna array. Also, in this chapter, it was concluded that the beam forming / null steering algorithm has a significant performance advantage over the simple power minimization algorithm. This is due to the fact that beam forming / null steering is able to point a beam (providing antenna gain) in the direction of the desired signal, while allowing the remaining degrees of freedom to null interfering signals; whereas, simple power minimization maintains the response of the reference element only and then uses the remaining degrees of freedom to null interfering signals. Since the reference element is a patch antenna distributed upon the top of a non-planar surface, it will already have a poor response in the direction of GPS low elevation satellites making it very difficult to receive them, especially in the presence of interfering signals. One may then think, why does one choose to use simple power minimization if their is a significant performance advantage in implementing beam forming / null steering? The reason why simple power minimization is utilized is because it is low cost and requires no *a priori* knowledge of the desired signal direction or the antenna array response in the desired signal direction; whereas, beam forming

/ null steering is a high cost implementation that does require *a priori* knowledge of the desired signal direction as well as the antenna array response at the carrier frequency in the particular direction of the desired signal. Therefore, there is a trade off between attainable performance level and cost of the hardware (antenna and antenna electronics).

In Chapter 4, it was shown that for a convex non-planar antenna array, the larger the amount of curvature of the surface, the more AJ performance improvement one can attain. This was shown from moving from a planar surface (zero curvature) up to a six inch high convex non-planar surface. The results held true for both L1 and L2 GPS frequencies, as well as, both adaptive algorithms for the seven and ten element distributions investigated. Therefore, further examination of the six inch high geometry regarding the number of elements as well as the element distributions was the focus of Chapter 5. It was concluded that the best distribution for the six inch high geometry was a two ring distribution, with a reference element located at the top of the hemisphere, and the remaining elements distributed between an inner ring of height 4.24 inches and an outer ring located along the bottom of the hemisphere. The other distributions that were studied was a one ring distribution, with the reference element located at the apex of the hemisphere and the auxiliary elements placed uniformly around the periphery of the hemisphere, and a two ring distribution, with a reference element placed at the top of the surface, and the remaining elements distributed either on an inner ring that was three inches high, or along an outer ring on the bottom of the surface. Furthermore, it was concluded that if the antenna electronics is operating in the beam forming / null steering mode, one can pack the aperture as much as possible resulting in improved AJ performance. The limiting factors of attainable AJ performance are the physical size of the individual antenna elements and hardware cost (antenna and antenna electronics). It is important to note that the physical size of the individual antenna elements can be reduced by selecting a higher dielectric constant substrate [2]. However, reducing the size of individual elements results in poorer performance with respect to bandwidth as well as antenna gain. In the case of the AE operating in simple power minimization mode, it was shown that the point of diminishing returns in regards to AJ performance was achieved around twelve elements. Therefore, it was recommended that antenna array C11 (Figure 5.13) is selected as the best antenna array in regards to performance relative to both adaptive algorithms at the L1 and L2 bands. Antenna array C11 has one element distributed at the top of the hemisphere, three elements located along an inner ring 4.24 inches high, and the remaining eight elements distributed uniformly along the bottom of the surface.

The six inch high surface is a possibility for ground or ship-board application; however, it would not be desirable to the aerodynamic profile of an aircraft due to its physical size. Thus, the desired platform may not be able to tolerate a large height; however, one still desires the performance advantage given by the convex non planar surface. Therefore, in Chapter 6 we investigated two inch high geometries. The antenna elements were distributed on a two inch high surface, while maintaining a curvature relative to a spherical surface of ten inches. Furthermore, it was shown that as the antenna aperture becomes filled with antenna elements, there is an advantage to placing the elements along one ring instead of two rings; however, there is not a significant advantage between distributing antenna elements uniformly or non-uniformly. Again, we observed that when the antenna electronics is operating in the beam forming / null steering mode, increasing the number of antenna elements results in performance improvement. However, with respect to simple power minimization, there was not a significant increase in AJ performance observed with the addition of more elements. Moreover, it was shown that when the antenna arrays were operating in the simple power minimization mode, they were able to more effectively null jammers in the L1 band than in the L2 band, which has to do with the antenna aperture being electrically larger in the L1 band. The recommended antenna array was D13 (Figure 6.15), which contained twelve elements, with one element at the top of the surface and the remaining elements distributed non-uniformly around the bottom of the surface.

As a result, the performance advantage one can achieve moving from a twelve element planar geometry to the two inch high and six inch high convex non planar geometries is shown in Chapter 7. It is shown that the six inch high geometry drastically outperforms the two inch high as well as the planar geometries for both the

L1 and L2 bands. Also, it concludes that the two inch high geometry significantly outperforms the planar geometry in the L1 band; whereas, the improvement in the L2 band is only 4-6%.

In conclusion, if one desires to achieve the best performance possible, irrespective of cost. One should select a convex non-planar geometry with large curvature (i.e. six inch high geometry), fill the aperture as much as possible with antenna elements and implement the antenna electronics in the beam forming / null steering mode.

## 8.2 Future Work

In this thesis, we investigated convex non planar antenna arrays with all antenna elements being identical. The next step is to study the effect of directive (high gain) auxiliary elements. We still want the reference element at the top of the surface to yield a broad pattern over the entire upper hemisphere in order to receive all satellite signals. However, since the surface is convex non planar, all the antenna elements are not oriented in the same direction. We think that directive auxiliary elements, which are tilted in the direction of low elevation signals, will receive low elevation interfering signals with a higher gain; as a result, the antenna array will force a deeper, concise null in the incident jammer direction. This will lead to a reduction in nulling the desired signal; thus, it will improve the antenna array AJ performance.

Hereafter, one should build and test the antenna arrays to verify the presented achievable AJ performance using STAP based AE in the presence of real world wide-band signals. Due to the fact that most current antenna electronics only provide seven or eight channels for L1 and L2 band processing, the seven element antenna array should be built first. Moreover, we have demonstrated great promise for the two inch high and six inch high twelve element antenna arrays, and they should be constructed when future technology allows.

# BIBLIOGRAPHY


[1] A.K. Brown and B. Mathews. GPS Multipath Mitigation Using a Three Dimensional Phased Array. In *Proceedings of ION GNSS 2005*, Long Beach, CA, September 2005.

[2] Y. Zhou, C.-C. Chen, and J. L. Volakis, Dual Band Proximity-Fed Stacked Patch Antenna for Tri-Band GPS Applications, *IEEE Transactions on Antennas and Propagation*, 55(1):220-223, January 2007.

[3] I.J. Gupta et. al., Non-Planar Controlled Reception Pattern Antennas for GPS Receivers, In *Proceedings of ION GNSS 2006*, Fort Worth, TX, September 2006.

[4] I.J. Gupta and A.A. Ksienski. Dependence of Adaptive Array Performance on Conventional Array Design. *IEEE Transactions on Antennas and Propagation*, AP-30(4):549-553, July 1982.

[5] I.J. Gupta and A.A. Ksienski. Effect of Mutual Coupling on the Performance of Adaptive Arrays. *IEEE Transactions on Antennas and Propagation*, AP-31(5):785-791, September 1983.

[6] I.J. Gupta and A.A. Ksienski. Prediction of Adaptive Array Performance. *IEEE Transactions on Aerospace and Electronic Systems*, AES-19(3):380-388, May 1983.

[7] R.T. Compton Jr. A Method of Choosing Element Patterns in an Adaptive Array. *IEEE Transactions on Antennas and Propagation*, AP-30(3):489-493, May 1982.

[8] R.T. Compton Jr. *Adaptive Antennas, Concepts and Performance.* Prentice-Hall, Inc., 1988.

[9] R.T. Compton Jr. The Bandwidth Performance of a Two-Element Adaptive Array with Tapped-Delay Line Processing. *IEEE Transactions on Antennas and Propagation*, 36(1):5-14, January 1988.

[10] Y. Lee and S. Ganguly. Design of a Direction Dependent Uniform Scan Array. In *Proceedings of ION GNSS 2005*, Long Beach, CA, September 2005.

[11] T.D. Moore, *Analytic Study of Space-Time and Space-Frequency Adaptive Processing For Radio Frequency Interference Suppression*, PhD Dissertation, The Ohio State University, 2002.

[12] M.L. Rankin, *The Effect of Sampling Rate on STAP Based RFI Suppression Systems*, Master's Thesis, The Ohio State University, 2004.

[13] I.J. Gupta, J.A. Ulrey and E.H. Newman. Effects Antenna Element Bandwidth on Adaptive Array Performance. *IEEE Transactions on Antennas and Propagation*, 53(7):2332-2336, July 2005.

[14] J.A. Ulrey, *Optimum Element Distribution For Planar Circular Adaptive Antenna Arrays*, Master's Thesis, The Ohio State University, 2006.

[15] FEKO, http://www.feko.info/.